Design, Pharmacokinetic and Pharmacodynamic Evaluation of Nanocarriers for Raloxifene Hydrochloride in the EffectiveTreatment of Post-menopausal Osteoporosis

THESIS

Submitted in partial fulfilment
of the requirements for the degree of
DOCTOR OF PHILOSOPHY

by

N. ADITYA

ID. No. 2010PHXF033H

Under the Supervision of

Dr. PUNNA RAO RAVI

BIRLA INSTITUTE OF TECHNOLOGY AND SCIENCE

PILANI (RAJASTHAN) INDIA

2014

BIRLA INSTITUTE OF TECHNOLOGY AND SCIENCE

PILANI (RAJASTHAN)

CERTIFICATE

This is to certify that the thesis entitled **"Design, Pharmacokinetic and Pharmacodynamic Evaluation of Nanocarriers for Raloxifene Hydrochloride in the Effective Treatment of Post-menopausal Osteoporosis"** submitted by **N. ADITYA**, ID.No:2010PHXF033H for award of Ph.D. Degree of the institute embodies original work done by him under my supervision.

Date: **Signature in full of the Supervisor**_____

Name in capital Block letters: **PUNNA RAO RAVI**

Designation : Assistant Professor

ACKNOWLEDGEMENT

Words cannot express my heartfelt gratitude to my mentor and guide, Dr Punna Rao Ravi, Assistant Professor, Department of Pharmacy, BITS Pilani, Hyderabad Campus. He has been a constant source of support and inspiration to me throughout my course of work. His boundless enthusiasm coupled with his sharp intellectual abilities has left an indelible mark on me. His moral support and timely advice at crucial times are unforgettable. I am highly indebted to him and sincerely acknowledge his help at all times.

It is my duty to express my sincere thanks to the Chancellor, BITS Pilani for providing necessary infrastructural support to carry out my research work. I am thankful to Prof. Bijendra Nath Jain, Vice Chancellor, BITS Pilani for facilitating my research work at the institute. I am also thankful to Prof. V.S. Rao, Director, BITS Pilani, Hyderabad Campus for his support during the course of my stay at this campus. I am thankful to Prof S.K. Verma, Dean, Academic Research Division, BITS Pilani, for his co-operation and encouragement at every stage of this research work.

I am thankful to Dr V. Vamsi Krishna, Head, Department of Pharmacy and senior professors, Dr D Sriram and Dr Yogeeswari Sriram for providing me with all the laboratory facilities and moral support during the course of my stay at the campus.

I sincerely acknowledge the help provided by other faculty members, Dr Srikant Charde, Dr Swati Biswas, Dr Sajeli Begum, Dr Balram Ghosh, Dr Onkar Kulkarni and Dr Arti Dhar for sharing their vast experience and technical knowledge with me at needy times.

I am also grateful to the non-teaching staff, Mrs Saritha, Mr Rajesh, Mr Ramu, Mr Srinivas and Mrs Rekha for their support in maintaining the supply of chemicals, glassware and animals during the course of my research work.

I am very grateful to my colleagues and friends, Mr Rahul Vats, Mr Praveen Kumar, Mr Shailender, Mr Mahibalan, Mr Srikant, Mr Suman, Mr Anup and many others for their invaluable support, encouragement and help at all times. They have been extremely patient

and bearing with me and have helped in gaining a lot through mutual exchange of knowledge. Their constructive criticism and technical inputs have been invaluable for my work.

The undergraduate and postgraduate students of pharmacy department deserve a special mention here. I cannot forget the help rendered by our students, Mr Himanshu Kathuria, Mr Srinivas Malekar, Mr Uday Sai Ranjan, Ms Rashmi Sinha and Ms Nancy Malik.

I acknowledge the help of University Grants Commission (UGC) for providing financial assistance through a major research grant (UGC Ref. No.: 39-176/2010 (SR)) for the project. I also thank SERB, Department of Science and Technology, Govt. of India and BITS-Pilani for providing travel assistance to present my research work at various conferences in India and abroad.

This section would be incomplete without thanking my family for their unwavering support throughout this period. My heartfelt thanks to my parents, Mr Narasimha Murthy and Mrs Nagamani Murthy for being pillars of my life and for providing me with unconditional support at all times. I can hardly find words to express my gratitude to my in laws, uncles and my wife Swetha for their patience and sacrifice. Lastly, I thank my six month old son Aprameya for bringing immense joy and excitement to my life!

Aditya N

List of Abbreviations and Symbols	
µg	Microgram
AFM	Atomic Force Microscopy
AP-2	Assembly Polypeptide 2
AUC	Area Under concentration versus time Curve
AUMC	Area Under first Moments Curve of concentration versus time profile
BBB	Blood Brain Barrier
Caco-2	Colorectal adenocarcinoma cells
CI	Confidence Intervals
Cl	Clearance
Cl/F	Clearance scaled by bioavailability
C_{max}	Maximum concentration of the drug
CME	Clathrin Mediated Endocytosis
CNS	Central Nervous System
CPCSEA	Committee for the Purpose of Control and Supervision of Experiments on Animals
CR	Complement Receptor
CYP	Cytochrome P450 enzyme system
DDS	Drug Delivery System
DLS	Dynamic Light Scattering
DSC	Differential Scanning Calorimetry
EE	Entrapment Efficiency
EPR	Enhanced Permeation and Retention
F	Absolute Bioavailability
FAE	Follicle Associated Epithelium
FDA	Food and Drug Administration

Frel	Relative Bioavailability
g	gram
GALT	Gut-associated Lymphoid Tissue
GIT	Gastrointestinal Tract
GMS	Glyceryl Monostearate
GDS	Glyceryl Distearate
GB	Glyceryl Behenate
GTS	Glyceryl Tristearate
GTO	Glyceryl Trioleate
h	hour
HPLC	High Performance Liquid Chromatography
HQC	Higher Level Quality Control Standard
IAEC	Institutional Animal Ethics Committee
ICH	International Conference on Harmonization
J	Joules
k	Degradation rate constant
K	Release rate constant
K_e	Rate of elimination of the drug
KHB	Krebs-Henseleit Buffer
L	Litre
LCMS	Liquid Chromatography coupled with Mass Spectroscopy
LCNPs	Lecithin-Chitosan Nanoparticles
LDL	Low Density Lipoprotein
LOD	Limit of Detection
Log D	Log of oil/water partition coefficient at a given pH

Log P	Log of oil/water partition coefficient
LOQ	Limit of Quantification
LQC	Lower Level Quality Control Standard
M	Molar
MAT	Mean Absorption Time
M-Cells	Manifold Cells
MEC	Minimum Effective Concentration
mg	milligram
min	Minutes
mm	Millimeter
MPS	Mononuclear Phagocyte System
MQC	Medium Level Quality Control Standard
MRT	Mean Retention Time
N	Newton
NCs	Nanocapsules
NDDS	Novel Drug Delivery System
NF	National Formulary
ng	Nano gram
NLC	Nanostructured Lipid Carriers
O/W	Oil-in-water
^{o}C	Degree Centigrade
O-MALT	Mucosa Associated Lymphoid Tissue
P188	Poloxamer 188
P407	Poloxamer 407
PCL	Poly(ε-caprolactone)

PCS	Photon correlation spectroscopy
PD	Pharmacodynamics
PDI	Polydispersity Index
PECA	Poly(ethyl cyanoacrylate)
PEG	Polyethylene glycol
PK	Pharmacokinetics
PLA	Poly Lactic acid
PLGA	Poly(lactide-co-glycolic acid) copolymer
PMO	Postmenopausal Osteoporosis
PSD	Particle size distribution
PVA	Polyvinyl Alcohol
QC	Quality Control Standard
R^2	Regression coefficient
RES	Reticuloendothelial System
RESOLV	Rapid expansion of supercritical solution into liquid solvent
RESS	Rapid expansion of supercritical solution
R_f	Retention Factor
RI	Recrystallization Index
RLX	Raloxifene hydrochloride
rpm	Revolutions per minute
RSD	Relative Standard Deviation
RT	Room Temperature (25 ± 2 ºC/60 ± 5% RH)
s	Seconds
SA	Stearic Acid
SD	Standard Deviation

SEM	Scanning Electron Microscopy
SERMs	Selective Estrogen Receptor Modulators
SGF	Simulated Gastric Fluid
SIF	Simulated Intestinal Fluid
SLN	Solid Lipid Nanoparticles
$T_{1/2}$	Half-life
TEM	Transmission Electron Microscopy
T_f	Tailing Factor
TG-LPs	Triglycerides rich lipoproteins
T_{max}	Time to reach maximum concentration of the drug
USP	United States Pharmacopoeia
UV	Ultraviolet Light
V_d	Volume of distribution
Vis	Visible Light
VLDL	Verly Low Density Lipoproteins
w/o/w	water-in-oil-in-water
WAXS	Wide angle X-ray Scattering
Δ H	Melting Enthalpy
ε	Epsilon
ζ-potential	Zeta Potential
λmax	Wavelength Maxima for UV-Absorbance

Abstract

The objective of this work was to design and evaluate different nanocarriers for oral delivery of raloxifene hydrochloride. Raloxifene hydrochloride is a selective estrogen receptor modulator (SERM) and is useful in treatment of postmenopausal osteoporosis and breast cancer. It exhibits low oral bioavailability (less than 2%) and high inter-patient variability in humans due to its poor solubility across GIT and extensive intestinal glucuronidation. In order to achieve the broader objective of this work, analytical and bioanalytical methods were first developed and validated for accurate and precise estimation of Raloxifene in both bulk and biological samples. Extensive preformulation studies were carried out to establish physicochemical properties of Raloxifene that could further aid in selection of appropriate excipients and manufacturing conditions.

Lipid based and polymeric nanocapsules/nanoparticles were developed for delivery of raloxifene. Biodegradable materials of synthetic (poly-ε-caprolactone) and natural origin (lipids, soy lecithin & chitosan) were used to produce different types of carrier systems for raloxifene. All the formulations were extensively characterized and evaluated. Manufacturing conditions for the formulations were optimized using design of experiments approach. In some cases, hybrid designs were used to get a better understanding of the factors affecting properties of nanocarriers like particle size, surface charge and drug entrapment efficiency. Optimized formulations were subjected to extensive pharmacokinetic evaluation (after oral and intravenous administration) in female Wistar rats. Further, time-dependent bio-distribution patterns for both free drug and nanocarriers were obtained. Mechanistic studies in presence of various cell uptake inhibitors like chlorpromazine and nystatin were performed to decipher the mechanisms involved in the intestinal uptake of these nanocarriers. For lipid

based nanoparticles, role of lymphatic uptake in bioavailability enhancement of raloxifene was established.

In all the cases, significant improvement in oral bioavailability of raloxifene was noticed. However, depending on the degree of enhancement, the formulations could be arranged as: soy lecithin-chitosan hybrid nanoparticles (~4.2 folds) > solid lipid nanoparticles (~3.4 folds) > poly-ε-caprolactone nanocapsules (~2.1 folds). Significant improvement in oral bioavailability was attributed to protection from intestinal glucuronidation and improvement in both active and passive uptake of raloxifene from the GIT.

Further, to assess the usefulness of these nanocarriers, pharmacodynamic screening was carried out in female Wistar rats. Rat model for postmenopausal osteoporosis was established by performing bilateral ovariectomy using the dorso-lateral approach. Three groups – Naïve rats, sham operated rats and ovariectomized rats were used in this study. Biomechanical investigations were carried out on rat femoral bones using three-point bending method. The bone stiffness and ultimate breaking force were taken as indicators of bone strength. Drug content was estimated in plasma and bone marrow at the endpoint of the study. Results from these studies indicated that drug loaded into soy lecithin-chitosan hybrid nanocarriers accumulate to a significantly greater extent than the free drug in the bone marrow. Moreover, there was evidence that rats treated with nanocarriers had significantly greater bone strength compared to rats treated with vehicle alone or free drug. It is prudent to note that these studies are only preliminary in nature. Nevertheless, they provide evidence that nanocarriers could be useful for effective delivery of estrogens/SERMs and could further prove to be a new strategy in managing chronic disease like postmenopausal osteoporosis.

Chapter 1

Introduction

1.1 Post-menopausal osteoporosis and its treatment

Osteoporosis is a skeletal disorder characterized by compromised bone strength predisposing a person to an increased risk of fracture. Bone strength primarily reflects the integration of bone density and bone quality [1]. There are many causes for osteoporosis, but by far the most common and most important is postmenopausal osteoporosis (PMO), which affects most women during senescence [2]. Despite an increasing awareness of the importance of osteoporosis in some sections of the population, many women are still not sufficiently aware of the condition, do not appreciate the way in which it may affect their lives and, most importantly, do not understand that it is preventable.

About 30-40% of women in the world are estimated to suffer bone fracture attributed to osteoporosis. It is estimated that osteoporosis causes over 1.5 million fractures each year in the USA. It also accounts for 70% of all fractures for people over 45 years in USA and 80% of these cases of osteoporosis occur in women [3]. Seventeen billion dollars was the estimated cost of osteoporotic fracture treatment in United States in 2005, thus indicating the economic bearing that the disease has on the society [4]. Asia fares no better in prevalence of osteoporosis. About 37% of Japanese women aged 50 years and above are estimated to suffer vertebral fracture due to osteoporosis. Women in other Asian countries like Malaysia, China and Thailand also suffer from increased risk of fractures due to osteoporosis.

Indian scenario on prevalence of this disease is unclear as there is very little data available on the incidence of osteoporosis in India. Indirect estimates suggest some 25 million people are osteoporotic and further 25 million have low bone mass [5]. This figure may be an underestimate of the problem as Indian women have low peak bone mass on account of low blood calcium levels due to low dietary calcium and vitamin D intake [6, 7] and accelerated loss due to genetic estrogen receptor polymorphism [8]. This makes social and economic burden of osteoporosis immense in a developing country like India, where

resources are scarce and per-capita spending on health care is less, even in comparison to other Asian countries.

Physiologically, osteoporosis is characterized by a decrease in bone mass (osteopenia) and a deterioration in bone micro-architecture which leads to an enhanced fragility of the skeleton, and therefore to a greater risk of fracture. Bone remodelling occurs throughout life of an individual at discrete sites within the skeleton and proceeds in an orderly fashion, with initial bone resorption being followed by bone formation, a phenomenon referred to as 'coupling'. This maintenance programme is necessary for both metabolic and mechanical skeletal functions. The process of bone resorption followed by synthesis of bone matrix and its subsequent mineralization, takes up to 6 months. If the process of bone resorption and bone formation is not matched, there is a 're-modelling imbalance'. Such an imbalance is magnified when the rate of initiation of new cycles of bone re-modelling increases, as it does in post-menopausal women in whom, at any time, some bone would have been resorbed and not yet replaced [9].

Postmenopausal osteoporosis is currently an important public health issue due to its widespread prevalence and the high socio-economic and healthcare impact it entails. This justifies the establishment of pharmacological and non-pharmacological measures aimed at treating this disease and at secondary prevention of the fractures associated with it [10].

Pharmacological measures for treating postmenopausal osteoporosis include use of drugs like activated vitamin D3, calcitonin, biphosphonates, Hormone Replacement Therapy (HRT) with estrogen, anabolic steroids, calcium supplements and use of selective estrogen receptor modulators. Though HRT is effective in treatment of postmenopausal osteoporosis, complications like deep vein thrombosis and occurrence of endometrial and breast cancer makes it less preferred as a first line of therapy. These limitations of HRT stimulated the

development of a series of non-hormonal compounds with high affinity for estrogen receptors that are capable of reproducing the beneficial effects of estrogens on the skeletal system (estrogen agonist effect), without the negative effects on the breast and endometrium (estrogen antagonist effect). These compounds were called Selective Estrogen Receptor Modulators or SERMs [11]. The SERMs include drugs like tamoxifen, raloxifene, toremifene, ospemifene, lasofoxifene, arzoxifene and bazedoxifene [12].

Currently, there are two classes of SERMs approved for clinical use: the first-generation triphenylethylene derivatives, which include tamoxifen and toremifene that are used in prevention and treatment of breast cancer, and raloxifene, a second-generation benzothiopene derivative that is prescribed for treatment and prevention of osteoporosis [13]. In recent years, raloxifene is also being prescribed for reduction of breast cancer incidence in high risk post-menopausal women [14]. It is noteworthy that all these drugs have beneficial effects on serum lipids [14]. However, adverse effects associated with them include hot flushes and an increased risk of venous thromboembolism [14].

Raloxifene, marketed as a raloxifene hydrochloride is the only SERM compound approved worldwide for the prevention and treatment of postmenopausal osteoporosis and fragility fractures. It has low solubility and poor oral bioavailability (of less than 2%) with high inter-patient variability in humans. Approximately 60% of oral dose is absorbed, but pre-systemic glucuronide conjugation is extensive, which limits its oral bioavailability [15]. The bioavailability of raloxifene hydrochloride varies across different species of animals. In rats and dogs, bioavailability of raloxifene hydrochloride was originally reported as 39% and 17%, respectively [16]. In contrast, according to more recent reports, bioavailability of raloxifene hydrochloride is 4% and 0% in rats and dogs respectively [17]. Further, bioavailability of raloxifene hydrochloride in pigs is reported as 7% [18]. Across all these species, low solubility and gut wall glucuronide conjugation is a major limiting factors for

oral bioavailability of raloxifene hydrochloride [19]. A more detailed discussion on physicochemical, pharmacokinetic and pharmacodynamic properties of raloxifene hydrochloride is available in chapter 2.

1.2 History of nanoparticles and their use as drug carriers

Though nanotechnology looks like the cutting edge of modern technology, intriguingly, it's not that new. From the Roman Lycurgus cup of 4th century AD to the iridescent metallic glazes of 'deruta ceramicists' in Italy (1450-1600 AD), nanotechnology in a variety of ways has existed for long [20]. However, it's only in the last few decades that our understanding and utilization of nanotechnology has grown by leaps and bounds.

Nanomedicine has been an important offshoot of nanotechnology. It is anticipated that nanomedicine could have a great bearing on human life because elementary biological units like DNA, proteins and cell membranes are of this dimension. Development of the concept of nanomedicine has followed two principal paths that have been termed "wet nanotechnology" in the biological tradition and "dry nanotechnology" in the mechanical tradition [21].

The use of modern concepts of nanotechnology in the design of pharmaceutical products took shape with the introduction of milled Danazol, a synthetic steroid derived from ethisterone. The bead-milled Danazol nanosuspension with mean particle size of 169 nm showed an enhanced oral bioavailability (~82 %) in comparison to conventional Danazol suspension (~5 %) [22]. Later, using micro-fluidization technology, sub-micron atovaquone was introduced with a mean particle size ranging from 0.1 to 3 μm. The first nanotechnology product to be approved by USFDA was Rapamune® that contained Sirolimus, an immunosuppressant developed by Wyeth pharmaceuticals. The next major nanotechnology based product to be approved by USFDA was Emend® (containing nanocrystalline anti-emetic drug, aprepitant). Subsequently, Abbott Laboratories launched nanocrystalline

Fenofibrate that was marketed as Tricor®. With Triglide®, another nanotechnology product containing Fenofibrate, SkyePharma and First Horizon Pharmaceuticals extended the life-term of the drug after its original patent had expired. Another product called Megace ES® containing nanocrystalline megesterol acetate (used in the treatment of eating disorders) was subsequently launched by Elan drug delivery and Par pharmaceutical companies. This product, like other nanocrystalline products, significantly improved the oral bioavailability and reduced fasting-fed variability in humans. It was also demonstrated for the first time that nanosuspension products could be commercially produced with adequate stability and shelf-life. Table 1.1 [23, 24] below showcases a list of marketed nanotechnology based drug products that have been approved by the USFDA.

Table 1.1: FDA approved nanomedicine products on the market

Product Name	Composition	Indication	Company
Abelcet	Amphotericin B/ lipid complex	Fungal infections	Enzon (Bridgewater, NJ, USA)
Amphotec	Amphotericin B/ colloidal dispersion	Fungal infections	InterMune (Brisbane, CA, USA) Ambisome
Ambisome	Liposomal Amphotericin B	Fungal infections	Gilead (Foster City, CA, USA), Fujisawa, (Osaka, Japan)
DaunoXome	Liposomal daunorubicin	Kaposi sarcoma	Gilead
Doxil/Caelyx	Liposomal doxorubicin	Cancer, Kaposi sarcoma	Ortho Biotech (Bridgewater, NJ, USA); Schering-Plough (Kenilworth, NJ, USA)
Depocyt	Liposomal cytarabine	Cancer	SkyePharma (London), Enzon
Epaxal Berna	Virosomal hepatitis vaccine	Hepatitis A	Berna Biotech (Bern, Switzerland)
Inflexal V Berna	Virosomal influenza vaccine	Influenza	Berna Biotech
Myocet	Liposomal doxorubicin	Breast cancer	Zeneus Pharma (Oxford, UK)
Visudyne	Liposomal verteporfin	Age-related macular degeneration	QLT (Vancouver, Canada), Novartis (Basel)

Adagen	PEG-adenosine deaminase	Immunodeficiency disease	Enzon
Neulasta	PEG-G-CSF	Febrile neutropenia	Amgen (Thousand Oaks, CA, USA)
Oncaspar	PEG-asparaginase	Leukemia	Enzon
Pegasys	PEG-α-interferon 2a	Hepatitis C	Nektar (San Carlos, CA, USA), Hoffmann-La Roche (Basel)
PEG-Intron	PEG- α -interferon 2b	Hepatitis C	Enzon, Schering-Plough
Macugen	Pegylated anti-VEGF aptamer	Age-related macular degeneration	OSI Pharmaceuticals (Melville, NY, USA), Pfizer (New York)
Somavert	PEG-HGH	Acromegaly	Nektar, Pfizer
Copaxone	Copolymer of alanine, lysine, glutamic acid and tyrosine	Multiple sclerosis	TEVA Pharmaceuticals (Petach Tikva, Israel)
Renagel	Crosslinked poly(allylamine) resin	Chronic kidney disease	Genzyme (Cambridge, MA, USA)
Emend	Nanocrystalline aprepitant	Antiemetic	Elan Drug Delivery (King of Prussia, PA, USA), Merck & Co. (Whitehouse Station, NJ, USA)
MegaceES	Nanocrystalline megesterol acetate	Eating disorders	Elan Drug Delivery, Par Pharmaceutical Companies (Woodcliff Lake, NJ, USA)
Rapamune	Nanocrystalline sirolimus	Immunosuppressant	Elan Drug Delivery, Wyeth Pharmaceuticals (Collegeville, PA, USA)
Tricor	Nanocrystalline Fenofibrate	Lipid regulation	Elan Drug Delivery, Abbott (Abbott Park, IL, USA)
Triglide	Nanocrystalline fenofibrate	Lipid regulation	SkyePharma, First Horizon Pharmaceuticals (Alpharetta, GA, USA)
Abraxane	Paclitaxel protein bound nanoparticles	Cancer	Abraxis BioScience (Schaumburg, IL, USA), AstraZeneca (London)

1.3 Nanoparticles – Types, preparation techniques and characterization tools

(A) Relative comparison of nanoparticles with other materials

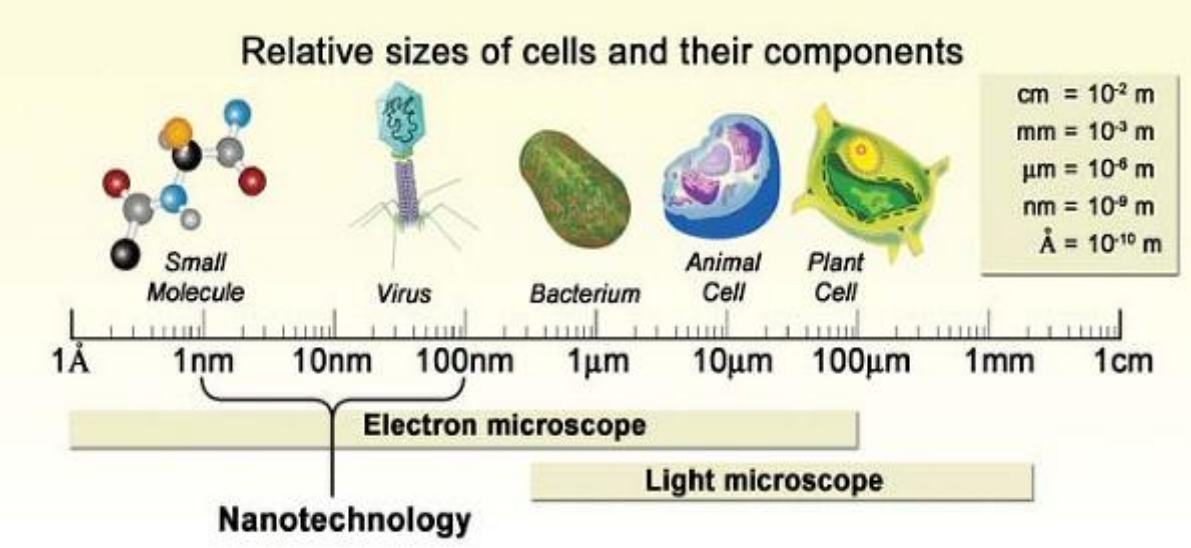

Fig. 1.1: Relative comparison of nanoparticles with other sub-micro and micro particles. Figure source: Majoros, I., et al., *Progress in Cancer Nanotechnology*, in *Progress in Molecular Biology and Translational Science*, R. Ruddon, Editor. 2010, Elsevier: Burlington. p. 193-236.

1.3 Approaches to manufacture nanotechnology based products:

There are two widely accepted approaches for manufacture of nanoparticles: (a) Top-down approach and (b) Bottom-up approach.

1.3.1 The top-down approach:

This approach uses external, macroscopic raw materials to get the desired nanomaterial. The processing of these macroscopic materials is externally well-controlled. Typical examples for this kind of approach include: etching, ball-milling, homogenization and application of severe plastic deformations [25].

1.3.2 The bottom-up approach:

In this approach, the raw material is taken in a pre-miniaturized form (molecular/atomic level) and later either allowed to self-assemble into nanomaterial or assembly is facilitated by addition of other catalysts. During the assembly process, other molecules of interest can be incorporated into the nanomaterial to finally get a composite nanoproduct. However, in both these approaches, it is important that the final product has to be 'stabilized' by some external means. Else, these inherently unstable nanoproducts demonstrate a tendency to aggregate upon storage [25].

1.4 Polymeric Nanoparticles

1.4.1 Methods for manufacture of polymeric nanoparticles [26]

The polymeric nanoparticles can be prepared by two ways: (1) from pre-formed polymers or (2) by direct polymerization of monomers using classical polymerization techniques. A brief overview of the available methods is illustrated in Fig. 1.2.

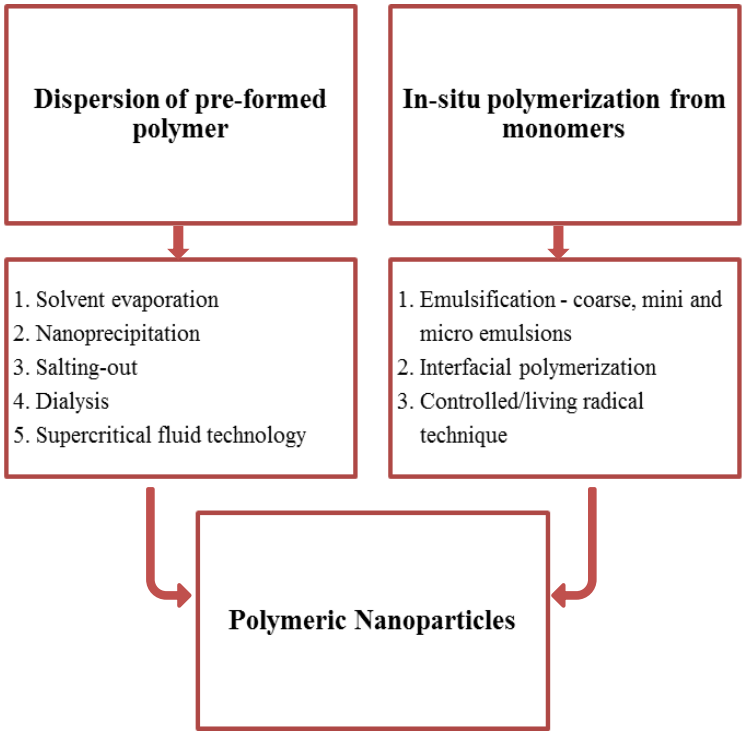

Fig. 1.2: Overview of methods available for manufacture of polymeric nanoparticles.

1.4.1.1 Dispersion of pre-formed polymers

In the following section, brief discussion on widely reported methods is presented.

A. Solvent evaporation method

This was one of the first methods to be reported for the manufacture of nanoparticles. This method is more popular with the polymer chemists. Nevertheless, the pharmaceutical industry has benefitted the most from this method. In this method, polymer solutions are prepared in carefully chosen volatile organic solvent(s) and an emulsion is formed using an aqueous immiscible phase. The emulsion is stabilized by suitable surfactant/blend of surfactants. To get the nanoparticle suspension, the organic phase is either evaporated or allowed to slowly diffuse out of the system. Common organic phase solvents that have been used are: dichloromethane and chloroform. However, more recently, ethyl acetate has replaced other solvents as an organic phase due to its low flammability potential and better toxicity profile [27]. The polymers employed in the manufacture of nanoparticles are mostly biodegradable in nature. Examples include, poly (organophosphazene), poly (ε-caprolactone), poly (D, L-lactic acid-co-glycolic acid), poly (L-lactic acid) and poly (lactide-co-glycolide fumarate) [27-33]. Choice of an appropriate surfactant is critical for stabilization of emulsion, and hence, the nanoparticle. Frequently used surfactants include: polyvinyl alcohol, tri-block co-polymers (pluronics), sodium cholate, span 40, poloxamine 908 and sodium dodecyl sulphate [27-30, 32]. Two types of emulsions can be obtained by this method: (1) Single emulsion (o/w or w/o) and (2) Double emulsion (w/o/w). The choice of the emulsion type, almost always depends on the solubility of the material to be loaded in the nanoparticle.

To achieve desired particle size, high-speed homogenization, ultrasonication or a combination of these methods can be used. The solvent evaporation can be accelerated by operating under reduced pressure conditions. The solidified nanoparticles are collected either

by centrifugation or dialysis process. The product is washed in repeated cycles with distilled water to remove excess surfactant. These nanoparticles are then either re-suspended in suitable buffer or lyophilized for storage.

The particle size and polydispersity could vary depending on the organic phase, stirring mechanism and speed and surfactant concentration used. In general, using this method, particle sizes ranging from 60 to 200 nm can be obtained.

B. Salting out method

A major drawback of the previous method is the use of hazardous organic solvents in the formulation. Therefore, Bindschaedler et al. [34] first reported the use of a solvent-free method for manufacture of nanoparticles that involved a salting-out process. In this method, a system is first formed with a solvent (e.g. acetone) that is totally miscible with water. The polymer is dissolved in the solvent. Then, emulsification is achieved without applying high-shear forces, by dissolving high concentration of salt or sucrose in the aqueous phase to get a salting-out effect. Magnesium chloride, calcium chloride and magnesium acetate are commonly used for salting-out effect. The reverse salting-out process can be obtained by diluting the emulsion with large quantities of water that leads to precipitation of polymer present in the organic phase of the emulsion. Both biodegradable and non-biodegradable polymers have been used in this method. Examples include, eudragit L100-55 [35], poly (D, L-lactic acid-co-glycolic acid) [36-38] and poly (methylacrylate) [39]. In this method, the effect of stirring speed and polymer concentration on the particle size is less pronounced because, in this case, unlike regular emulsions, only one phase is present [39]. The overall energy required to form droplet surface in this method is much lesser when compared to conventional bi-phasic emulsions.

C. Nanoprecipitation/Solvent displacement method

Fessi et al. [40] are credited for first reporting the development of nanoparticles using this method. The basic principle here is the interfacial deposition of polymer after it is displaced by a semi-polar, water miscible solvent from the organic phase. The rapid diffusion of solvent from the non-solvent phase results in a sudden decrease of the interfacial tension and an increase in surface area that results in formation of tiny droplets of organic phase. In a nanoprecipitation system, there are three basic components: (1) the polymer (synthetic or natural) (2) a solvent in which the polymer is soluble (solvent phase) and (3) another solvent in which the polymer is not soluble (non-solvent phase). Typically, organic solvents that are water-miscible, yet easily removable (e.g. ethanol and acetone) are used as solvent phases. Conversely, for the non-solvent phase, water (with or without surfactant/stabilizer) is almost always used. Polymers like poly (ε-caprolactone) [41-43], poly (D, L-lactic acid-co-glycolic acid) [44, 45], poly (L-lactic acid) [46, 47], polyalkylcyanoacrylate [48] and allylic starch [49] have been previously employed for preparation of nanoparticles by this method. Surfactants/stabilizers employed include PVA, various grades of pluronics and tweens.

In practice, the polymeric nanoparticles are produced by slowly adding the solvent phase to the non-solvent phase under mild stirring conditions. However, even if the addition order is reversed, nanoparticles can still be obtained. The important variables that affect the particle size and distribution in this method are: (1) Order and rate of addition of solvent phase to the non-solvent phase (2) Stirring rate and speed and (3) The ratio of solvent to non-solvent phase. Although nanoparticles can be obtained even without using surfactant/stabilizer, including them in the formulation helps in controlling both the nanoparticle size and its distribution. This is a simple, fast and reliable method for routine manufacture of nanoparticles.

D. Dialysis method

In this method, the polymer is dissolved in an organic phase and placed inside a dialysis tube with an appropriate molecular weight cut-off. This is then dialyzed against a non-solvent that is miscible with the organic phase. Due to progressive loss of solubility, the polymer slowly precipitates out and forms homogeneous nanoparticle dispersion inside the dialysis bag [50, 51]. Although the mechanism of nanoparticle formation is not fully understood, many scientists believe that the underlying principle is akin to nanoprecipitation [40].

E. Supercritical fluid technology

Two important methods employing supercritical fluid technology have been employed for development of nanoparticles:

i. Rapid expansion of supercritical solution (RESS)

In this method, the solute (polymer or pure active ingredient) is dissolved in a supercritical fluid and allowed to expand rapidly through a tiny orifice or a capillary nozzle into ambient air. This rapid pressure reduction along with a high degree of supersaturation results in controlled nucleation and formation of nanoparticles. In most of the cases, carbon dioxide is used as a solvent to dissolve the solute.

ii. Rapid expansion of supercritical solution into liquid solvent (RESOLV)

This method is a modified version of the RESS method. The modification is in the use of a liquid instead of ambient air as a medium for the rapidly expanding supercritical solution. The liquid medium apparently prevents the growth of micro particles and keeps most of the particle population in nano dimension. Many solvents can be used as supercritical fluids (e.g. carbon dioxide, carbon monoxide, n-pentane, ammonia and water). However, the choice of solvent depends on solubility of the solute (polymer) in a given supercritical fluid.

For the external liquid phase, either water or sodium chloride solution [52] have been employed.

1.4.1.2 Polymerization from monomers

In all the previously discussed techniques, pre-formed polymers were manipulated to obtain nanoparticles. In this section, methods that use monomers to build polymers are presented.

A. Emulsion polymerization method

This is one of the most common methods to obtain variety of polymers. In this method, water is used as a dispersion medium as it is environmentally friendly and also allows heat dissipation during the polymerization process. This method is further classified into two types depending on presence or absence of surfactant in the manufacturing process.

i. Conventional emulsion polymerization method

The basic ingredients used in this method are: (1) Water (2) A monomer with low water solubility (3) A water-soluble initiator and (4) A surfactant. The chain initiation occurs when a monomer molecule dissolved in the continuous phase collides with an initiator molecule that may be either an ion or a free radical. Phase separation and formation of solid particles occur once the polymerization reaction reaches completion. A range of particle sizes (50 to 300 nm) could be obtained depending on the nature of monomer used.

ii. Emulsion polymerization without surfactants

Removal of surfactant from the final product is a time-consuming and an expensive process. The reagents used in this method include (1) deionized water (2) water-soluble initiator (e.g. potassium persulfate) and (3) monomers (e.g. vinyl and acryl monomers). In absence of a surfactant, stabilization of nanoparticles occurs via ionisable initiators or ionic co-monomers used in the formulation [53].

B. Mini-emulsion polymerization method

A typical formulation in this method would contain water, monomer mixture, co-stabilizer, surfactant and an initiator [54]. The critical difference between this and the previously reported emulsion polymerization method is that, in this method, a low molecular mass co-stabilizer and a high-shear device (e.g. ultrasonicator) are used. The mini-emulsions are unstable and require a high-shear to reach a steady state; interfacial tension in a mini-emulsion is very high [54].

C. Micro-emulsion polymerization method

In this method, a water-soluble initiator is added to the aqueous phase of a thermodynamically stable micro-emulsion. The polymerization starts in the micro-emulsion phase that has monomers in a dissolved form. This method heavily relies on use of appropriate surfactants to obtain a thermodynamically stable micro-emulsion with an interfacial tension in o/w interface close to zero. The final particles are completely covered by excess surfactant added to the formulation. The critical variables in this process that control the droplet size of micro-emulsion (and hence, nanoparticles) are: type and concentration of initiator, surfactant type and concentration and the reaction temperature during formulation process [54].

D. Interfacial polymerization method

As the name suggests, in this method, the polymerization process takes place at the o/w interface. In each of the phases, reactive monomers or agents are added that interact with each other at the interface. This method is useful to encapsulate liquids and oils into polymer matrices. In this method, when aprotic solvents like acetone or acetonitrile are used, it results in formation of nanocapsules. On the other hand, when protic solvents like ethanol, n-butanol or isopropanol are employed, it results in the formation of both nanospheres and nanocapsules [55].

Alternatively, water-containing nanocapsules can be obtained by taking monomers in water-in-oil micro-emulsions. In the recent years, the membrane reactors have been used to prepare nanoparticles. A controlled addition of one reactant (the organic phase) to another reactant (the aqueous phase) can be achieved by membrane reactors. This process comparable to the membrane emulsification process, where the dispersed phase permeates through the membrane pores to form droplets in the continuous phase for preparation of emulsions [55].

1.5 Lipid based nanoparticles – Solid lipid nanoparticles and nanostructured lipid carriers

A systemic classification of lipid-based formulation for oral delivery was first given by Pouton [56] based on the nature of components present in the formulation. Table 1.2 below gives this lipid classification system.

Solid lipid nanoparticles (SLN) and more recently, nanostructured lipid carriers (NLC) have developed as an alternative to emulsions, liposomes, polymeric micro and nanoparticles. They show numerous advantages over other nanocarriers. Some of them are:

a) No inherent cytotoxic effects or granulocyte formation like polymeric nanoparticles [57]
b) No impairment of reticuloendothelial system (RES). Polymeric nanoparticles degrade slowly and can impair the RES up to 4 weeks [57].
c) Most of the lipids and surfactants used in the production of SLN and NLC have an approved status, e.g. Generally Recognized as Safe (GRAS status) due to their low toxicity profile. Organic solvents are minimally used for lipid nanoparticles.
d) Better physical stability and drug loading–lesser chance of drug leakage when compared to polymeric nanocapsules or liposomes.

e) Easy to scale-up and commercialize as compared to other polymeric nanoparticles due to excellent reproducibility and cost effectiveness (e.g. methods like high pressure homogenization can be easily scaled-up) [58].

Table 1.2: Pouton's classification of lipid-based formulations for oral delivery [56]

Formulation Characteristics	**Type I**	**Type II**	**Type IIIA (fine emulsion)**	**Type IIIB (micro emulsion)**	**Type IV (surfactant blend)**
Nature of the formulation	Only triglyceride oils (no surfactant)	Oils with water insoluble surfactants (HLB <12)	Oils with surfactants and small amount of co-solvents[$]	Oils with surfactants and greater amount of co-solvents[$]	No oils; only water soluble surfactants and co-solvents used
Dispersibility	Non-dispersing	Self-emulsifying in nature (SEDDS)	SEDDS and SMEDDS formed with water-soluble components	SEDDS and SMEDDS formed with water-soluble components; low oil content	Dispersion into micellar systems
Digestibility	Requires digestion before absorption (lipase/co-lipase)	Easily digestible (lipase/co-lipase)	No digestion necessary before absorption	No digestion necessary before absorption	Limited digestion
Digestion products	FFA and MG	At low surfactant concentrations, FFA and MG generated; At high concentrations* digestion is less important	Partial digestion of lipids may occur, but digestion is not a pre-requisite for absorption	Lipid digestion eliminated because large part of TG oil is replaced by co-solvents	No lipids available for digestion; if TG is present as surfactant, it may be partially digested
Absorption from the gut	Form mixed micelles with bile salts and are absorbed through gut	Form mixed micelles with bile salts and are absorbed through gut	Absorption from gut is rapid	Drug release is independent of digestion kinetics and absorption is extremely rapid	Absorption is independent of digestion. Depending on the micelle size and nature, absorption rate varies

FFA – Free fatty acid; MG – Monoglycerides; SEDDS - Self-emulsifying drug delivery systems; SMEDDS - Self-microemulsifying drug delivery systems; [$]co-solvents commonly used are alcohol and propylene glycol; *high concentration of surfactants is 20 to 60% w/w in the formulation.

1.5.1 Solid lipid nanoparticles (SLN)

The first idea of lipid based particulate systems carrying active ingredients was conceived in the late 1980s when Speiser and group reported the production of lipid microparticles by spray congealing method [59]. Later, the same group focused on further size reduction of lipid microparticles by using high-speed stirring and ultrasonication techniques [60]. It was in 1990s that the first experiments on lipid nanoparticles were performed in the lab. The lipid nanoparticles were developed in parallel by M. R. Gasco in Turin, Italy, and by R. H.Müller and J. S. Lucks in Berlin, Germany [61, 62]. The first of the many patents on SLN were filed by them. The high pressure homogenization technique to produce lipid nanoparticles was introduced by Muller et al. in 1993 [62]. From several studies conducted by Muller's group (and other groups), it was demonstrated that this technique was superior to any the other available techniques to produce lipid nanoparticles [63]. While, the trade name 'SLN^{TM}' has been registered in the pharmaceutical sector, for cosmetic applications, SLN is registered under the trade name 'Lipopearls^{TM}'[64].

SLN consist of a solid lipid matrix that is in solid state at both room and body temperatures. The SLNs are prepared in a similar manner to an oil-in-water (o/w) emulsion except that the oil phase of the emulsion is replaced by a solid lipid or a blend of solid lipids. High carbon chain fatty acids, fatty acid esters and waxes are used as solid lipids in the SLN. Typically, the SLN particle size ranges from 80 to 1000 nm [65]. It is difficult to produce SLN with a mean particle size lower than 80 nm as these small particles do not re-crystallize during the manufacturing process [66, 67].

The SLN dispersion can be directly used as a nanosuspension or it can also be incorporated into solid dosage forms like tablet and pellets by using SLN dispersion during granulation process [68]. Alternatively, SLN aqueous dispersion can be transformed into a

dry powder by spray-drying or lyophilisation [68]. This will enhance the SLN's long-term stability and when required, it may be reconstituted with water to produce a nanosuspension. The ingredients commonly used in preparation of SLN are listed in Table 1.3 and 1.4 below [69].

Table 1.3: List of excipients commonly used in the manufacture of lipid nanoparticles

Lipids	Surfactants		Miscellaneous lipophilic excipients
Triglycerides	Surfactant	HLB Value	
1. Trimyristin (Dynasan 114)	1. Lecithin	4–9	
2. Tripalmitin (Dynasan 116)	2. Poloxamer 188	29	
3. Tristearin (Dynasan 118)	3. Poloxamer 407	21.5	
Mixtures of mono, di and triglycerides	4. Tyloxapol	13	
1. Witeposol bases	5. Polysorbate 20	16.7	
2. Glyceryl monostearate (Imwitor 900)	6. Polysorbate 60	14.9	
3. Glyceryl behenate (Compritol 888 ATO)	7. Polysorbate 80	15	
4. Glyceryl palmitostearate (Precirol ATO 5)	8. Sodium cholate	18	
Waxes	9. Sodium glycocholate	14.9	
1. Beeswax	10. Taurodeoxycholic acid sodium	13–14	
2. Cetyl palmitate	11. Butanol and Butyric acid	7–9	
Solid fatty acids	12. Cetylpyridinium chloride	~15	
1. Stearic acid	13. Sodium dodecyl sulphate	40	
2. Palmitic acid	14. Sodium oleate	18	
3. Behenic acid	15. Polyvinyl alcohol	15–19	
Other lipids	16. Cremophor EL	12–14	
1. Miglyol 812			
2. Paraffin			

Oleic acid, Soya fatty acids, D-α-Tocopherol (vitamin E), Corn oil mono-di-triglycerides, Propylene glycol esters of fatty acids

Table 1.4: Physicochemical properties of lipids used in the manufacture of SLN and NLC

Name of the fatty acid	Number of carbon atoms (chain length)	Melting range (ºC)
1. Caprylic acid	08	16.5
2. Capric acid	10	31.6
3. Lauric acid	12	44.8
4. Myristic acid	14	54.4
5. Palmitic acid	16	62.9
6. Stearic acid	18	70.1
7. Oleic acid	18	16.0
8. Linoleic acid	18	-5.0
9. γ-Linoleic acid	18	-11.0
10. Ricinoleic acid	18	6.0
11. Arachidic acid	20	76.1
12. Behenic acid	22	80.0

1.5.1.1 Drug incorporation into SLN

The SLNs can alter the inherent properties of the drug incorporated in them. They act by enhancing the dissolution rate (thus, improving oral bioavailability of many drugs) [70], improving tissue distribution [71], targeting organs and protecting the drug from in-vivo processes like metabolism in the gut/liver [70, 71].

Numerous factors like solubility of the drug in the lipid matrix, physicochemical properties of the drug, nature of the lipid and surfactant used and manufacturing method play an important role in determining the amount of drug loaded into the SLN [63]. Currently, there are four different models describing the drug incorporation into SLN. These are schematically represented in Fig. 1.3 below [63, 72]

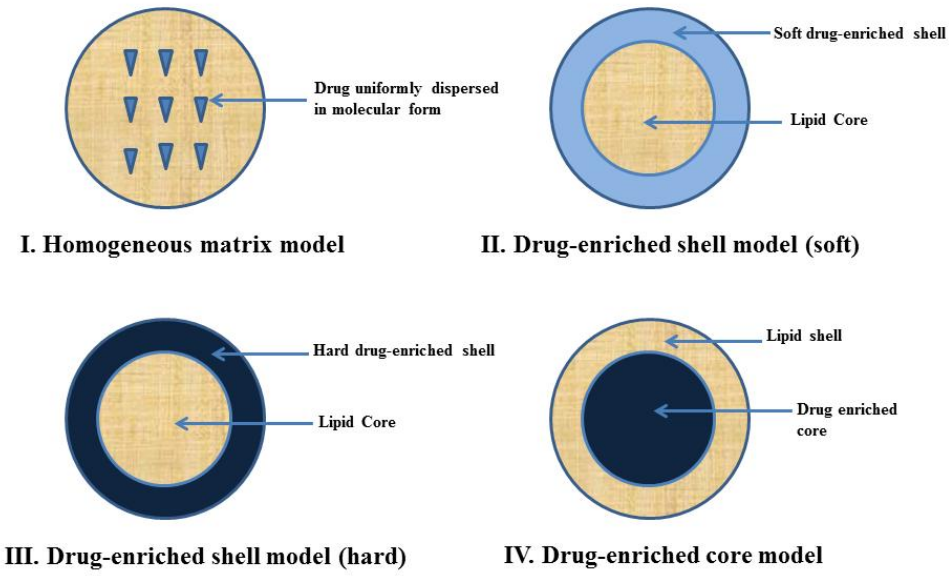

Fig. 1.3: Schematic representation of models describing drug incorporation into SLN

I. Homogeneous matrix model for incorporation of drug in SLN

This model is also called solid solution model. It is achieved when the drug incorporated into SLN exists in completely dissolved, molecular form. The drug may remain as amorphous clusters within the lipid matrix. This type of drug loading into SLN can be obtained by both cold and hot homogenization methods [63]. The in-vitro drug release from these systems is determined by the rate of drug diffusion within the solid lipid matrix. Therefore, in this model, the drug is released in a controlled manner from the lipid matrix [63].

II. Soft and hard drug-enriched shell models

In both of these models, lipid is present in the core and this solid lipid core is surrounded by a drug-enriched outer shell. SLN manufactured by hot homogenization process have a higher tendency to demonstrate this kind of behaviour. When hot microemulsion cools down, phase separation between the dissolved drug and the lipid phase leads to the generation of core-shell type SLN. Initially, the drug partitions into the external aqueous environment of o/w emulsion. This leads to drug-enrichment of the peripheral SLN regions and upon complete cooling, shell-enriched SLN are obtained [63, 72].

Depending on the type of interaction between drug and lipid, either shell-enriched soft or hard types of SLN are obtained. In the shell-enriched hard type SLN, the drug's structural characteristics enable them to fit together to form a strong, brick-like solid layer [63, 72]. In soft shell-enriched SLN, the drug and lipid do not fit tightly like brick-model described earlier [63, 72]. However, in both the cases, a rapid in-vitro drug release (burst release) profile is obtained [63, 72].

III. Drug-enriched core

In case of the drug-enriched core model SLN, incorporation of drug in SLN involves the formation of a drug-enriched core surrounded by a shell that is relatively free of drug. The model can be obtained when the concentration of a drug is close to the saturation solubility of the drug in the lipid phase of the SLN formulation [72]. Due to this, the entire drug remains at the core and the layers of lipid above the core gradually cool down to entrap the drug. The formulations that show an initial lag followed by more controlled release at later stage are best described by this SLN model [63, 72].

1.5.2 Nanostructured lipid carriers (NLC)

The shortcomings of SLN (low drug loading and drug expulsion from the lipid matrix upon storage) led to development nanostructured lipid carriers (NLC) [67]. The perfect crystalline nature of solid lipids was identified as the main cause for drug expulsion from lipid matrix [64, 67, 73]. The pure solid lipids are crystalline in nature and prefer to exist in a low energy and a highly ordered state called the β-polymorphic state [64, 74]. During manufacture of SLN, when the lipid is molten and allowed to cool, it re-arranges to less stable forms: α-polymorphic form and/or β'-polymorphic form. Both these forms of the lipid are amorphous and allow drug retention within the lipid matrix [73]. However, upon prolonged storage, especially in warmer temperature, the less ordered amorphous forms of the lipid tend to change to more ordered crystalline form. This change reduces the number of imperfections in the lipid matrix leading to subsequent expulsion of drug in a phased manner [67]. This eventually leads to loss of entrapped drug and decrease in potency of SLN [67].

To overcome the problems associated with classical SLN, researchers developed techniques to maintain imperfections in the lipid matrix, even after prolonged storage. They achieved this by partially replacing a part of pure solid lipid with liquid lipid(s). The

researchers proved that adding a small amount of liquid lipid/oil to the solid lipid matrix created less ordered crystal lattice structures and increased the number of imperfections where the amorphous drug clusters could be accommodated [67, 75, 76]. Moreover, the liquid lipids also helped in increasing the loading capacity of the lipid nanocarriers. Thus, this hybrid lipid system could not only support higher drug loading, it also reduced the drug expulsion from the lipid matrix upon storage. The concept of drug expulsion from SLN upon ageing [73] is schematically represented in Fig. 1.4.

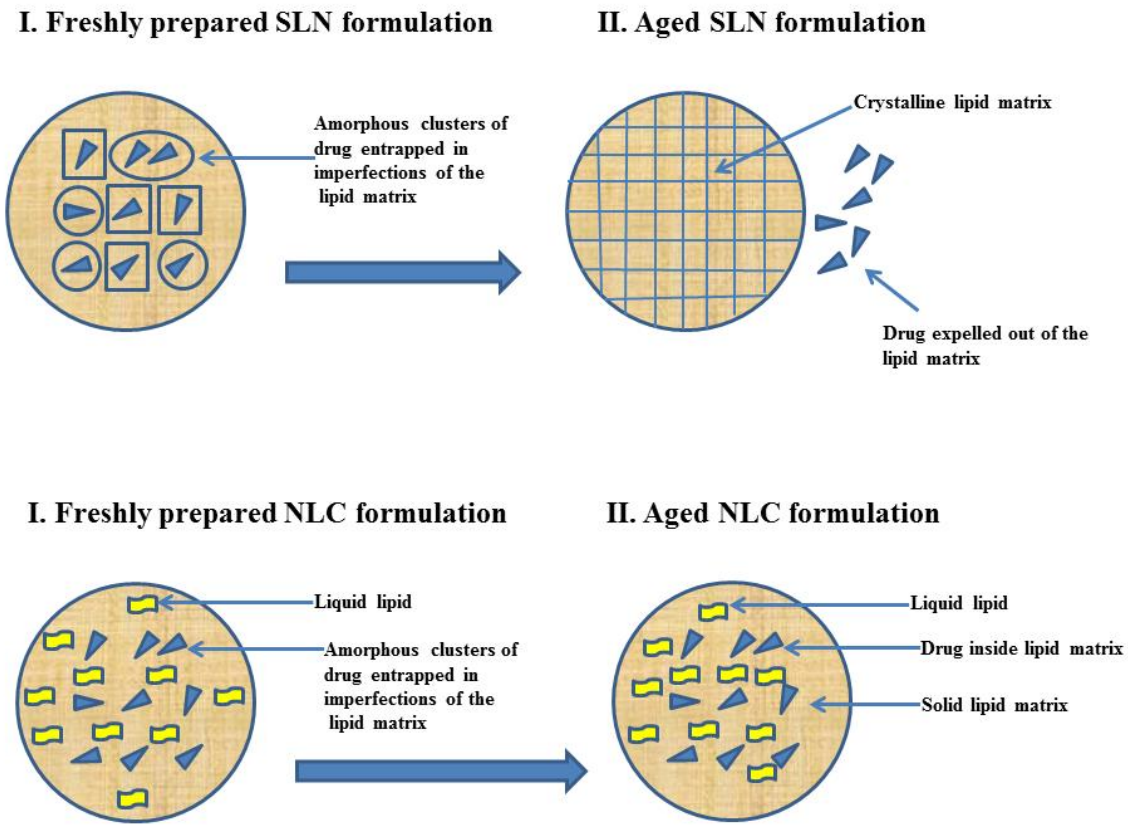

Fig. 1.4: Effect of ageing on drug expulsion in (a) SLN formulations and (b) NLC formulations

1.5.2.1 Drug incorporation into NLC

Three possible models have been postulated for understanding the drug incorporation into NLC [67].

I. Imperfect crystal type model

This type of model is applicable when two chemically dissimilar lipids are combined together [67, 73]. Following recrystallization, these lipids form a highly disordered crystal lattice structure with many imperfections that can accommodate higher amount of drug, leading to higher loading capacity in the NLC [67].

II. Amorphous type model

This type of model can be obtained when lipids like hydroxyoctacosanylhydroxy stearate and isopropyl myristate are used along with other solid lipids in the matrix, which, once molten, fail to re-crystallize back. Thus, they create a permanent amorphous polymorphic structure (α-polymorph modification) that tends to retain the drug incorporated into them [67].

III. Multiple emulsion type model

This model describes a situation in which tiny drug-containing oil droplets are dispersed uniformly into SLN that are in turn dispersed into water. So, effectively, it is an "oil-in-lipid-in-water" (O/L/W) system [67]. These types of NLC are based on the assumption that, in general, the drugs will have better solubility in oil than in solid lipids [67]. Therefore, theoretically, the drug loading into such NLC formulations should be much higher than conventional SLN or NLC formulations. Initially, during the process of manufacture, the hot oil and the lipid form a single homogenous micro-emulsion. However, upon cooling, the oil droplets tend to phase separate and mutually coalesce producing two

distinct phases that co-exist in the same system [67, 77]. Subsequent re-crystallization of lipid tends to "encapsulate" the drug containing oil droplets within the lipid matrix [67, 77].

1.5.3 Production methods of lipid nanoparticles

I. High pressure homogenization

The high pressure homogenization method can be further divided as (a) hot homogenization and (b) cold homogenization method.

a. Hot homogenization method:

It involves homogenization of lipids at an elevated temperature (above the melting range of the lipid). In this method, the drug to be incorporated is dissolved in the molten lipid which is then dispersed into a hot aqueous surfactant solution using a high-speed stirrer (e.g. Ultra Turrax). This results in formation of a coarse pre-emulsion. This coarse pre-emulsion is then homogenized using a high pressure homogenizer (e.g. APV Gaulin LAB 40) at a pressure ranging from 100 to 1500 bar [66]. For a typical formulation, one to three homogenization cycles are used. The homogenized nanoemulsion is then cooled to room temperature that causes lipids to crystallize and finally results in the formation of SLN. This method is useful to encapsulate lipophilic and water-insoluble drugs. However, it is not well-suited for loading hydrophilic drugs. For highly hydrophilic drugs, temperatures 5 to 10 ºC below the melting point of lipid are preferred [66]. At this temperature, the lipid is softened but is not in a liquid state. Hence, it can prevent the drug from completely leaching out into the aqueous media, ensuring decent drug encapsulation in the SLN [64].

b. Cold homogenization technique:

This technique is well-suited for encapsulation of hydrophilic drugs. In this method, the drug is first solubilized in molten lipid matrix. If the drug's solubility in the lipid matrix is low, hydrophobic surfactants are added to the molten lipid to increase drug's solubility. Then,

the drug-lipid-surfactant matrix is cooled in dry ice or liquid nitrogen that makes the lipid brittle and eases the subsequent milling process. After milling, the obtained microparticles (5 to 100 µm) are dispersed in a cold aqueous surfactant solution. This lipid suspension is then homogenized at room temperature or at 0 ºC [72]. The solid state of the matrix prevents partitioning of the drug into the aqueous phase. Thermosensitive drugs can be incorporated into SLN using this method as the drug is exposed to high temperatures for very short periods of time [77]. In both hot and cold homogenization techniques, the particle size is usually below 500 nm. However, in general, larger particle size and broader size distribution are observed in SLN produced by cold homogenization compared to hot homogenization [77, 78].

II. Preparation via o/w micro-emulsion:

In this method, lipid nanoparticles are produced by precipitation of the fine lipid droplets obtained by breaking the micro-emulsion [79]. This method was first developed and introduced by Gasco [80]. In this method, the formation of SLN occurs by dispersing warm o/w micro-emulsion into a cold aqueous medium under mechanical stirring. To form the primary micro-emulsion, the lipid is held in a molten condition and an aqueous surfactant/co-surfactant solution, isothermal with the molten lipid phase is added to it under continuous mechanical stirring or sonication. The warm micro-emulsion is then dispersed into cold water (below 5 ºC) under mechanical stirring. This quenches the micro-emulsion into SLN while maintaining the small particle size. Typically, the volume ratios of hot micro-emulsion to that of cold water is 1:25 to 1:50 [79, 80]. This method is more suited for fatty acids and lipids (e.g. stearic acid, glyceryl monostearate and glyceryl behenate) with low melting point (50 to 70 ºC) [81]. The major disadvantage of this method is the removal of excess water and surfactant/co-surfactant from the final formulation.

III. Preparation by solvent emulsification-evaporation/diffusion:

In this method, the lipid is dissolved in an organic solvent and is then emulsified with an aqueous phase containing surfactant/co-surfactant mixture. Stirring ensures formation of an o/w type emulsion while an ambient temperature is maintained. The solvent is removed under reduced pressure to precipitate the lipids and yield nanoparticles [81]. Depending on the lipid type and surfactant, the particle size of nanoparticles formed by this method varies from 30 to 100 nm [82]. The most important advantage of this method is the avoidance of high temperatures to melt the lipids.

As an alternate, lipid nanoparticles can also be produced by injection-moulding method. In this method, the lipid is dissolved in a water-miscible organic solvent and heated to its melting point. Then, it is rapidly injected into an aqueous surfactant solution that is under continuous stirring. The resulting dispersion is filtered to remove larger lipid aggregates. In general, preparation by either of the above mentioned methods involves the use of organic solvents that may have unacceptable toxicity profile. Moreover, in both these methods, the final SLN formulation is diluted (15% w/v) when compared to high-pressure homogenization method (80% w/v) [83]. This dilution can have implications on dosing volume, dose accuracy, patient compliance and formulation stability.

IV. Double emulsion method (Water-in-oil-in-water or w/o/w method):

In this method, an aqueous drug solution with surfactants is emulsified with lipid melt using a high-speed homogenizer (e.g. Ultra Turrax) at an elevated temperature. This warm nanoemulsion is then dispersed into water containing stabilizers and allowed to cool to 2-3 ºC to complete the w/o/w emulsion [84, 85].

V. High shear homogenization and/or ultrasonication:

This method involves the production of lipid nanoparticles without using solvents. The drug-lipid matrix is directly emulsified with hot surfactant solution using high shear forces [86]. Again in this case, the formulation's re-dispersibility is poor and particle size can vary considerably.

1.5.4 Characterization of nanoparticles:

Overview

As with conventional formulations, for the reasons of repeatability and quality, it is important to characterize nanoparticles by analytical tools. However, the small size of nanoparticles and their sensitivity to the immediate environment complicates the analytical process. In general, most of the analytical tools used to evaluate nanoparticles require manipulation of the test sample in some way. Thus, there is a risk of de-stabilizing the nanoparticle system or changing the physical characteristics of the nanoparticles like kinetic behaviour, crystallization pattern or lipid's polymorphic state during the course of analysis [66]. Therefore, it is prudent to understand the consequences of sample manipulation before choosing an analytical tool to characterize the nanoparticle formulations.

Both in-process and final quality control tests are essential to assure the quality of the final formulation. Depending on the type of the formulation and need, a wide variety of analytical tools are employed to characterize nanoparticles. However, most widely employed analytical tools are: measurement of particle size, polydispersity index, entrapment efficiency of the active, loading capacity of nanoparticles, assay, in-vitro drug release behaviour and stability in various pH conditions, surface morphology, polymorphism and crystallinity

(especially for lipid nanoparticles), stability studies (accelerated and long-term stability studies), degradation kinetics and identification/quantification of degradation products [66].

1.5.4.1 Particle size and polydispersity index (PDI)

By definition, nanoparticles are particles of colloidal size. Many nanoparticles show a time-dependent aggregation leading to generation of particle aggregates that have an overall particle size of 1 μm or greater. Therefore, it is essential to monitor the particle size and particle size distribution (PSD) of nanoparticles [87]. This can be accomplished by using photon correlation spectroscopy (PCS)/dynamic light scattering (DLS) technique [87]. In this technique, the random motion of sub-micron particles (caused due to collisions between particles and the molecules of the media – the Brownian motion) is measured as a function of time. It is based on the basic principle that, in a given medium, smaller particles move with greater velocities than larger particles. When a laser beam illuminates the path of a dilute, colloidal, sub-micron suspension, it gets diffracted which is detected by a detector. In addition to this, the Brownian motion of the particles also allows the scattered light to fluctuate; the intensity of fluctuation is measured by a photomultiplier placed at a given scattering angle [66, 87]. The intensity of fluctuation is then transmitted to an autocorrelation function, G(τ), that decays exponentially. The microprocessor in the PCS calculates the diffusion coefficient (D) of the particles in the given dispersion media (at given temperature and viscosity) [88]. The value of D is then related to particle size by Stokes-Einstein equation.

Stokes-Einstein equation to determine particle size

$$D = \frac{kT}{3\pi\eta d}$$

Where,

$D =$ *Diffusion coefficient of the particles*
$k =$ *Boltzmann's constant* $(1.3806488 \times 10^{-23}\ m^2\ kg\ s^{-2}\ K^{-1})$
$T =$ *Absolute temperature* $(\mathrm{K} = {}^{\circ}\mathrm{C} + 273.15)$
$\eta =$ *Viscosity of the dispersion medium*
$d =$ *Diameter of a spherical particles*

The Stokes-Einstein equation relates diffusion coefficient to particle size assuming that the particles are spherical in nature. For non-spherical particles (e.g. rod-shaped particles), the mean particle size will be larger than spherical particles since these particles have lower diffusion coefficient values [88]. Hence, this measurement technique should be supported with other methods to measure surface morphology like scanning electron microscopy (SEM) or transmission electron microscopy (TEM).

The PCS/DLS technique is useful in determination of particle sizes ranging from 3 to 3000 nm [88]. However, when particle size exceeds 3000 nm, this method becomes less accurate in measuring the particle size. Therefore, for reasons of accuracy, it is recommended that PCS should be used in tandem with other complimentary analytical techniques like laser diffraction (LD) which can determine particle sizes above 3 µm [89, 90]. The particle size data is represented as volume distribution diameters of d50, d90, d95 and d99 percentages. The value of d99% indicates that 99% of the total particle population in the dispersion medium are below a given size or volume distribution [91].

Polydispersity index (PDI) is a measure of the width of PSD. The decay of autocorrelation function, G(τ) is mono-exponential when the colloidal dispersion has particles with uniform size (monodispersed particles). Similarly, when the particle size is polydisperse, the decay of G(τ) is poly-exponential [92]. Simply put, PDI measures the deviation from a mono-exponetial decay of G(τ), and typically ranges from 0 to 1 [92]. A value of PDI

between 0.03-0.06 refers to a monodisperse system. However, in practice, such small values of PDI are difficult to obtain. Hence, a colloidal system is considered to have a narrow size distribution if the values of PDI lie in the range of 0.1 to 0.2. PDI values of 0.2 to 0.5 are indicative of a polydisperse colloidal system [92].

1.5.4.2 Electrophoretic mobility and Zeta potential of nanoparticles

During long term storage of nanoparticle dispersion, the value of zeta potential becomes an important parameter to provide stability and to prevent aggregation of the particles [87, 91]. Zeta potential is defined as the electrical potential prevalent at the hydrodynamic shear plane. The hydrodynamic shear plane is an imaginary surface on the particle that separates a thin-layer of liquid constituting counter-ions and is bound to a moving charged surface [91]. The magnitude of zeta potential depends on the chemical groups present in the particle, the pH on the medium in which the particles are suspended and the charge and number of ions present in the medium itself. Fig.1.5 gives a schematic representation of the surface charge (zeta potential) of the particles.

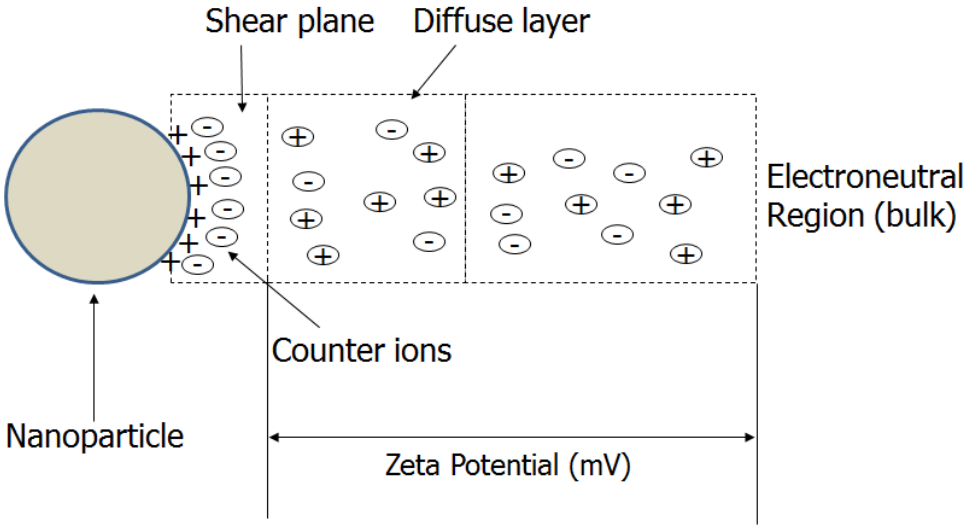

Fig. 1.5: Schematic representation of surface charge present on the particles

For an aqueous colloidal dispersion, the zeta potential is measured by determining the electrophoretic mobility of the particle using Laser Doppler Anemometry (LDA) and then applying the Helmholtz-Smoluchowsky equation to get the value [93].

Helmholtz-Smoluchowsky equation to calculate zeta potential

$$\vartheta = \frac{\varepsilon\xi}{\eta}$$

Where,

$\vartheta = Electrophoretic\ mobility$
$\varepsilon = Dielectric\ constant\ (permittivity\ of\ the\ environment)$
$\xi = Zeta\ potential$
$\eta = Viscosity\ of\ the\ dispersion\ medium$

The value of zeta potential is usually considered important to the stability of a colloidal dispersion. It indicates the possible effects of storage on aggregation and hence, the stability of the colloidal dispersion. Zeta potential with values of less than -30 mV or more than +30 mV are considered suitable for the stability of colloidal dispersions [87, 91]. This is true only in case of colloidal dispersions purely stabilized by electrostatic forces. However, in practice, a combination of electrostatic stabilizers and stearic stabilizers are used in the preparation. If a stearic stabilizer is used, the zeta potential values are usually lower because the shear plane gets shifted due to the surface presence of the stearic stabilizer molecules [66].

1.5.4.3 Microscopic techniques for characterization of size, shape and morphology

i. Scanning electron microscopy

Scanning electron microscopy (SEM) has been used to determine the size, shape and surface morphology of nanoparticles. In this technique, a small drop of nanoparticle dispersion is placed on a metal stub/graphite strip and allowed to dry. Drying may be done at room temperature (by leaving it overnight) or accelerated using a vacuum oven at low temperature (25-30 ºC). It is critical to maintain low temperature because the integrity of nanoparticles is disturbed at higher temperatures either due to melting (SLN and NLC) or deformation (polymeric nanoparticles). Following drying, the sample is made conductive to electrons by coating with metals like gold, palladium or platinum [94]. Then, a high-energy electron beam is targeted at the sample and a three dimensional image of the sample is obtained on the screen. The sample is observed at various zoom levels and finally, the image is captured using the software attached to the SEM instrument. One of the limitations of this method is that, the process of drying, analysis under vacuum and use of accelerated voltage can cause the sample to shrink and can also alter the surface morphology [94].

ii. Transmission electron microscopy

Akin to SEM, transmission electron microscopy **(**TEM) is used as a tool to get information about the particle size, shape and surface morphology in colloidal dispersions [95]. However, in contrast to SEM, the TEM generates two dimensional images of the sample. The image resolution in TEM is generally higher than that of SEM and it can give valuable information about the PDI of the colloidal dispersion [95]. The sample preparation in TEM analysis is slightly different than that of SEM. Here, the sample is either stained of freeze-fractured before analysis. The sample preparation method depends on the need of the user. For size, shape and morphology analysis, a simple staining technique with a dye like phosphotungstic acid is adequate [95]. The sample to be analysed is initially deposited onto a

copper grid coated with a carbon film. Then, the sample is allowed to dry for a period of 30 seconds. Following drying, it is stained with a dye like phosphotungstic acid and again dried under controlled conditions for 30 seconds. After drying, the sample is visualized and data captured using TEM instrument.

1.5.4.4 Crystallographic and polymorph analysis

For lipid-based nanoparticles, it is important to conduct thorough crystallographic analysis as crystallinity and polymorphism are closely related [96]. Moreover, drug incorporation and drug release kinetics depends on the polymorphic nature of the nanoparticles. Two techniques, namely, differential scanning calorimetry (DSC) and wide angle X-ray scattering (WAXS) have been extensively used for this purpose [96]. These tools are used to characterize the crystalline structure, modifications occurring in the bulk lipid (after processing or incorporating API), modifications occurring to the API (after it is dispersed in the lipid matrix) and to determine the physical states of both lipids and API in the formulation. DSC and WAXS have also been used to confirm the absence of super-cooled melts during formulation and optimization processes [96, 97].

i. Differential Scanning Calorimetry (DSC)

DSC works on the principle that different modifications/polymorphs of the same material possess different physical properties like melting point. DSC is frequently used to elucidate the changes in the degree of crystallinity of bulk lipid, bulk API and the formulation [98]. It is also an important quality control tool to establish the stability of the formulation in different storage conditions over a period of time. The information obtained from a DSC thermogram is illustrated in Fig. 1.6.

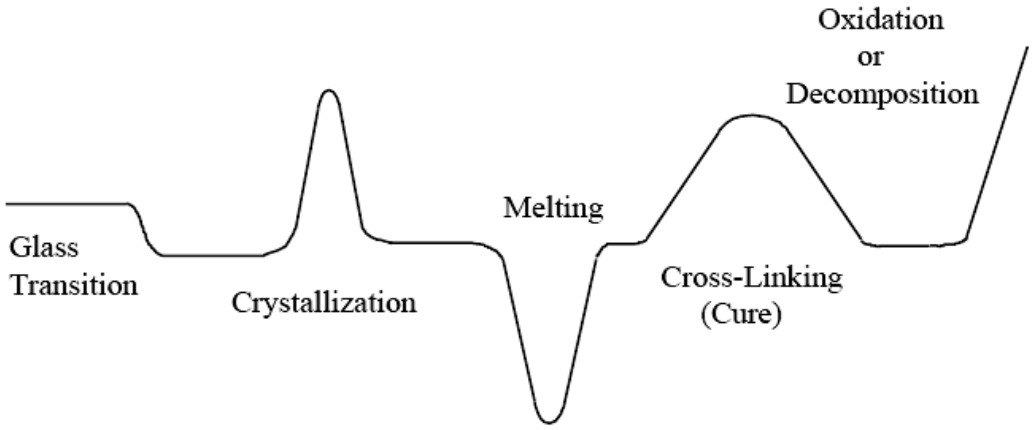

Fig. 1.6: Various phase transitions in a typical DSC thermogram

DSC instrument measures the differences in heat flow to a test substance and a reference substance as a function of sample temperature when both the samples are subjected to a controlled temperature program. In other words, the DSC measures how physical properties of a material change alongwith temperature, against time [99]. During the course of change in temperature, the DSC captures the quantity of heat that is radiated or excessively absorbed by the sample on the basis of temperature difference between the sample and the reference material [99].

In the literature, based on the mechanism of working, DSC instruments are classified into two types: (1) the heat flux DSC and (1) the power compensated DSC [99]. In the heat flux DSC, sample to be analysed is crimped into a metal pan (e.g. aluminium pan) and covered with a lid of the same material. The DSC sample holder in a heat flux DSC consists of two slots for two such pans and is heated by a single furnace. While the sample holding pan is placed on one of the slots, the other slot is reserved for an empty crimped pan (reference pan) of the same material. Once both the pans are positioned, the heating furnace

is switched on and a linear heating rate (5 to 10 ºC per minute) is maintained. The heating furnace effectively transfers heat to these pans through a thermoelectric disk [98]. Due to the inherent heat capacity (Cp) of the sample in one of the pans, there will be a temperature difference between both the pans. This difference in heat between sample and reference pans is measured by a thermocouple and consequent heat flow is determined using a formula that is a thermal counterpart of the famous Ohm's law. The formula is given in the equation below.

Formula used in DSC to determine heat flow in a sample

$$q = \frac{\Delta T}{R}$$

Where,

q = sample heat flow
ΔT = temperature difference between sample and reference pans
R = resistance of thermoelectric disk

In the power compensated DSC, two separate furnaces, heated by separate heaters are used for the pans. The sample and reference pans are maintained at the same temperature and the difference in the thermal power required to maintain isothermal conditions between both the pans is measured and plotted as a function of temperature and time. From the molar melting enthalpy (ΔH) obtained via DSC thermograms of SLN and NLC, a parameter called re-crystallization index (RI) can be obtained [100]. The RI is a measure of percentage of lipid matrix that has recrystallized during storage period of the nanopartic1es [100, 101]. The RI for an aqueous SLN or NLC formulation can be calculated using the equation given below.

Formula to calculate re-crystallization index using enthalpy data

$$RI\ (\%) = \frac{\Delta H_{aqueous\ SLN\ or\ NLC}}{\Delta H_{bulk\ lipid}\ X\ lipid\ conc.}\ X\ 100$$

ii. Wide angle X-ray diffraction (WAXS)

This method is widely used to understand the lamellar arrangement of lipid molecules, polymorphism and degree of crystallinity of fatty acid chains in triglycerides (TG) [101, 102]. The principle of WAXS in lipid crystallinity measurement is based on the fact that the WAXS measures the length of long/short spacing between alkyl side chains within the TG lipid layer. These appear as reflections in the WAXS spectrum. We can differentiate between crystalline and amorphous forms of the lipid by observing the WAXS spectral data. While the crystalline forms demonstrate many reflection bands (sharp peaks) on a WAXS spectrum, the amorphous forms show minimum reflection bands, sometimes yielding straight lines [102]. In conjugation with DSC, WAXS provides valuable information to elucidate the crystallinity and polymorphic nature of lipids in SLN and NLC. In many cases, the nature of API (bulk and entrapped API) can be ascertained with the use of these techniques.

1.5.4.5 Drug loading and encapsulation efficiency determination

Both drug loading and encapsulation efficiency are important parameters in all nanoparticle formulations because they affect the choice of the matrix forming material and drug release characteristics from the material [103]. The loading capacity of a formulation is expressed as the amount of drug loaded (or encapsulated) in the nanoparticles to the total amount of matrix forming material used [63]. The loading capacity depends on factors like relative solubility of drug and matrix forming material in a given solvent (for polymeric nanoparticles), solubility of the drug in the matrix forming material (for SLN and NLC) and

polymorphic nature of the matrix forming material and method used for the manufacture of nanoparticles [65]. The loading capacity is given by the following formula:

$$LC = \frac{(Total\ amount\ of\ drug) - (Amount\ of\ free\ drug)}{Total\ amount\ of\ lipid\ phase}$$

The entrapment efficiency is another important parameter that takes into account the total amount of drug (in percentage) incorporated into the nanoparticle dosage form. It is a measure of how efficient the method of manufacture was in encapsulating the drug into the nanoparticle formulation [67, 104]. During the manufacture of nanoparticles, high entrapment efficiencies are desired (>80%) because, when the entrapment efficiency is low, a significant amount of drug gets wasted during the "washing" process. Washing of the formulation in either buffer or water is practiced to separate free drug from the nanoparticle formulation. The entrapment efficiency (EE) is calculated using the following formula:

$$EE(\%) = \frac{(Total\ amount\ of\ drug) - (Amount\ of\ free\ drug)}{Total\ amount\ of\ drug} X\ 100$$

1.6 Fate of nanocarriers after oral delivery

Intestinal mucosa acts as a major barrier for entry of any particulate system, more so for the nanoparticles [105]. If the nanoparticles manage to cross the mucosal barrier, the cargo-carrying nanoparticles are encountered with yet another challenge – transport across the intestinal epithelium. The transport across intestinal epithelium can take place through paracellular pathways, transcytosis and receptor-mediated transcytosis by enterocytes and M-cells [105]. The pharmacokinetics and in-vivo behaviour of the "cargo" depends on whether it is transported in an encapsulated form or in a free form [105].

Post per-oral administration, the nanocarriers are encountered with a variety of hostile conditions in the GI tract. From the extremes in the pH (pH 1-3 in stomach and pH 6-8 in

small intestine) to various enzyme systems, many factors affect the stability and the in-vivo fate of the nanoparticles. The composition of nanoparticles has a significant role in its stability in the GI tract; nanoparticles comprising insoluble polymers or high-carbon chain length lipids are neither degraded immediately nor do they release their cargo rapidly [106].

1.6.1 The mucus barrier

After extreme pH and hostile enzymes, the next major barrier that orally delivered nanoparticles encounter is the mucus layer on the GI tract. The luminal surface of the GI tract is entirely protected by a highly viscoelastic mucus layer [107]. This layer acts as a 'net' to trap many sub-micron particles and organisms [108]. The nanoparticles that get bound to the mucosa are effectively cleared from the body during the frequent mucus turnover cycles [108]. It is now known that viruses pass through this mucus net and travel "upstream" towards the epithelial layer [109]. Once they reach the epithelium, they get entry into the body through various mechanisms that will be discussed later. To be effective, oral nanoparticles should essentially mimic the strategy of viruses. Therefore, akin to viruses, orally delivered nanoparticles should ideally have sizes below 200 nm [109]. However, there are also several reports in the literature where nanoparticles larger than 200 nm have been taken up into the body after oral administration [107].

For over a decade now, many research groups have been working on design of mucoadhesive nanoparticles using polymers like chitosan and its derivatives [110]. The mucoadhesion is brought about by forces like hydrogen bonding, van der Walls interactions, polymer chain interpenetration and electrostatic/ionic interactions [110]. Moreover, the surface charge on the nanoparticles plays an important role in determining its fate. Indeed, smaller particles carrying strong positive charge readily bind to the mucosa (that carries an

overall negative charge due to the glycocalix). Compared to other nanoparticle formulations, these nanoparticles exhibit longer residence time in the GI tract [110].

Among other strategies, coating/bonding the nanoparticle surface with polyethylene glycol (PEG) ensures rapid transport across the mucosal barrier [111]. Dense coating with PEG minimizes the nanoparticle-mucus interactions and thus helps their rapid transit towards epithelial layer. Further, researchers like Carter and Carrier [109] have previously shown that positively charged particles are caught-up in the mucus net while, the negatively charged particles move 20-30 times faster towards the epithelium [109].

In conclusion, for an effective oral delivery, a fine balance between mucoadhesion and mucus-penetration should be maintained [111]. Because positively charged particles immobilized by mucus are rapidly cleared from the body, negatively charged mucus-penetrating nanoparticles of sizes below 200 nm are most suitable for oral drug delivery. In summary, the nanoparticles must be tiny enough to pass through the mucus net to avoid significant steric inhibition by the fibre mesh and should avoid adhesion to mucin fibres [111].

1.6.2 Endocytic uptake mechanisms for nanoparticles from GI Tract

To develop effective nanocarriers for oral delivery, it is imperative to understand the underlying uptake mechanisms for nanocarriers from GI tract. Though several in-vitro methods are available to elucidate the uptake mechanism of nanoparticles (e.g. everted gut-sac model, intestinal closed loop model and Ussing chambers), by far, studies using Caco-2 monolayer cells are most reliable. More recently, co-culture of Caco-2 cells with HT29 cells (to produce mucus) [112] and Raji cells (to mimic follicle-associated epithelium (FAE)) [113] have been developed. A combination of quantitative measurement techniques along

with confocal microscopy (to visualize the localization of nanoparticles) have been reportedly used by many research groups to gain insights into GI uptake of nanoparticles [114].

The uptake of nanoparticles in GI tract can involve both paracellular and transcellular routes. However, paracellular's contribution to uptake is negligible as it utilizes only 1% of the total available mucosal surface [115]. Further, the tight junctions between the epithelial cells restrict the entry of particles over through the paracellular route. The tight junctions are the closely associated areas between two epithelial cells that form an almost impermeable barrier. They are composed of a group of transmembrane and cytosolic proteins, including occludins, claudins, actins and zona occludens [116]. Moreover, there are other special densely packed proteins in this region called the 'tight junction associated proteins' [116]. They are designated as ZO-1, ZO-2 and ZO-3; these proteins not only interact with each other, but also serve as links between occludin and actin filaments. Between all this meshwork of proteins, the paracellular space is defined. This space ranges from 3 to 10 Å [116]. However, in some literature, the paracellular space is simply put as <1 nm [117, 118].

Chitosan, a high molecular weight polysaccharide acts as an oral permeation enhancer [117]. It mainly enhances the paracellular transport of drugs. Its permeation enhancing properties have been attributed to its mucus-binding properties (due to its positive charge in acidic environment and interpenetration of polymeric chains with mucus) and its effect on gating properties of the tight junction mediated through cellular signalling mechanism [117]. Fig. 1.7 below illustrates the mechanism of chitosan as an oral permeation enhancer [117].

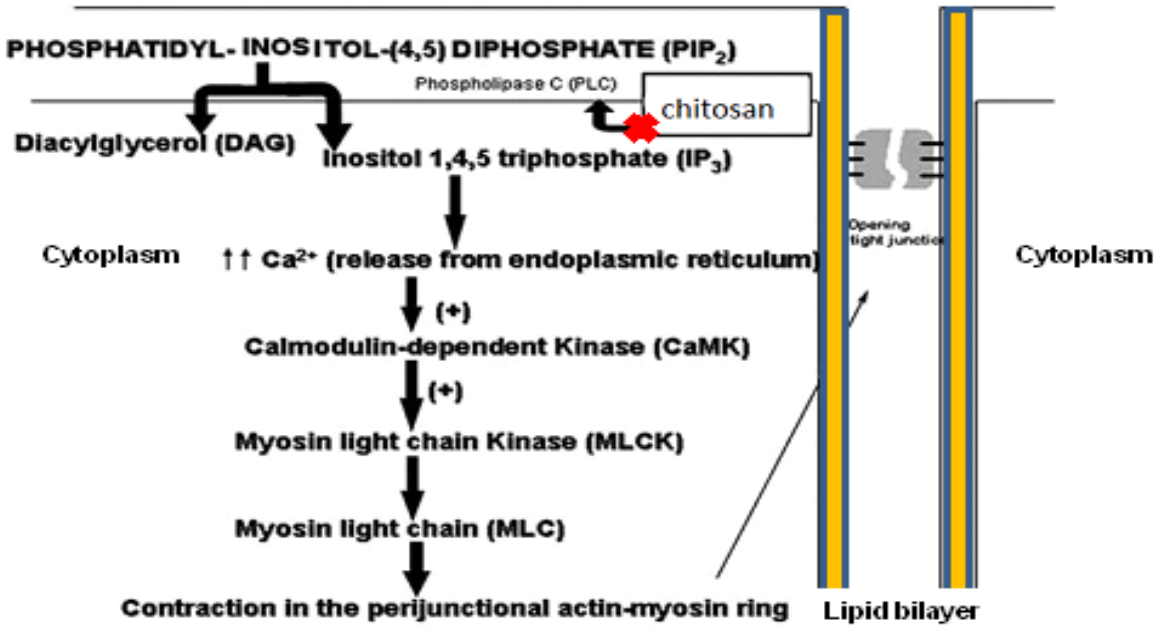

Fig. 1.7: Cellular mechanism of chitosan as an oral permeation enhancer. Figure adapted with modifications from: Dodane, V., M. Amin Khan, and J.R. Merwin, *Effect of chitosan on epithelial permeability and structure*. Int J Pharm, 1999. **182**(1): p. 21-32.

1.6.3 Transcellular transport of nanoparticles

This is a major transport mechanism for uptake of orally administered nanoparticles [115]. The steps involved on transcellular transport of nanoparticles can be subdivided as: (a) Uptake process at the apical side of the cell (b) Transport through the cell and (c) Release at the basolateral side of the cell.

The intestinal epithelium is made up of different types of cells – Enterocytes (absorptive cells), Goblet cells (mucus secreting cells), enteroendocrine cells (that secrete hormones such as cholecystokinin and gastrin into the blood), the paneth cells (that secrete a number of antimicrobial molecules into the lumen) and the M-cells (manifold cells).

i. The M-cells

The M-cells are specialized cells that make up the mucosa-associated lymphoid tissues (O-MALT) and consist of lymphoid follicles that are arranged to form distinct structures like Payer's patches [119]. The M-cells are characterized by their ability to transport the antigens from the luminal side of the small intestine to the cells of the immune system [119]. Targeting M-cells could be a good option for orally delivered nanoparticles and vaccines. However, uptake is limited since M-cells constitute less than 1% of the intestinal epithelial cell population [120]. The access of nanocarriers to systemic circulation is limited after M-cells transport as nanoparticles often get trapped in local lymph nodes. Moreover, lymph flow is limited in comparison to blood flow (1:500), and is highly variable depending on the physiological conditions [121, 122]. Consequently, for drugs that need to reach the blood circulation, it is more prudent to target them to absorptive epithelial cells (or the enterocytes).

ii. The Enterocytes

The transcellular transport across enterocytes is an energy-dependent process. Uptake of nanoparticles through enterocytes can be described by several energy dependent pinocytic processes [123]. They include macropinocytosis, clathrin-mediated endocytosis, caveolae-mediated endocytosis and clathrin- and caveolae-independent endocytosis [124]. Following diagram (Fig. 1.8) illustrates different endocytic pathways for nanoparticle uptake through enterocytes.

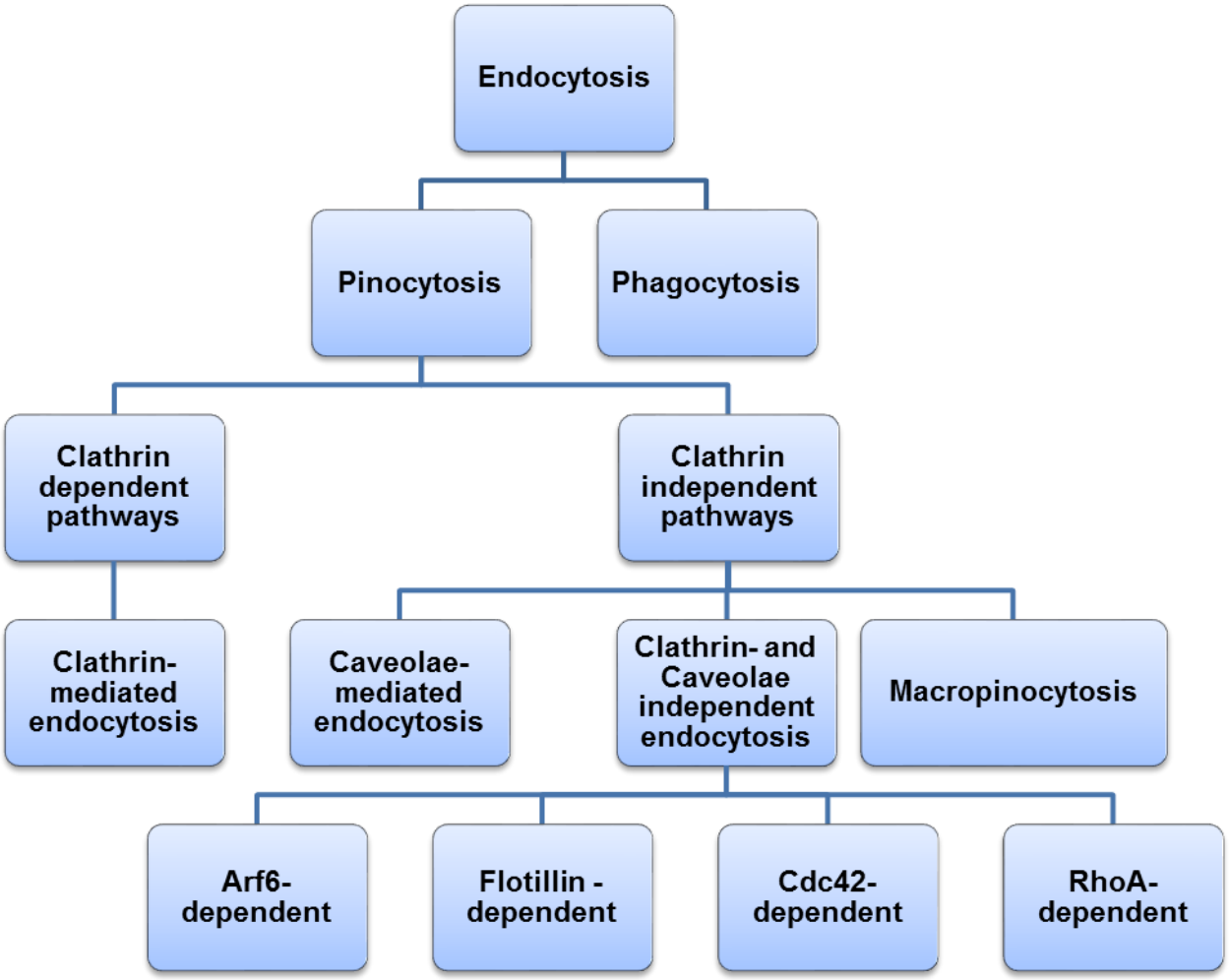

Fig. 1.8: Classification of endocytic pathways depending on the protein involved in the entry of particles into the cells [125]**.** Figure source: Sahay, G., D.Y. Alakhova, and A.V. Kabanov, *Endocytosis of nanomedicines*. J Control Release, 2010. **145**(3): p. 182-95.

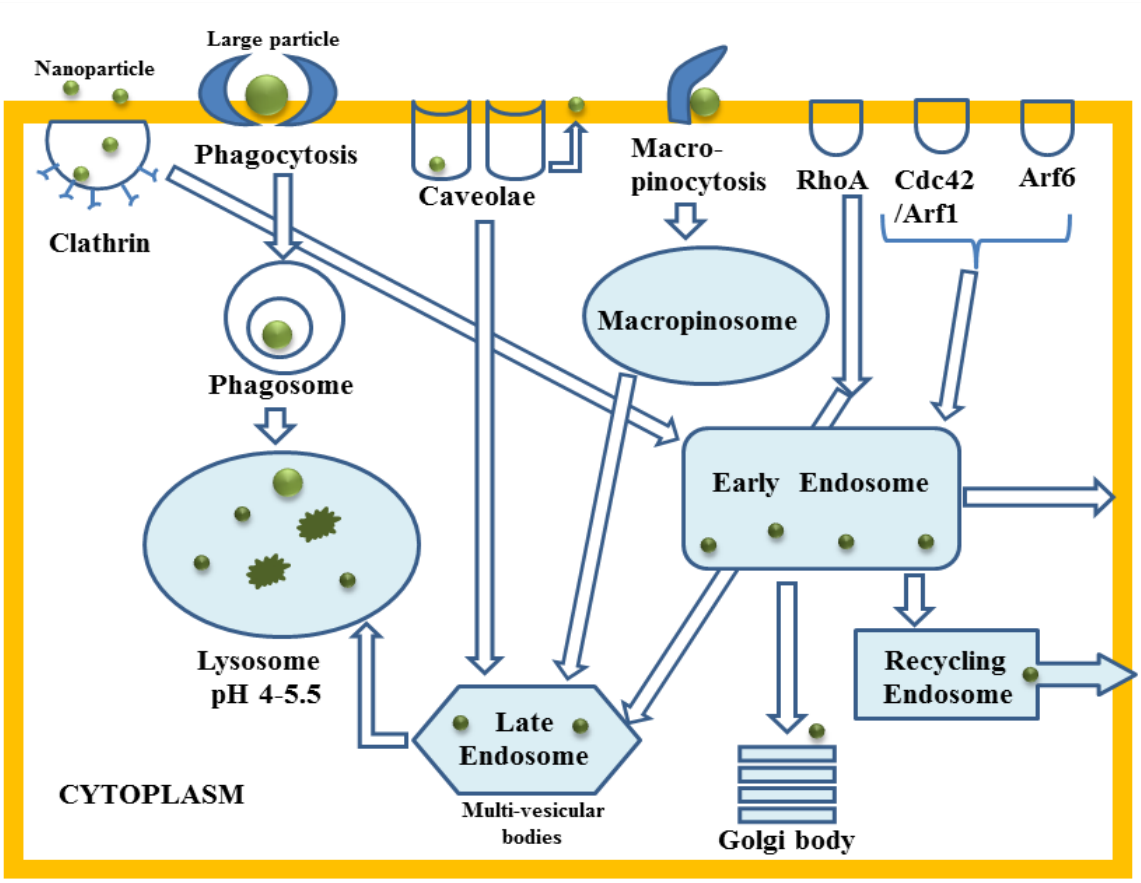

Fig. 1.9: An overview of different endocytic uptake pathways and the fate of cargo after uptake [126]

iii. Macropinocytosis:

The macropinocytosis is an actin-dependent, clathrin-, caveolae- and dynamin-independent non-specific transport mechanism driven by Rho-family GTPases [127]. It is not mediated by any receptors and hence non-specific. The macropinocytosis is initiated by transient activation of receptor tyrosine kinases by growth factors [127]. This mediates a signalling cascade that leads to changes in the actin cytoskeleton and triggers formation of 'membrane ruffles'. These membrane ruffles protrude to engulf the surrounding fluid and nutrients in the extracellular milieu [128].

Here, a large (0.5 to 2 µm) heterogeneous, dynamic, vesicular structures at the cell surface called, macropinosome is formed; particles smaller than 2 µm can be internalized into enterocytes by this mechanism [128]. The intracellular fate of the particle depends on the cell type. In most cases, it will be acidified and shrinks or it fuses with the lysosomal compartment of the cell [127]. Macropinocytosis is differentiated from other types of endocytosis by its unique susceptibility to inhibitors of Na+/H+ exchange [129]. Amiloride, a potassium-sparing diuretic inhibits macropinocytosis by lowering sub-membranous pH and preventing Rac1 and Cdc42 signalling [129].

iv. Clathrin-mediated endocytosis (CME):

The CME is a "classical route" of entry for particles into the cell that is present in all mammalian cells [125]. It is a common route for uptake of physiologically important molecules like cholesterol (carried into cells by low density lipoproteins (LDL)) via the LDL receptor, or iron carried by transferrin (Tf) via the Tf receptor [125]. Another important physiological function of CME is the down-regulation of cell signalling by internalization and degradation of receptors and maintenance of cellular homeostasis [125].

Clathrin is a three-legged structure (called triskelion) formed by three heavy chains. Each of the heavy chains is associated with lighter clathrin chains [130]. The CME can occur as specific ligand-receptor interaction or via non-specific endocytosis [130]. The specific CME involves concentration of high-affinity transmembrane receptors and their bound ligands into "coated pits" on the plasma membrane [130]. The assembly of clathrin molecules on the coated pit induces an invagination of the membrane and forms a clathrin-coated vesicle (100 to 120 nm) that requires GTPase activity of dynamin and actin polymerization to form. This endocytosis pathway is initiated when the endocyted material interacts with the assembly polypeptide (AP)-2 and phosphoinositol biphosphate. The cargo containing

invagination is pinched-off from the cell membrane to form vesicles that are further degraded by acidified early and late endosomes [123, 131]. Hypertonic sucrose solution, K+ depletion, chlorpromazine and actin polymerization inhibitors (CytoD, LatA) can all act as inhibitors for CME [125]. Fig. 1.10 below illustrates the CME process in cells.

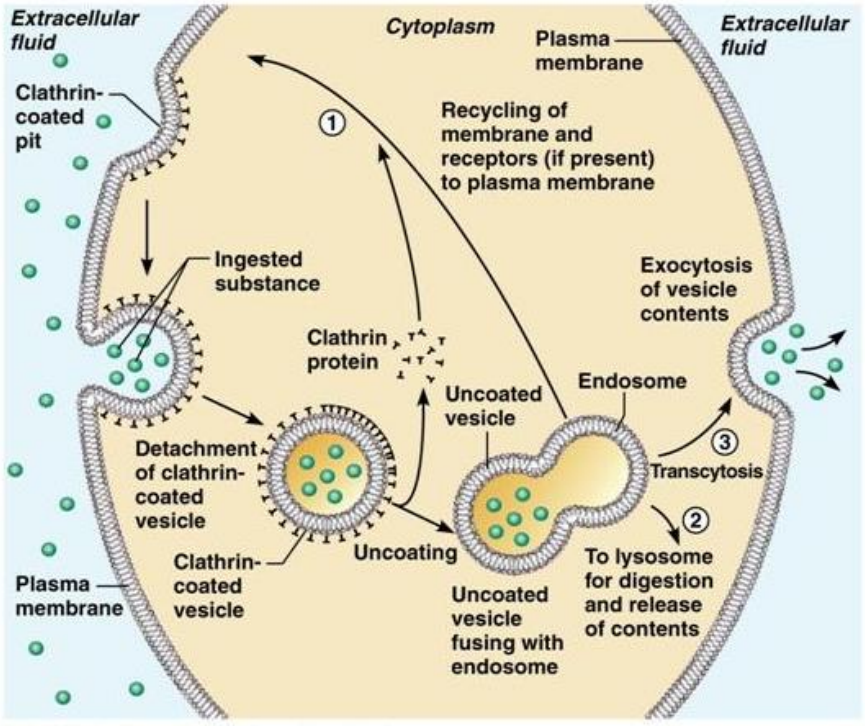

Fig. 1.10: Clathrin-mediated endocytic uptake process in cells. Figure Copyright © 2006 Pearson Education, Inc., publishing as Benjamin Cummings

v. Caveolae-mediated endocytosis

This pathway was first observed 50 years ago, and is associated with cholesterol and sphingolipid-rich microdomains of the cell membrane [123]. Caveolae are special type of "lipid rafts" rich in cholesterol and sphingolipids. They are flask-shaped invaginations on the plasma membrane that can engulf cargo molecules or carriers binding to their surface [123]. These invaginations are static structures with a size of 50 to 100 nm at the plasma membrane [123, 131, 132]. The term 'lipid raft' refers to the tiny membrane microdomains, which are defined as "small heterogeneous membrane domains" enriched in cholesterol, glycol-

sphingolipid, sphingo-myelin, phospholipids, glycol-phosphatidyl-inositol-linked proteins and some membrane-spanning proteins [125, 132]. In contrast to CME, this pathway is a highly regulated process involving complex signalling pathways. The fission of caveolae from membrane, mediated by GTPase dynamin generates cytosolic caveolar vesicles (caveosomes) which do not contain any enzymes [133]. Therefore, this pathway is employed by many pathogens to escape degradation by lysosomal enzymes [133].

Ligands known to be internalized by caveolae-mediated endocytosis include folic acid, albumin and cholesterol [131]. Caveolae is one type of cholesterol-rich microdomain, but other "rafts" also exist. They are small structures, approximately 40 to 50 nm in diameter, that diffuse freely on the cell surface. These microdomains allow endocytosis independent of clathrin- and caveolin-coated pits. These small rafts can be captured by and internalized within any endocytic vesicle [115, 131].

Caveolae-mediated endocytosis was originally discovered as the way by which SV40 viruses enter into the cells [134]. In the past, it was common understanding that materials taken into the cell by caveolae-mediated endocytosis would be transferred into specialized structures called 'caveosomes' that would help in transcytosis of the cargo without fusing into the destructive endosomes [134]. However, recent studies indicate that caveosome itself is an artefact in cells over-expressing different constructs of caveolin-1 and that the term caveosome no longer should be used [134, 135]. Therefore, literature describing uptake of nanoparticles into caveosomes by caveolae-mediated endocytosis of nanoparticles (into caveosomes) may need to be viewed in this new light [134]. It is now understood that the caveolae that pinch-off from the cell membrane fuse with the endosomes and the cargo is degraded in the acidic environment of the endosomes [136]. Fig. 1.11 and 1.12 below illustrate the components of caveola.

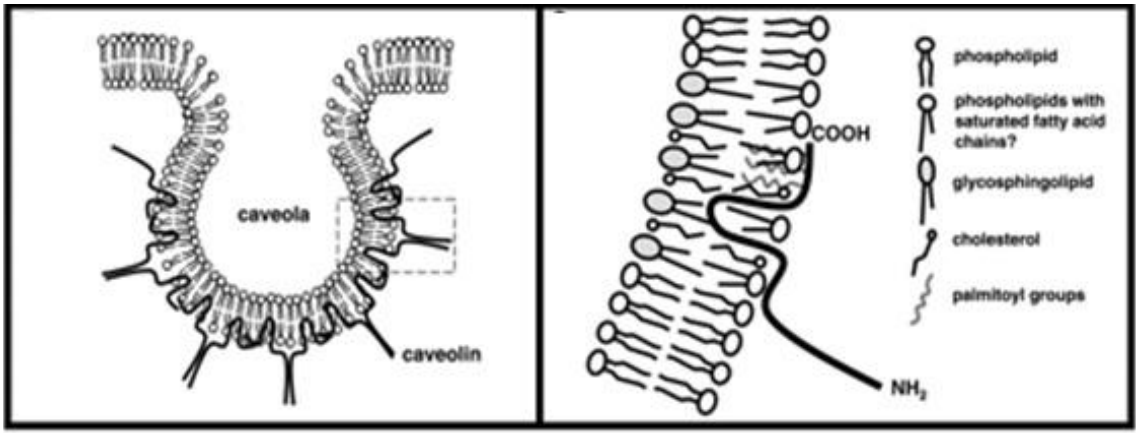

Fig. 1.11: Schematic for structure of Caveolae and its components. Figure Source: Tuma, P. and A.L. Hubbard, *Transcytosis: crossing cellular barriers.* Physiol Rev, 2003. **83**(3): p. 871-932.

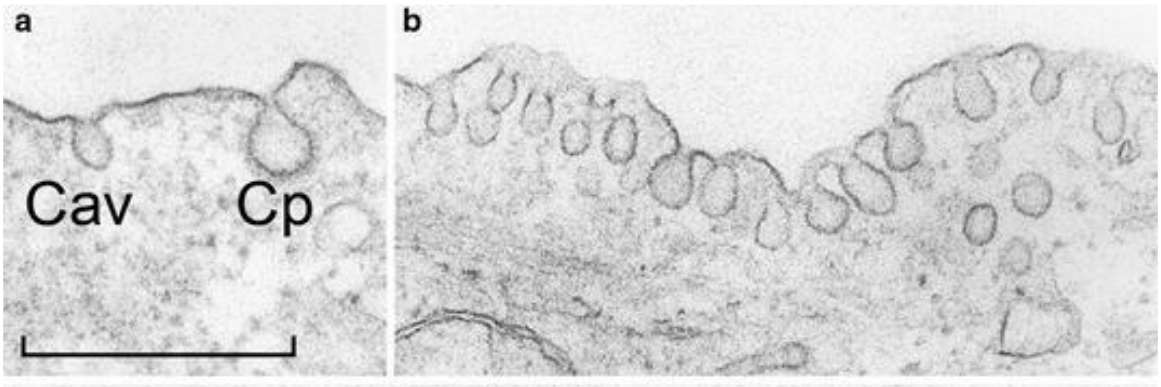

Fig. 1.12: Appearance of caveolae in myoepithelial cells. In **(a)** is seen a single caveola (*Cav*) and for comparison a clathrin-coated pit (*Cp*). **(b)** Shows a group of caveolae at the plasma membrane. Figure Source: Sandvig, K., et al., *Clathrin-independent endocytosis: from nonexisting to an extreme degree of complexity.* Histochem Cell Biol, 2008. **129**(3): p. 267-76.

vi. Clathrin- and caveolae-independent endocytosis

It is known that cellular entry can occur in cells devoid of both CME and caveolin-1 [125]. Based on the mechanism, the caveolae- and clathrin-independent pathways are presently classified as: Arf6-dependent, flotillin-dependent, Cdc42-dependent and RhoA-

dependent pathways [125, 137, 138]. All these pathways generally require some specific lipid compositions and are mostly dependent on cholesterol [125, 137]. Moreover, most of these pathways are dynamin-independent. Not many nanocarriers have been reported to utilize different sub-types of the clathrin- and caveolae-independent endocytosis. Examples reported in the literature include nanoparticles and polymers modified with folate [139]. It is known that the folate binds to GPI-anchored folate receptor, 'FRα' that is overexpressed in tumor cells [139]. However, the folate entry is a complicated process. Along with clathrin- and caveolae-independent endocytosis it can also involve CME in specific cell types [139].

vii. Phagocytosis

Phagocytosis occurs primarily in phagocytic cells like macrophages, monocytes, neutrophils and dendritic cells [133]. It is also reported that non-phagocytic cells like fibroblasts, epithelial and endothelial cells, may also display some phagocytic activity, but to a much lesser extent. The phagocytic pathway consists of three distinct steps [125]:

1) Recognition of the particles by opsonisation in the bloodstream

2) Adhesion of the opsonized particles onto the cell membrane and

3) Ingestion of the particle by the cells

The opsonization of nanoparticles occurs through adsorption of proteins, such as immunoglubulins (IgG and IgM), complement components (C3, C4, C5) and blood serum proteins (including laminin, fibronectin, etc.) [140]. The opsonized particle then attaches to the macrophage surface through specific receptors. (E.g. Fc receptor (FcR) or complement receptors (CR) [141]. Mannose/fructose and scavenger receptors also play a role in phagocytosis [125]. The receptor–ligand interaction leads to signal cascades, which result in actin rearrangement and formation of a phagosome. The size of the phagosome formed can vary greatly depending on the size of the cargo. It can range from few hundred nanometers to

dozens of microns [125]. The phagosome and its cargo undergo series of modifications to reach late endosomes from where they ultimately fuse with lysosome to form phagolysosome [125, 141].

1.6.3 Oral uptake mechanisms for lipid-based nanoparticles

Upon oral administration, drugs loaded into lipid carriers can access the blood/lymphatic transport system by three mechanisms: (1) Through M-cells and gut-associated lymphoid tissue that consist of lymphoidal follicles forming Peyer's patches (2) Stimulating chylomicron production and transport via triglyceride-rich lipoproteins and (3) Digestion of lipid by lipases and formation of vesicles/micelles. In the second case, the triglyceride-rich lipoproteins preferentially access lymphatic capillaries where cells are arranged in an overlapped manner with gaps. Thus, they gain entry into lymphatic system bypassing the portal hepatic circulation [142]. This is illustrated in Fig. 1.13 below.

Following ingestion of a lipid-based formulation, the process of lipid digestion is initiated in the stomach by the enzyme gastric lipase [142, 143]. Mechanical mixing (propulsion, grinding and retropulsion) in stomach further contributes to lipid digestion. The lipid is initially broken down to amphiphilic products (diglyceride and fatty acid) which when combined with mechanical mixing and aqueous medium produce a crude emulsion [142]. This crude emulsion is propelled further into small intestine where the pancreatic lipase together with its co-factor, co-lipase further breaks this down to diglycerides, monoglycerides and fatty acids. It is widely reported that the pancreatic lipase always acts on sn-1 and sn-3 positions of triglycerides to produce 2-monoglycerides and fatty acid [142, 143]. The pancreatic phospholipase A2 hydrolyses a single fatty-acid molecule from the sn-2 position of phospholipid to yield lyso-phosphatidylcholine and fatty acid. The presence of exogenous lipids in the intestine in turn stimulates the secretion of some endogenous lipids like bile salts,

phospholipids and cholesterol from the gall-bladder [142]. In presence of bile salts, the partially digested exogenous lipids form series of colloidal structures, including multi-lamellar and unilamellar vesicles, mixed micelles and micelles [142]. The lipophilic drug, along with these vesicles/micelles is absorbed through the intestine.

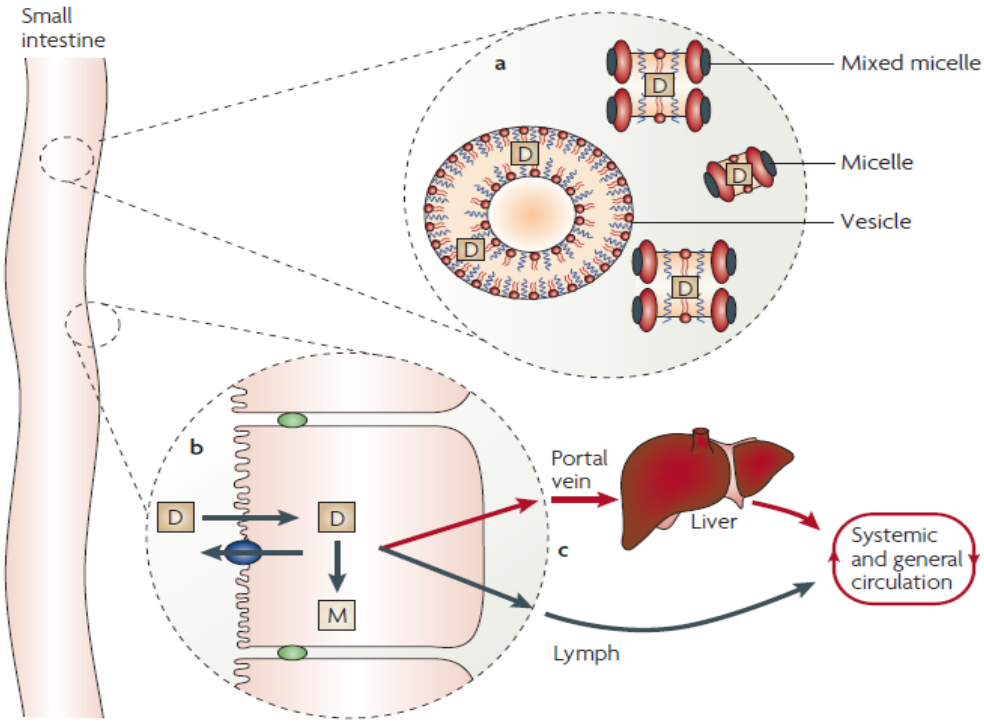

Fig. 1.13: An overview of the potential effect of lipids and lipidic excipients on drug absorption. Figure source: Porter, C.J.H., N.L. Trevaskis, and W.N. Charman, *Lipids and lipid-based formulations: optimizing the oral delivery of lipophilic drugs.* Nat Rev Drug Discov, 2007. **6**(3): p. 231-248.

Lipids can affect drug absorption in three ways: (a) enhancing drug solubilisation in the intestinal milieu through alterations to the composition and character of the colloidal environment; (b) interacting with enterocyte-based transport and metabolic processes, thereby potentially changing drug uptake, efflux, disposition and the formation of metabolites within the enterocyte and (c) altering the pathway (portal vein versus intestinal lymphatic system) of drug transport to the systemic circulation.

Following uptake into enterocytes, the products of lipid breakdown (monoglyceride and fatty acid) are re-synthesized to triglycerides in the smooth endoplasmic reticulum and are subsequently assembled into triglyceride-rich lipoproteins (TG-LPs) [144]. Lipoproteins are colloidal particles synthesized in the liver and small intestine that consist of a hydrophobic core (containing triglyceride and cholesteryl esters) and a relatively hydrophilic surface (containing phospholipids, cholesterol and apolipoproteins). TG-LPs facilitate the transport of lipids and lipophilic substances around the body [145]. These TG-LPs are then exocytosed into the lamina propria where the tight-junctions (between cells) and presence of an underlying basement membrane prevent their easy access to blood capillaries [145, 146]. Instead the TG-LPs selectively access the lymphatic systems where the adjacent cells overlap resulting in 'gaps' where colloidal species like TG-LPs have enhanced permeability [146]. TG-LPs include chylomicrons and very low-density lipoproteins (VLDL). Chylomicrons are larger (50–500 nm) and less dense lipoproteins than VLDL, and are formed exclusively in the small intestine following the ingestion of lipids (dietary derived or formulation-derived) [142, 147].

In contrast, the VLDL are small (20–50 nm) and more dense lipoproteins than chylomicrons, and are formed in the liver and the small intestine, primarily in fasting state [142]. Some drugs and excipients can block the formation of chylomicrons and thus, block the lymphatic uptake mechanism. For example, Pluronic-L81, colchicine and cycloheximide block intestinal chylomicron flow into the lymph and therefore inhibit lymphatic drug transport [142].

Most of the low molecular weight drugs are absorbed through portal vein as the rate of fluid flow in portal blood is approximately 500-fold higher than that of intestinal lymph. However, the lymphatic system can be a significant absorption pathway for highly lipophilic drugs [142, 147]. For highly lipophilic drugs (typically with log P >5 and solubility >50 mg

in long-chain TG lipid) partitioning into developing TG-LPs in the enterocyte provides a preferential access mechanism to the intestinal lymph [142].

Although the exact mechanism remains unknown, it is thought to involve drug association with lipoproteins during transport through the enterocyte [142]. The lymphatically transported compounds such as DDT (dichlorodiphenyltrichloroethane), aryl and alkyl hydrocarbons and halofantrine are transported in lymph within the apolar lipid core of lymph lipoproteins [142]. Fig. 1.14 gives a schematic representation of lipid and drug transport by the mesenteric lymph or portal blood upon oral delivery.

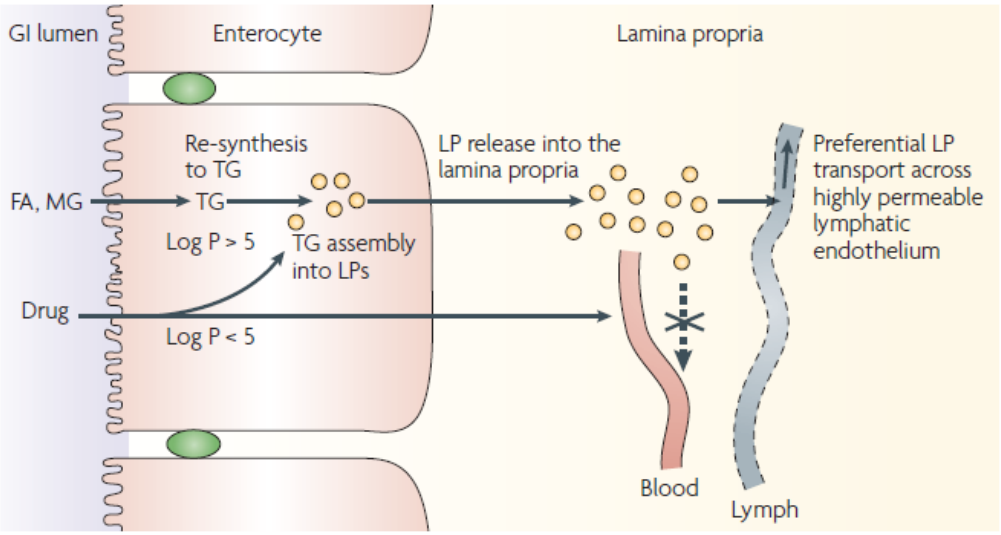

FA-Fatty acid; MG-Monoglyceride; TG-Triglyceride and LPs-Triglyceride-rich lipoproteins

Fig. 1.14: Schematic representation of lipid and drug transport by the mesenteric lymph or portal blood upon oral delivery. Figure source: Porter, C.J.H., N.L. Trevaskis, and W.N. Charman, *Lipids and lipid-based formulations: optimizing the oral delivery of lipophilic drugs.* Nat Rev Drug Discov, 2007. **6**(3): p. 231-248.

1.6.4 Factors affecting uptake, pharmacokinetics and bio-distribution of nanoparticles

i. Effect of the particle charge

Surface charge of nanoparticles certainly affect cellular uptake [125]. Presently, the reports suggest that majority of the positively charged nanoparticles are taken up by CME, while some small fraction use macropinocytosis [125, 148]. For example, cationic particles with different core materials like PLGA, chitosan and PEG-co-PLA are taken up by CME. One exception to this is PEI-based polyplexes that are strongly cationic, yet are taken up by caveolae-mediated endocytic process [149]. One reason for this could be that the excessive cationic charge attracts serum proteins that bind to the nanoparticle surface and neutralize the surface charge [150].

On the other hand, negatively charged particles, for example, DOXIL®, micelles and quantum dots mostly use caveolae-mediated endocytic uptake process [151-153]. Again there are few exceptions like carboxylate-modified polystyrene nanoparticles [154, 155] and negatively charged PLGA particles that utilize clathrin- and caveolae-independent uptake pathways. Because the cell membrane surface is negatively charged it is generally accepted that uptake of negatively charged nanoparticles is relatively slow in comparison to positively charged particles of the same size [125]. Again, exceptions here are the negatively charged quantum dots that are taken up much faster than positively charged ones [152].

There is still ambiguity in the literature regarding the uptake of neutral charge particles. It has been shown that Pluronic® micelles with neutral charge prefer CME uptake process [156]. However, this could be due to inhibition of caveolae-mediated pathways above certain micellar concentrations [156].

The particle charge also affects the pharmacokinetics of the nanoparticles. It has been shown that liposomes of ~200 nm with different surface charges show differences in their

tissue distribution properties [157]. The study demonstrated that rate of clearance of strongly negatively charged liposomes (ζ-potential of ~ -40 mV) was significantly higher than that of neutral liposomes (ζ-potential of ±10 mV) [158]. It was also shown that negatively charged liposomes were taken up to a greater extent by macrophages in liver and contributed towards faster elimination from the body [158]. Further, it was shown that PEGylation of these liposomes reduced the surface charge to ~ -15 mV; the PEGylated liposomes were taken-up to a lesser extent in the liver and showed higher circulation time in the body [158].

On the contrary, the positively charged particles tend to aggregate in presence of serum proteins when administered by intravenous (IV) injection [159]. These aggregates are large and often occlude the tiny capillaries in the lungs. The particles are slowly dissociated and then transported to the liver. Thus, strongly positively charged nanoparticles (ζ-potential of ~ +40 mV) show rapid clearance from plasma and tend to accumulate in liver and lungs [159]. Akin to their negatively charged counterparts, PEGylation increases the circulation time of positively charged nanoparticles in the body [159].

ii. Effect of the particle size

The very basis of nanomedicine is the size of the dosage form. For long, it was believed that particle size was crucial for uptake of nanoparticles. Researchers recommended a size of 10-100 nm for a nanoparticles to show endocytic uptake into the cells [125]. However, recent studies indicate that, though small particle size may help in rapid endocytic uptake of the particle, it is not always essential. Particles upto 5 µm have been shown to undergo endocytic uptake by pinocytosis [150]. Macropinocytosis allows for uptake of all large particles, though this process is albeit slow compared to other uptake processes. One study showed that negatively charged nanoparticles of 43 nm were taken up by CME process while, 25 nm particles of the same material and charge underwent caveolae-mediated uptake

[160]. As most of the nanoparticle preparations are polydisperse, it is difficult to understand the size-dependence on particle uptake [125].

Size of the nanoparticles also affects the bio-distribution and other pharmacokinetic properties. In one study, polystyrene nanoparticles with consistent composition but varying particles sizes from 50 to 500 nm showed that, larger particles have a greater tendency to aggregate and accumulate in the liver [161]. It was suggested that, for larger particles, the process of opsonisation followed by phagocytic uptake resulted in greater hepatic accumulation [161]. The size of nanoparticle has significant effect on protein adsorption. In another study, small (<100 nm), medium (100-200 nm) and large (>200 nm) nanoparticles of the same material were incubated with serum proteins for 2h [162]. Results indicated that, for smaller particles, protein adsorption was 6%; the medium and larger nanoparticles showed protein adsorption upto 23 and 34% respectively [162]. From the study, it was also concluded that the blood clearance of larger particles was twice as fast as that for smaller nanoparticles [163]. In summary, it has been consistently shown that PEGylated nanoparticles of less than 100 nm size have a reduced plasma adsorption, reduced phagocytic uptake, reduced hepatic filtration and a prolonged circulation time [164].

iii. Effect of the particle geometry

From recent studies, [165] it is known that the shape/geometry of the particle could affect both endocytic uptake and bio-distribution. It was shown that geometrically specific mechanisms of uptake, primarily CME for spherical particles and macropinocytosis or phagocytosis for cylindrical and worm-like particles exists [166].

It was hypothesized that this phenomena was due to the actual orientation of the nanoparticles when they interact with the cell surface [166]. For example, a spherical nanoparticle will have only one ‘face’ with which it can interact with the cell surface, while

cylindrical and worm-like nanoparticles have multiple ‘faces’ with large variations in size in each dimension [167]. Moreover, the *effective size* of the nanoparticle in that dimension matters. A sphere of 200 nm easily undergoes CME; cylindrical and worm-like particles have two distinct sizes in two dimensions – smaller axes (~200 nm) and the larger axes (400 to 1300 nm) [168]. A spherical particle is too large for caveolin-mediated endocyotsis and too small for phagocytosis, unless the spheres aggregate [169]. On the contrary, it is more probable that macropinocytosis and/or phagocytosis are the mechanisms of uptake for cylindrical and worm-like particles due to their relatively large size [170]. This is shown in Fig. 1.15 below.

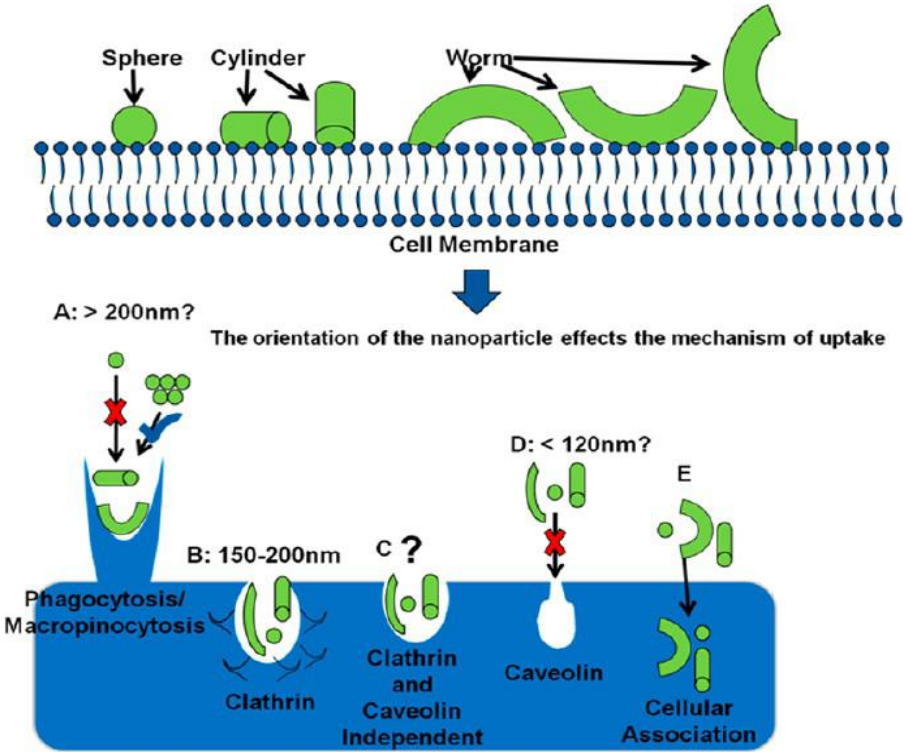

Fig. 1.15: Schematic representation describing the influence of nanoparticle orientation on mechanism of uptake. Figure source: Herd, H., et al., *Nanoparticle Geometry and Surface Orientation Influence Mode of Cellular Uptake.* ACS Nano, 2013. **7**(3): p. 1961-1973.

Discher et al. [171] produced a worm-like particle using a diblock co-polymer. They established the pharmacokinetics of nanoparticles after administration to mice. Their study results indicate that the worm-like nanoparticles showed unusually large circulation time in the blood (~5 days after administration). Subsequent studies using macrophages indicated that the worm-like nanoparticles produce a strong drag force by the flowing fluid such that they are carried away by the flow even before macrophages can engulf them [172].

1.7 Concluding remarks

The reticuloendothelial system (RES) or mononuclear phagocyte system (MPS) contribute significantly towards nanoparticle uptake and clearance from the body. For prolonging the circulation time in the body, the best method is to reduce opsonisation and thus reduce MPS clearance. Approaches to improve pharmacokinetics of nanoparticles include: maintaining the size around 100 nm, keeping the ζ-potential in neutral zone (~10 mV), grafting PEG onto the nanoparticle surface and designing nanoparticles with elongated structure (cylindrical, rod-like or worm-like structure) [157].

The FDA-approved nanoparticle formulation for cancer therapy, Doxil (liposomal doxorubicin), fits all of these criteria except for the geometrical requirements [125]. However, even non-PEGylated nanoparticles can be specifically used to target the MPS. For example, AmBisome (liposomal amphotericin B), another FDA-approved product is non-PEGylated and useful in targeting MPS for treatment of fungal infections.

References

1. *Electronic Package Insert: Evista® ((raloxifene hydrochloride): Tablet for Oral Use.* 2011, Eli Lilly and Company: Lilly USA, LLC, Indianapolis, IN 46285, USA.

2. Stevenson, J.C. and M.S. Marsh, *An atlas of osteoporosis*. 2nd ed. The encyclopedia of visual medicine series. 2000, New York: Parthenon Pub. Group. 109 p.

3. *International Osteoporosis Foundation. Facts and statistics about osteoporosis and its impact.* . [cited 2010 August 08].

4. Burge, R., et al., *Incidence and economic burden of osteoporosis-related fractures in the United States, 2005-2025.* J Bone Miner Res, 2007. **22**(3): p. 465-75.

5. Malhotra, N. and A. Mithal, *Osteoporosis in Indians.* Indian J Med Res, 2008. **127**(3): p. 263-8.

6. Goswami, R., et al., *Prevalence and significance of low 25-hydroxyvitamin D concentrations in healthy subjects in Delhi.* Am J Clin Nutr, 2000. **72**(2): p. 472-5.

7. Arya, V., et al., *Vitamin D status and its relationship with bone mineral density in healthy Asian Indians.* Osteoporos Int, 2004. **15**(1): p. 56-61.

8. Mitra, S., M. Desai, and M.I. Khatkhatay, *Association of estrogen receptor alpha gene polymorphisms with bone mineral density in postmenopausal Indian women.* Mol Genet Metab, 2006. **87**(1): p. 80-7.

9. Albertazzi, P. and D.W. Purdie, *Oestrogen and selective oestrogen receptor modulators (SERMs): current roles in the prevention and treatment of osteoporosis.* Best Pract Res Clin Rheumatol, 2001. **15**(3): p. 451-68.

10. Brown, J.P., R.G. Josse, and C. Scientific Advisory Council of the Osteoporosis Society of, *2002 clinical practice guidelines for the diagnosis and management of osteoporosis in Canada.* CMAJ, 2002. **167**(10 Suppl): p. S1-34.

11. Rey, J.R., et al., *Raloxifene: mechanism of action, effects on bone tissue, and applicability in clinical traumatology practice.* Open Orthop J, 2009. **3**: p. 14-21.

12. Maximov, P.Y., T.M. Lee, and V.C. Jordan, *The discovery and development of selective estrogen receptor modulators (SERMs) for clinical practice.* Curr Clin Pharmacol, 2013. **8**(2): p. 135-55.

13. Muchmore, D.B., *Raloxifene: A selective estrogen receptor modulator (SERM) with multiple target system effects.* Oncologist, 2000. **5**(5): p. 388-92.

14. Delmas, P.D., et al., *Effects of raloxifene on bone mineral density, serum cholesterol concentrations, and uterine endometrium in postmenopausal women.* N Engl J Med, 1997. **337**(23): p. 1641-7.

15. Hochner-Celnikier, D., *Pharmacokinetics of raloxifene and its clinical application.* Eur J Obstet Gynecol Reprod Biol, 1999. **85**(1): p. 23-9.

16. Lindstrom, T.D., N.G. Whitaker, and G.W. Whitaker, *Disposition and metabolism of a new benzothiophene antiestrogen in rats, dogs and monkeys.* Xenobiotica, 1984. **14**(11): p. 841-7.

17. Deguchi, T., et al., *Human pharmacokinetic prediction of UDP-glucuronosyltransferase substrates with an animal scale-up approach.* Drug Metab Dispos, 2011. **39**(5): p. 820-9.

18. Thorn, H.A., et al., *Extensive intestinal glucuronidation of raloxifene in vivo in pigs and impact for oral drug delivery.* Xenobiotica, 2012. **42**(9): p. 917-28.

19. Mizuma, T., *Intestinal glucuronidation metabolism may have a greater impact on oral bioavailability than hepatic glucuronidation metabolism in humans: a study with raloxifene, substrate for UGT1A1, 1A8, 1A9, and 1A10.* Int J Pharm, 2009. **378**(1-2): p. 140-1.

20. Heiligtag, F.J.M.N., *The fascinating world of nanoparticle research.* Mater Today, 2013. **7/8**(16): p. 262-272.

21. Freitas, R., *The Prospect of Nanomedicine*, in *Nanomedicine, Volume I: Basic Capabilities*. 1999, Landes Bioscience: Texas, U.S.A. p. 27.

22. Liversidge, G.G. and K.C. Cundy, *Particle size reduction for improvement of oral bioavailability of hydrophobic drugs: I. Absolute oral bioavailability of nanocrystalline danazol in beagle dogs.* Int J Pharm, 1995. **125**(1): p. 91-97.

23. Shegokar, R. and R.H. Müller, *Nanocrystals: Industrially feasible multifunctional formulation technology for poorly soluble actives.* Int J Pharm, 2010. **399**(1-2): p. 129-139.

24. Wagner, V., et al., *The emerging nanomedicine landscape.* Nat Biotechnol, 2006. **24**(10): p. 1211-7.

25. *Introduction to Nanoparticles*, in *Microwaves in Nanoparticle Synthesis: Fundamentals and Applications*, S.S. Horikoshi, Nick Editor. 2013, Wiley-VCH Verlag GmbH & Co. KGaA: Wiley-VCH Verlag GmbH & Co. KGaA. p. 8-10.

26. Rao, J.P. and K.E. Geckeler, *Polymer nanoparticles: Preparation techniques and size-control parameters.* Prog Polym Sci, 2011. **36**(7): p. 887-913.

27. Zambaux, M.F., et al., *Influence of experimental parameters on the characteristics of poly(lactic acid) nanoparticles prepared by a double emulsion method.* J Control Release, 1998. **50**(1-3): p. 31-40.

28. Vandorpe, J., et al., *Poly(organo phosphazene) nanoparticles surface modified with poly(ethylene oxide).* Biotechnol Bioeng, 1996. **52**(1): p. 89-95.

29. Song, C.X., et al., *Formulation and characterization of biodegradable nanoparticles for intravascular local drug delivery.* J Control Release, 1997. **43**(2-3): p. 197-212.

30. Lemoine, D. and V. Préat, *Polymeric nanoparticles as delivery system for influenza virus glycoproteins.* J Control Release, 1998. **54**(1): p. 15-27.

31. Musyanovych, A., Schmitz-Wienke, J., Mailänder, V., Walther, P. and Landfester, K. , *Preparation of Biodegradable Polymer Nanoparticles by Miniemulsion Technique and Their Cell Interactions.* Macromol Biosci, 2008. **8**: p. 127-139.

32. Bilati, U., E. Allemann, and E. Doelker, *Sonication parameters for the preparation of biodegradable nanocapsules of controlled size by the double emulsion method.* Pharm Dev Technol, 2003. **8**(1): p. 1-9.

33. Potineni, A., et al., *Poly(ethylene oxide)-modified poly(β-amino ester) nanoparticles as a pH-sensitive biodegradable system for paclitaxel delivery.* J Control Release, 2003. **86**(2–3): p. 223-234.

34. Bindschaedler C., R.G., Doelker E, *Process for preparing a powder of water-insoluble polymer which can be redispersed in a liquid phase, the resulting powder and utilization thereof.* 1990: US Patent 4,968,350.

35. Allémann, E., R. Gurny, and E. Doelker, *Preparation of aqueous polymeric nanodispersions by a reversible salting-out process: influence of process parameters on particle size.* Int J Pharm, 1992. **87**(1–3): p. 247-253.

36. De Jaeghere, F., et al., *Formulation and Lyoprotection of Poly(Lactic Acid-Co-Ethylene Oxide) Nanoparticles: Influence on Physical Stability and In Vitro Cell Uptake.* Pharm Res, 1999. **16**(6): p. 859-866.

37. Nguyen, C.A., et al., *Synthesis of a novel fluorescent poly(d,l-lactide) end-capped with 1-pyrenebutanol used for the preparation of nanoparticles.* Eur J Pharm Sci, 2003. **20**(2): p. 217-222.

38. Zweers, M.L.T., et al., *In vitro degradation of nanoparticles prepared from polymers based on dl-lactide, glycolide and poly(ethylene oxide).* J Control Release, 2004. **100**(3): p. 347-356.

39. Galindo-Rodríguez, S.A., et al., *Comparative scale-up of three methods for producing ibuprofen-loaded nanoparticles.* Eur J Pharm Sci, 2005. **25**(4–5): p. 357-367.

40. Fessi, H., et al., *Nanocapsule formation by interfacial polymer deposition following solvent displacement.* Int J Pharm, 1989. **55**(1): p. R1-R4.

41. Limayem Blouza, I., et al., *Preparation and characterization of spironolactone-loaded nanocapsules for paediatric use.* Int J Pharm, 2006. **325**(1-2): p. 124-31.

42. Zili, Z., S. Sfar, and H. Fessi, *Preparation and characterization of poly-ε-caprolactone nanoparticles containing griseofulvin.* Int J Pharm, 2005. **294**(1–2): p. 261-267.

43. Moinard-Checot, D., et al., *Mechanism of nanocapsules formation by the emulsion-diffusion process.* J Colloid Interface Sci, 2008. **317**(2): p. 458-68.

44. Nehilla, B.J., et al., *Purified and surfactant-free coenzyme Q10-loaded biodegradable nanoparticles.* Int J Pharm, 2008. **348**(1-2): p. 107-114.

45. Yallapu, M.M., et al., *Fabrication of curcumin encapsulated PLGA nanoparticles for improved therapeutic effects in metastatic cancer cells.* J Colloid Interface Sci, 2010. **351**(1): p. 19-29.

46. Seyler, I., et al., *Macrophage Activation by a Lipophilic Derivative of Muramyldipeptide within Nanocapsules: Investigation of the Mechanism of Drug Delivery.* J Nanopart Res, 1999. **1**(1): p. 91-97.

47. Legrand, P., et al., *Influence of polymer behaviour in organic solution on the production of polylactide nanoparticles by nanoprecipitation.* Int J Pharm, 2007. **344**(1–2): p. 33-43.

48. Yordanov, G. and C. Dushkin, *Preparation of poly(butylcyanoacrylate) drug carriers by nanoprecipitation using a pre-synthesized polymer and different colloidal stabilizers.* Colloid Polym Sci, 2010. **288**(9): p. 1019-1026.

49. Tan, Y., et al., *Designing Starch-Based Nanospheres to Make Hydrogels with High Mechanical Strength.* Macromol Mater Eng, 2009. **294**(12): p. 855-859.

50. Jeon, H.J., et al., *Effect of solvent on the preparation of surfactant-free poly(DL-lactide-co-glycolide) nanoparticles and norfloxacin release characteristics.* Int J Pharm, 2000. **207**(1-2): p. 99-108.

51. Jeong, Y.-I., et al., *Preparation of poly(DL-lactide-co-glycolide) nanoparticles without surfactant.* J Appl Polym Sci, 2001. **80**(12): p. 2228-2236.

52. Meziani, M.J., et al., *Polymeric Nanofibers from Rapid Expansion of Supercritical Solution.* Ind Eng Chem Res, 2005. **44**(13): p. 4594-4598.

53. Thickett, S.C. and R.G. Gilbert, *Emulsion polymerization: State of the art in kinetics and mechanisms.* Polymer, 2007. **48**(24): p. 6965-6991.

54. Asua, J.M., *Emulsion polymerization: From fundamental mechanisms to process developments.* J Polym Sci Part A Polym Chem, 2004. **42**(5): p. 1025-1041.

55. Chern, C.S., *Emulsion polymerization mechanisms and kinetics.* Prog Polym Sci, 2006. **31**(5): p. 443-486.

56. Pouton, C.W., *Formulation of poorly water-soluble drugs for oral administration: Physicochemical and physiological issues and the lipid formulation classification system.* Eur J Pharm Sci, 2006. **29**(3-4): p. 278-287.

57. Müller, R.H., et al., *Solid lipid nanoparticles (SLN) as potential carrier for human use: interaction with human granulocytes.* J Control Release, 1997. **47**(3): p. 261-269.

58. Shegokar, R., K.K. Singh, and R.H. Müller, *Production and stability of stavudine solid lipid nanoparticles—From lab to industrial scale.* Int J Pharm, 2011. **416**(2): p. 461-470.

59. Speiser, P., *Lipid nano-pellets as excipient system for perorally administered drugs*. 1989, Google Patents.

60. Gasco, M.R., *Method for producing solid lipid microspheres having a narrow size distribution*. 1993, Google Patents.

61. Gasco, M.R., *Solid lipid nanospheres from warm micro-emulions.* Pharm Tech Eur, 1997. **9**: p. 52-58.

62. Schwarz, C., et al., *Solid lipid nanoparticles (SLN) for controlled drug delivery. I. Production, characterization and sterilization.* J Control Release, 1994. **30**(1): p. 83-96.

63. Müller, R.H., K. Mäder, and S. Gohla, *Solid lipid nanoparticles (SLN) for controlled drug delivery – a review of the state of the art.* Eur J Pharm Biopharm, 2000. **50**(1): p. 161-177.

64. Müller, R.H., M. Radtke, and S.A. Wissing, *Solid lipid nanoparticles (SLN) and nanostructured lipid carriers (NLC) in cosmetic and dermatological preparations.* Adv Drug Deliver Rev, 2002. **54, Supplement**(0): p. S131-S155.

65. Wissing, S.A., O. Kayser, and R.H. Müller, *Solid lipid nanoparticles for parenteral drug delivery.* Adv Drug Deliver Rev, 2004. **56**(9): p. 1257-1272.

66. Mehnert, W. and K. Mäder, *Solid lipid nanoparticles: Production, characterization and applications.* Adv Drug Deliver Rev, 2001. **47**(2-3): p. 165-196.

67. Muller, R.H., M. Radtke, and S.A. Wissing, *Nanostructured lipid matrices for improved microencapsulation of drugs.* Int J Pharm, 2002. **242**(1-2): p. 121-8.

68. Tan, A., S. Rao, and C.A. Prestidge, *Transforming lipid-based oral drug delivery systems into solid dosage forms: an overview of solid carriers, physicochemical properties, and biopharmaceutical performance.* Pharm Res, 2013. **30**(12): p. 2993-3017.

69. Kalepu, S., M. Manthina, and V. Padavala, *Oral lipid-based drug delivery systems – an overview.* Acta Pharm Sin B, 2013. **3**(6): p. 361-372.

70. Qi, J., Y. Lu, and W. Wu, *Absorption, disposition and pharmacokinetics of solid lipid nanoparticles.* Curr Drug Metab, 2012. **13**(4): p. 418-28.

71. Wang, J., et al., *Absorption, pharmacokinetics and disposition properties of solid lipid nanoparticles (SLNs).* Curr Drug Metab, 2012. **13**(4): p. 447-56.

72. Muller, R.H., A.Lippacher and S.,Gohla, *Solid lipid nanoparticles (SLN) as a carrier systen for the controlled release of drugs*, in *Hand of Pharmaceutical Controlled Release Technology*, D.L. Wise, Editor. 2000, Mercel Dekker: New York. p. 377-389.

73. Müller, R.H., et al., *Nanostructured lipid carriers (NLC) in cosmetic dermal products.* Adv Drug Deliver Rev, 2007. **59**(6): p. 522-530.

74. Pardeike, J., A. Hommoss, and R.H. Müller, *Lipid nanoparticles (SLN, NLC) in cosmetic and pharmaceutical dermal products.* Int J Pharm, 2009. **366**(1-2): p. 170-184.

75. Tiwari, R. and K. Pathak, *Nanostructured lipid carrier versus solid lipid nanoparticles of simvastatin: Comparative analysis of characteristics, pharmacokinetics and tissue uptake.* Int J Pharm, 2011. **415**(1-2): p. 232-243.

76. Zhuang, C.-Y., et al., *Preparation and characterization of vinpocetine loaded nanostructured lipid carriers (NLC) for improved oral bioavailability.* Int J Pharm, 2010. **394**(1-2): p. 179-185.

77. Souto, E.B., Muller R.H., *Lipid nanoparticles (SLN and NLC) for drug delivery*, in *Nanoparticles for Pharmaceutical Applications*, Y.T. A. J. Domb, M. N. V .R. Kumar and S. Farber, Editor. 2007, American Scientific Publishers: Stevenson Ranch, California. p. 102-122.

78. Muller, R.H.S., Runge, *Solid lipid nanoparticles (SLN) for controlled drug delivery*, in *Submicron emulsion in drug targeting and delivery*, B. S, Editor. 1998, Harwood Academic Publishers: The Netherlands. p. 219-234.

79. Cavalli, R., et al., *Sterilization and freeze-drying of drug-free and drug-loaded solid lipid nanoparticles.* Int J Pharm, 1997. **148**(1): p. 47-54.

80. Gasco, M.R., *Solid lipid nanospheres from warm micro-emulsions.* Pharm Technol Eur, 1997. **9**: p. 52-58.

81. Igartua, M., et al., *Development and characterization of solid lipid nanoparticles loaded with magnetite.* Int J Pharm, 2002. **233**(1-2): p. 149-57.

82. Siekmann, B., K., Westesen *Investigations on solid lipid nanoparticles prepared by precipitation in o/w emulsions.* Eur J Pharm Biopharm, 1996. **43**: p. 104-109.

83. Trotta, M., F. Debernardi, and O. Caputo, *Preparation of solid lipid nanoparticles by a solvent emulsification-diffusion technique.* Int J Pharm, 2003. **257**(1-2): p. 153-60.

84. Morel, S., et al., *Thymopentin in solid lipid nanoparticles.* Int J Pharm, 1996. **132**(1–2): p. 259-261.

85. Cortesi, R., et al., *Production of lipospheres as carriers for bioactive compounds.* Biomaterials, 2002. **23**(11): p. 2283-2294.

86. Mei, Z., et al., *Solid lipid nanoparticle and microemulsion for topical delivery of triptolide.* Eur J Pharm Biopharm, 2003. **56**(2): p. 189-96.

87. Heurtault, B., et al., *Physico-chemical stability of colloidal lipid particles.* Biomaterials, 2003. **24**(23): p. 4283-300.

88. Jores, K., et al., *Investigations on the structure of solid lipid nanoparticles (SLN) and oil-loaded solid lipid nanoparticles by photon correlation spectroscopy, field-flow fractionation and transmission electron microscopy.* J Control Release, 2004. **95**(2): p. 217-27.

89. Keck, C.M. and R.H. Müller, *Drug nanocrystals of poorly soluble drugs produced by high pressure homogenisation.* Eur J Pharm Biopharm, 2006. **62**(1): p. 3-16.

90. Keck, C.M. and R.H. Müller, *Size analysis of submicron particles by laser diffractometry—90% of the published measurements are false.* Int J Pharm, 2008. **355**(1–2): p. 150-163.

91. Radomska-Soukharev, A., *Stability of lipid excipients in solid lipid nanoparticles.* Adv Drug Deliv Rev, 2007. **59**(6): p. 411-8.

92. Zimmermann, L., *Possibilities and limitations of laser light scattering techniques for particle size analysis*, in *Particle and Surface Characterization Methods*, R.H. Muller, W. Mehnert, Editor. 1997, Medpharm: Stuttgart. p. 19-26.

93. Kuo, Y.-C. and T.-W. Lin, *Electrophoretic Mobility, Zeta Potential, and Fixed Charge Density of Bovine Knee Chondrocytes, Methyl Methacrylate−Sulfopropyl Methacrylate, Polybutylcyanoacrylate, and Solid Lipid Nanoparticles.* J Phys Chem B, 2006. **110**(5): p. 2202-2208.

94. Dubes, A., et al., *Scanning electron microscopy and atomic force microscopy imaging of solid lipid nanoparticles derived from amphiphilic cyclodextrins.* Eur J Pharm Biopharm, 2003. **55**(3): p. 279-282.

95. Hou, D., et al., *The production and characteristics of solid lipid nanoparticles (SLNs).* Biomaterials, 2003. **24**(10): p. 1781-1785.

96. Bunjes, H., K. Westesen, and M.H.J. Koch, *Crystallization tendency and polymorphic transitions in triglyceride nanoparticles.* Int J Pharm, 1996. **129**(1–2): p. 159-173.

97. Westesen, K., B. Siekmann, M. H. J., Koch, *Investigations on the physical state of solid lipid nanoparticles by synchrom radiation X-ray diffraction.* Int J Pharm, 1993. **93**: p. 189-199.

98. Coleman, N.J., D. Q. M., Craig, *Modulated temperature differential scanning calorimetry: a novel approach to pharmaceutical thennal analysis.* Int J Pharm, 1996. **136**: p. 13-29.

99. Flynn, J.H., *Analysis of DSC results by integration.* Thermochemica Acta, 1993. **217**: p. 129-149.

100. Souto, E.B., W. Mehnert, and R.H. Müller, *Polymorphic behaviour of Compritol®888 ATO as bulk lipid and as SLN and NLC.* J Microencap, 2006. **23**(4): p. 417-433.

101. Freitas, C., R. H., Mulller, *Correlation between long-term stability of solid lipid nanoparticles (SLN^{TM}) and crystallinity of the lipid phase.* Eur J Pharm Biopharm, 1999. **47**: p. 125-132.

102. Teeranachaideekul, V., et al., *Cetyl palmitate-based NLC for topical delivery of Coenzyme Q10 – Development, physicochemical characterization and in vitro release studies.* Eur J Pharm Biopharm, 2007. **67**(1): p. 141-148.

103. Joshi, M. and V. Patravale, *Nanostructured lipid carrier (NLC) based gel of celecoxib.* Int J Pharm, 2008. **346**(1-2): p. 124-32.

104. You, J., et al., *Preparation and characteristic of vinorelbine bitartrate-loaded solid lipid nanoparticles.* Int J Pharm, 2007. **343**(1–2): p. 270-276.

105. Ensign, L.M., R. Cone, and J. Hanes, *Oral drug delivery with polymeric nanoparticles: the gastrointestinal mucus barriers.* Adv Drug Deliv Rev, 2012. **64**(6): p. 557-70.

106. Singh, R. and J.W. Lillard Jr, *Nanoparticle-based targeted drug delivery.* Expt Mol Patho, 2009. **86**(3): p. 215-223.

107. Tang, B.C., et al., *Biodegradable polymer nanoparticles that rapidly penetrate the human mucus barrier.* Proc Natl Acad Sci, 2009.

108. Cone, R.A., *Barrier properties of mucus.* Adv Drug Deliv Rev, 2009. **61**(2): p. 75-85.

109. Crater, J.S. and R.L. Carrier, *Barrier properties of gastrointestinal mucus to nanoparticle transport.* Macromol Biosci, 2010. **10**(12): p. 1473-83.

110. Lai, S.K., Y.-Y. Wang, and J. Hanes, *Mucus-penetrating nanoparticles for drug and gene delivery to mucosal tissues.* Adv Drug Deliver Rev, 2009. **61**(2): p. 158-171.

111. Huang, Y., et al., *Molecular aspects of muco- and bioadhesion: tethered structures and site-specific surfaces.* J Control Release, 2000. **65**(1-2): p. 63-71.

112. Nollevaux, G., et al., *Development of a serum-free co-culture of human intestinal epithelium cell-lines (Caco-2/HT29-5M21).* BMC Cell Biol, 2006. **7**: p. 20.

113. Yin, L., et al., *Drug permeability and mucoadhesion properties of thiolated trimethyl chitosan nanoparticles in oral insulin delivery.* Biomaterials, 2009. **30**(29): p. 5691-5700.

114. Schmidt, C., et al., *W1266 Confocal Laser Endomicroscopy (CLE) Reveals Mucosal Accumulation of Plga-Nanoparticles in Ulcerous Lesions of Patients With Inflammatory Bowel Diseases.* Gastroenterology, 2010. **138**(5): p. S-687.

115. Plapied, L., et al., *Fate of polymeric nanocarriers for oral drug delivery.* Curr Opin Colloid Interface Sci, 2011. **16**(3): p. 228-237.

116. Cano-Cebrian, M.J., et al., *Intestinal absorption enhancement via the paracellular route by fatty acids, chitosans and others: a target for drug delivery.* Curr Drug Deliv, 2005. **2**(1): p. 9-22.

117. Dodane, V., M. Amin Khan, and J.R. Merwin, *Effect of chitosan on epithelial permeability and structure.* Int J Pharm, 1999. **182**(1): p. 21-32.

118. Yeh, T.-H., et al., *Mechanism and consequence of chitosan-mediated reversible epithelial tight junction opening.* Biomaterials, 2011. **32**(26): p. 6164-6173.

119. Gebert, A., H.-J. Rothkötter, and R. Pabst, *M Cells in Peyer's Patches of the Intestine*, in *Int Rev Cytol*, W.J. Kwang, Editor. 1996, Academic Press. p. 91-159.

120. Kreuter, J., *Peroral administration of nanoparticles.* Adv Drug Deliver Rev, 1991. **7**(1): p. 71-86.

121. O'Hagan, D.T., *Intestinal translocation of particulates — implications for drug and antigen delivery.* Adv Drug Deliver Rev, 1990. **5**(3): p. 265-285.

122. Roger, E., et al., *Biopharmaceutical parameters to consider in order to alter the fate of nanocarriers after oral delivery.* Nanomedicine (Lond), 2010. **5**(2): p. 287-306.

123. Conner, S.D. and S.L. Schmid, *Regulated portals of entry into the cell.* Nature, 2003. **422**(6927): p. 37-44.

124. Snoeck, V., B. Goddeeris, and E. Cox, *The role of enterocytes in the intestinal barrier function and antigen uptake.* Microbes Infect, 2005. **7**(7-8): p. 997-1004.

125. Sahay, G., D.Y. Alakhova, and A.V. Kabanov, *Endocytosis of nanomedicines.* J Control Release, 2010. **145**(3): p. 182-95.

126. Parton, R.G. and K. Simons, *The multiple faces of caveolae.* Nat Rev Mol Cell Biol, 2007. **8**(3): p. 185-94.

127. Kerr, M.C. and R.D. Teasdale, *Defining macropinocytosis.* Traffic, 2009. **10**(4): p. 364-71.

128. Jones, A.T., *Macropinocytosis: searching for an endocytic identity and role in the uptake of cell penetrating peptides.* J Cell Mol Med, 2007. **11**(4): p. 670-84.

129. Koivusalo, M., et al., *Amiloride inhibits macropinocytosis by lowering submembranous pH and preventing Rac1 and Cdc42 signaling.* J Cell Biol, 2010. **188**(4): p. 547-63.

130. Brodsky, F.M., et al., *Biological basket weaving: formation and function of clathrin-coated vesicles.* Annu Rev Cell Dev Biol, 2001. **17**: p. 517-68.

131. Bareford, L.M. and P.W. Swaan, *Endocytic mechanisms for targeted drug delivery.* Adv Drug Deliv Rev, 2007. **59**(8): p. 748-58.

132. Mayor, S. and R.E. Pagano, *Pathways of clathrin-independent endocytosis.* Nat Rev Mol Cell Biol, 2007. **8**(8): p. 603-12.

133. Hillaireau, H. and P. Couvreur, *Nanocarriers' entry into the cell: relevance to drug delivery.* Cell Mol Life Sci, 2009. **66**(17): p. 2873-2896.

134. Iversen, T.-G., T. Skotland, and K. Sandvig, *Endocytosis and intracellular transport of nanoparticles: Present knowledge and need for future studies.* Nano Today, 2011. **6**(2): p. 176-185.

135. Hayer, A., et al., *Caveolin-1 is ubiquitinated and targeted to intralumenal vesicles in endolysosomes for degradation.* J Cell Biol, 2010. **191**(3): p. 615-629.

136. Scita, G. and P.P. Di Fiore, *The endocytic matrix.* Nature, 2010. **463**(7280): p. 464-73.

137. Sandvig, K., et al., *Clathrin-independent endocytosis: mechanisms and function.* Curr Opin Cell Biol, 2011. **23**(4): p. 413-20.

138. Doherty, G.J. and H.T. McMahon, *Mechanisms of endocytosis.* Annu Rev Biochem, 2009. **78**: p. 857-902.

139. Lu, Y. and P.S. Low, *Folate-mediated delivery of macromolecular anticancer therapeutic agents.* Adv Drug Deliv Rev, 2002. **54**(5): p. 675-93.

140. Rabinovitch, M., *Professional and non-professional phagocytes: an introduction.* Trends Cell Biol, 1995. **5**(3): p. 85-7.

141. Aderem, A. and D.M. Underhill, *Mechanisms of phagocytosis in macrophages.* Annu Rev Immunol, 1999. **17**: p. 593-623.

142. Porter, C.J.H., N.L. Trevaskis, and W.N. Charman, *Lipids and lipid-based formulations: optimizing the oral delivery of lipophilic drugs.* Nat Rev Drug Discov, 2007. **6**(3): p. 231-248.

143. Chapus, C., et al., *Mechanism of pancreatic lipase action. 1. Interfacial activation of pancreatic lipase.* Biochemistry, 1976. **15**(23): p. 4980-7.

144. Lehner, R. and A. Kuksis, *Biosynthesis of triacylglycerols.* Prog Lipid Res, 1996. **35**(2): p. 169-201.

145. Hussain, M.M., et al., *Microsomal triglyceride transfer protein: a multifunctional protein.* Front Biosci, 2003. **8**: p. s500-6.

146. Hussain, N., V. Jaitley, and A.T. Florence, *Recent advances in the understanding of uptake of microparticulates across the gastrointestinal lymphatics.* Adv Drug Deliver Rev, 2001. **50**(1-2): p. 107-142.

147. Phan, C.T. and P. Tso, *Intestinal lipid absorption and transport.* Front Biosci, 2001. **6**: p. D299-319.

148. Harush-Frenkel, O., et al., *Surface Charge of Nanoparticles Determines Their Endocytic and Transcytotic Pathway in Polarized MDCK Cells.* Biomacromolecules, 2008. **9**(2): p. 435-443.

149. Rejman, J., A. Bragonzi, and M. Conese, *Role of clathrin- and caveolae-mediated endocytosis in gene transfer mediated by lipo- and polyplexes.* Mol Ther, 2005. **12**(3): p. 468-74.

150. Gratton, S.E., et al., *The effect of particle design on cellular internalization pathways.* Proc Natl Acad Sci U S A, 2008. **105**(33): p. 11613-8.

151. Xiao, Y., et al., *Dynamics and mechanisms of quantum dot nanoparticle cellular uptake.* J Nanobiotechnology, 2010. **8**: p. 13.

152. Zhang, L.W. and N.A. Monteiro-Riviere, *Mechanisms of quantum dot nanoparticle cellular uptake.* Toxicol Sci, 2009. **110**(1): p. 138-55.

153. Sahay, G., et al., *The exploitation of differential endocytic pathways in normal and tumor cells in the selective targeting of nanoparticulate chemotherapeutic agents.* Biomaterials, 2010. **31**(5): p. 923-33.

154. Panyam, J. and V. Labhasetwar, *Dynamics of endocytosis and exocytosis of poly(D,L-lactide-co-glycolide) nanoparticles in vascular smooth muscle cells.* Pharm Res, 2003. **20**(2): p. 212-20.

155. Qaddoumi, M.G., et al., *The characteristics and mechanisms of uptake of PLGA nanoparticles in rabbit conjunctival epithelial cell layers.* Pharm Res, 2004. **21**(4): p. 641-8.

156. Sahay, G., E.V. Batrakova, and A.V. Kabanov, *Different Internalization Pathways of Polymeric Micelles and Unimers and Their Effects on Vesicular Transport.* Bioconjugate Chemistry, 2008. **19**(10): p. 2023-2029.

157. Li, S.D. and L. Huang, *Pharmacokinetics and biodistribution of nanoparticles.* Mol Pharm, 2008. **5**(4): p. 496-504.

158. Levchenko, T.S., et al., *Liposome clearance in mice: the effect of a separate and combined presence of surface charge and polymer coating.* Int J Pharm, 2002. **240**(1-2): p. 95-102.

159. Zhang, J.S., F. Liu, and L. Huang, *Implications of pharmacokinetic behavior of lipoplex for its inflammatory toxicity.* Adv Drug Deliv Rev, 2005. **57**(5): p. 689-98.

160. Lai, S.K., et al., *Characterization of the intracellular dynamics of a non-degradative pathway accessed by polymer nanoparticles.* J Control Release, 2008. **125**(2): p. 107-11.

161. Nagayama, S., et al., *Time-dependent changes in opsonin amount associated on nanoparticles alter their hepatic uptake characteristics.* Int J Pharm, 2007. **342**(1–2): p. 215-221.

162. Fang, C., et al., *In vivo tumor targeting of tumor necrosis factor-alpha-loaded stealth nanoparticles: effect of MePEG molecular weight and particle size.* Eur J Pharm Sci, 2006. **27**(1): p. 27-36.

163. Fang, Z. and B. Bhandari, *Encapsulation of polyphenols - a review.* Trends in Food Science & Technology, 2010. **21**(10): p. 510-523.

164. Alexis, F., et al., *Factors affecting the clearance and biodistribution of polymeric nanoparticles.* Mol Pharm, 2008. **5**(4): p. 505-15.

165. de Wolf, H.K., et al., *Effect of cationic carriers on the pharmacokinetics and tumor localization of nucleic acids after intravenous administration.* Int J Pharm, 2007. **331**(2): p. 167-75.

166. Huang, C., et al., *Role of nanoparticle geometry in endocytosis: laying down to stand up.* Nano Lett, 2013. **13**(9): p. 4546-50.

167. Tao, L., et al., *Lithographically defined uniform worm-shaped polymeric nanoparticles.* Nanotechnology, 2010. **21**(9): p. 095301.

168. Loverde, S.M., M.L. Klein, and D.E. Discher, *Nanoparticle shape improves delivery: rational coarse grain molecular dynamics (rCG-MD) of taxol in worm-like PEG-PCL micelles.* Adv Mater, 2012. **24**(28): p. 3823-30.

169. Herd, H., et al., *Nanoparticle Geometry and Surface Orientation Influence Mode of Cellular Uptake.* ACS Nano, 2013. **7**(3): p. 1961-1973.

170. Smith, B.R., et al., *Shape matters: intravital microscopy reveals surprising geometrical dependence for nanoparticles in tumor models of extravasation.* Nano Lett, 2012. **12**(7): p. 3369-77.

171. Discher, B.M., Y.Y., Won , D.S., Ege, J.C., Lee, F.S., Bates, D.E., Discher, D.A., Hammer., *Polymersomes: tough vesicles made from diblock copolymers.* Science, 1999. **14**(284): p. 1143-1146.

172. Albanese, A., P.S. Tang, and W.C. Chan, *The effect of nanoparticle size, shape, and surface chemistry on biological systems.* Annu Rev Biomed Eng, 2012. **14**: p. 1-16.

Objectives of the study

Post-menopausal osteoporosis is a chronic disease that affects majority of women in senescence. Selective estrogen receptor modulators (SERMs) are a class of drugs that are frequently prescribed in the prevention and treatment of post-menopausal osteoporosis. Presently, raloxifene hydrochloride is the only SERM that is marketed in the US and many countries for treatment and prevention of osteoporosis. However, there are two major drawbacks with this drug – poor oral bioavailability (~2%) and high inter-patient variability in the pharmacokinetic properties. Intestinal glucuronidation followed by excretion results in both the problems. Nanocarriers for oral delivery (solid lipid nanoparticles, nanostructured lipid carriers and polymeric nanocapsules) can protect the drug from intestinal degradation and also enhance the drug's bioavailability. The latter is possible because orally delivered nanocarriers can selectively access lymphatic system through endocytic uptake via M-cells and enterocytes in the intestine.

The important objectives of this study were:

1. To acquire physicochemical data about raloxifene hydrochloride that would assist in designing novel nanocarriers from both empirical studies and the literature.
2. To develop and validate suitable analytical and bioanalytical methods for accurate estimation of raloxifene hydrochloride in the formulation and other biological matrices (e.g. rat/rabbit plasma, urine and faeces).
3. To study the influence of different formulation and process variables on structure, size, surface charge, loading capacity and in-vitro drug release behaviour from the nanocarriers; to optimize the formulation using design of experiments (DOE) approach.
4. To carry out in-vivo pharmacokinetic evaluation and ex-vivo studies of selected nanocarrier formulations in suitable animal models.

Chapter 2

Drug Profile

2.0 Introduction

2.1 Raloxifene hydrochloride

Raloxifene hydrochloride (Fig. 2.1) is chemically methanone[6-hydroxy-2-(4-hydroxyphenyl) benzo[b]thien-3-yl]-[4-[2-(1-piperidinyl)ethoxy] phenyl] hydrochloride. Raloxifene hydrochloride occurs as off-white to pale-yellow solid powder that contains not less than 97.5 percent and not more than 102.0 percent of $C_{28}H_{27}NO_4S \cdot HCl$, calculated on the dried basis [1].

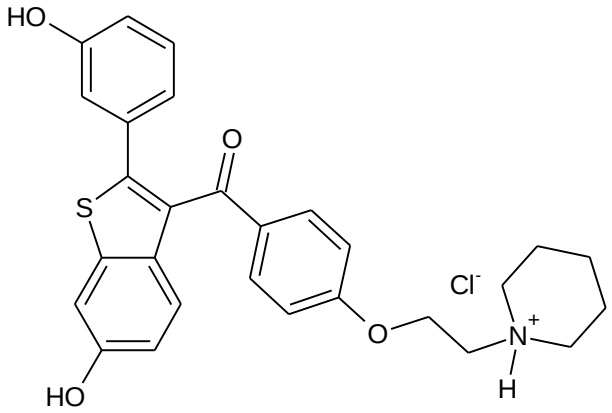

Fig. 2.1 Chemical structure of raloxifene hydrochloride

2.2 Physicochemical properties of raloxifene hydrochloride

Table 2.1: Physicochemical properties and drug information for raloxifene hydrochloride

Parameter	Description
Drug Name	Raloxifene hydrochloride
Category	Selective Estrogen Receptor Modulator (SERM)
Therapeutic class	Prevention and treatment of post-menopausal osteoporosis
Chemical class	Benzothiophenes
Chemical name	10-hydroxy-2-methyl-5-(1-methylethyl)-1-[2-(1-methylethyl)-4-thiazolyl]-3,6-dioxo-8,11-bis(phenylmethyl)-2,4,7,12-tetraazatridecan-13-oic acid, 5-thiazolylmethyl ester, [5S-(5R*,8R*,10R*,11R*)]
Chemical formula	$C_{37}H_{48}N_6O_5S_2$
Generic name	Raloxifene hydrochloride
Proprietary name	Evista
Proprietor	Eli Lilly and Company
CAS registry number	82640-04-8

Melting point	267.3-268.5 °C
Molecular weight	510.04
Water solubility	Very slightly soluble in water (less than 0.25 mg per Liter)
Physical state	Off-white to pale-yellow solid powder
Hydrophobicity (LogP and cLogP)	5.2 and 5.45
Ionization constant (pKa)	8.44, 9.12, 10.0 (extrapolated aqueous pKas')
pH of saturated raloxifene solution at 25ºC in water	4.5
Optical activity	Inactive
Hygroscopicity	Non-hygroscopic
Physical stability	Stable under room temperature
Photostability	Stable under normal conditions

2.3 Clinical Pharmacology

2.3.1 Mechanism of action

Raloxifene is a selective estrogen modulator that belongs to the chemical class of benzothiophenes. It has estrogen agonist effects on bone and lipid metabolism, and estrogen antagonist effect in uterine and breast tissues. Like estrogen, raloxifene's biological actions are mediated through high-affinity binding to estrogen receptors and regulation of gene expression. The binding results in differential expression of multiple estrogen-regulated genes in different tissues [2].

The classical estrogens, particularly estradiol enters the nucleus of the target organ cells and binds to series of inactive proteins called estrogen receptors (ER). The ER has two different isoforms, ERα (predominantly activating form) and ERβ, which inhibits the former. These proteins, after binding with estradiol transform with a different spatial configuration (E_2-ER) enabling them to simultaneously dimerize and subsequently interact with a specific sequence of DNA known as Estrogen Responding Element (ERE). Another specific group of genes that are responsible for synthesis of proteins that result in estrogenic activity on tissues like uterus and breast depend on the ERE for their action [2, 3].

Additionally, there are two specific areas in the ER that are known as Activation Factors (AF). The first AF, called AF-1 is located at the site of interaction with specific DNA sequence, and the second one, called AF-2 is located at the site where the ligands bind (Figure 2.2). For activation and protein synthesis (gene expression), the E_2 side-chain must interact with the AF-2 region. It is also known that ER does not have a single binding site, rather there are two separate binding sites: one for estrogens and another for anti-estrogens and SERMs like raloxifene (Figure 2.2). Therefore, depending on the binding site occupied, a compound may show complete estrogen agonist activity, partial estrogen agonist activity or estrogen antagonist activity [2, 3].

Thus, considering all these factors, it is currently believed that ER does not act in the same way on all the tissues. The actual action on a given tissue depends on – (a) the type of ER predominant in the given tissue (alpha or beta sub-type) (b) nature of the ligand binding to them (estrogen, anti-estrogen or SERM) (c) on the cell transcription machinery (ERE and AF) and (d) presence or absence of helper or regulating proteins [4-6]. Although this accounts for the varied action of raloxifene in different tissues (pure agonist action in tissues where ERα is predominant and pure antagonist action where ERβ is predominant), the precise mechanism of raloxifene still remains unknown [7-9].

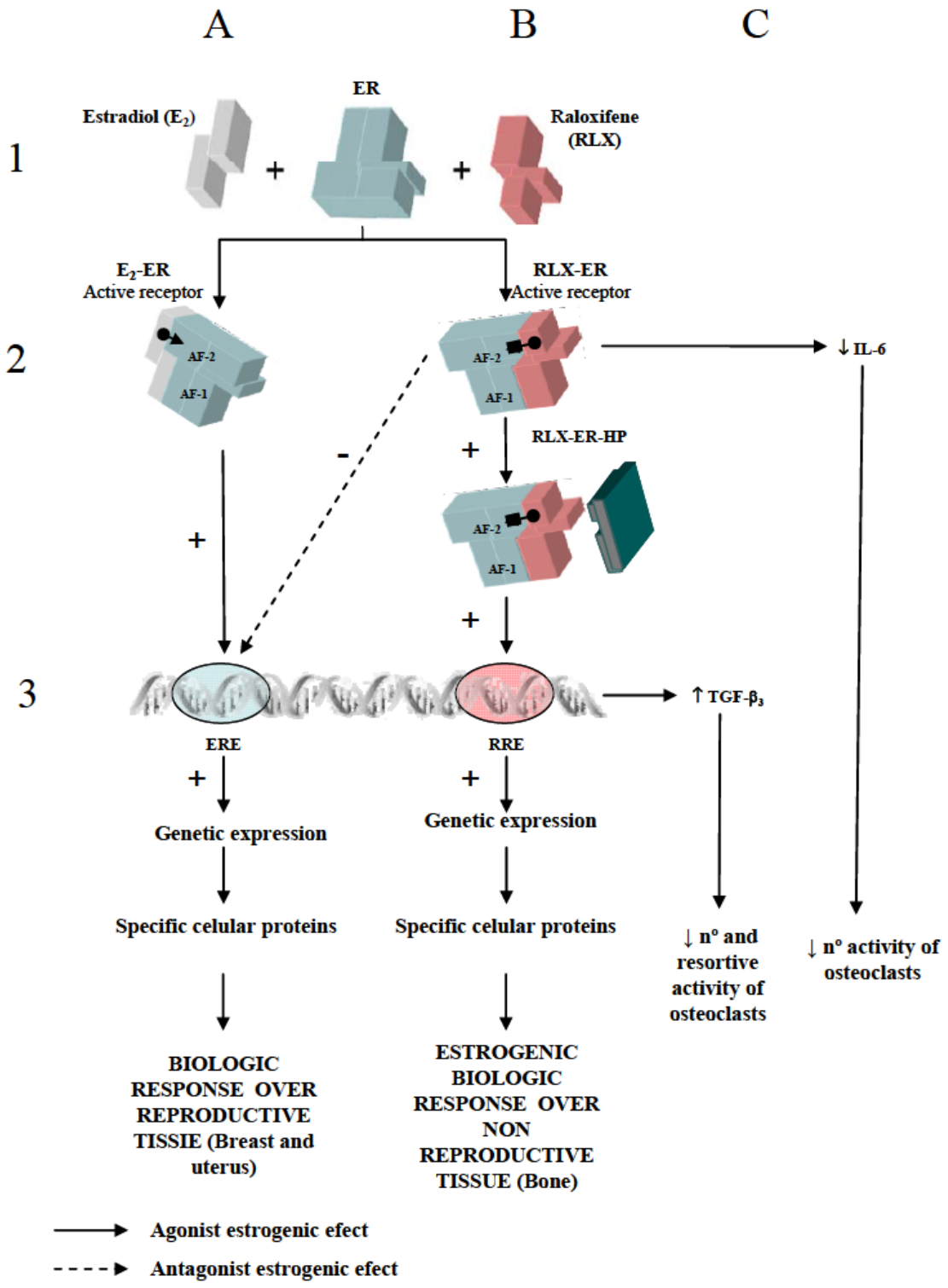

Fig. 2.2: Mechanism of action of raloxifene. Figure source: Rey, J.R., et al., *raloxifene : mechanism of action, effects on bone tissue, and applicability in clinical traumatology practice.* Open Orthop J, 2009. **3**: p. 14-21.

2.3.2 Pharmacodynamic activities of raloxifene

2.3.2.1 Effects on skeletal system

From adulthood to middle age, the bones undergo continuous remodelling process. The bone mass lost due to resorption is continually replaced by new bone formation, i.e. both bone loss and bone formation are balanced. Thus, in this period, the bone mass and volume remain relatively constant [10-13]. In women, ovarian estrogen is important to maintain this balance. Post oophorectomy or menopause, there is a marked reduction in estrogen levels and correspondingly, a marked reduction in the bone turnover. There is an accelerated bone loss that increases the risk of fracture. After menopause, the bone mass is lost rapidly because the compensatory bone remodelling is inadequate. This imbalance between bone resorption and bone turnover can be due to both reduction in estrogen and the aging osteoblasts.

Hormonal therapy with estrogen improves bone turnover and prevents osteoporosis by inhibiting the formation and actions of osteoclasts [11, 14, 15]. These effects on bone are marked by reduction in markers of bone turnover in plasma and urine and an increase in bone mineral density (BMD) [16, 17]. Raloxifene also increases BMD, but to a lesser extent as compared to estrogen. Further, raloxifene's ability to improve the osteoporotic condition is evidenced by a marked reduction in osteoporosis markers both in serum and urine [16].

2.3.4 Pharmacokinetics

Raloxifene shows high within-subject variability (30%) of most pharmacokinetic parameters as evident from the data in 292 women [18]. Table 2.1 summarizes the pharmacokinetic parameters of raloxifene.

Table 2.2: Summary of pharmacokinetic parameters of raloxifene in healthy postmenopausal women

	Cmax[a] (ng/mL)/ (mg/kg)	**t½ (hr)**	**$AUC_{0-\infty}$[a] (ng•hr/mL)/ (mg/kg)**	**CL/F (L/kg•hr)**	**V/F (L/kg)**
Single Dose					
Mean	0.50	27.7	27.2	44.1	2348
CV(%)	52	10.7 to 273[b]	44	46	52
Multiple Dose					
Mean	1.36	32.5	24.2	47.4	2853
CV(%)	37	15.8 to 86.6[b]	36	41	56

Abbreviations: Cmax = maximum plasma concentration, $t_{½}$ = half-life, AUC = area under the curve, CL = clearance,
V = volume of distribution, F = bioavailability, CV = coefficient of variation.
a data normalized based on dose in mg and body weight in kg
b range of observed half-life

Table source: Rey, J.R., et al., *raloxifene : mechanism of action, effects on bone tissue, and applicability in clinical traumatology practice.* Open Orthop J, 2009. **3**: p. 14-21.

2.3.4.1 Absorption

After oral administration, raloxifene is rapidly absorbed. Approximately, 60% of the oral dose is absorbed, but presystemic glucuronide conjugation is extensive. Absolute bioavailability of raloxifene is 2% [14]. The T_{max} and bioavailability of raloxifene are functions of systemic inter-conversion and enterohepatic cycling raloxifene and its glucuronide metabolites [14]. Absorption of raloxifene with a standard high-fat meal increases its aborption slightly, but does not provide clinically significant increase in bioavailability. Therefore, it can be administered without regards to meals [19].

2.3.4.2 Distribution

Following oral administration of a single dose (30 to 150 mg) the apparent volume of distribution is 2348 L/kg and is not dose dependent [14, 20]. Both raloxifene and its mono-glucuronide conjugate are highly bound to plasma proteins. The parent compound binds to both albumin and α1-acid glycoprotein but not to globulin that binds to other sex steroids [2].

2.3.4.3 Metabolism

Raloxifene undergoes extensive first-pass metabolism to glucuronide conjugates: raloxifene-4'-glucuronide, raloxifene 6-glucuronide and raloxifene-6, 4'-diglucuronide. Raloxifene is not metabolized by cytochrome P450 pathways. The unconjugated raloxifene comprises of less than 1% of the total administered raloxifene in plasma. The terminal log-linear portion of the plasma concentration curve for raloxifene and its glucuronide metabolites are usually parallel. This is consistent with inter-conversion of raloxifene and its metabolites [2, 5, 20-22]. Following intravenous administration, raloxifene is cleared from the body at a rate approximating hepatic blood flow. Apparent oral clearance of raloxifene is 44.1 L/kg.hr. Increasing the dose of raloxifene (from 30 to 150 mg) results in slightly less than a proportional increase in the area under curve (AUC) [1, 5, 20, 21, 23, 24].

2.3.4.4 Excretion

Raloxifene is primarily excreted in faeces, and negligible amount is excreted unchanged in urine [1, 21, 25]. Less than 6% of the dose is eliminated in urine as glucuronide conjugates.

2.3.4.5 Toxicity

Dose upto 600 mg/day was found to be safely tolerated for 8 weeks in 63 postmenopausal women [1]**.**

2.3.4.6 Special populations and conditions

a. Gender

Total extent of exposure and oral clearance (normalized to body weight) are not significantly different between male and female volunteers of the same age [25].

b. Race

There is no discernable difference in raloxifene's plasma concentration between Caucasians, Asians, Hispanics and Black population [1, 14]. However, the influence of race on pharmacokinetics of raloxifene is not fully evident as the study used small number of non-Caucasians [14].

c. Renal insufficiency

Since negligible amounts of raloxifene are eliminated in urine, there is no study available on pharmacokinetics of raloxifene in renal impaired patients. In patients with osteoporosis and a creatinine clearance as low as 21 ml/min, no change in pharmacokinetic parameters of raloxifene or its metabolites was noted [26].

d. Hepatic insufficiency

Pharmacokinetics of raloxifene was studied in patients with Class A cirrhosis with total serum bilirubin ranging from 0.6 to 2.0 mg/dl. In this case, the plasma concentration of raloxifene was 2.5 times higher than the control group and correlated with the increase in bilirubin concentrations [9, 14, 20]. However, in-depth safety and efficacy data for raloxifene in patients with hepatic insufficiency is unavailable.

2.3.5 Storage and stability

Store at temperature ranging from 15º to 30 ºC [1].

2.3.6 Dosage form, composition and packaging

Raloxifene hydrochloride is marketed as EVISTA and is available as 60 mg (equivalent to 55.71 mg free base) immediate release tablets for oral administration. Inactive ingredients in the tablet include anhydrous lactose, crospovidone, FD&C blue #2 aluminium lake colour, hydroxypropyl methylcellulose, lactose monohydrate, magnesium stearate, polysorbate 80, povidone, macrogol 400 and titanium dioxide E171 [1].

EVISTA 60-mg tablets are white, elliptical and film coated. They are imprinted with tablet code 4165 in blue ink on one side. It is available in blister package of 28 tablets.

2.3.7 Indications and clinical use

Raloxifene hydrochloride is indicated for: (1) The treatment of osteoporosis in postmenopausal women, (2) The prevention of osteoporosis in postmenopausal women and (3) As second line drug in treatment of breast cancer in postmenopausal women.

References:

1. *Electronic Package Insert: Evista® (raloxifene hydrochloride): Tablet for Oral Use.* 2011, Eli Lilly and Company: Lilly USA, LLC, Indianapolis, IN 46285, USA.

2. Rey, J.R., et al., *raloxifene : mechanism of action, effects on bone tissue, and applicability in clinical traumatology practice.* Open Orthop J, 2009. **3**: p. 14-21.

3. Hibner, M., et al., *Effects of raloxifene hydrochloride on endometrial cancer cells in vitro.* Gynecologic Oncology, 2004. **93**(3): p. 642-646.

4. Dogiparthi, A., et al., *Comparative evaluation of raloxifene versus estrogen: Progestin on symptomatology, endometrium, and lipid profile in postmenopausal women.* J Midlife Health, 2010. **1**(1): p. 14-8.

5. Clemett, D. and C.M. Spencer, *raloxifene : a review of its use in postmenopausal osteoporosis.* Drugs, 2000. **60**(2): p. 379-411.

6. Cranney, A. and J.D. Adachi, *Benefit-risk assessment of raloxifene in postmenopausal osteoporosis.* Drug Saf, 2005. **28**(8): p. 721-30.

7. Cosman, F., *Selective estrogen-receptor modulators.* Clinics in Geriatric Medicine, 2003. **19**(2): p. 371-379.

8. Dardes, R.C., et al., *Regulation of Estrogen Target Genes and Growth by Selective Estrogen-Receptor Modulators in Endometrial Cancer Cells.* Gynecologic Oncology, 2002. **85**(3): p. 498-506.

9. Snyder, K.R., N. Sparano, and J.M. Malinowski, *raloxifene hydrochloride.* Am J Health Syst Pharm, 2000. **57**(18): p. 1669-75; quiz 1676-8.

10. Heaney, R.P., *Is the paradigm shifting?* Bone, 2003. **33**(4): p. 457-65.

11. Hartke, J.R., *Preclinical development of agents for the treatment of osteoporosis.* Toxicol Pathol, 1999. **27**(1): p. 143-7.

12. Kleerekoper, M., *Prevention of postmenopausal bone loss and treatment of osteoporosis.* Semin Reprod Med, 2005. **23**(2): p. 141-8.

13. Peterson, G.M., et al., *Lasofoxifene: selective estrogen receptor modulator for the prevention and treatment of postmenopausal osteoporosis.* Ann Pharmacother, 2011. **45**(4): p. 499-509.

14. Hochner-Celnikier, D., *Pharmacokinetics of raloxifene and its clinical application.* Eur J Obstet Gynecol Reprod Biol, 1999. **85**(1): p. 23-9.

15. Messalli, E.M. and C. Scaffa, *Long-term safety and efficacy of raloxifene in the prevention and treatment of postmenopausal osteoporosis: an update.* Int J Womens Health, 2010. **1**: p. 11-20.

16. Delmas, P.D., et al., *Effects of raloxifene on bone mineral density, serum cholesterol concentrations, and uterine endometrium in postmenopausal women.* N Engl J Med, 1997. **337**(23): p. 1641-7.

17. Diab, T., et al., *Effects of the combination treatment of raloxifene and alendronate on the biomechanical properties of vertebral bone.* J Bone Miner Res, 2011. **26**(2): p. 270-6.

18. Wempe, M.F., et al., *Pharmacokinetics of raloxifene in male Wistar-Hannover rats: influence of complexation with hydroxybutenyl-beta-cyclodextrin.* Int J Pharm, 2008. **346**(1-2): p. 25-37.

19. Scott, J.A., C.C. Da Camara, and J.E. Early, *raloxifene : a selective estrogen receptor modulator.* Am Fam Physician, 1999. **60**(4): p. 1131-9.

20. Balfour, J.A. and K.L. Goa, *raloxifene* . Drugs Aging, 1998. **12**(4): p. 335-41; discussion 342.

21. Aronson, J.K., *raloxifene* , in *Meyler's Side Effects of Drugs: The International Encyclopedia of Adverse Drug Reactions and Interactions*, J.K.A. Editor: , Editor. 2006, Elsevier: Amsterdam. p. 3019-3021.

22. Blake, J., *Menopause: evidence-based practice.* Best Practice & Research Clinical Obstetrics & Gynaecology, 2006. **20**(6): p. 799-839.

23. Cohen, I.R., et al., *The reversible effects of raloxifene on luteinizing hormone levels and ovarian morphology in mice.* Reproductive Toxicology. **14**(1): p. 37-44.

24. Cosman, F., *Selective estrogen-receptor modulators.* Clin Geriatr Med, 2003. **19**(2): p. 371-9.

25. Archer, D.F., *The gynecologic effects of lasofoxifene, an estrogen agonist/antagonist, in postmenopausal women.* Menopause, 2011. **18**(1): p. 6-7.

26. Czock, D., et al., *raloxifene pharmacokinetics in males with normal and impaired renal function.* Br J Clin Pharmacol, 2005. **59**(4): p. 479-82.

Chapter 3

Analytical Method Development and Validation

3.1 Introduction

An accurate and precise analytical method is an integral part of formulation development and pharmacokinetic evaluation of dosage forms. An insensitive and inaccurate analytical method results in erroneous conclusions about the drug product. This is even truer in case of biological samples. The biological samples (e.g. plasma, serum, urine, faeces etc.) inherently contain proteins, fats and other biological material that interfere with the actual drug analysis. Therefore, it is obligatory that the analytical method developed must be selective towards the drug and should be able to resolve the drug peak from other junk peaks.

As an antecedent to formulation development, analytical method development and validation was undertaken. Though there are several methods described in the literature for the analysis of raloxifene hydrochloride in both drug product and biological samples, we developed and validated in-house methods that were customized to suit our needs. For analysis of raloxifene hydrochloride, both ultraviolet (UV) and high performance liquid chromatography (HPLC) methods were developed and validated.

3.2 Analytical methods for estimation of raloxifene hydrochloride

In the literature, several analytical methods have been described for estimation of raloxifene hydrochloride in a variety of study samples like the bulk, formulation and biological samples [1]. High performance liquid chromatographic (HPLC) methods [2-4] for detection and estimation of raloxifene hydrochloride in quality control studies have been reported. Many methods based on UV and visible spectrophotometry for determination of raloxifene hydrochloride with application in bulk drug and formulation analyses have also been reported [1, 5, 6]. A method for quantitative assay of raloxifene hydrochloride by capillary electrophoresis [7] and another method with resonance Rayleigh scattering using gold nanoparticle as a probe has been described [8].

Further, a HPLC method for estimation of raloxifene in rat plasma and its pharmacokinetic application has also been described [9]. In this method the lower limit of detection for the drug was reported as 200 ng/ml. Another bioanalytical method describes the procedure for estimation of raloxifene in human urine by LC-MS-MS with high sensitivity [10]. More recently, the pharmacokinetics of raloxifene hydrochloride in male Wistar–Hannover rats was studied and raloxifene and its glucuronide metabolites were simultaneously quantified using LC-MS [11].

Although it is indisputable that some of the earlier reported methods are sensitive and accurate, they mostly rely on the use of LC-MS technique that makes them expensive and involve many steps for sample preparation and processing. Only a few HPLC methods for analysis of raloxifene hydrochloride in plasma samples are reported, albeit with low sensitivity. Hence, there was a need for a sensitive, simple, rapid and cost effective analytical and bioanalytical method for quantification of raloxifene hydrochloride in the drug product and for pharmacokinetic evaluation of the developed drug product in suitable animal models. In the following section, the development and validation of in-house UV and HPLC methods are reported.

3.3 Materials

3.3.1 Chemicals and Reagents

Raloxifene hydrochloride was obtained as a gift sample from Apotex Research Pvt Ltd., Bangalore. HPLC grade ammonium acetate, glacial acetic acid and sodium citrate were purchased from Merck, Mumbai, India. HPLC grade acetonitrile and methanol were purchased from Sigma Aldrich, India. Milli-Q® water purification system (Millipore®, MA) was used to obtain high quality HPLC grade water.

3.3.2 Instruments

A double-beam Jasco (Jasco, Japan) UV-Visible spectrophotometer, model V570 connected to a computer loaded with Spectra Manager software was employed for development of spectrophotometric method development. The instrument had an automatic wavelength correction accuracy of 0.1 nm. Pair of matched quartz cells of 10 mm path length was used for holding the samples during analysis.

The liquid chromatography system employed was Shimadzu HPLC (Shimadzu, Japan) with solvent delivery system from binary pumps (Model LC-20AD, Prominence Liquid Chromatograph, Shimadzu, Japan), auto injector (Model SIL-20A HT, Prominence Auto Sampler, Shimadzu, Japan) and photo diode array (PDA) UV detector (Model SPD-M20A, Prominence UV Detector, Shimadzu, Japan). Data collection and integration was accomplished using LC Solutions, 1.25 version software.

Other instruments used in the method development and validation include vortex mixer (Model VX-200, Labnet International Inc., USA), sonicator (Model SONICA® 2200 MH, Soltec, Italy), refrigerated centrifuge (Model C-24 BL, Remi, India) and deep freezer (Model BFS-345-S, Celfrost Innovations Pvt. Ltd., India). pH meter (Model pHTestr 30, Eutech Instruments, Singapore) was used for measuring pH of all buffer systems used. Membrane filters of 0.22 µm (Millipore, USA) were used for filtration of aqueous phase of mobile phase system.

3.4 Method I: UV-Visible Spectrophotometric method for analysis of raloxifene hydrochloride

3.4.1 Spectrophotometric conditions

Absorption spectra were recorded from 190 to 800 nm at a speed of 400 nm/min with a 0.2 nm data interval, keeping 1 nm bandwidth. The quantitative analysis was carried out at a fixed wavelength (289 nm).

3.4.2 Preparation of stock and standard solutions

Selection of the solvent media was done based on the solubility data of raloxifene hydrochloride generated in-house and also based on the available literature. The primary stock of 100 µg/ml was prepared by dissolving 10 mg raloxifene hydrochloride in 100 ml of pure methanol. Subsequently, various concentrations, viz., 2.5, 5.0, 7.5. 10, 15, 20 and 25 µg/ml of raloxifene hydrochloride were prepared by transferring aliquots of stock solution into series of 10 ml standard flasks and making up the volume with a solvent media consisting of methanol: water (50:50 %v/v). On each day of validation, three separate series of seven calibration standards were prepared freshly and absorbance values were recorded at a wavelength of 289 nm against blank solvent system.

Formulations standards were prepared by adding known amount of drug to both the placebo tablet blend and blank nanoparticles at five levels 50, 75, 100, 125 and 150% of the labelled claim. Similarly, placebo standards were prepared without the addition of the drug. The standards were analysed at a wavelength of 289 nm.

3.4.3 Sample preparation

A quantity of the product, powdered tablets (Fiona® 60 mg tablets) or nanoparticles equivalent to 6 mg raloxifene hydrochloride were weighed and taken into a 100 ml

volumetric flask. In case of nanoparticles, the samples were subjected to ultrasonication using a probe sonicator (Vibra cell, Sonics, USA) for specific time period at fixed amplitude (30 W output). This helped in the digestion of nanoparticles and release of entrapped drug from the nanoparticle matrix. In all the cases, the volume was made up to 100 ml with the solvent system (methanol: water 50:50, %v/v), vortex mixed for 5 minutes and centrifuged (Remi, Mumbai, India) at 10, 000 rpm for 15 minutes. A clear supernatant was obtained in each case; 1 ml of the supernatant was transferred to 10 ml calibrated volumetric flasks and the volume as made with the solvent media.

3.4.4 Development of spectroscopic method

In the beginning, several solvent systems were studied to develop a selective and sensitive method for analysis of raloxifene hydrochloride from the formulations. The solvents/solvent systems were selected based on criteria like ease of sample preparation, analyte stability, preparation time, cost of sample processing and comprehensive applicability. The selection of wavelength was based on criteria like sensitivity, reproducibility, selectivity towards drug and robustness. Absorbance of raloxifene hydrochloride standard solutions was determined in selected media at the optimized wavelength and parameters like molar absorptivity, specific absorptivity and Sandell's coefficient were calculated using standard formulae. The robustness of the method was studied by accounting for variables like change in pH, buffer strength and composition of the solvent media. All the analyses were performed at an ambient temperature (25 ºC) after instrument stabilization for 15 minutes.

3.4.5 Spectroscopic method validation

The developed spectroscopic method was validated for selectivity, linearity, range, precision, accuracy and sensitivity. This method was also employed for analysis of raloxifene

hydrochloride from the commercial tablet formulation and the in-house nanoparticle formulations.

3.4.5.1 Selectivity

The selectivity of the method was determined using both placebo and drug-spiked placebo samples (formulation standards) of tablets and nanoparticles. To determine the variability, two sets of both placebo and formulation standards were prepared on three consecutive days (n = 3, at each level). Each day, one sample from each group was scanned for the absorption spectrum from 190 to 800 nm. The other sets were used to measure absorbance at 289 nm for the quantitative estimation of raloxifene hydrochloride. Obtained spectra were compared for the change in absorption profile with freshly prepared calibration standard spectrum. The mean absorbance at each level was compared using t-test at 95% significance level.

3.4.5.2 Linearity and range

For establishing linearity, a set of seven concentrations ranging from 2.5 to 25 µg/mL were analysed to establish the linearity range for the method. The least square linear regression analysis was performed on the calculated average absorbance values at each concentration level. The linear regression equation was used to calculate the corresponding predicted concentrations.

3.4.5.3 Accuracy and precision

To assess the accuracy of the method, drug-spiked placebo samples were used. Different recovery methods were tried individually for the tablets and nanoparticles. Two methods, viz. placebo-spiking method and standard addition method were used to determine the accuracy of the analytical method. In the placebo-spiking method, a known amount of

pure raloxifene hydrochloride standard at 50, 75, 100, 125 and 150% of the labelled claim of the individual drug product was added into the blank placebo mix. Similarly, in the standard addition method, formulations containing 50 and 100% of the labelled claim (60 mg) for individual drug products were added. On three consecutive days, each concentration was processed separately in six replicates and scanned for absorbance values. The mean absolute recovery from both the methods and percentage relative standard deviation (% RSD) and % bias was estimated.

Three quality control (QC) standards, lower (LQC = 2.5 µg/ml), middle (MQC = 10µg/ml) and higher (HQC = 25µg/ml) were evaluated to check the repeatability (intra-batch) and intermediate (inter-batch) precision of the method. Six series of three QC standards were freshly prepared and analysed on the same day and on three consecutive days to establish intra-batch and inter-batch precision.

3.4.5.4 Sensitivity

The sensitivity of the method was assessed by using seven calibration standards and was expressed as limit of detection (LOD) and limit of quantification (LOQ) for raloxifene hydrochloride. The LOD and LOQ were determined using standard deviation of intercept (σ) and slope (s) of the calibration curve. Following equations were used to determine LOD and LOQ values:

$$(1)\ LOD = \frac{3.3\sigma}{s} \qquad (2) LOQ = \frac{10\sigma}{s}$$

3.4.5.5 System precision and drug stability

To evaluate the precision of the instrument, ten freshly prepared calibration standards (5 µg/ml) were analysed in triplicates over the duration of 48 h. The same readings were

compared to evaluate the stability of raloxifene hydrochloride in the solvent medium under the selected test conditions.

3.4.5.6 Analysis of raloxifene hydrochloride in drug products

For tablet samples, twenty tablets (Fiona® 60 mg tablets) were individually weighed and pulverized using glass mortar and pestle. A quantity of powder blend equivalent to 6 mg raloxifene hydrochloride was accurately weighed and processed as described earlier. For the nanoparticle samples, freeze dried formulations equivalent to 6 mg raloxifene hydrochloride was accurately weighed and processed as described earlier. After appropriate dilution, the absorbance values were recorded at 289 nm using UV-Vis spectrophotometer.

3.4.6 Results and Discussion

3.4.6.1 Spectroscopic method development

The preliminary investigations showed no significant change at 289 nm in methanol and water. In different pH conditions (0.1 N HCl and 0.1 N NaOH), some variation in absorbance values for raloxifene hydrochloride were observed. However, this variation was minimal at a wavelength of 289 nm. Moreover, this wavelength provided sensitivity and high repeatability in absorbance values and hence was selected for all further studies. Additionally, at this wavelength, the method was highly selective for raloxifene hydrochloride and there was least interference from other excipients present in the drug products.

The molar absorptivity (l/mol.cm) at 289 nm was found to be 3.6×10^4 and the Sandell's sensitivity coefficient ($\mu g/cm^2$) in the selected solvent system (methanol: water, 50:50, v/v) was calculated as 0.0149×10^{-1}.

Thus, the selected wavelength proved meritorious in terms of superior sensitivity and repeatability with good selectivity towards raloxifene hydrochloride. The UV-visible spectrum of raloxifene hydrochloride is shown in Fig. 3.1.

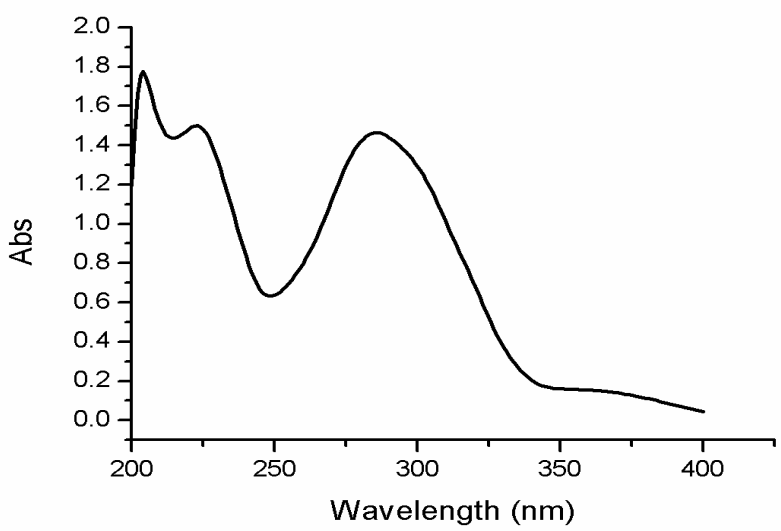

Fig. 3.1: UV absorption spectrum of raloxifene hydrochloride in 50:50 %v/v methanol: water

3.4.6.2 Spectroscopic method validation

The UV absorption spectrum of raloxifene hydrochloride in presence of placebo (tablet and nanoparticles) showed negligible interference. The formulation standards and test samples showed no significant change in the absorption spectrum when compared with calibration standards. The method resulted in consistently high recoveries (>95% of the spiked drug amount) at all the tested concentrations. The calculated t-values were lower than the critical t-values and there was no statistically significant difference between mean absorbance of the formulation and calibration standards. The data are presented in Table 3.1 below.

Table 3.1: Summary of data obtained from the UV-spectroscopic method development

S.No.	Parameter	Data Value
1.	Calibration Range	2.5 to 25 µg/ml
2.	Regression coefficient (R^2) of the calibration curve	0.9996
3.	Linear regression equation (y -Abs; x-conc. in µg/ml)	y = 0.0588x + 0.0129
4.	Confidence interval of slope [a] (at 0.05 significance level)	0.0550 to 0.0649
5.	Confidence interval of intercept [a] (at 0.05 significance level)	0.00874 to 0.0226
6.	Standard deviation of the intercept (σ)	0.00279
7.	Standard error of estimate [c] (µg/ml)	0.18234
8.	Limit of detection (LOD) (µg/ml)	0.160
9.	Limit of quantification (LOQ) (µg/ml)	0.475
10.	Absolute recovery of raloxifene hydrochloride	96.2 – 102.1 %
11.	Precision (% RSD) a. Repeatability (intra-batch) b. Intermediate precision (inter-batch) c. System precision (*n* = 10)	 3.41% 2.14 % 1.1 %
12.	Molar absorptivity (l/M.cm)	2.95×10^4
13.	Sandell's sensitivity (µg/cm^2)	0.149×10^{-1}
14.	Selectivity (resolution) wavelength	Selective at 289 nm

[a] When n < 30, Confidence Interval = $x \pm t_{\alpha/2} \times (\sigma/\sqrt{n})$, where, x = sample mean; σ = sample standard deviation; α = 0.05 and α/2 = 0.025; $t_{\alpha/2}$ = value from the t-table.

[b] calculated from intercept using the formula ($t_{df} = (C-\alpha)/\sigma$)

[c] calculated using the formula: $Std\ error\ of\ estimate = \sqrt{\frac{\sum y - y_{est}}{n}}$, where, y is actual value and y_{est} is the estimated value and n is the number of observations.

From the above table, it is evident that the proposed method demonstrates adequate sensitivity and selectivity within the selected range.

3.4.6.3 Linearity and range

From the least square regression analysis, a linear response was obtained over a range of 2.5 to 25 µg/ml with a regression coefficient (R^2) value of 0.9996. The best-fit linear

equation obtained was y = 0.0588x + 0.0129, where y is the absorbance (AU) and x is the concentration of raloxifene hydrochloride in µg/ml. Over the entire tested analytical range, the standard deviation and % RSD were low (< 5%). The selected model showed minimum bias with a low standard error of estimate (0.18234) indicating a goodness of fit. The absorbance values at individual concentration points are presented in Table 3.2 given below.

Table 3.2: Linearity of raloxifene hydrochloride by UV-Vis spectrophotometric estimation

Nominal concentrations (µg/ml)	**Average absorbance [a] ± standard deviation**	**RSD (%)**	**Back calculated concentrations (from the equation) (µg/ml)**	**Accuracy [b] (%)**	**Bias [c] (%)**
2.5	0.153 ± 0.002	1.63	2.38	95.31	4.69
5	0.309 ± 0.007	2.14	5.04	100.73	-0.73
7.5	0.467 ± 0.017	3.67	7.72	102.90	-2.90
10	0.607 ± 0.016	2.59	10.10	100.98	-0.98
15	0.898 ± 0.030	3.36	15.05	100.34	-0.34
20	1.215 ± 0.035	2.92	20.45	102.26	-2.26
25	1.473 ± 0.048	3.27	24.83	99.31	0.69

a Each value represents the average of six independent determinations (n = 6);

$b\ Accuracy = \frac{Back\ calculated\ conc}{Nominal\ conc}\ x\ 100$ $c\ Bias = \frac{Nominal\ conc - Back\ calculated\ conc}{Nominal\ conc}\ x\ 100$

3.4.6.4 Accuracy and precision

With the proposed method, the drug showed consistent and high absolute recoveries at all the tested concentration levels. The mean absolute recovery ranged from 96.2–102.1 %. From the placebo-spiking method results, it was evident that data was normally distributed around the mean and the %RSD was lower (< 3%) across all the concentration levels. Thus, it was concluded that there was no significant interference from the excipients during analysis.

Further, the method was found to be accurate with low % bias values (Table 3.3). The results of standard addition method collated well with the results from placebo-spiking method. In both the cases, the drug recovery from the placebo matrix was consistently higher. From

these studies, it was concluded that the proposed method could be used to analyse raloxifene hydrochloride without further modifications.

Table 3.3: Recovery studies by placebo-spiking and standard addition methods for UV-spectroscopic method

Drug products	Method	Amount of drug added [a] (% of label claim)	Mean Absolute Recovery ± SD (%)	% RSD	% Bias
Tablets	Placebo-spiking	50	98.10 ± 1.22	1.24	+1.90
		75	100.60 ± 2.24	2.22	-0.60
		100	99.45 ± 2.11	2.12	+0.55
		125	99.82 ± 0.92	0.92	+0.18
		150	100.27 ± 1.00	0.99	-0.27
	Standard addition [b]	50	99.62 ± 1.88	1.89	+0.38
		100	99.45 ± 1.93	1.94	+0.55
Nanoparticles	Placebo-spiking	50	99.09 ± 2.54	2.56	+0.91
		75	100.23 ± 1.51	1.51	-0.23
		100	100.50 ± 2.62	2.61	-0.50
		125	99.69 ± 1.64	1.64	0.33
		150	99.70 ± 1.68	1.69	0.30
	Standard addition [c]	50	100.42 ± 2.16	2.15	-0.42
		100	100.14 ± 1.46	1.45	-0.14

[a] Each level was processed independently and analysed in six replicates (n = 6); [b] Commercial tablet preparation containing powder equivalent to 60 mg raloxifene hydrochloride; [c] In-house nanoparticle formulation containing powder equivalent to 6 mg raloxifene hydrochloride.

Precision is repeatability of the data. When freshly prepared quality control (QC) standards (n = 6, at each level) were scanned for absorbance at 289 nm, they showed no significant variation in the measured response which demonstrated the repeatability of the data. This was confirmed by the low % RSD (< 3%) values. Lastly, the % RSD for inter-batch variability was significantly lower (< 2 %) further confirming the repeatability of the data. Table 3.4 gives a summary of recovery and precision data.

Table 3.4: Results of intra and inter-batch precision study for UV-spectroscopic method

QC Levels	Intra-batch precision						Inter-batch precision	
	Trial – 1		Trial – 2		Trial – 3			
	Mean [a] ± SD	% RSD	Mean [a] ± SD	% RSD	Mean [a] ± SD	% RSD	Mean ± SD	% RSD
LQC	2.50 ± 0.06	2.36	2.44 ± 0.07	2.81	2.49 ± 0.03	1.15	2.48 ± 0.03	1.30
MQC	9.92 ± 0.20	1.99	9.82 ± 0.29	2.96	10.08 ± 0.12	1.18	9.94 ± 0.13	1.32
HQC	24.40 ± 0.37	1.53	24.53 ± 0.60	2.45	24.98 ± 0.45	1.80	24.64 ± 0.30	1.24

[a] Each value is the average of six independent determinations

3.4.6.5 Sensitivity

The LOD and LOQ of the UV spectroscopic method were calculated as 0.16 and 0.475 µg/ml respectively. From table 3.1, it is evident that the slope has high magnitude and the standard error is low. Repeat analysis at LOQ demonstrated high mean recovery with lower % bias and % RSD values. Thus, the method was found to be accurate with high sensitivity with an ability to detect low concentrations of raloxifene hydrochloride.

3.4.6.6 System precision and drug stability

The repeatability test at a fixed concentration indicated very low variability in the response with a low % RSD (< 1%). Stability test for samples stored at room temperature (48 h) indicated no significant change in absorption values when compared to initial values indicating the stability of raloxifene hydrochloride in the selected solvent medium. Thus, the test samples could be stored at room temperature for at least 48 h without affecting the drug analysis.

3.4.6.7 Analysis of raloxifene hydrochloride in drug products

The mean recovery values were found to be in good agreement with the label claim of the drug products (tablets and nanoparticles). The recovery ranged from 96.2 – 102.1 % for both the drug products. There was no significant interference from the excipients in either of

the formulations. Therefore, the method was found suitable for analysis of raloxifene hydrochloride from both the drug products.

3.5 Method II: Analytical method development using HPLC

3.5.1 Instrument details

The liquid chromatographic system and other methods employed were same as that described under method I (analytical method development validation).

3.5.2 Chromatographic conditions

An endcapped C8 reverse phase analytical column (Zorbax SB-C8, 150 mm long and 4.6 mm internal diameter, particle size 5 µm, Agilent technologies, USA) was used for the study. Mobile phase consisted of 20 mM ammonium acetate buffer (pH adjusted to 4.5 with glacial acetic acid) and acetonitrile (63:37 v/v). The buffer was filtered through 0.22 µm Millipore® filtration membrane. The HPLC system was stabilized by running the mobile phase for 1 h at a flow rate of 1 ml/min prior to actual analysis. raloxifene hydrochloride was monitored at a wavelength of 289 nm with a mobile phase flow rate of 1 ml/min. The run time was fixed at 10 min and the injection volume was 50 µl.

3.5.3 Analytical method development using HPLC

In the analytical method, mobile phase composition, pH and other chromatographic conditions were optimized considering their effects on peak shape, tailing factor and retention time (RT). The stock solution, analytical standard and samples were prepared as explained earlier under UV-spectroscopic method development.

3.5.3.1 Calibration standards

Primary stock of raloxifene hydrochloride (1 mg/ml) was prepared by dissolving 10 mg of raloxifene hydrochloride in 10 ml of methanol and water pre-mix (50:50, %v/v). Secondary stock solutions of raloxifene hydrochloride (25, 50, 100, 250, 500, 750, 1000, 1500 ng/ml) and analytical quality control samples (LQC = 75 and 150, MQC = 600 and HQC = 1300 ng/ml) were prepared by making appropriate dilutions with the same solvent system.

3.5.4 Analytical method validation of the HPLC method

3.5.4.1 Selectivity

Selectivity was assessed using placebo of the drug products (tablets and nanoparticles) and absence of interference with the drug peak was evaluated using drug-spiked placebos. A similar sample processing method (as described earlier under UV-spectroscopic method validation section) was used to process the samples. Obtained chromatograms were compared with fresh calibration standards.

3.5.4.2 Linearity and range

For establishing linearity and range for the method, concentrations ranging from 25–1500 ng/ml were prepared and analysed. The average peak area (AUC) at each concentration level was calculated and plotted against individual concentration levels. Linear regression analysis was performed and a calibration equation was obtained that was used to calculate the predicted concentrations. One-way ANOVA was performed on each replicate response obtained for different concentration levels.

3.5.4.3 Accuracy and precision

As described earlier (under UV-spectroscopic method validation), recovery studies for the drug were carried out by placebo-spiking and standard addition methods. The spiked drug concentrations were same as that used for UV-spectroscopic method validation. Each concentration level was processed in six replicates on three different days (n = 18) and the results were expressed as mean recoveries, % RSD and % bias.

For determining the repeatability and precision of the analytical method, intra-batch and inter-batch variations were assessed. For the study, three QC standards, lower (LQC = 75 ng/ml), medium (MQC = 600 ng/ml) and high (HQC = 1300 ng/ml) were used. The precision was expressed as % RSD of the assay results. Repeatability (intra-batch) was assessed using six series of three QC standards that were freshly prepared. For inter-batch repeatability, similar QC standards were prepared and analysed on three consecutive days.

3.5.4.4 Sensitivity

Sensitivity of the analytical method was determined from standard deviation of the intercepts (σ) and mean of the slopes of the calibration curves (n = 18). The LOD and LOQ were calculated using the formulae described earlier under UV-spectroscopic method.

3.5.4.5 Analysis of raloxifene hydrochloride in drug products

raloxifene hydrochloride was quantified using the proposed method in drug products (marketed tablet formulation and in-house nanoparticle formulation). A similar procedure, as described under UV-spectroscopic method validation, was followed for preparation and processing of the samples. In all the cases, after processing, the final samples were collected and analysed using the proposed method. Injection volume was kept constant at 50 µl for all the samples.

3.5.5 Results and discussion

3.5.5.1 Optimization of chromatographic conditions

As raloxifene hydrochloride exhibits a basic character (pKa 8.44, 9.12 and 10.0) [12], it was hypothesized that acidic pH could improve the ionization efficiency of the drug. Therefore, pH of 4.5 was maintained and consequently, good separation of peaks in the column was obtained. The mobile phase composition was finalized after several trials with different solvent systems. It was found that, use of methanol with water or pH 4.5 ammonium acetate buffers caused peak broadening with substantial loss of peak area. A composition comprising of 63 parts of 20 mM ammonium acetate buffer (pH 4.5) and 37 parts of acetonitrile was found to be optimal for good separation and for obtaining a sharp peak of raloxifene hydrochloride.

Peak tailing was a major criterion for selection of the stationary phase. Initial trials with C18 columns of two different makes, (Phenomenex® C18, 250 mm long and 4.6 mm internal diameter, particle size 5 µm and Kromasil C18, 250 mm long and 4.6 mm internal diameter, particle size 5 µm) showed prominent peak tailing (tailing factor over 1.5). To solve the problem of peak tailing, approaches like addition of tri-ethyl amine to the solvent system, increase in buffer strength (from 10 mM to 20 mM of pH 4.5 ammonium acetate buffer) were attempted, however, without much success. It is reported in the literature [13] that tertiary amines with pKa > 9.0 are greatly affected by free silanol groups present in the column; use of a C18 endcapped column was an option to resolve peak tailing problem. However, C18 endcapped columns are much pricier than the regular C18 columns. As we intended to develop a cost effective method for regular analysis, it was excogitated to use a regular C8 column (Zorbax SB-C8, 150 mm long and 4.6 mm internal diameter, particle size 5 µm). The C8 column was selected based on the hypothesis that the peak tailing problem of

lipophilic drug raloxifene hydrochloride could reduce if the carbon chain length, and hence, the lipophilicity of the column could be reduced. Moreover, conventional C8 columns are less expensive than endcapped C18 columns.

With the C8 column, a statistically significant reduction in tailing factor from 1.67 ± 0.09 (C18 column) to 1.21 ± 0.03 (C8 column) [t_{cal} = 10.04 and t_{crit} = 4.30, α = 0.05 and df = 2] was observed. Further, a significant improvement [t_{cal} = 3839.67 and t_{crit} = 4.30, α = 0.05 and df = 2] in the Height equivalent to theoretical plates (HETP) values were also observed when C8 column (HETP value of 0.12 ± 0.005 mm) was used in place of C18 column (HETP value of 0.28 ± 0.01 mm).

Study of various parameters to check the robustness of the method, and their effect on the peak parameters yielded interesting results. It was observed that varying the mobile phase flow rate between 0.8 to 1.2 ml/min affected the area as well as the retention time of the drug (Fig. 3.2a). A flow rate of 1.0 ml/min was found optimum for the method.

Further, change in the mobile phase composition also affected retention time and the peak area (Fig. 3.2b). We found that decreasing the proportion of aqueous phase (20mM ammonium acetate buffer) yielded sharper peaks, albeit with lower retention times. The reverse was also true. A composition containing 50:50 (% v/v) of 20mM ammonium acetate buffer (pH 4.5) and acetonitrile showed a retention time of 3.05 minutes, whilst a composition containing 70:30 (% v/v) of the same solvent system showed retention time of 11.67 minutes. As we intended to develop a rapid method for analysis of raloxifene hydrochloride, a composition containing 63:37 (% v/v) of 20mM ammonium acetate buffer (pH 4.5) and acetonitrile was chosen as optimum. In this composition, the retention time was found to be 5.6 ± 0.12 min (for n = 6, 99% confidence interval between 5.45 and 5.75) with tailing factor of 1.12 ± 0.03 (for n = 6, 99% confidence interval between 1.083 and 1.157).

Varying the column temperature also affected the retention time and peak area of the drug. Based on the trials, an optimum column temperature of 40 ºC was selected for further trials.

The hydrogen ion concentration (pH) of the mobile phase was found to affect both peak separation and peak shape critically. It was found that, with decreasing pH values (from pH 6.8 to pH 4.5), the peak area increased and the retention time decreased (as the drug became more ionized at lower pH). The peak tailing was also found to decrease with decreasing pH (Fig. 3.2c). From these trials, a pH of 4.5 (ammonium acetate buffer, pH adjusted with glacial acetic acid) was found optimum as it yielded sharp chromatograms with tailing factor less than 1.5 and retention time of 5.6 minutes. Trials below pH 4.5 were not attempted as low pH could adversely affect the integrity of the stationery phase in long run.

The strength of buffer used in the method also affected retention time of the drug. Increasing buffer strength from 1 to 20 mM (ammonium acetate buffer) saw a decrease in RT values from 30 minutes (for 1mM buffer strength) to 5.6 minutes (for 20mM buffer strength). Buffer strength of 20mM ammonium acetate buffer was found optimum for the final method. Finally, effect of change in injection volume on peak area and peak shapes were examined. A linear increase in peak area was found when injection volume was increased from 25 to 100 µL.

Based on these results, the final optimum chromatographic conditions were for analysis of raloxifene hydrochloride were: mobile phase consisting 20 mM ammonium acetate buffer (adjusted to pH 4.5 with acetic acid) and acetonitrile in the ratio 63:37, v/v, flow rate of 1 ml/min, C8 analytical column and an operating temperature of 40 ºC.

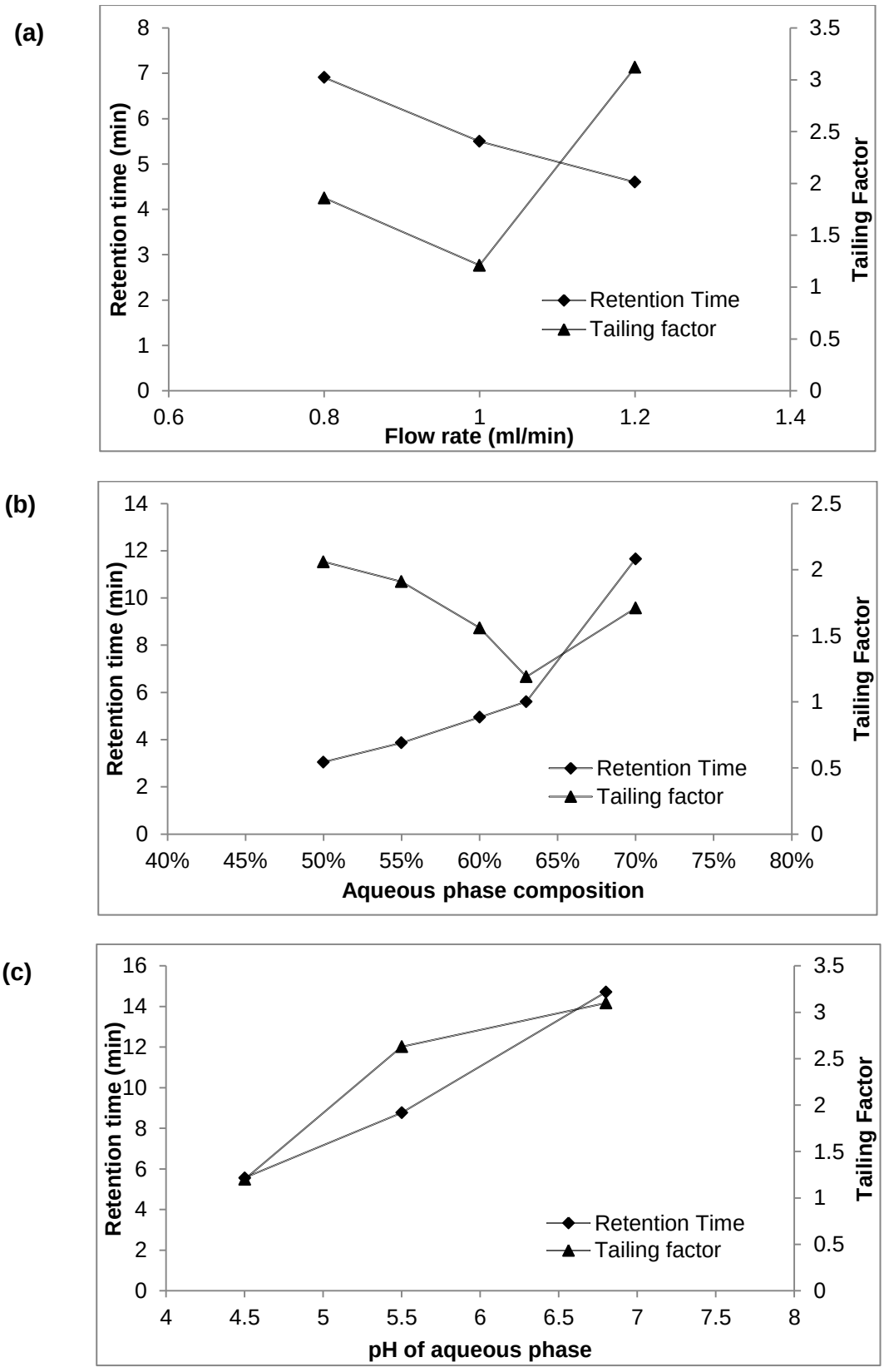

Fig. 3.2: Effect of chromatographic conditions on retention time and tailing factor of raloxifene hydrochloride

3.5.5.1 Selectivity

There was no interference from placebo samples in the vicinity of the drug peak. This indicated that the proposed method was selective towards raloxifene hydrochloride even in presence of formulation excipients (Fig. 3.3).

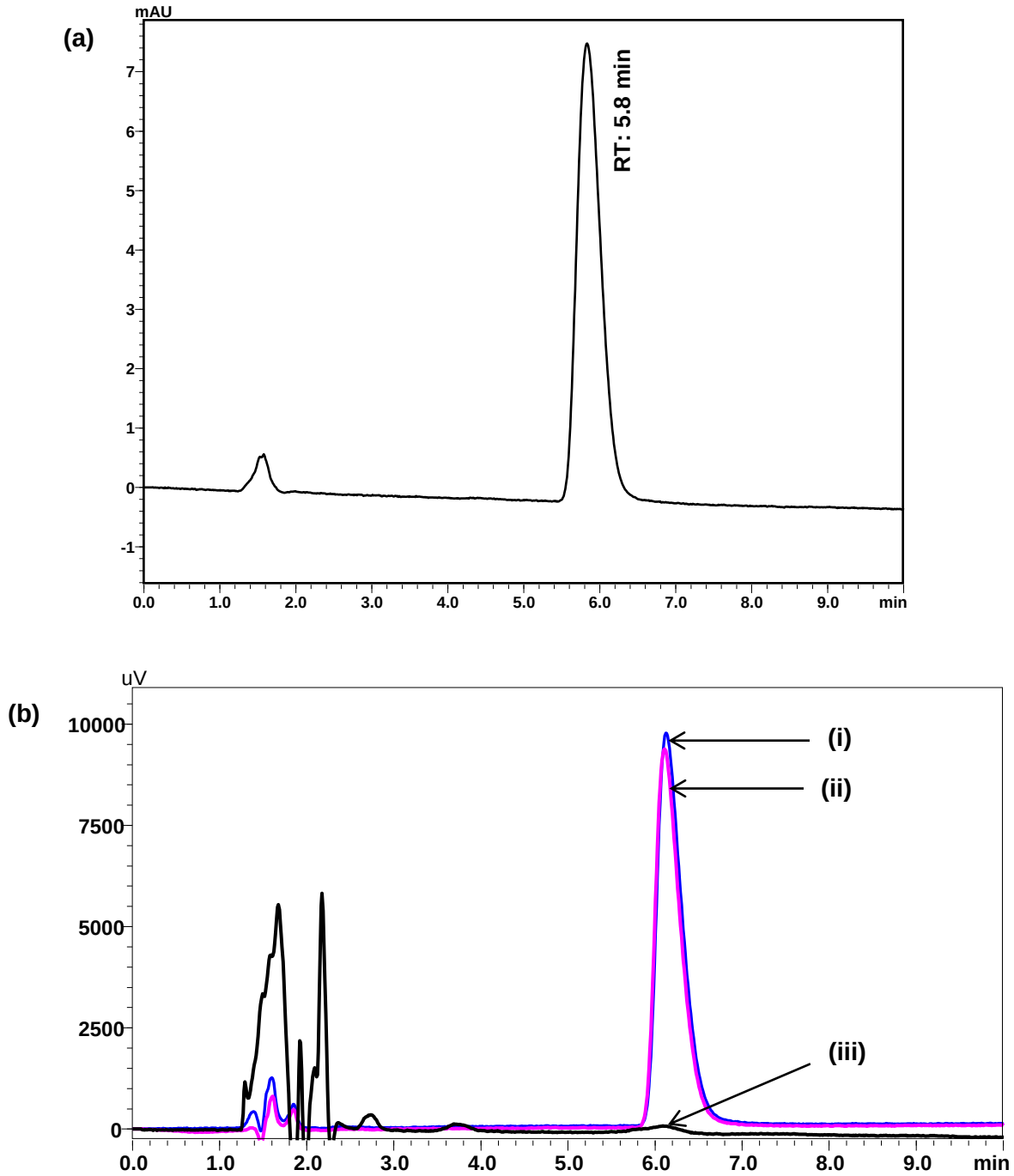

Fig. 3.3: Representative chromatograms of (a) Pure raloxifene hydrochloride (b) (i) raloxifene hydrochloride in in-house nanoparticle formulation (ii) raloxifene hydrochloride standard (1.2 µg/ml) and (iii) Nanoparticle placebo

3.5.5.2 Linearity and range

From the least square regression analysis, a linear response was obtained over a range of 25–1500 ng/ml with a regression coefficient (R^2) value of 0.9995. The best-fit linear equation obtained was y = 169.87x – 251, where y is the area (AUC) and x is the concentration of raloxifene hydrochloride in ng/ml. Over the entire tested analytical range, the standard deviation and % RSD were low (<5%). The selected model showed minimum bias with a low standard error of estimate indicating goodness of fit. The absorbance values at individual concentration points are presented in Table 3.5 given below.

Table 3.5: Linearity of raloxifene hydrochloride by chromatographic method

Nominal concentrations (ng/ml)	Average area [a] ± standard deviation	RSD (%)	Back calculated concentrations (from the equation) (µg/ml)	Accuracy [b] (%)	Bias [c] (%)
25	3590 ± 77	2.14	23.91	95.64	4.36
50	7433 ± 125	1.68	48.54	97.08	2.92
100	16288 ± 468	2.88	97.36	97.36	2.64
250	40361 ± 636	1.58	239.08	95.63	4.36
500	81193 ± 2089	2.58	479.45	95.88	4.11
750	124934 ± 1467	1.74	736.95	98.25	1.74
1000	171671 ± 1376	0.80	1012.08	101.20	-1.20
1500	255833 ± 2584	1.10	1507.53	100.50	-0.50

a Each value represents the average of six independent determinations (n = 6);

$$b\ Accuracy = \frac{Back\ calculated\ conc}{Nominal\ conc}\ x\ 100 \quad c\ Bias = \frac{Nominal\ conc - Back\ calculated\ conc}{Nominal\ conc}\ x\ 100$$

3.5.5.3 Accuracy and precision

With the proposed HPLC method, raloxifene hydrochloride showed consistent and high absolute recoveries at all the tested concentration levels. The mean absolute recovery ranged from 98.4–101.2 %. From the placebo-spiking method results, it was evident that there was normal distribution of data around the mean and the %RSD was lower (<3%)

across all the concentration levels. Thus, it was concluded that there was no significant interference from the excipients during analysis. Moreover, the method demonstrated a low % bias indicating the accuracy of the proposed method for analysis of raloxifene hydrochloride. In both the cases, recovery of drug from placebo matrices was consistently high. The recovery data is presented in Table 3.6.

Table 3.6: Recovery studies in HPLC method by placebo-spiking and standard addition methods

Drug products	Method	Amount of drug added [a] (% of label claim)	Mean Absolute Recovery ± SD (%)	% RSD	% Bias
Tablets	Placebo-spiking	50	96.98 ± 4.02	4.15	+3.02
		75	99.19 ± 4.04	4.03	-0.81
		100	99.08 ± 4.27	4.31	+0.92
		125	100.90 ± 4.71	4.67	-0.90
		150	100.71 ± 3.09	3.07	-0.71
	Standard addition [b]	50	99.13 ± 3.73	3.76	+0.87
		100	100.12 ± 2.19	2.19	-0.12
Nanoparticles	Placebo-spiking	50	97.94 ± 4.82	4.93	+2.06
		75	101.56 ± 4.76	4.68	-1.56
		100	99.76 ± 2.44	2.45	+0.24
		125	98.95 ± 4.02	4.06	+1.05
		150	100.16 ± 4.32	4.31	-0.16
	Standard addition [c]	50	101.60 ± 4.27	4.20	-1.60
		100	99.82 ± 3.18	3.19	+0.18

[a] Each level was processed independently and analysed in six replicates (n = 6); [b] Commercial tablet preparation containing powder equivalent to 60 mg raloxifene hydrochloride; [c] In-house nanoparticle formulation containing powder equivalent to 6 mg raloxifene hydrochloride.

Precision of the method was assessed using freshly prepared QC standards (n = 6, at each level). The results showed no significant variation in the measured response which demonstrated the repeatability of the data. This was confirmed by the low % RSD (< 3%) values. Moreover, the % RSD for inter-batch variability was also significantly lower (< 3 %) further confirming the repeatability of the data. Table 3.7 gives a summary of recovery and precision data.

Table 3.7: Results of intra- and inter-batch precision study by HPLC method

QC Levels	Intra-batch precision						Inter-batch precision	
	Trial – 1		Trial – 2		Trial – 3			
	Mean [a] ± SD	% RSD	Mean [a] ± SD	% RSD	Mean [a] ± SD	% RSD	Mean ± SD	% RSD
LQC (75 ng/ml)	73.57 ± 2.05	2.79	76.47 ± 2.22	2.81	79.47 ± 1.91	1.15	76.17 ± 3.46	4.54
MQC (600 ng/ml)	619.33 ± 17.67	2.85	623.13 ± 8.56	1.37	662.93 ± 7.83	1.18	635.13 ± 24.15	3.80
HQC (1300 ng/ml)	1345.30 ± 15.74	1.17	1324.30 ± 15.56	1.17	1344.73 ± 10.06	0.85	1344.78 ± 20.50	1.52

[a] Each value is the average of six independent determinations

3.5.5.4 Sensitivity

The LOD and LOQ values for the HPLC method were calculated as 9.33 and 28.28 ng/ml respectively. For practical purposes, the LOD and LOQ were considered as 10 and 30 ng/ml respectively. Repeat analysis at LOQ indicated high mean recovery with lower % bias and % RSD values. From these data, the method was found to be accurate, precise, sensitive and selective towards raloxifene hydrochloride.

3.6 Method III: Bioanalytical method development and validation using HPLC

The chromatographic conditions for the bioanalytical method were maintained similar to that of the analytical method. The method was validated as per regulatory guidelines in rabbit plasma.

3.6.1 Collection of Blood and Separation of Plasma

Blood samples were collected by marginal ear vein puncture of New Zealand white rabbits into microfuge tubes containing sodium citrate solution (3.8 %w/v) as an anticoagulant. The plasma was obtained by centrifuging the blood samples in a cooling centrifuge at 3400 rpm, 4 ºC for 10 min. The supernatant clear plasma was collected carefully and frozen at -20 ºC till further use.

3.6.2 Calibration Curve and Quality Control Standards

Primary stock of raloxifene hydrochloride (1 mg/ml) was prepared by dissolving 10 mg of raloxifene hydrochloride in 10 ml of acetonitrile and water pre-mix (1:1). Secondary stock solutions of raloxifene hydrochloride, analytical standards for studying the absolute recovery from 'plasma standards' (50, 100, 250, 500, 750, 1000, 1500 ng/ml) and analytical quality control samples for studying the absolute recovery of 'plasma quality control samples' (150, 600, 1300 ng/ml) were prepared by making appropriate dilutions in acetonitrile and water pre-mix (1:1).

Plasma calibration standards and plasma quality control samples were prepared by spiking 10 µl of appropriate standard solutions of raloxifene hydrochloride in 90 µl of drug-free rabbit plasma to obtain final concentrations of 50, 100, 250, 500, 750, 1000, 1500 ng/ml for calibration curve; same procedure was followed for 150, 600 and 1300 ng/ml which were considered as lower quality control (LQC), medium quality control (MQC) and higher quality control (HQC) samples respectively. Blank sample was prepared by spiking 10 µl of acetonitrile and water pre-mix (1:1) in 90 µl of blank plasma. All solutions were stored at 4 ^{o}C till further use.

3.6.3 Extraction Technique

A simple, single-step protein precipitation method was followed for extraction of raloxifene hydrochloride from rabbit plasma. 100 µl of drug spiked plasma sample was pipetted into a RIA vial; 150 µl of acetonitrile (protein precipitating solvent) and 50 µl of pH 4.5 ammonium acetate buffer were added to it. The sample was then vortex-mixed for 2 min. This was followed by centrifugation of samples at 10,000 rpm in 4 ^{o}C for 20 min. From the centrifuged samples, 250 µl of the clear supernatant was transferred to a sample loading vial and injected into the HPLC system.

3.6.4 Bioanalytical method development

For mobile phase optimization, various buffers of different pH and in varying proportions with acetonitrile and methanol were investigated. Optimization of mobile phase consisting of aqueous phase (20 mM ammonium acetate) and acetonitrile (63:37 v/v) was based on peak properties (retention time, tailing factor and asymmetric factor) and sensitivity (height and area), ease of preparation and applicability of the method for in vivo studies in rabbits.

3.6.5 Validation of the bioanalytical method

The developed method was validated according to standard guidelines [14] and suitable statistical tests were performed to test the significance of results obtained. Selectivity was established by comparing six different lots of drug-free rabbit plasma samples and raloxifene hydrochloride spiked plasma samples. Calibration curves were constructed from blank sample and seven non-zero samples ranging from 50 ng/ml to 1500 ng/ml. Linearity of the method was assessed by plotting peak area against the nominal concentrations of raloxifene hydrochloride. Calibration curves were fitted using unweighted linear regression analysis. Precision and accuracy were determined across the three quality control (QC) samples, LQC (150 ng/ml), MQC (600 ng/ml) and HQC (1300 ng/ml). Intra-day precision and accuracy were assessed by replicate analysis (n = 3) twice in a day at each QC levels. Inter-day precision and accuracy were determined by replicate analysis of the same QC samples on three different days (n = 18). The %RSD was calculated from the predicted concentration obtained by regression equation.

Sensitivity was assessed by determination of lowest limit of quantification (LLOQ), the minimum quantifiable concentration with less than 20% RSD. The quantification limit and detection limit were also determined using standard deviation of response and the slope

of calibration curve obtained from the linear regression analysis [14]. Recovery of the drug was determined at all concentration levels (including the three QC levels) in triplicate by comparing the peak area obtained from plasma (extracted) samples with analytical standard (unextracted) samples at the same nominal concentration.

The stability of raloxifene hydrochloride was evaluated under three different stress conditions: three freeze and thaw cycles, long-term storage up to 15 days at -20 ºC and post extraction storage in an auto injector up to 24 h. Stability was determined by triplicate analysis of LQC, MQC and HQC samples in each of the above conditions. The percentage deviation from the mean concentrations observed at zero time was calculated. The stability of raloxifene hydrochloride stock solution was also established by storing it at room temperature for a period of 24 h and comparing the response for 1000 ng/ml solution prepared from this stock solution (after 24 h storage period) against the same concentration prepared using a fresh stock solution.

3.6.6 Pharmacokinetic Application

Raloxifene hydrochloride formulation for intravenous (IV) bolus administration was prepared by dissolving the drug in optimized solvent mixture of ethanol and water just before the commencement of study. Formulation was administered through marginal ear vein in female New Zealand white rabbits (n = 3), weighing 2.2 to 2.5 kg, at a dose of 10 mg/kg. Blood samples were drawn from marginal ear veins at 5, 15, 20, 30, 45, 60, 150, 360 and 480 min post dose in microfuge tube pre-treated with sodium citrate solution (3.8% w/v). A baseline blank plasma sample was drawn from each animal before drug administration. All samples were processed according to the procedure described earlier and analysed using the validated HPLC method. Various pharmacokinetic parameters were calculated from measured raloxifene hydrochloride plasma concentrations verses time profiles after IV bolus

administration using non-compartmental model and compartmental models in WinNonlin Professional software (Version 4.0, Pharsight Corporation, USA).

3.7 Results and Discussion

3.7.1 Method Validation

3.7.1.1 Selectivity

Simple and efficient one-step precipitation technique was used to separate raloxifene hydrochloride from rabbit plasma. The technique was found to be suitable and selective for estimation of raloxifene hydrochloride from bio-matrix with no interference from endogenous protein impurities which is evident from overlaid chromatograms of blank plasma, in vivo test sample and plasma calibration standard (Fig. 3.4).

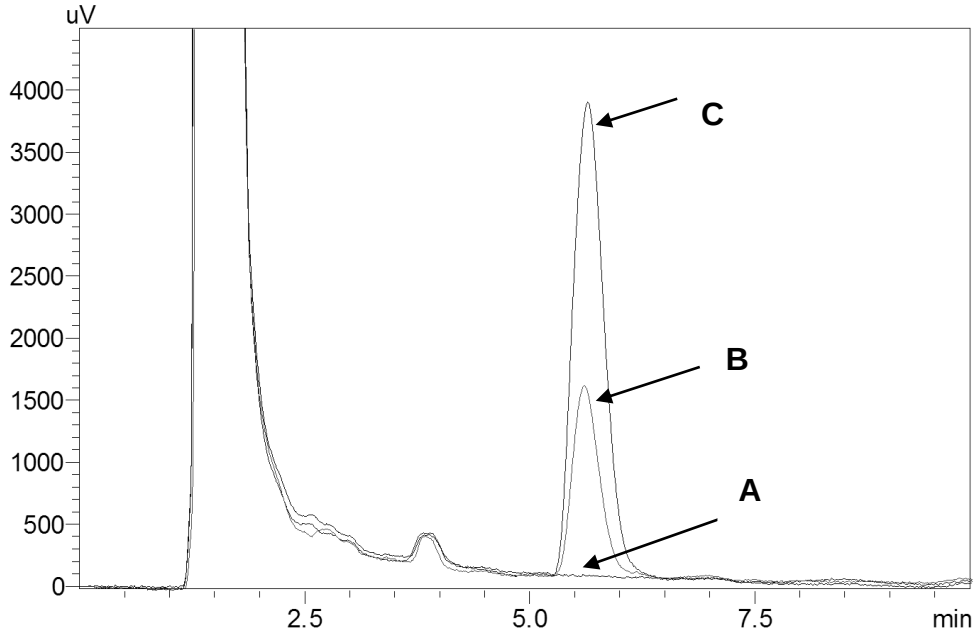

Fig. 3.4: Overlaid chromatograms of (A) blank plasma, (B) in-vivo test sample and (C) plasma calibration standard (1000 ng/ml)

3.7.1.2 Linearity

Calibration curve was linear in the selected concentration range of 50 ng/ml to 1500 ng/ml. At all the concentration levels, %RSD values did not exceed 5.11. According to linear regression analysis, the slope (± standard error) and intercept (± standard error) were found to be 57.8 (± 1.9) and -150.6 (± 170.3) respectively with a regression coefficient value of 0.996. Lower F_{cal} value of 1.66×10^{-2} in comparison to F_{crit} (8, 63) value of 2.08 at $p < 0.001$, further confirmed precision of the proposed method.

3.7.1.3 Accuracy

All three quality control samples (LQC = 150 ng/ml, MQC = 600 ng/ml and HQC = 1300 ng/ml) showed an accuracy ranging from –2.20% to 2.11% with maximum %RSD of 2.36 across the entire QC range, establishing the accuracy of method for raloxifene hydrochloride estimation in rabbit plasma (Table 3.8).

Table 3.8: Accuracy and absolute recovery data for the proposed method in plasma by HPLC method

QC Level	Predicted concentration[a] (ng/ml)			Mean accuracy[e] (%)	Recovery	
	Range	Mean[b] ± SD[c]	%RSD[d]		% Mean recovery[f] ± SD[c]	%RSD[d]
LQC (150 ng/ml)	149.18 – 160.52	153.17 ± 3.62	2.36	2.11	98.15 ± 1.06	1.08
MQC (600 ng/ml)	588.60 – 598.80	592.83 ± 3.43	0.57	-2.20	98.27 ± 0.59	0.60
HQC (1300 ng/ml)	1289.73 – 1301.49	1295.42 ± 3.92	0.30	-1.46	99.92 ± 0.16	0.16

[a]Each value is mean of six independent determinations ($n = 6$); [b]Predicted concentration of raloxifene hydrochloride was calculated by linear regression equation. [c]Standard deviation; [d]Percentage relative standard deviation; [e]Accuracy is given in relative error % = [100 × (predicted concentration – nominal concentration)/nominal concentration.)]; [f]Percent drug recovery = [(Peak area of plasma standard/peak area of analytical standard of same concentration) ×100].

3.7.1.4 Precision

In repeatability study, the %RSD ranged from 0.30 to 2.39 across all QC samples (Table 3.9). The %RSD values for intra-day variation were not more than 2.39 and for inter-day variation were less than 2.36 (Table 3.9). Acceptable %RSD values indicated the repeatability and intermediate precision of the method.

Table 3.9: Results of intermediate precision study in rabbit plasma by HPLC method

Level	Intra-day repeatability (%RSD[a]) (*n* = 3)			Inter-day repeatability (%RSD[a]) (*n* = 18)
	Day-1	Day-2	Day-3	
LQC	2.39	2.31	2.39	2.36
	2.13	2.10	2.12	
MQC	0.58	0.82	0.52	0.58
	0.95	0.74	0.54	
HQC	0.37	0.42	0.35	0.30
	0.45	0.63	0.30	

[a]Percentage relative standard deviation

3.7.1.5 Quantification limit

The mean percentage accuracy of six independent samples of 50 ng/ml, calculated against linear regression equation was found to be 97.72 with %RSD value of 5.11. The quantification limit and detection limit determined using standard deviation of response and the slope calibration curve were found to be 45.78 ng/ml and 15.11 ng/ml respectively. Hence, LLOQ of 50 ng/ml was considered to be reliable, reproducible and accurate for the proposed method.

3.7.1.6 Recovery

The absolute recovery of raloxifene hydrochloride from the spiked rabbit plasma samples, when compared with analytical standards of same concentration, was within 98.1% to 99.8% with %RSD less than 1.08 at each of the concentration levels. The high (nearly 100%) mean per cent recovery values (Table 3.8) precludes the use of internal standard in the method. Low %RSD values (%RSD < 5.0) established the extraction efficiency of selected solvent for precipitation. The mean per cent recovery and %RSD values of raloxifene hydrochloride form spiked plasma samples at the three QC levels are shown in Table 3.8.

3.7.1.7 Stability

The stability of raloxifene hydrochloride in rabbit plasma was evaluated using QC samples under different stress conditions and the results obtained are shown in Fig. 3.5 (a – c). In freeze thaw stability, no significant degradation of raloxifene hydrochloride was observed up to three cycles over a period of three days. The deviation from the zero time concentration was found to be between -1.73% and 1.62% at the end of three freeze thaw cycles as shown in Fig. 3.5a raloxifene hydrochloride was found to be stable for a period of 24 h in the post-preparative study of processed samples kept in the auto sampler. The deviation from the zero time concentration was found to be between -1.43% and 1.02% as shown in Fig. 3.5b. In long-term stability studies, raloxifene hydrochloride was found stable for 28 days when stored at –20 ºC. The deviation in recoveries of raloxifene hydrochloride after analysis at 7, 14, 21 and 28 days of sample preparation were found to be within acceptable limits. Results of this study indicate that storage temperature of -20 ºC was adequate for storing the samples for at least 28 days. The deviation from the zero day concentration was found to be between -1.28% and 0.64% as shown in Fig. 3.5c. The areas obtained for both the samples (prepared from fresh stock solution and stock solution stored at

room temperature for 24 h) were found to be nearly same with a deviation of -0.10%. Hence, it was concluded that stock solution was stable at room temperature for a period of 24 h.

3.7.1.8 Pharmacokinetic Application

The developed and validated HPLC method for raloxifene hydrochloride estimation in rabbit plasma was applied to pharmacokinetic study after IV bolus administration of raloxifene hydrochloride solution in rabbits. The mean plasma concentration versus time profile of raloxifene hydrochloride following IV administration is given in Fig. 3.6. The time course of plasma drug concentration was found to follow a bi-exponential equation, Concentration = $9473.92\ e^{-0.0457t} + 602.75\ e^{-0.0012t}$ with a good correlation coefficient (R^2 = 0.9967) indicating that the drug follows two compartment open model in rabbits.

The pharmacokinetic parameters obtained from the study using non-compartmental and compartmental were area under the curve (AUC) = 589550.73 ± 3879.24 min ng/ml, mean retention time (MRT) = 299.01 ± 10.17 min, concentration at time zero (C_o) = 10076.68 ± 502.63 ng/ml, volume of distribution (V_{ss}) = 19095.71 ± 256.44 ml, elimination rate constant from central compartment (K_{10}) = 0.0144 ± 0.001 per min, distribution rate constant from central to peripheral compartment (K_{12}) = 0.0286 ± 0.002 per min, distribution rate constant from peripheral to central compartment (K_{12}) = 0.0039 ± 0.0003 per min, total plasma clearance (Cl_s) = 35.77 ± 2.01 ml/min and volume of distribution (V_{ss}) = 19095.71 ± 479.85 ml.

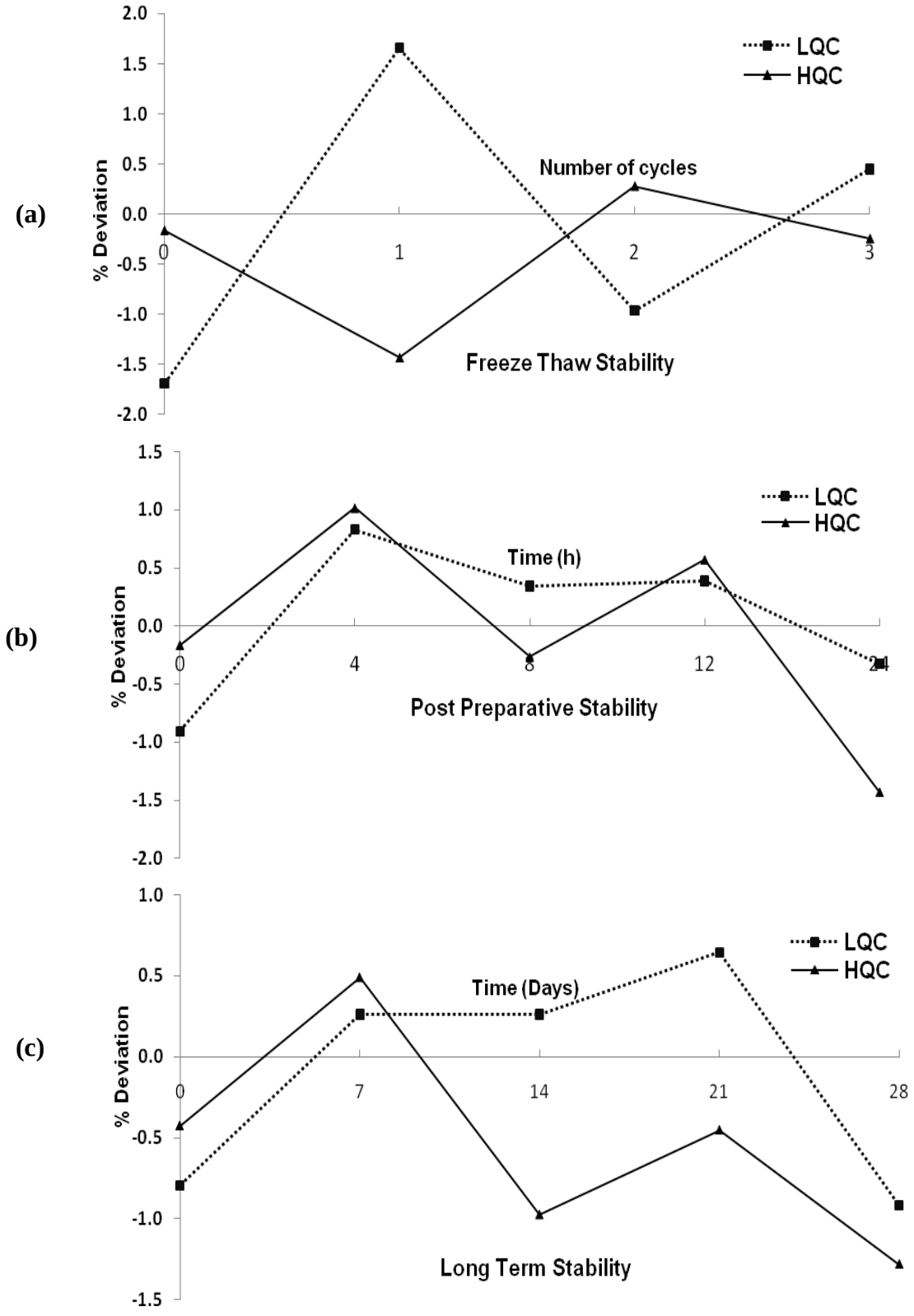

Fig. 3.5: Stability study of raloxifene hydrochloride in rabbit plasma (a) Freeze thaw stability; (b) Post preparative stability; (c) Long term stability. Each point represents mean of three independent determinations.

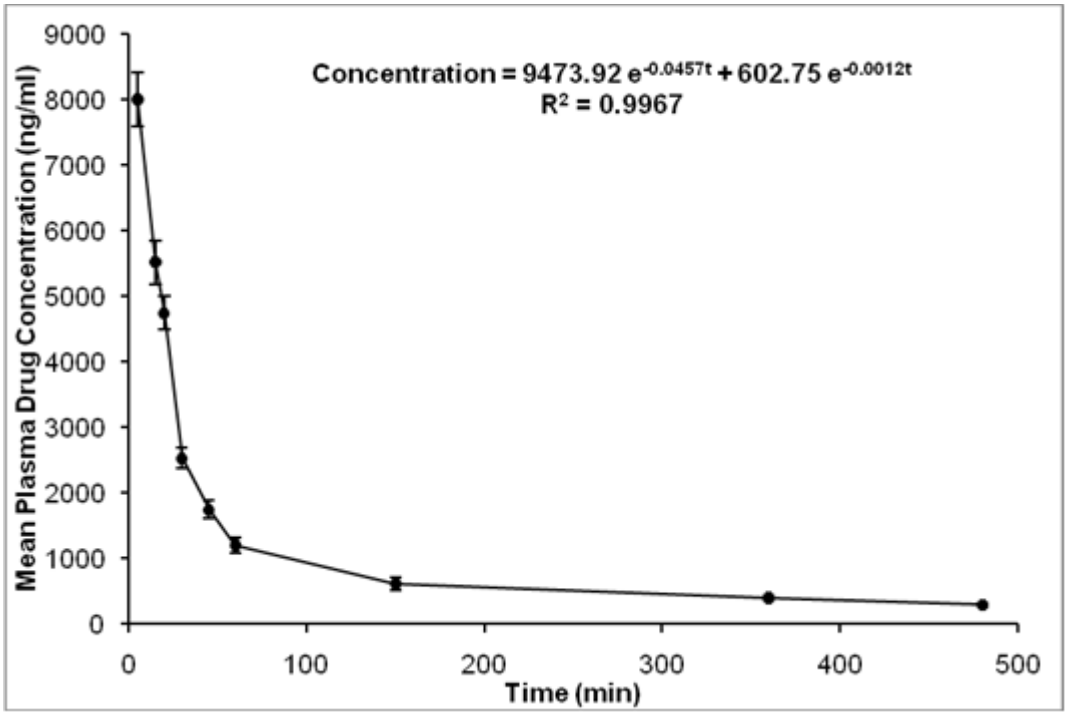

Fig. 3.6: The mean plasma concentration versus time profile of raloxifene hydrochloride in rabbits after IV bolus administration of the drug (10 mg/kg, *n* = 3)

3.7.2 Partial validation of analytical method for estimation of raloxifene hydrochloride in various biological matrices from rats

The bioanalytical method was initially developed and validated for estimation of raloxifene hydrochloride in rabbit plasma. However, due to practical reasons, female Wistar rat was chosen as an animal model for all future pharmacokinetic and pharmacodynamic evaluations. Therefore, it is prudent that this method should be partially validated to understand its applicability in analysing raloxifene from biological samples of rat origin.

Partial validation was done in rat biological matrices like rat plasma, rat faeces, tissue matrices sand bone marrow. Method was validated for: selectivity, accuracy and quantification limit. The data is presented in Table 3.10.

Table 3.10: Accuracy and absolute recovery data for the proposed method in different biological matrices by HPLC method

Biological matrix	QC Level	Predicted concentration[a] (ng/ml)			Mean accuracy[e] (%)	Recovery	
		Range	Mean[b] ± SD[c]	%RSD[d]		% Mean recovery ± SD[c]	%RSD[d]
Rat plasma	**MQC (600 ng/ml)**	578.22 – 596.41	588.98 ± 7.79	1.32	-1.83	96.34 ± 2.09	2.17
Rat liver		567.40 – 595.20	583.11 ± 11.17	1.91	-2.81	95.80 ± 3.14	3.28
Rat spleen		575.40 – 603.71	590.10 ± 11.57	1.96	-1.65	97.21 ± 2.84	2.93
Rat lungs		584.82 – 624.21	607.46 ± 16.62	2.73	1.24	98.38 ± 4.21	4.28
Rat kidneys		578.31 – 593.52	584.33 ± 6.59	1.13	-2.61	96.41 ± 3.8	3.94
Rat faeces		606.5 – 633.4	617.41 ± 11.56	1.87	2.90	98.52 ± 4.28	4.34
Rat bone marrow		570.23 – 593.41	584.27 ± 10.09	1.72	-2.62	95.42 ± 4.86	5.09

[a]Each value is mean of six independent determinations (n = 6); [b]Predicted concentration of raloxifene hydrochloride was calculated by linear regression equation. [c]Standard deviation; [d]Percentage relative standard deviation; [e]Accuracy is given in relative error % = [100 × (predicted concentration – nominal concentration)/nominal concentration.)].

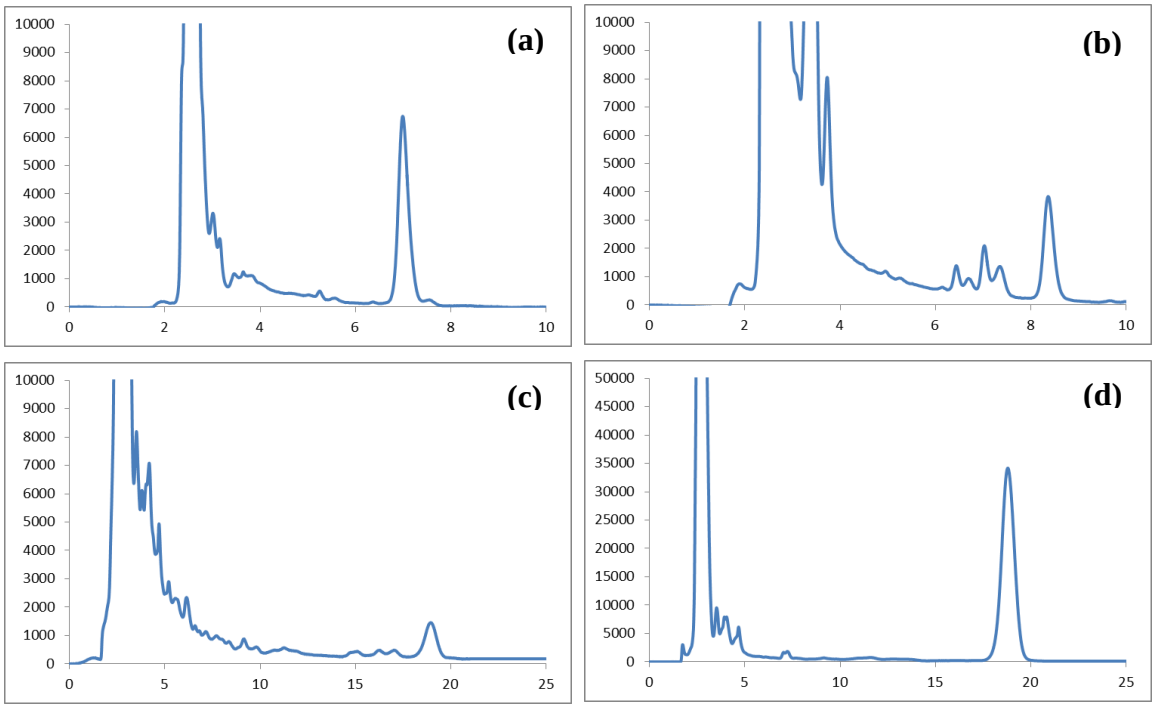

Fig 3.7: Representative chromatograms of raloxifene hydrochloride in: (a) rat plasma matrix (b) rat faeces (c) rat spleen matrix and (d) rat liver matrix

3.7.3 Conclusion

The developed and validated method for estimation of raloxifene hydrochloride in rabbit plasma was found to be rapid, precise, specific, reproducible and cost effective. Recovery of raloxifene hydrochloride from plasma samples by protein precipitation technique using acetonitrile was found to be efficient with nearly complete recovery. In addition, the drug was found to be stable under various processing and storage conditions. The method allows high sample throughput due to simple procedure for sample preparation and relatively short run time. The method was successfully employed in determining the pharmacokinetic parameters of the drug following IV bolus administration in rabbits. Further, partial validation for the method was performed in various biological matrices. The results indicated that the method was selective and accurate in determining raloxifene hydrochloride in different biological matrices. No significant *matrix effect* was evident across species (rabbit and rat) while analysing the drug.

References

1. Pavithra, D. and L. Sivasubramanian, *New spectrophotometric determination of Raloxifene hydrochloride in tablets.* Ind J Pharm Sci, 2006. **68**(3): p. 375-376.

2. Basavaiah, K., U.R. Anil Kumar, and K. Tharpa, *Gradient HPLC analysis of raloxifene hydrochloride and its application to drug quality control.* Acta Pharm, 2008. **58**(3): p. 347-56.

3. Yang, Z., X. He, and Y. Zhang, *The determination of raloxifene in rat tissue using HPLC.* Biomed Chromatogr, 2007. **21**(3): p. 229-33.

4. Trontelj, J., et al., *HPLC analysis of raloxifene hydrochloride and its application to drug quality control studies.* Pharmacol Res, 2005. **52**(4): p. 334-9.

5. Basavaiah, K., et al., *Optimized and validated spectrophotometric methods for the determination of raloxifene in pharmaceuticals using permanganate.* Arch Pharm Res, 2009. **32**(9): p. 1271-9.

6. Basavaiah, K., et al., *Validated spectrophotometric methods for the determination of Raloxifene hydrochloride in pharmaceuticals.* J Chil Chem Soc, 2008. **53**: p. 1635-1639.

7. Perez-Ruiz, T., et al., *Development and validation of a quantitative assay for raloxifene by capillary electrophoresis.* J Pharm Biomed Anal, 2004. **34**(5): p. 891-7.

8. Liu, S.P., et al., *Resonance Rayleigh scattering spectral method for the determination of raloxifene using gold nanoparticle as a probe.* Anal Chim Acta, 2007. **598**(2): p. 304-11.

9. Yang, Z.Y., et al., *Validation of a Novel HPLC Method for the Determination of Raloxifene and Its Pharmacokinetics in Rat Plasma.* Chromatographia, 2007. **65**(3-4): p. 197-201.

10. Trdan, T., et al., *Determination of raloxifene and its glucuronides in human urine by liquid chromatography-tandem mass spectrometry assay.* J Chromatogr B Analyt Technol Biomed Life Sci, 2011. **879**(23): p. 2323-31.

11. Wempe, M.F., et al., *Pharmacokinetics of raloxifene in male Wistar-Hannover rats: influence of complexation with hydroxybutenyl-beta-cyclodextrin.* Int J Pharm, 2008. **346**(1-2): p. 25-37.

12. Teeter, J.S. and R.D. Meyerhoff, *Environmental fate and chemistry of raloxifene hydrochloride.* Environ Toxicol Chem, 2002. **21**(4): p. 729-36.

13. Gasco-Lopez, A.I., A. Santos-Montes, and R. Izquierdo-Hornillos, *The effect of different amines added to eluents as silanol masking agents on the chromatographic behavior of some diuretics in reversed-phase high-performance liquid chromatography using C18 packings.* J Chromatogr Sci, 1997. **35**(11): p. 525-35.

14. *Guidance for Industry: Analytical procedures and methods validation for drugs and biologics*, C.f.D.E.a.R. (CDER), Editor. 2014: Rockville, MD.

Chapter 4

Preformulation Studies

4.1 Introduction

Preformulation studies include both physicochemical evaluation and determination of its biopharmaceutical properties of the drug molecule. The data generated from the preformulation studies arm the formulator with the knowledge of drug's behaviour within and outside the body. The formulator uses the preformulation data to improve drug's solubility, permeability, stability, selection of appropriate excipients and processing conditions for the dosage form [1-3].

Physicochemical properties of raloxifene hydrochloride like pH solubility, dissociation constant and partition co-efficient have been reported in literature [3, 4]. However, it is prudent that we confirm these parameters again and also determine other parameters like melting point, purity, stability under various processing conditions and polymorphic form of the drug sample before delving into the actual formulation development. Moreover, as a part of preformulation studies, we also established the compatibility of raloxifene hydrochloride with various excipients that we planned to use in the formulation of nanoparticles.

4.2 Materials

4.2.1 Chemicals and Reagents

Raloxifene hydrochloride was obtained as a gift sample from Apotex Research Pvt Ltd. (Bangalore, India). Poly-ε-caprolactone (PCL) and Chitosan (medium molecular weight) were purchased from Polysciences, Inc. (Warrington, USA). Poloxamer 407 (P407), Poloxamer 188 (P188), Poly vinyl alcohol (PVA) and Mannitol (Pearlitorl SD) were procured form Signet Chemicals (Mumbai, India). Polyethylene glycol 400 (PEG 400), Sodium lauryl sulfate (SLS), Polysorbate 80 (Tween 80) were purchased from Merck Ltd. (Mumbai, India).

The lipids – Stearic acid, Glyceryl monostearate, Glyceryl distearate, Glyceryl tristearate (Dynasan 118), Glyceryl tribehenate (Compritol ATO 888) and Soya bean lecithin (soyalecithin) were purchased from Himedia Pvt. Ltd. (Hyderabad, India). All the other chemicals and reagents were of analytical grade.

4.2.2 Instruments

A digital pH meter equipped with a glass electrode and automatic thermal compensation probe (pH Tutor, Eutech Instruments, Singapore); calibrated digital analytical balance (Sartorius 2244S-CW, Goettingen, Germany); temperature controlled water bath with shaker (Remi, Mumbai, India); humidity and temperature controlled cabinet (Remi, Mumbai, India); rotary flash evaporator (Rotavapor R-215, Bucchi Labortechnik AG, Postfach, Switzerland); ultrasonicator (Vibracell, Sonics, Connecticut, USA); vortex mixer (Vortex 3, Ika India Pvt Ltd., Bengaluru, India) were used for these studies. All the analytical instruments were calibrated prior to use.

4.2.3 Methods

4.2.3.1 Preparation of reagents and buffers

Preparation of buffered solutions

Various buffers (0.1 M strength) ranging from pH 1.2 to 7.4 were prepared in accordance to procedures described in the United States Pharmacopeia [5]. Triple distilled water (TDW) was used as a solvent in all the cases.

4.2.3.2 Procedures and Protocols

Previously validated UV Spectroscopic method (described in Chapter 3) was used for analysis of all the samples in solubility and partition coefficient determination studies. A

validated HPLC method (Chapter 3) was used for analysis of samples from solid state and solution state stability studies.

I. Identity confirmation and bulk drug characterization

Following tests were employed to identify and quantify raloxifene hydrochloride in bulk form: Fourier-transform infrared (FT-IR) absorption spectrum, thermal analysis using differential scanning calorimetry (DSC), identification of absorption spectrum ultra-violet spectroscopy and determination of purity by HPLC [6].

(a) FT-IR absorption spectrum of raloxifene hydrochloride

The FT-IR spectrum of pure raloxifene hydrochloride was recorded in solid state using KBr as a dispersion medium (1:10) using JASCO FT/IR-4200 (Jasco Inc., Maryland, USA) spectrometer in the range of 4000–400 cm^{-1}. An average of 40 scans were taken per sample.

(b) Ultra-violet absorption spectrum

The absorption maxima of raloxifene hydrochloride (1 µg/ml) in methanol: water (50:50, % v/v) was determined using a double beam UV-visible spectrophotometer (Jasco Inc., Maryland, USA). The absorption maximum was obtained after scanning the compound from 200-800 nm in triplicates.

(c) Thermal analysis using DSC

Thermal analysis was carried out using DSC 60 (Shimadzu, Kyoto, Japan) instrument. For the study, accurately weighted samples were taken in aluminium pan and crimp sealed. In the DSC chamber, samples were allowed to equilibrate at 25 °C. Then, the samples were subjected to heating run over temperature range of 25 to 300 °C at a heating rate of 5 °C per

min. DSC thermograms were directly obtained from the software supplied with the instrument.

(d) Assay and purity assessment

For assessment of purity of the drug and to quantify the drug from the bulk sample, an in-house validated HPLC method (as described in Chapter 3) was used.

(e) Molecular weight confirmation by LC-MS

To confirm the molecular weight of the drug, a solution of pure raloxifene hydrochloride in HPLC grade methanol was prepared (1 µg/ml) and injected into LC-MS system (Shimadzu LCMS-2020, Shimadzu Corporation, Kyoto, Japan). The peaks were captured in both M+1 and M-1 modes.

II. Determination of drug solubility

Drug substance administered by any route must possess some aqueous solubility for systemic absorption and therapeutic response. Poorly soluble compounds (e.g. less than 10mg/ml aqueous solubility) may exhibit incomplete, erratic, and slow absorption and thus produce minimal response at desired dosage [1]. Therefore, it is prudent that the saturation solubility of drug in various pH conditions be determined as a part of preformulation studies.

The equilibrium solubility of raloxifene hydrochloride was determined in buffered solutions with pH ranging from 1.2 to 7.4 at 37 ºC. In all the cases, known excess of raloxifene hydrochloride (25 mg) was added to 25 ml buffered solutions, bath sonicated for 2 min and kept under shaking on a rotary shaker (Remi, Mumbai, India) for 48 h at 37 ºC. After 48 h, samples were centrifuged 5000 x g for 15 min to get a clear supernatant. The clear supernatant was then suitably diluted and analysed at 289 nm using a validated UV-

spectrophotometric method against respective blank samples. Three replicates were taken for each sample and final values were expressed as mean ± S.D.

III. Determination of octanol/water partition coefficient

Partition coefficient is the ratio of concentrations of a compound in a mixture of two immiscible liquids at equilibrium. These coefficients indicate the differences in solubility of the compound in the two immiscible phases. Partition coefficient of raloxifene hydrochloride was determined using *n*-octanol /water (pH 5.5) system by shake flask method. The *n*-octanol phase was pre-saturated for 24 h with water at room temperature (25 ± 2 ºC). After pre-saturation, the *n*-octanol layer was separated by centrifugation (80 x g, 2 min) from the aqueous layer. To 10 ml of this pre-saturated *n*-octanol phase, equal proportion of water (also previously pre-saturated with *n*-octanol) was added. To 20 ml of the total mixture, 0.1 ml aliquot of 1 mg/ml raloxifene hydrochloride in methanol was added. The flasks were incubated on a rotary shaker (125 rpm), maintained at 25 ± 2 ºC for 24 h. After 24 h period, triplicate samples from each phase were collected from the flasks and analysed for drug content using validated HPLC method. All the experiments were performed in triplicate and the results were expressed as log $K_{o/w}$. The partition coefficient of raloxifene hydrochloride was calculated using the following formula:

$$\boldsymbol{K_{o/w} = C_{n-octanol} / C_{water}}$$

Where, $\boldsymbol{C_{n-octanol}}$ and $\boldsymbol{C_{water}}$ are the concentration of raloxifene hydrochloride in *n*-octanol and pure water respectively.

The saturation solubility of raloxifene hydrochloride in *n*-octanol was independently determined by incubating a known excess of raloxifene hydrochloride in *n*-octanol. After

equilibration for 24 h at 25 ºC, the samples were centrifuged (15,000 x g), supernatant collected and analysed by HPLC method as discussed in chapter 3.

The stability of raloxifene hydrochloride in *n*-octanol was confirmed by comparing the time zero values with values obtained after 3 days of incubation at 25 ºC. All the experiments were performed in triplicates and a validated HPLC method was used to carry out the analysis of the samples.

IV. Stability Studies

The stability studies were performed in order to evaluate the stability of raloxifene hydrochloride under various pH, temperature and moisture conditions. If the drug is extensively degraded, it may substantially reduce the potency of the drug. Moreover, the degradation products of the drugs may be toxic to the consumer [7]. Drug degradation can also bring unprecedented changes in drug product performance i.e. dissolution/bioavailability. During the process of manufacture, storage or in the in-vivo system, the drug may encounter one or more of these conditions. Therefore, to select the manufacturing, storage conditions and to protect the drug after administration, the stability studies for raloxifene hydrochloride were preformed both in liquid and solid states.

a) Liquid state stability studies

The liquid state stability for raloxifene hydrochloride was studied on various un-buffered and buffered pH solutions. Raloxifene hydrochloride stock solution (1 mg/ml) was prepared in methanol and appropriate volume of this stock was spiked into various buffered and unbuffered solutions with pH ranging from 1.2 to 10. The final concentration in each case was 10 µg/ml. Three sets of samples were also prepared in TDW.

All the samples were placed on a temperature controlled water bath shaker (Remi, Mumbai, India) at fixed temperature of 25 ± 2 ºC. At pre-determined time points (0, 2, 4, 6, 12 and 24 h and 2, 4, 8, 15, 30, 45 and 60 days), a aliquot of sample was withdrawn and analysed for drug content using previously described validated HPLC method. The amount of drug remaining in the solution was plotted as a function of time. The order of degradation kinetics and the degradation rate constants were determined for un-buffered solutions.

b) Solid state stability studies

The thermal stability studies for raloxifene hydrochloride were conducted as a part of drug-excipient compatibility studies.

V. Drug-excipients compatibility studies

Excipients play an important role in determining the stability of the final formulation. It is common knowledge that formulation stability is affected by:

1. Drug and excipient: chemical structure, moisture content, particle size, surface area and charge.
2. Formulation: drug: excipient ratio, processing method and nature of packaging.
3. Environment: Temperature, relative humidity, packaging material used, light and oxygen.

Drug: excipient compatibility studies form an important part of preformulation studies. In the following section, the actual protocol followed for these studies is presented.

The purpose of this protocol is to describe the procedure for investigation of possible changes in the physicochemical characteristics and the purity of raloxifene hydrochloride in presence and/ or absence of excipients.

Sample details

Raloxifene hydrochloride manufactured by Apotex Research Pvt Ltd. was used for the preformulation compatibility study. The details of raloxifene hydrochloride to be used for compatibility study are tabulated as shown in below Table 4.1.

Table 4.1: Details of the API used in drug: excipient compatibility studies

Sr. No.	Name of the API	Batch No. / Lot No.	Mfg. by
1.	Raloxifene HCl	RAL-A127-37	APIL

The details of individual excipients to be used in compatibility study are tabulated as shown below in Table-4.2. Individual excipient shall be sifted through # 40 ASTM SS sieve.

Table 4.2: Details of excipients used in drug: excipient compatibility studies

Sr. No.	Excipient	General Function	Mfg. by
1.	Mannitol	Cryoprotectant	Roquette Pharma
2.	Sucrose	Cryoprotectant	Domino
3.	Tween 80	Non-ionic Surfactant	Sigma Aldrich
4.	Poloxamer 188 (P188)	Non-ionic Surfactant	Sigma Chemicals
5.	Poloxamer 407 (P407)	Non-ionic Surfactant	Sigma Chemicals
6.	Poly vinyl alcohol	Non-ionic Surfactant	Sigma Aldrich
7.	Poly-ε-caprolactone (PCL)	Polymer	Polysciences Inc.
8.	Chitosan (Medium Mol wt)	Polymer	Polysciences Inc.
9.	Sodiul lauryl sulfate (SLS)	Anionic Surfactant	Sigma Aldrich
10.	Stearic acid	Lipid	Himedia
11.	Glyceryl monostearate	Lipid	Himedia
12.	Glyceryl tristearate (Dynasan 118)	Lipid	Himedia
13.	Glyceryl behenate (Compritol ATO 888)	Lipid	Himedia
14.	Soyalecithin	Lipid/Surfactant	Himedia

Sample preparation

a. Samples were kept in different conditions as given in Table – 4.3 Sifting of the mixed material was done using # 40 ASTM Sieve.

b. A blend containing raloxifene hydrochloride (with or without excipients as given in Table 4.3) was filled into clean glass sample holders with screw cap and wrapped with aluminium foil. All sample holders were filled with blend containing at least 100 mg raloxifene hydrochloride, except for the vials containing placebos (mixture of only excipients without raloxifene hydrochloride) and individual excipients.

c. After filling, all the sample holders were closed with a rubber stopper and sealed with aluminium tear-off seals. Post sealing, the central portion of the aluminium seal was manually removed to expose the underlying rubber stopper. With the help of a needle, five holes were punctured into the rubber stopper to enable the entry of moisture in to all the glass vials. Rubber stoppers of vials kept at 2-8 °C (control) and 60 °C (thermal stability sample) were not punctured.

d. Placebo and individual excipients were also exposed in a similar manner at all conditions.

    1. The samples were stored at 40 °C/75% RH, 60 °C and 25 °C/60%RH. The placebo mixtures, individual excipients and samples of 2-8 °C were considered as *control* and were analyzed only when required. All other samples were subjected to following analyses: Physical description and assay; DSC analysis and IR-spectroscopic analysis.

Summary of Test Conditions:

1. 2-8 °C – control samples which were analysed only when required.
2. 40 °C/75% RH – samples were kept in this condition to study the combined effect of temperature and humidity on raloxifene hydrochloride in presence and/ or in absence of excipients.
3. 60 °C temperature – samples were kept at this condition to study the effect of only temperature on raloxifene hydrochloride in presence and/ or absence of excipients.
4. 25 °C/60%RH – samples under this condition simulate the effects at room temperature.

Table 4.3: Details of different samples, drug: excipient ratios and test conditions used for drug: excipient compatibility studies

SL. NO.	SAMPLE	DRUG: EXCIPIENT RATIO	2-8° C (CONTROL SAMPLES)	INITIAL	40°C/75%RH		60°C		25^0C/60%RH	
					AFTER 14 DAYS	AFTER 28 DAYS	AFTER 14 DAYS	AFTER 28 DAYS	AFTER 14 DAYS	AFTER 28 DAYS
1.	Raloxifene HCl	-		√	√	√	√	√	√	√
2.	Raloxifene HCl + Mannitol	1:9		√	√	√	√	√	√	√
3.	Raloxifene HCl + PCL	1:9		√	√	√	√	√	√	√
4.	Raloxifene HCl + Chitosan	1:9		√	√	√	√	√	√	√
5.	Raloxifene HCl + Stearic acid	1:9		√	√	√	√	√	√	√
6.	Raloxifene HCl + Glyceryl Monostearate	1:9		√	√	√	√	√	√	√
7.	Raloxifene HCl + Glyceryl Behenate	1:9		√	√	√	√	√	√	√
8.	Raloxifene HCl + P188	1:1		√	√	√	√	√	√	√
9.	Raloxifene HCl + P407	1:1		√	√	√	√	√	√	√
10.	Raloxifene HCl + SLS	1:1		√	√	√	√	√	√	√
11.	Raloxifene HCl + PVA	1:1		√	√	√	√	√	√	√
12.	Raloxifene HCl + Sucrose	1:9		√	√	√	√	√	√	√
13.	Raloxifene HCl + Soyalecithin	1:9		√	√	√	√	√	√	√

14.	Mannitol	1		√	√	√	√	√	√	√
15.	PCL	1		√	√	√	√	√	√	√
16.	Chitosan	1		√	√	√	√	√	√	√
17.	Stearic acid	1		√	√	√	√	√	√	√
18.	Glyceryl Monostearate	1		√	√	√	√	√	√	√
19.	Glyceryl Behenate	1		√	√	√	√	√	√	√
20.	P188	1		√	√	√	√	√	√	√
21.	P407	1		√	√	√	√	√	√	√
22.	SLS	1		√	√	√	√	√	√	√
23.	PVA	1		√	√	√	√	√	√	√
24.	Sucrose	1		√	√	√	√	√	√	√
25.	Soyalecithin	1		√	√	√	√	√	√	√
26.	Raloxifene HCl + Glyceryl Behenate + P407	1:20:10		√	√	√	√	√	√	√
27.	Raloxifene HCl + Chitosan + Soyalecithin + P407	2:6:2.5:4		√	√	√	√	√	√	√
28.	Raloxifene HCl + PCL + P407	1:5:5		√	√	√	√	√	√	√
29.	Glyceryl Behenate + P407	2:1		√	√	√	√	√	√	√
30.	Chitosan + Soyalecithin + P407	6:2.5:4		√	√	√	√	√	√	√
31.	PCL + P407	1:1		√	√	√	√	√	√	√

Note: Sign for sample kept: √, Sign for sample not kept: X

4.3 Results and discussion

I. Identification and bulk characterization of raloxifene hydrochloride

(a) FT-IR absorption spectrum

The infrared absorption spectrum of the pure drug showed characteristic absorption peaks at 3220 (O-H stretching), 1642 (C=O stretching), 1596 (conjugated ketone –C-O-C- stretching), 1122 (Aliphatic -C-O- stretching) and 705 (-C-S- stretching) which are in agreement with the reported values from the literature [8]. The FT-IR spectrum for bulk raloxifene hydrochloride is shown in Fig. 4.1.

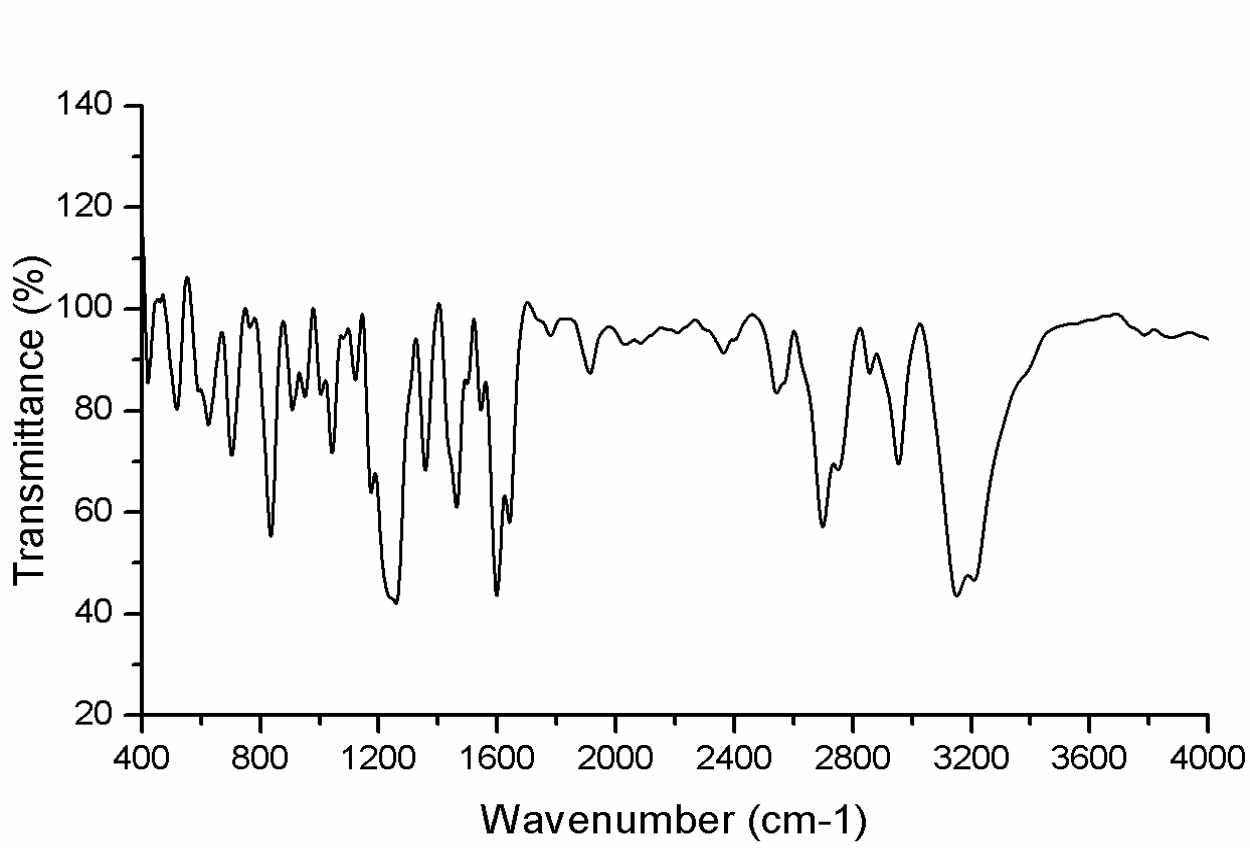

Fig 4.1: FT-IR spectrum of raloxifene hydrochloride in bulk form

(b) Ultra-violet absorption spectrum

The ultra-violet absorption spectrum of raloxifene hydrochloride in methanol: water (50:50, % v/v) showed maximum absorption at 289 nm (Fig. 4.2). This is in agreement with the value reported in the literature [9].

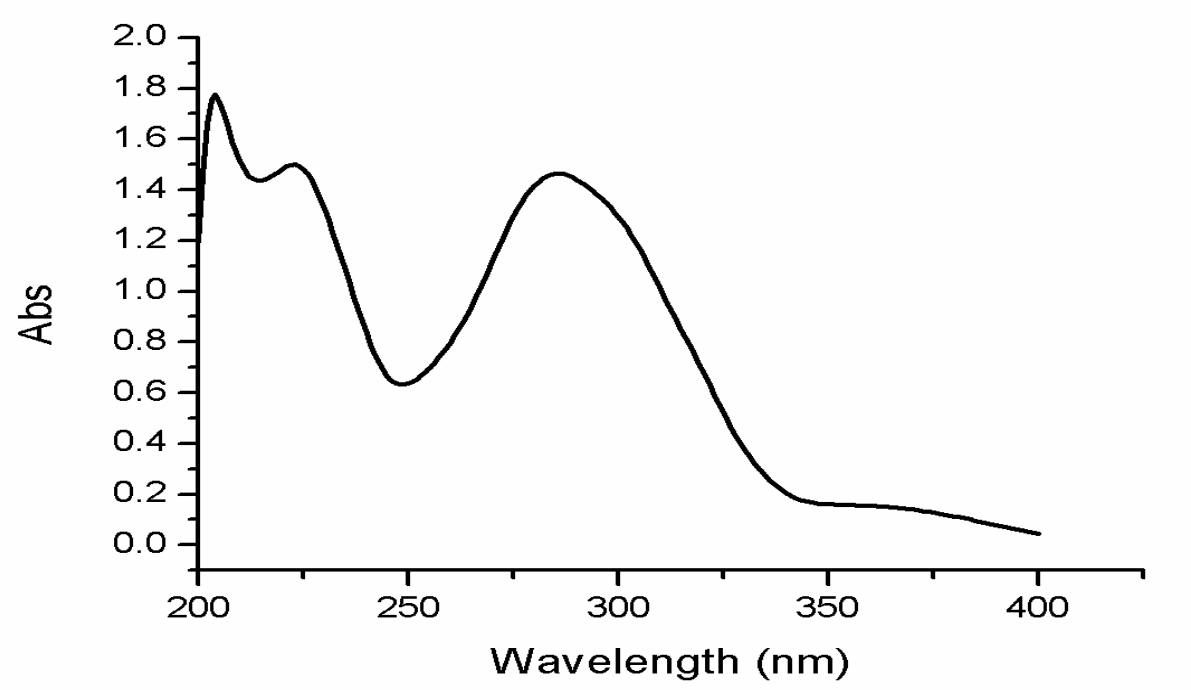

Fig. 4.2: UV absorption spectrum of raloxifene hydrochloride in 50:50, % v/v methanol: water

(c) Thermal analysis using DSC

The DSC thermogram of pure drug demonstrated a single strong endothermic peak onset at 257.88 ºC and peak endset 267.64 ºC. The average melting peak appeared at 263.98 (~ 267 ºC) which is in close agreement with the value reported in the literature [10]. The single strong endothermic peak indicates that the sample of raloxifene hydrochloride is crystalline in nature. The DSC thermogram and other data are presented in Fig. 4.3 below.

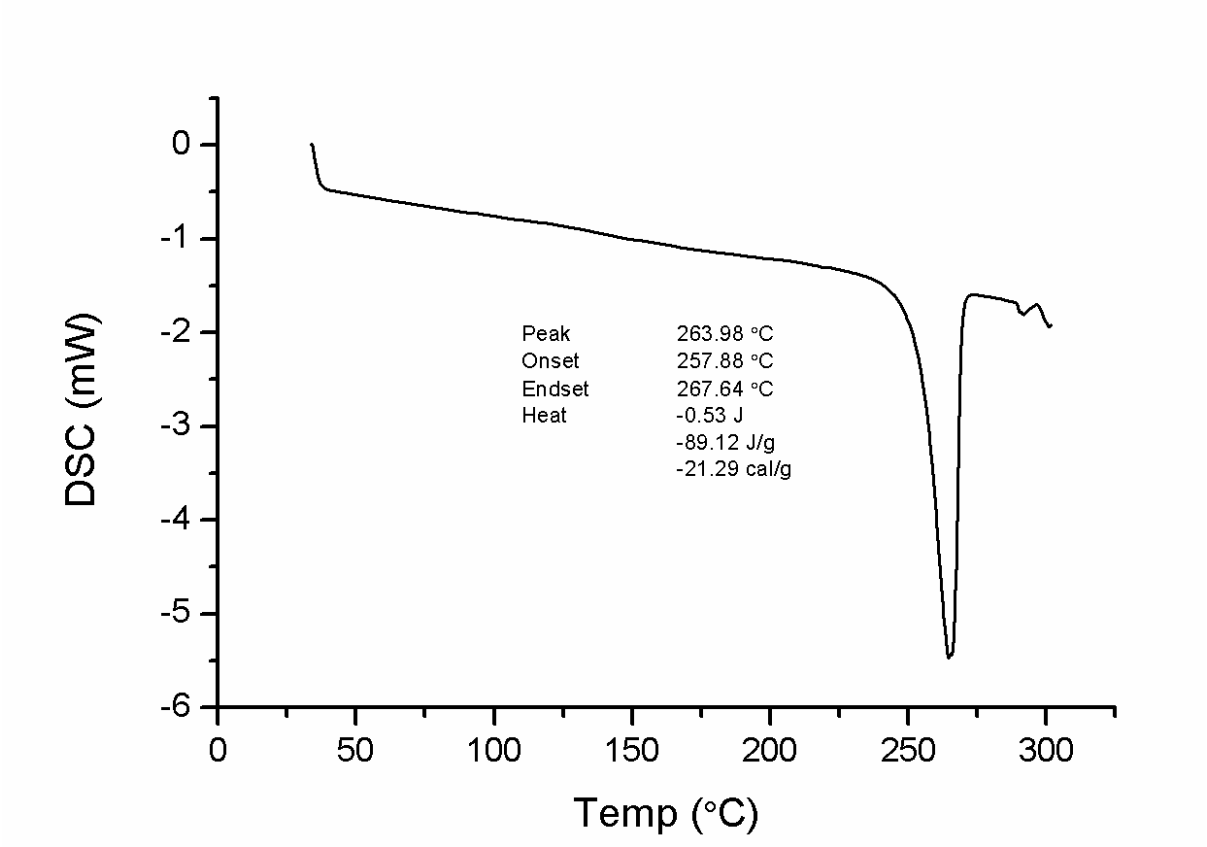

Fig. 4.3: DSC thermogram of pure raloxifene hydrochloride

(d) Molecular weight confirmation by LC-MS

The mass spectrum for pure raloxifene hydrochloride in M-1 mode showed two distinct peaks at following m/z values – 472 and 508. The molecular weight of raloxifene hydrochloride is reported in the literature as 509.08 g/mol. The two peaks obtained with our sample correspond to the salt Raloxifene hydrochloride (508 g/mol) and base form of Raloxifene (508 – 36 = 472 g/mol). From this study, molecular weight of present sample of Raloxifene hydrochloride was confirmed as 509 g/mol which is in agreement with the reported values. The data are represented in Fig. 4.4 below.

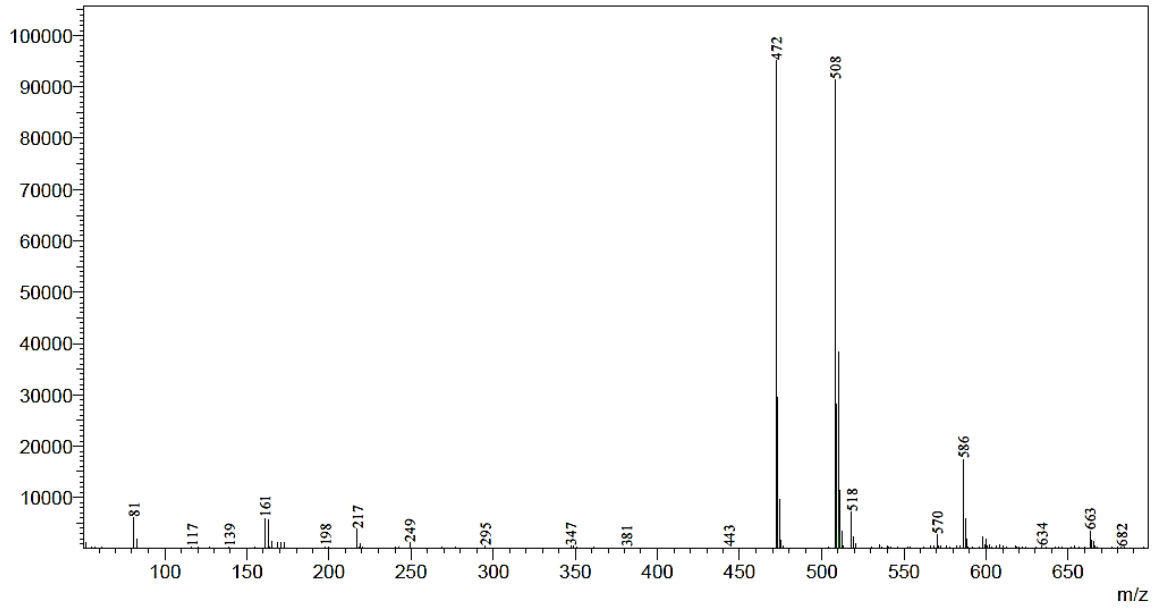

Fig. 4.4: Mass spectrum of raloxifene and raloxifene hydrochloride in negative mode

(e) Assay and purity assessment

The assay results showed that the raloxifene hydrochloride used in the study has a purity of 99.95%.

II. Determination of drug solubility

The data from solubility studies in different pH conditions is presented in Fig. 4.5. From the figure, it is evident that raloxifene hydrochloride demonstrates a pH-dependent solubility. Raloxifene hydrochloride demonstrated highest solubility of 384.6 ± 7.9 µg/ml solubility in water (pH 4.5 to 5.5). In buffered pH solutions, as the pH increased, there was a progressive decrease in the solubility of raloxifene hydrochloride. Maximum solubility for raloxifene hydrochloride was observed in pH 4.5 acetate buffer (277.9 ± 4.8 µg/ml).

Raloxifene hydrochloride is zwitter ionic in nature and simultaneously possesses both anionic and cationic charges over the pH range of 7 to 11 [4]. However, it becomes increasingly insoluble as pH moves towards 7. The solubility minimum is predicted around

pH 8.9 (~ pK_a of basic nitrogen). Teeter and Meyerhoff have proposed a hypothesis to explain this solubility behaviour of raloxifene hydrochloride [4]. According to them, raloxifene hydrochloride undergoes intramolecular folding to satisfy both the cationic and anionic charges of the zwitterion. In the folded state, raloxifene hydrochloride exhibits a hydrophobic character as both the charges are poorly accessible to the solvent. Nevertheless, raloxifene hydrochloride is highly soluble in strong basic condition (pH > 11) [4] due to dissociation of hydroxyl groups; the base nitrogen in this condition would be charge neutral [4].

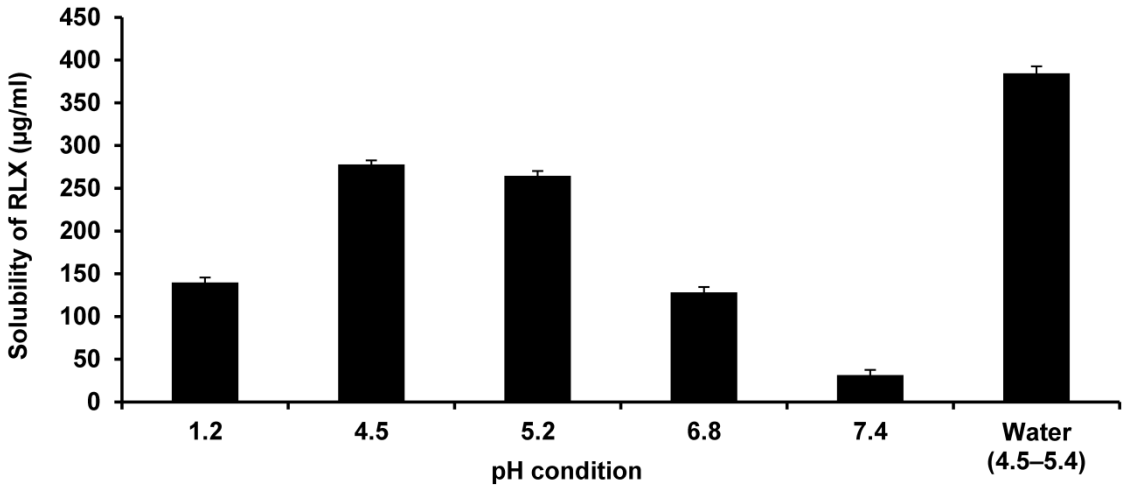

Fig. 4.5: Solubility profile of raloxifene hydrochloride (RLX) in various buffered solutions and water. Each observation represents mean ± SD (n = 3).

III. Octanol/water partition coefficient

The solubility of raloxifene hydrochloride in *n*-octanol was determined to ascertain that, at equilibrium, the concentration of raloxifene hydrochloride in *n*-octanol was not limited by its solubility. The saturation solubility of raloxifene hydrochloride in *n*-octanol was found to be 48.2 ± 4.1 µg/ml by independent experiments. The octanol/water (pH 5.5)

partition coefficient ($K_{o/w}$) of raloxifene hydrochloride was found to be 497 ± 26 (mean ± SD, n = 3). The log $K_{o/w}$ value of the mean observation was calculated as 2.69 which is in close agreement with the reported value of 2.71 [4].

IV. Stability studies

a) Liquid state stability studies

To estimate the stability of raloxifene hydrochloride in various pH conditions, the logarithm of percentage raloxifene hydrochloride unchanged was plotted against time in days (Fig. 4.6) and degradation rate constants (K_d) were obtained. The obtained K_d values indicated that the degradation of raloxifene hydrochloride followed first-order rate kinetics with high correlation coefficient values (Table 4.4). The data indicated that raloxifene hydrochloride degrades faster in higher pH conditions. The higher rates of degradation of raloxifene hydrochloride in alkaline conditions may be due to hydroxide ion catalysis [4]. During transit through GIT, degradation of drug is less likely to impact the in-vivo fate of raloxifene hydrochloride because it is relatively more stable in pH conditions below 7. From these studies, it was concluded that raloxifene hydrochloride must be processed in neutral or slightly acidic conditions and prolonged exposure to alkaline conditions must be avoided.

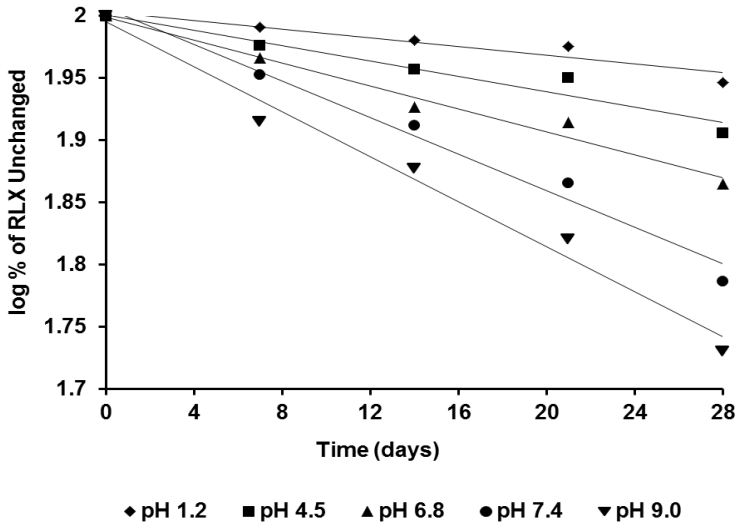

Fig 4.6: First-order plot of raloxifene hydrochloride (RLX) degradation in various pH conditions at 25 ºC.

Table 4.4: First-order degradation rate constants (K_d) and respective regression coefficients for raloxifene hydrochloride under different pH conditions

pH condition	K_d x 10^2 (per day)	Regression co-efficient (R^2)
1.2	0.17	0.9075
4.5	0.31	0.9422
6.8	0.46	0.9779
7.4	0.74	0.9811
9.0	0.91	0.9817

V. Drug-excipient compatibility studies

The compatibility of various drug substance/excipient combinations was studied for all excipients which were considered to find potential use in raloxifene hydrochloride nanocarrier formulation. The table below (Table 4.5) summarizes the compatibility study results for the various excipients proposed to be employed in the formulation of raloxifene hydrochloride nanocarriers. The sample mixtures were prepared in different excipients/active ratio as proposed for the nanocarrier formulation and exposed to different conditions, viz. 60 °C and 40 °C/75% RH for 2 weeks and 4 weeks.

Table 4.5: Compatibility analysis data of raloxifene hydrochloride with selected excipients

Sample Name	Interval and condition	Assay (%) (mean ± SD, *n* = 3)	Thermal analysis			Wavenumber (cm^{-1}) from IR spectrum			
			Type of phase transition	Peak (ºC)	Deviation from pure raloxifene hydrochloride (ºC)	3220 (-OH $_{str}$)	1642 (-C=O- $_{str}$)	1596 (-C-O-C-)	705 (-C-S_{str})
Raloxifene hydrochloride	Initial	99.5 ± 2.4	Endo	263.9	NA	3220	1642	1596	705
	14 Days – 40°C /75%RH	98.5 ± 1.4	Endo	264.5	NA	NC	NC	NC	NC
	14 Days – 60°C	97.5 ± 3.2	Endo	263.1	NA	NC	NC	NC	NC
	28 Days – 40°C /75%RH	96.4 ± 2.8	Endo	264.2	NA	NC	NC	NC	NC
	28 Days – 60°C	97.3 ± 3.6	Endo	263.2	NA	NC	NC	NC	NC
Raloxifene hydrochloride + Mannitol	Initial	99.6 ± 3.1	Endo	239.5	-24.4	3117	1703	1503	723
	14 Days – 40°C /75%RH	98.4 ± 2.9	Endo	238.6	-25.9	3214	1669	1513	717
	14 Days – 60°C	96.3 ± 2.5	Endo	236.8	-26.3	3226	1649	1571	721
	28 Days – 40°C /75%RH	95.1 ± 2.2	Endo	239.4	-24.5	3241	1672	1579	733
	28 Days – 60°C	94.8 ± 4.1	Endo	238.4	-25.5	3161	1683	1581	709
Raloxifene hydrochloride + PCL	Initial	97.6 ± 3.1	Endo	274.8	+10.9	3446	1667	ND	713
	14 Days – 40°C /75%RH	96.2 ± 4.5	Endo	273.2	+8.7	3231	1671	ND	847
	14 Days – 60°C	95.0 ± 3.6	Endo	272.8	+9.7	3225	1714	ND	743
	28 Days – 40°C /75%RH	95.5 ± 2.9	Endo	271.3	+7.1	3178	1664	ND	834
	28 Days – 60°C	96.5 ± 1.6	Endo	276.1	+12.9	3265	1653	ND	839

Sample Name	Interval and condition	Assay (%) (mean ± SD, *n* = 3)	Thermal analysis			Wavenumber (cm^{-1}) from IR spectrum			
			Type of phase transition	Peak (°C)	Deviation from pure raloxifene hydrochloride (°C)	3220 (-OH $_{str}$)	1642 (-C=O- $_{str}$)	1596 (-C-O-C-)	705 (-C-S_{str})
Raloxifene hydrochloride + Chitosan	Initial	94.6 ± 4.1	Endo	259.8	-4.1	3242	1607	1567	800
	14 Days – 40°C /75%RH	97.3 ± 3.8	Endo	258.2	-6.3	3244	1618	1554	808
	14 Days – 60°C	96.2 ± 2.9	Endo	260.2	-3.0	3216	1664	1571	806
	28 Days – 40°C /75%RH	97.4 ± 3.7	Endo	259.4	-4.8	3228	1617	1593	794
	28 Days – 60°C	98.4 ± 2.8	Endo	258.3	-4.9	3135	1661	1581	772
Raloxifene hydrochloride + Stearic acid	Initial	96.4 ± 3.2	Endo	263.7	-0.2	3241	1607	1568	742
	14 Days – 40°C /75%RH	95.4 ± 2.7	Endo	264.3	-0.2	3228	1618	1587	696
	14 Days – 60°C	98.3 ± 1.3	Endo	265.5	+2.4	3218	1661	1590	698
	28 Days – 40°C /75%RH	96.3 ± 3.1	Endo	264.1	-0.1	3340	1641	1578	718
	28 Days – 60°C	99.4 ± 4.1	Endo	263.4	+0.2	3311	1638	1589	691
Raloxifene hydrochloride + Glyceryl Behenate	Initial	96.2 ± 2.9	Endo	268.3	+4.4	3182	1637	1590	694
	14 Days – 40°C /75%RH	96.3 ± 3.4	Endo	265.2	+0.7	3224	1646	1598	705
	14 Days – 60°C	98.1 ± 2.2	Endo	264.3	+1.2	3225	1645	1591	707
	28 Days – 40°C /75%RH	97.2 ± 3.4	Endo	267.2	+3.0	3341	1673	1587	717
	28 Days – 60°C	98.2 ± 3.4	Endo	267.5	+4.3	3228	1741	1608	709

Sample Name	Interval and condition	Assay (%) (mean ± SD, *n* = 3)	Thermal analysis	Wavenumber (cm^{-1}) from IR spectrum					
			Type of phase transition	Peak (ºC)	Deviation from pure raloxifene hydrochloride (ºC)	3220 (-OH $_{str}$)	1642 (-C=O- $_{str}$)	1596 (-C-O-C-)	705 (-C-S_{str})
Raloxifene hydrochloride + Glyceryl monostearate	Initial	93.2 ± 3.2	Endo	271.9	+8.0	3206	1640	1595	715
	14 Days – 40°C /75%RH	98.1 ± 2.8	Endo	273.4	+8.9	3274	1677	1598	724
	14 Days – 60°C	97.1 ± 3.2	Endo	268.7	+5.6	3218	1638	1590	734
	28 Days – 40°C /75%RH	95.1 ± 4.3	Endo	269.4	+5.2	3227	1648	1604	726
	28 Days – 60°C	92.8 ± 3.9	Endo	272.3	+9.1	3219	1639	1589	709
Raloxifene hydrochloride + Soyalecithin	Initial	94.1 ± 2.1	Endo	248.5	-15.4	3160	ND	1596	ND
	14 Days – 40°C /75%RH	97.5 ± 3.2	Endo	254.3	-10.2	3224	ND	1591	ND
	14 Days – 60°C	95.4 ± 2.7	Endo	242.9	-20.2	3168	ND	1562	ND
	28 Days – 40°C /75%RH	96.4 ± 3.1	Endo	244.5	-19.7	3220	ND	1598	ND
	28 Days – 60°C	95.3 ± 2.7	Endo	252.3	-10.9	3219	ND	1564	ND
Raloxifene hydrochloride + Glyceryl Behenate + P407	Initial	96.4 ± 3.4	Endo	269.4	+6.5	3221	1651	1589	714
	14 Days – 40°C /75%RH	X	X	X	X	X	X	X	X
	14 Days – 60°C	X	X	X	X	X	X	X	X
	28 Days – 40°C /75%RH	X	X	X	X	X	X	X	X
	28 Days – 60°C	X	X	X	X	X	X	X	X

Sample Name	Interval and condition	Assay (%) (mean ± SD, *n* = 3)	Thermal analysis	Wavenumber (cm^{-1}) from IR spectrum					
			Type of phase transition	Peak (ºC)	Deviation from pure raloxifene hydrochloride (ºC)	3220 (-OH $_{str}$)	1642 (-C=O- $_{str}$)	1596 (-C-O-C-)	705 (-C-S_{str})
Raloxifene hydrochloride + Chitosan + Soyalecithin	Initial	94.5 ± 2.9	Endo	258.4	-4.8	2904	ND	1559	817
	14 Days – 40°C /75%RH	X	X	X	X	X	X	X	X
	14 Days – 60°C	X	X	X	X	X	X	X	X
	28 Days – 40°C /75%RH	X	X	X	X	X	X	X	X
	28 Days – 60°C	X	X	X	X	X	X	X	X
Raloxifene hydrochloride + PCL + P407	Initial	96.4 ± 3.3	Endo	274.8	+10.9	3217	ND	1592	837
	14 Days – 40°C /75%RH	X	X	X	X	X	X	X	X
	14 Days – 60°C	X	X	X	X	X	X	X	X
	28 Days – 40°C /75%RH	X	X	X	X	X	X	X	X
	28 Days – 60°C	X	X	X	X	X	X	X	X

Abbreviations: Endo – Endothermic melting peak; ND – Not Detected; NC – No significant change in the value compared to initial sample; SD – Standard deviation; PCL – Poly (ε-caprolactone); P407 – Poloxamer 407; X – Not Analysed.

References

1. Bharate, S.S. and R.A. Vishwakarma, *Impact of preformulation on drug development.* Expert Opin Drug Deliv, 2013. **10**(9): p. 1239-57.

2. Ceresole, R., et al., *Drug-excipient compatibility studies in binary mixtures of avobenzone.* J Cosmet Sci, 2013. **64**(5): p. 317-28.

3. Chadha, R. and S. Bhandari, *Drug-excipient compatibility screening--role of thermoanalytical and spectroscopic techniques.* J Pharm Biomed Anal, 2014. **87**: p. 82-97.

4. Teeter, J.S. and R.D. Meyerhoff, *Environmental fate and chemistry of raloxifene hydrochloride.* Environ Toxicol Chem, 2002. **21**(4): p. 729-36.

5. *US Pharmacopoeia XXX*. Vol. I. 2007, Rockville, MD: US Pharamcopoeial Convention.

6. Perioli, L. and C. Pagano, *Preformulation studies of mucoadhesive tablets for carbamazepine sublingual administration.* Colloids Surf B Biointerfaces, 2013. **102**: p. 915-22.

7. Jiang, S., et al., *Preformulation study of methazolamide for topical ophthalmic delivery: physicochemical properties and degradation kinetics in aqueous solutions.* Int J Pharm, 2013. **448**(2): p. 390-3.

8. Patil, P.H., et al., *Solubility Enhancement of Raloxifene Using Inclusion Complexes and Cogrinding Method.* J Pharm, 2013. **2013**: p. 9.

9. Pavithra, D. and L. Sivasubramanian, *New spectrophotometric determination of Raloxifene hydrochloride in tablets.* Ind J Pharm Sci, 2006. **68**(3): p. 375-376.

10. Jagadish, B., et al., *Enhanced Dissolution and Bioavailability of Raloxifene Hydrochloride by Co-grinding with Different Superdisintegrants.* Chem Pharm Bull (Tokyo), 2010. **58**(3): p. 293-300.

Chapter 5

Formulation design and pharmacokinetic evaluation

Lipid based nanoparticles

5.1 Introduction

Lipid based nanoparticles can be successfully developed by giving a careful consideration to the formulation objectives [1]. A systematic development approach must include the following: pre-selection of lipid excipients based on transition temperature; composition of fatty acid; HLB values of the lipid(s); digestibility and disposability of the lipid; drug solubility in selected lipids [1]; identification of a suitable technique to manufacture the lipid nanoparticles [1]; optimization of process and formulation related parameters; characterization of nanoparticles; in-vitro evaluation; selection of appropriate animal model to predict in-vivo performance of the nanoparticles [1] and long-term stability assessment of the nanoparticles.

As the name suggests, solid lipid nanoparticles (SLN) consist of a lipid matrix that is in solid state at both room and body temperatures [2]. The SLNs are prepared in a similar manner to an oil-in-water (o/w) emulsion except that the oil phase of the emulsion is replaced by a solid lipid or a blend of solid lipids. High carbon chain fatty acids, fatty acid esters and waxes are used as solid lipids in the SLN [3]. Typically, the SLN particle size ranges from 80 to 1000 nm [4].

5.1.1 Factors to be considered in design of SLN for oral delivery

Factors that affect absorption and stability (both in-vitro and in-vivo) of SLN are given due consideration in the design of SLN formulation. These include: lipids, emulsifiers and other miscellaneous factors [5].

a) Selection of lipids

The SLNs can be formulated either with glycerides or waxes as matrix forming materials [5]. While most of the available literature focuses on glycerides as matrix forming material, newer studies have shown that wax-based SLN are also equally effective [5].

Notwithstanding their superior stability characteristics over glycerides, the wax-based SLN suffer from one major setback – poor drug encapsulation efficiency. The highly ordered crystalline structures of waxes results in both poor encapsulation and drug expulsion from the matrix upon standing. An ideal lipid must possess both; high drug encapsulation ability and stability upon storage.

From the studies of Radomska-Soukharev [6], we know that selection of lipid excipients depends on chemical stability of lipid itself and later on the stability of SLN. They showed that SLNs that comprised of higher percentage of triglycerides showed very low degradation when incubated at 25 ºC. Among the lipids tested, Dynasan 118 (Tristearin) showed highest chemical stability after 2 years of storage at 25 ºC. For most of the lipids tested, degradation was between 2-5% over 2 years when stored at 25 ºC.

The type of lipid also affects properties of SLN like particle size. It is reported that, with increasing melting point of the lipid, the particle size of the SLN also increases [7]. This is because, with increasing melting point of the lipid, the viscosity of the dispersion also increases. The energy required to break-down the viscous lipid into tiny nanosized droplets is enormous. Moreover, the particle size and size distribution are also influenced by the proportion of lipid used in the formulation [7]. This is often seen when the lipid content in a formulation exceeds 10% w/v [7].

Another important parameter that affects the stability of SLNs is the rate of cooling of lipid. Lipids tend to recrystallize upon cooling. If recrystallization of lipids is not enforced by cooling below a critical recrystallization temperature, the lipid in the SLN remains in a metastable form for long time and the formulation behaves more like an emulsion rather than a suspension [8]. The metastable SLNs may be unstable in GIT and can lead to burst release of the loaded drug [8].

The nature of lipid used in SLN can also affect its in-vivo drug release behaviour. Higher carbon chain length lipids result in higher plasma concentrations of the loaded drug. SLNs formulated with higher chain length triglycerides show better resistance to the intestinal lipase, co-lipase system and hence release the drug more slowly [9, 10]. Moreover, for these lipids, higher AUC and lower clearance rates (longer circulation times in the body) are observed [9, 10].

Lastly, selection of lipid affects drug loading capacity into SLN. Higher loading is usually achieved when the drug is soluble in the lipid matrix. With higher loading efficiency, the amount of lipid required to hold a given dose of drug can be reduced [11]. Higher loading into lipid matrix is usually well correlated with its partitioning behaviour in the external aqueous phase. Higher drug solubility in lipid ensures that more drug is available in the lipid layer and less of it is partitioned out into the external aqueous layer [11].

b) Selection of emulsifiers/surfactants

As defined earlier, SLNs can be considered as microemulsions in which the lipid is in solid state at room and body temperatures. Hence, as with other emulsions, the emulsifier or the surfactant plays a significant role in both formation and stability of SLNs. In the hot molten state, emulsifiers get distributed to the o/w interface and facilitate the formation of SLN. In the solidified sate, the surfactants provide charge-based or stearic stability that keeps the SLNs apart and prevents them from agglomeration.

Selection of both appropriate surfactant and concentration are critical to produce stable SLN with good entrapment efficiency. Surfactants that are more hydrophilic increase the drug solubility in the external aqueous phase leading to fall in the entrapment efficiency of the drug in the SLN matrix. Excessive use of surfactant (more than 5% w/v) may be counterproductive because, the excess surfactant tends to adsorb on the surface of SLN which

reduces its hydrophobicity and hence, its chances of lymphatic uptake when administered by oral route is minimized [12].

c) Miscellaneous factors

There is range of other formulation and process related factors that affect the particle size, surface charge, stability and ultimately, the in-vivo behaviour of SLNs. In general, the drug's melting point should be higher than the melting point of the lipids. Else, it leads to heterogeneous crystallization of drug-loaded SLNs [13]. Choice of the method of manufacture and heating and cooling rates affect both particle size and distribution. Erratic heating and cooling rates result in uneven crystallization of lipids within the SLN matrix which in turn results in erratic drug release behaviour. Other parameters that affect SLN properties are homogenization speed and time, polarity of the solvent used (in emulsification-evaporation method), manufacturing vessel capacity, volume of internal and external phases etc.

The process flow followed in development of SLNs for raloxifene hydrochloride is depicted in Fig. 5.1 and 5.2 below:

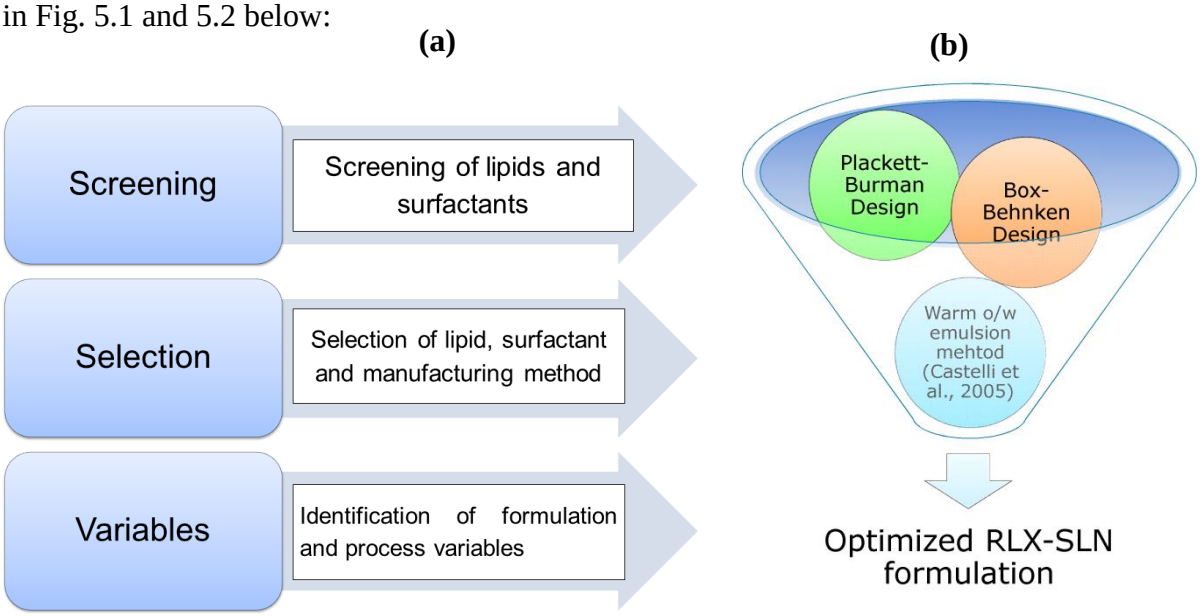

Fig. 5.1: Process flow chart for formulation development of raloxifene hydrochloride loaded SLN – Initial screening and selection of lipid, surfactant and process (a) and optimization of manufacturing conditions using hybrid-design approach (b).

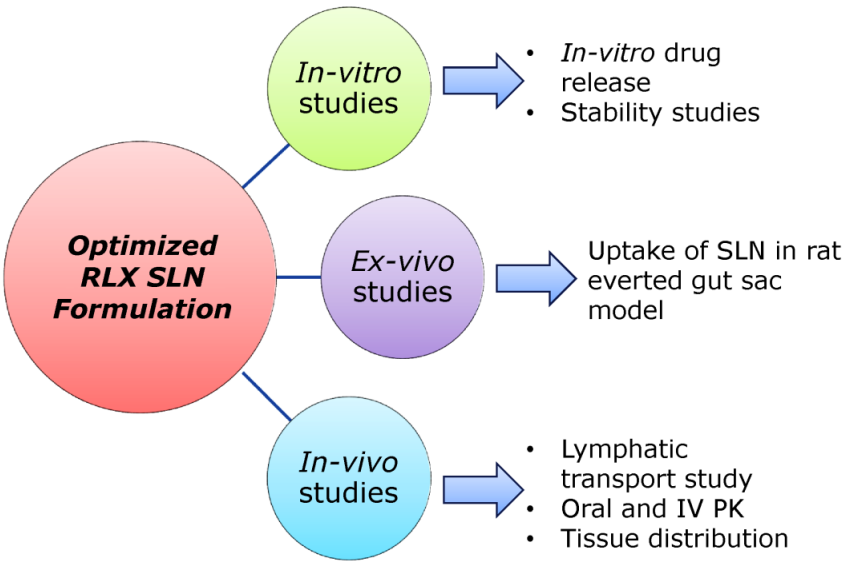

Fig. 5.2: Scheme for in-vitro, ex-vivo and in-vivo evaluation of optimized SLN formulation.

5.1.2 Materials

Raloxifene hydrochloride was obtained as a gift sample from Apotex Research Pvt. Ltd. Bangalore, India. High purity lipids (stearic acid (SA), glyceryl monostearate (GMS), glyceryl distearate (GDS), glyceryl tristearate (GTS), glycerol trioleate/Triolein (GTO) and GB (GB) (C69H134O6, molecular weight 1059.8)) were purchased from M/s Himedia Pvt. Ltd. (Hyderabad, India). Poloxamer 407 (P407), Poloxamer 188 (P188), polysorbate 80 (Tween 80) and mannitol were procured form Signet Chemicals, Mumbai, India. All other chemicals used were of analytical grade and the solvents were of HPLC grade. Freshly collected Milli-Q water (Millipore, Billerica, MA) was used in preparation of aqueous mobile phase of HPLC analysis.

5.2 Methodology

5.2.1 Screening and selection of lipids for preparation of SLN

Selection of lipids for production of raloxifene hydrochloride loaded SLN was based on: (a) solubility of raloxifene hydrochloride in the lipid matrix, (b) in-vitro stability of SLN (loss of entrapped drug on standing) and (c) in-vivo stability of the lipid to lipase/co-lipase enzyme system. From the literature [14], we know that triglycerides based nanoparticles of shorter carbon chain length are susceptible to intestinal lipase, co-lipase enzyme system. This can be a major deterrent for orally administered SLN. Conversely, higher carbon chain lipids like GB (Compritol 888 ATO) are relatively more resistant to this enzyme system [14].

Determination of raloxifene hydrochloride solubility in various lipid matrices

Saturation solubility of raloxifene hydrochloride in different lipid matrices was determined by using previously reported method, with slight modifications [15]. Briefly, accurately weighed amount of raloxifene hydrochloride (10 mg) was added to a screw-capped glass vial. To this, individual lipids (stearic acid (SA), glyceryl monostearate (GMS), glyceryl distearate (GDS), glyceryl tristearate (GTS), glyceryl trioleate (GTO) or glyceryl behenate (GB)) were added in incremental amounts while maintaining the temperature of the vial 5-10 ^{o}C above the melting point of the lipid. Initially, solubilisation was visually monitored. Absence of any suspended particles in the molten lipid was considered as a visual end-point for drug solubilisation.

5.2.2 Screening and selection of surfactants for preparation of SLN

Selection of surfactant for the SLN formulation was based on both prior literature and experimental results. To start with, we selected two distinct types of surfactants: tri-block co-polymers (poloxamer) and PEG-ylated sorbitan esters of fatty acids (polysorbate). From the

literature, it is known that nanoparticles stabilized by block co-polymers like poloxamer show distinctly reduced protein adsorption and low phagocytic uptake, achieving longer circulation time in the body [14]. Further, to achieve good entrapment efficiency, it is important that raloxifene hydrochloride must have higher solubility in the lipid phase and lower solubility in the aqueous phase. Therefore, to understand the solubility behaviour of raloxifene hydrochloride in surfactant solutions, we determined the solubility of raloxifene hydrochloride in aqueous surfactant solutions at different concentrations.

Determination of solubility of raloxifene hydrochloride in aqueous surfactant solutions

Briefly, a known excess of the drug was incubated with 1, 2.5, 5 and 7.5 w/v aqueous solutions of poloxamer 407 and 0.5, 1, and 2.5% w/v of Tween 80. These samples were placed in sealed glass vials on an orbital shaker (Remi, Mumbai, India) for 48 h at 25 ± 0.5 ºC and 75 ± 0.5 ºC. Thereafter, the resulting suspensions were centrifuged at 12,000 x g for 10 min to settle the suspended drug particles. The supernatant was carefully collected and filtered through Millex-VV 0.1 µm, PVDF syringe filter (the filter was previously validated for absence of drug adsorption). Filtrates were suitably diluted with methanol and analysed using a validated HPLC method. All the experiments were done in triplicates and results expressed as mean ± S.D.

5.3 Results and discussion

5.3.1 Screening and selection of lipids

Solubility of raloxifene hydrochloride in various lipid matrices was established by two methods. In the first method, we determined the amount of lipid required to dissolve 10 mg of raloxifene hydrochloride. The results from this experiment are presented in Fig 5.3

below. In this experiment, lower the amount of lipid required to solubilise the drug, better will be the loading efficiency in the SLN.

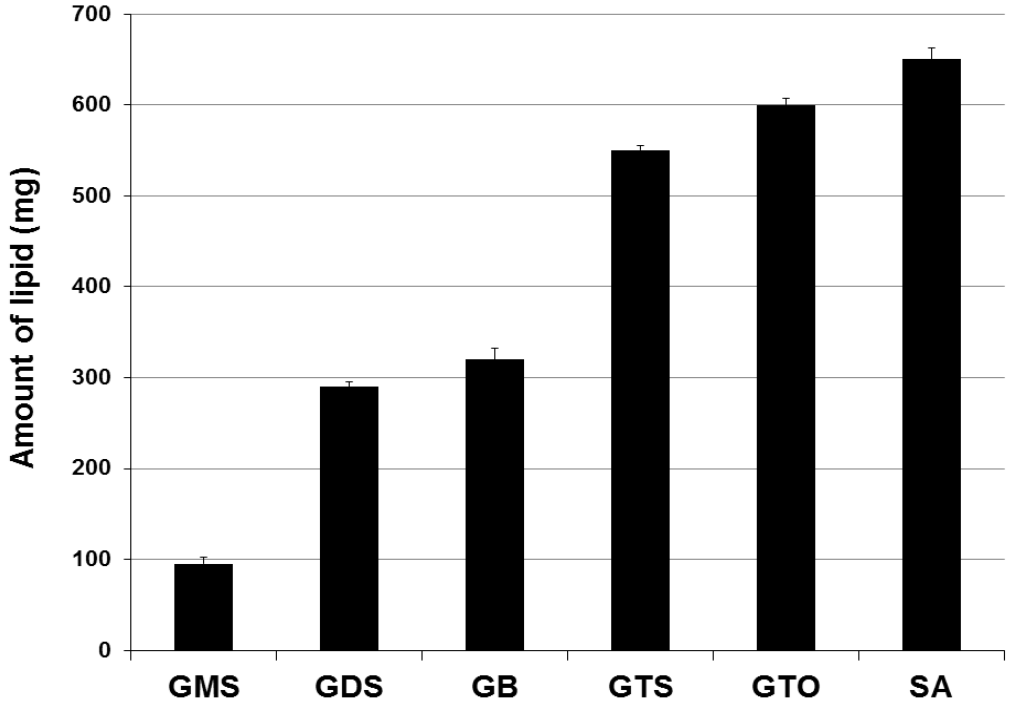

Fig 5.3: Solubility profile of raloxifene hydrochloride in different lipids. Each value represents mean ± SD of three independent observations. GMS – glyceryl monostearate; GDS – glyceryl distearate; GB – glyceryl behenate; GTS – glyceryl tristearate; GTO – glyceryl trioleate; SA – stearic acid.

The solubility of raloxifene hydrochloride was highest in GMS. This may be explained by the composition of GMS which comprises of ~50% monoglycerides; GMS behaves like a surfactant and demonstrates low surface activity in aqueous solutions [16]. On the contrary, GTS and GTO are triglycerides of high molecular weight and low surface activity. Based on these results, top three lipids (GMS, GDS and GB) were selected for formulation of raloxifene hydrochloride loaded SLNs.

5.3.2 Solubility of raloxifene hydrochloride in aqueous surfactant solutions

From the results, apparently, no significant difference in solubility of the drug at different concentrations of aqueous poloxamer 407 solutions was evident. To simulate the actual experimental condition encountered during preparation of SLN, we also estimated the solubility of drug at elevated temperature (75 ± 0.5 ºC). However, even in this case, no significant difference in solubility of drug across different concentrations of poloxamer 407 was noticed. Moreover, in preparation of SLN, we used 20 mL of hot surfactant solution (for forming primary emulsion) with drug-lipid dispersion. Therefore, considering the small volume of hot surfactant solution used and drug's high lipid solubility, it is expected that encapsulation efficiency of drug does not change appreciably for trials with maximum amount of lipid. The actual encapsulation efficiency of raloxifene hydrochloride in SLN is a result of interplay of drug's solubility in both lipid and surfactant solution.

In case of Tween 80, the solubility of raloxifene hydrochloride was much higher and it progressively increased with increasing concentration and incubation temperature. This may be due to lower CMC value of Tween 80 compared to poloxamer 407. It is desirable to elucidate the actual partitioning behaviour of the drug in lipid and aqueous surfactant solution at 75 ± 0.5 ºC (conditions that simulate actual preparation steps in SLN). However, this could not be accomplished because mixing lipid and aqueous surfactant solution resulted in formation of an in-situ emulsion that did not yield two distinct phases for estimation of drug partitioning.

Table 5.1: Solubility of raloxifene hydrochloride in different aqueous surfactant solutions

	Concentration of surfactant (% w/v)	**Equilibrium solubility of drug (µg/mL) (At zero hour) (*n* = 3)**	**Equilibrium solubility of drug (µg/mL) (After 48 h at 37±0.5 ºC) (*n* = 3)**	**Equilibrium solubility of drug (µg/mL) (After 48h at 75±0.5 ºC) (*n* = 3)**
Poloxamer 407	1.0	210 ± 2	212 ± 4	241 ± 3
	2.5	316 ± 3	321 ± 4	348 ± 4
	5.0	352 ± 2	359 ± 3	362 ± 3
	7.5	351 ± 4	355 ± 3	371 ± 4
Tween 80	0.5	476 ± 7	498 ± 4	523 ± 3
	1.0	670 ± 2	694 ± 6	721 ± 4
	1.5	884 ± 3	874 ± 5	909 ± 8

5.4 Formulation of raloxifene hydrochloride loaded SLNs

As indicated earlier, we selected GMS, GDS and GB as lipids for formulation of raloxifene hydrochloride loaded SLN. Initial trials with these lipids were taken employing the well-reported warm oil-in-water micro-emulsion technique with minor modifications [17]. The surfactant concentration was kept constant (poloxamer 407, 5 %w/v) for all these trials. However, it was noticed that with GDS, primary emulsion was not formed and hence no nanoparticles could be obtained. The SLNs formulated with GMS showed low particle size (< 200 nm) and high entrapment efficiency (> 80%). Nevertheless, upon standing for 24 h, these SLNs aggregated and led to an increase in particle size (>1 µm) and change in particle size distribution. Therefore, for all further trials, it was only prudent to use GB as the lipid phase and poloxamer 407 as the emulsifier.

We hypothesized that oral bioavailability of raloxifene hydrochloride can be improved significantly if higher carbon chain lipid like GB was used in conjunction with poloxamer 407 as emulsifier-stabilizer. Therefore, primary objective of this work was to prepare raloxifene hydrochloride loaded SLN with GB and P407 for oral administration.

Because manufacture of SLN is a multi-step process with many variables, for reproducibility, it is important to understand the interplay of formulation/process variables and to optimize manufacturing conditions. For this, we used design of experiments (DOE) to optimize the manufacturing process of SLN. However, in a process where many variables are involved, a single design is not always adequate. Therefore, we followed a hybrid-design approach: Plackett Burman design (PBD) for initial screening, followed by Box-Bhenken design (BBD), a sub-type of response surface methodology (RSM) design for process optimization. We selected particle size and entrapment efficiency percentage (EE %) as responses in the design because both of these responses affect *in vitro* and *in vivo* performance of SLN.

The PBD is particularly useful when large number of variables have to be screened with fewer runs. This design uses only a fraction of trials used in full factorial design and is suitable for initial screening of critical variables [18]. However, with PBD alone, we cannot detect interaction effects between variables.

For this, we need more sophisticated RSM design like BBD. We selected BBD because it requires fewer runs and is particularly useful when extreme treatment combinations need to be avoided. Using BBD, we identified multi-factor interactions between manufacturing variables.

We assessed the capability of SLN in enhancing oral BA of raloxifene hydrochloride by carrying out extensive pharmacokinetic evaluation and tissue distribution studies in female Wistar rats. Finally, to decipher the mechanism of intestinal uptake of SLN, we performed permeation studies in presence and absence of uptake inhibitors. To evaluate the role of lymphatic transport in oral delivery of SLN, we also conducted comparative pharmacokinetic studies in presence and absence of lymph flow inhibitor, cycloheximide.

5.4.1 Experimental Design

We used low resolution PBD to screen critical variables in the manufacturing process. Eleven variables were studied at two levels to determine their effect on two responses, viz., EE% and particle size of RLX-SLN formulations. Variables studied were: type of surfactant (polysorbate 80 and P407), concentration of surfactant (1% and 5% w/v), temperature of surfactant solution (25 and 75 °C), volume of external phase (10 and 30 ml), speed of homogenization (7500 and 12500 rpm), time of homogenization (2 and 16 min), amount of lipid (0.5 and 1.5 g), time of ultrasonication (5 and 15 min), ultrasonication amplitude (70% and 100%), ultrasonication pulse (continuous and pulse mode) and temperature during homogenization (60 and 75 °C).

From PBD, we selected three most influential variables (X_1 = surfactant concentration, X_2 = amount of lipid and X_3 = ultrasonication time) that influence EE (Y_1) and particle size (Y_2) of SLN. Further, these variables were examined for individual and interaction effects using higher resolution BBD, fixing other variables. The BBD comprised 17-runs and 3-factors, studied at 3-levels. Five center point trials were included to assess reproducibility of the method. Using BBD, we also constructed following second order polynomial model for optimization of the manufacturing process:

$$Y = b_0 + b_1X_1 + b_2X_2 + b_3X_3 + b_{11}X_1^2 + b_{22}X_2^2 + b_{33}X_3^2 + b_{12}X_1X_2 + b_{13}X_1X_3 + b_{23}X_2X_3$$

Where, the b_i (for i =1, 2 and 3) are the linear effects, the bii's are the quadratic effects, the bij's (for i, j = 1, 2 and 3, i<j) are the interactions between the i^{th} and the j^{th} variables; the b_0 is the intercept. Design Expert 8.0.7 software (Full version 8.0.7.1, Stat-Ease Inc., Minneapolis, MN) was used for both designing experiments and for statistical analysis of data. Selection of optimized formulation was done based on 'Goals' mentioned in table 5.2.

Table 5.2: Variables and their levels used in Box-Behnken design

Factor	Levels used		
	-1	0	+1
Independent variables			
X_1= Surfactant concentration (% w/v)	2.5	5.0	7.5
X_2=Lipid amount (mg)	500	1000	1500
X_3= Ultra sonication time (min)	2.0	4.0	6.0
Dependent factors		**Constraints**	
Y_1= Particle size (nm)		Minimize	
Y_2= Entrapment efficiency (%)		Maximize	

5.4.2 Preparation of solid lipid nanoparticles

For preparation of RLX-SLN, previously reported warm oil-in-water micro-emulsion technique [17] was employed, albeit with minor modifications. Briefly, GB (quantity varied as per experimental design) was held in a molten state at 75 °C. In this, accurately weighed quantity of raloxifene hydrochloride (50 mg) was dispersed thoroughly to form homogenous dispersion. This formed the lipid phase of emulsion. Aqueous phase was prepared by dissolving P407 (quantity varied as per experimental design) into double-distilled high purity water. Aqueous phase was heated until it became isothermal with lipid phase. Both phases were together homogenized (Polytron PT 3100D, Kinematica, Lucerne, Switzerland) at 10,000 rpm for 10 min, while maintaining temperature at 75 ± 0.5 °C. The obtained micro emulsion was then quickly ultrasonicated using a probe sonicator (Vibra cell, Sonics, USA) for specific time period at fixed amplitude (300 W output). This resulted in o/w nano-emulsion that was then cooled down in an ice-bath to form SLN. Final volume was adjusted to 200 ml with cold deionized high purity water. SLN dispersions were freeze-dried in lyophilizer (Coolsafe 110-4, Scanvac, Lynge, Denmark) for 12 h with 5% mannitol as a cryoprotectant to obtain free flowing powder. Lyophilized powder was stored in air-tight glass containers at room temperature till further use. The scheme of preparation is illustrated in Fig. 5.4 below.

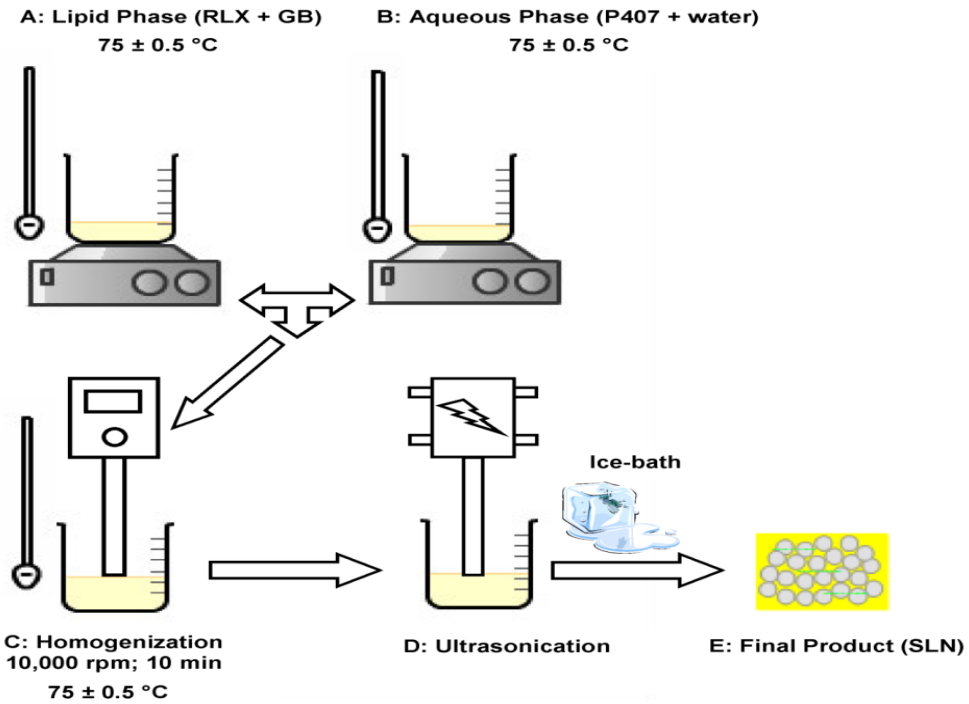

Fig 5.4: Preparation method for raloxifene loaded solid lipid nanoparticles

5.4.3 HPLC method for analysis of raloxifene hydrochloride

5.4.3.1 Method for analysis of EE, assay and in-vitro drug release study samples

Samples from EE, assay and in-vitro drug release studies were analyzed after suitable dilution and processing by a validated HPLC method as described.

5.4.3.2 Method for analysis of biological samples

The procedure described earlier under bioanalytical method development and validation section was used for analysis of biological samples.

5.4.4 Characterization Studies

5.4.4.1 Particle Size and Zeta Potential

Particle size, polydispersity index (PDI) and zeta potential of the SLN were measured by Zetasizer nano ZS 90 instrument (Malvern Instruments, Worcestershire, UK). Intensity of scattered light was measured at an angle of 90°. The samples were appropriately diluted with double-distilled high purity water before measurement. The instrument was set for 10 min in

serial mode; sample measurement time was 30 ms. Values of zeta potential and PDI were directly obtained from the software provided with the instrument.

5.4.4.2 Entrapment Efficiency (EE)

The EE (%) was obtained by ultrafiltration (regenerated cellulose membrane, molecular cut-off 10,000 Da, Milipore, Billerica, MA) method after suitable dilution. We selected filter for ultrafiltration based on independent adsorption and particle penetration studies performed earlier. Following equation was used to calculate EE:

$$EE\ (\%) = \ (W_{total} - W_{SN})/W_{total} \ \times 100$$

Where, W_{SN} is the amount of free raloxifene hydrochloride obtained in filtrate; W_{total} is total amount of raloxifene hydrochloride added to formulation. Drug content was determined using a validated HPLC method.

5.4.4.3 Scanning electron microscopy (SEM) analysis

Raloxifene hydrochloride-SLNs were examined for surface morphology under scanning electron microscope (JSM-6360LV Scanning Microscope; Tokyo, Japan). Before analysis, 100 µl of SLN suspension was dried overnight on aluminum stub under vacuum. This was then sputter-coated using a thin gold-palladium layer under an argon atmosphere using a gold sputter module in a high-vacuum evaporator (JFC-1100 fine coat ion sputter; Tokyo, Japan). These coated samples were then scanned and photomicrographs were taken at an acceleration voltage of 15 kV.

5.4.4.4 Differential scanning calorimetry (DSC)

Calorimetric analysis was carried out using DSC 60 (Shimadzu Corporation, Kyoto, Japan) instrument. Briefly, accurately weighted sample was taken in aluminum pan and crimp sealed. In the DSC chamber, samples were allowed to equilibrate at 25 °C. Then, the samples were subjected to heating run over temperature range of 25 to 300 °C at a heating rate of 5 °C

per min. DSC thermograms were directly obtained from the software supplied with the instrument.

5.4.4.5 Powder X-ray diffraction studies (pXRD)

The pXRD studies were carried out at ambient temperature with Philips XPert Pro X-ray diffractometer (Almelo, The Netherlands); target Cu (λ= 1.54 A°); filter Ni; voltage 40 kV; time constant 5 mm/s; scanning rate 1°/min.

5.5 In-vitro evaluation of SLN

5.5.1 In-vitro drug release studies

We used previously reported method to perform in-vitro drug release study [19]. Briefly, RLX-SLN (equivalent to 1 mg raloxifene hydrochloride) were dispersed in 200 ml PBS (phosphate buffer solution, pH 7.4) containing 0.1% w/v polysorbate 80 and incubated at 37 °C under uniform stirring. At pre-determined time intervals, 1 ml samples were withdrawn from the dissolution media using syringe fitted with Medical Millex-VV 0.1 µm, PVDF, 33 mm filter (Millipore, MA, USA) for analysis. The RLX-SLN pulled into the syringe filter during sampling were returned back to dissolution media by "back washing" same volume of drug-free media through the syringe [20]. The filtered samples were analyzed for drug content by validated HPLC method. Obtained data was fitted into zero order, first order, Higuchi and reciprocal-powered time mathematical models for evaluation of drug release kinetics [21]. Regression coefficient (r^2) and time for 50% drug release ($t_{50\%}$) were calculated for the best-fit model. Models used to fit the drug release data are listed below:

Zero order model: $F = k_0 t$,
First order model: $\ln(1 - F) = -k_f t$,
Higuchi model: $F = k_H \sqrt{t}$,
Reciprocal powered time model: $(1/F - 1) = m/t\text{^}b$

Where, F is fraction of drug released up to time t; k_0, k_f, k_H, m and b are model parameters.

5.5.2 Stability studies

We subjected optimized RLX-SLN formulation to stability testing as per International Conference on Harmonization (ICH) Q1A (R2) guidelines. Optimized RLX-SLN formulation (n = 3) were stored in sealed glass vials at 25 ± 2 °C/60 ± 5% RH in a stability chamber (Remi, Mumbai, India) for period of 3 months. Control samples at corresponding time intervals were stored at 2-8 °C. Statistical evaluation was done using GraphPad Prism version 5.03 for Windows software (GraphPad Software, San Diego, USA).

5.6 In-vivo and ex-vivo studies using SLN

5.6.1 In-vivo pharmacokinetic studies in rats

Female Wistar rats, weighing 180–220 g, were used in the study. The experimental protocol was approved by the Institutional Animal Ethics Committee. Experimental animals were fasted overnight (12 h) before dosing and were continued under fasting until 4 h post-administration. Thereafter, rat chow diet was provided *ad libitum*. In all the studies, freshly prepared SLN formulations were administered.

Pharmacokinetic studies were conducted post-oral (15 mg/kg) and post-intravenous (IV, 4 mg/kg) administration of free raloxifene hydrochloride and RLX-SLN. For both oral and IV pharmacokinetic study, two groups with six animals in each group were made. While control group received free raloxifene hydrochloride (suspended in 0.5% w/v methyl cellulose, molecular weight 14,000 Da, viscosity 15 cps), treatment group received optimized RLX-SLN formulation. Similarly, in IV pharmacokinetic study, control group received free raloxifene hydrochloride solution (dissolved in PEG 400: water pre-mix (1:1)), while the treatment group received RLX-SLN formulation.

Blood samples (0.15ml) were collected from the orbital sinus into microfuge tubes containing anti-coagulant (3.8 %w/v sodium citrate) at pre-dose (0.0), 0.17, 0.25, 0.5, 1, 2, 4, 6, 8 , 12, 24 and 48 h post dose for oral studies and at pre-dose (0.0), 0.17, 0.25, 0.5, 1, 2, 4,

6, 8, and 12 h post dose for IV studies. These samples were further harvested for plasma by centrifugation at 1000 x g at 4 °C for 10 min. Harvested plasma samples were stored at -70 °C until further analysis. Previously validated HPLC method was used for analyzing these samples.

5.6.2 Uptake of RLX-SLN into rat everted gut sac

Several endocytic uptake processes are described in the literature for intestinal uptake of lipid based nanoparticles. To understand the uptake mechanism of RLX-SLN, we conducted everted gut sac studies using rat intestinal segments [22, 23].

Briefly, female Wistar rats (n = 3) were fasted overnight for 12 h but allowed water *ad libitum* before the experiment. After anesthesia (urethane, 1.25 g/kg, i.p.), entire small intestinal segment was removed by cutting across the upper end of the duodenum and the lower end of ileum. The mesentery was separated by manual stripping. Intestine was washed carefully with normal saline (0.9% w/v NaCl) and different segments of small intestine were identified. A length of 8-10 cm was rapidly removed and gently everted over a glass rod. The everted intestine was then slipped off the glass rod and placed in a flat dish containing Krebs-Henseleit bicarbonate (KHB) buffer oxygenated with O_2/CO_2 (95%/5%) at 37 °C. One end of everted intestine was clamped and tied with a silk suture, while, from the open end, buffer at 37 °C was filled using 0.5 ml syringe. The intestinal sac was then slipped off the needle carefully and loose ligature at the proximal end was tightened. The sacs were then placed in individual incubation chambers containing either free raloxifene hydrochloride or RLX-SLN (effective concentration of raloxifene hydrochloride 4.0 µg/ml) prepared in oxygenated KHB buffer at 37 °C.

To discern uptake mechanism, everted gut sacs were incubated at 4 °C or in presence of specific endocytic inhibitors like chlorpromazine (CPZ) (10 µg/ml) and nystatin (NYT)

(25 µg/ml) at 37 °C. After pre-set incubation time of 30 min, intestinal sacs were carefully removed, blotted onto filter paper and contents were collected. Sacs were rinsed thrice with KHB buffer and rinsing was pooled with original content for analysis. Samples were analyzed with a validated HPLC method.

5.6.3 Lymphatic transport of RLX-SLN in rats

It is widely reported that lipid nanoparticles are taken up into enterocytes and are transported by lymphatic route to eventually reach systemic circulation [24-28]. To test this hypothesis, intestinal transport studies were carried out in presence and absence of a lymph transport inhibitor, cycloheximide (CXI). CXI is known to inhibit the secretion of chylomicrons from the enterocytes and therefore, inhibit lymphatic drug transport without causing damage to other active and passive absorption pathways [29-32].

In this study, six female Wistar rats weighing 180 to 220 g were randomly divided into two groups. Each group received either saline (control group) or CXI solution in saline (3 mg/kg) (treatment group) by i.p. route. One hour post-dosing, RLX-SLN formulation (15 mg/kg) was administered by oral gavage to rats from both groups. Blood samples (0.15 ml) were collected from rats at pre-dose (0.0), 0.17, 0.25, 0.5, 1, 2, 4, 6 and 8 h post-dose and samples were processed and analyzed as explained earlier.

5.6.4 Tissue-distribution study

This study was performed to understand the differences in tissue distribution pattern of free raloxifene hydrochloride and RLX-SLN. For this study, 36 female Wistar rats (180 ± 20 g) were divided into two groups with 18 rats in each group. Rats from each group were administered either free raloxifene hydrochloride suspension or RLX-SLN at a dose of 20 mg/kg via oral gavage. Three rats per group were sacrificed at 0.5, 1, 2, 4, 6 and12 h post-dosing. Immediately after sacrificing the animals, tissues of interest (spleen, liver, kidneys

and lungs) were collected and blotted dry on a tissue paper. Tissue samples were then frozen at -70 °C until further analysis. Prior to analysis, frozen tissue samples were thawed to room temperature, minced and water equivalent to tissue weight was added. Further, we homogenized these tissue samples to fine paste in a tissue homogenizer (Remi, Mumbai, India). The homogenized tissue samples were suitably processed by adding protein precipitating agent, acetonitrile (2 parts acetonitrile to 1 part of tissue homogenate) and centrifuged at 8000 x g for 20 min. Clear supernatant obtained was analyzed by HPLC method as described previously.

5.7 Statistical Analysis

Analysis of Variance (ANOVA) was used to examine significance of difference between experimental results in BBD. The *F*-test was used to determine an overall regression relationship between response variable *Y* and entire set of *X* variables at 95% ($\alpha = 0.05$) significance level. The co-efficient of multiple regression analysis (r^2) measured proportionate reduction of total variation in *Y* associated with set of *X* variables. Additionally, regression model validity was assessed using statistical assumptions and 'lack of fit' tests. Wilcoxon Signed Rank Test was used to identify statistically significant difference between actual and theoretical values for the optimized formulation at 95% ($\alpha = 0.05$) significance level. For analysis of everted gut sac study data, one way ANOVA at 95% ($\alpha = 0.05$) significance level was used. In lymphatic transport study, for assessing difference in plasma AUC_{0-t} of rats from control and treatment group, unpaired *t*-test was used at 95% ($\alpha = 0.05$) significance level.

5.8. Results and Discussion

5.8.1 Experiments using Plackett-Burman Design

Low resolution Plackett-Burman Design (PBD) was used to screen critical formulation and manufacturing variables in preparation of RLX-SLN. Influence of manufacturing variables like temperature, volume of external phase, homogenization time and speed, ultrasonication time, amplitude and mode on EE and particle size were determined. Additionally, effect of formulation variables like amount of lipid, type of surfactant and concentration of surfactant on EE and particle size was also investigated.

From PBD, amount of lipid, surfactant type, surfactant concentration and ultrasonication time were found to be most influential variables affecting EE and particle size. Two surfactants, polysorbate 80 and P407 were selected for evaluation. Formulations prepared with polysorbate 80 (1% w/v) as surfactant showed low particle size (172 ± 4 nm) and moderate EE (42 ± 2%). This moderate EE was attributed to higher saturation solubility of raloxifene hydrochloride in 1% w/v aqueous polysorbate 80 solutions (670 ± 2 µg/ml) which is also the external phase in preparation of SLN. In contrast, formulations with P407 showed low particle size (167 ± 3 nm) and high EE (93 ± 2%). Saturation solubility of raloxifene hydrochloride in 5 %w/v aqueous P407 solution was 358 ± 3 µg/ml. Therefore, P407 was selected as surfactant for further trials. Moreover, it has been previously reported [14] that tri-block co-polymers like P407 could provide stearic hindrance on SLN surface that would protect lipid from activity of lipase in the body which also influenced our selection of surfactant.

5.8.2 Box-Behnken design

5.8.2.1 Effect of formulation variables on particle size (Y_1)

The least-square second order polynomial equation for particle size at 95% confidence level is given below:

$$Particle\ size\ (Y_1) = 167.2 - 15.375(X_1) + 28.125(X_2) + 1(X_3) - 3.25(X_1X_2) + 2.5(X_1X_3) + 1(X_2X_3) + 80.525(X_1^2) + 23.525(X_2^2) + 21.775(X_3^2)$$

The quadratic model was found to be significant with F-value of 2174.22 ($P < 0.0001$). The value of regression co-efficient (r^2) for this equation was of 0.9893 indicating good correlation between response and selected factors. The residuals were distributed randomly around zero; there was no effect of experimental sequence on the trend of residuals. The regression co-efficients for X_1, X_2, X_1X_2, X_1X_3, X_1^2, X_2^2 and X_3^2 were significant. While particle size varied from 165 nm (run 16) to 319 nm (run 5), EE varied from 59% (run 9) to 94% (run 2). Results for all the runs are summarized in Table 5.3.

Table 5.3: Actual experimental design and obtained response

Run	Surfactant concentration (% w/v, X_1)	Lipid amount (mg, X_2)	Ultrasonication time (min, X_3)	Particle size (Y_1, nm)	Entrapment efficiency (Y_2, %)
1	7.5	1500	4.0	280	92
2	5.0	1500	2.0	238	94
3	5.0	1000	4.0	168	92
4	7.5	1000	6.0	258	76
5	2.5	1500	4.0	319	90
6	2.5	1000	2.0	287	73
7	7.5	1000	2.0	252	89
8	5.0	500	2.0	184	69
9	2.5	500	4.0	257	59
10	2.5	1000	6.0	282	73
11	5.0	1000	4.0	167	90
12	5.0	500	6.0	185	65
13	5.0	1500	6.0	243	85
14	5.0	1000	4.0	169	93
15	5.0	1000	4.0	168	91
16	5.0	1000	4.0	165	92
17	7.5	500	4.0	230	76

These results indicate that surfactant concentration and lipid amount significantly influence particle size of SLN, whereas, ultrasonication time alone has little impact. Ultrasonication time in interaction with surfactant concentration (X_1X_3) can influence particle size significantly. Effect of lipid amount and surfactant concentration on particle size at fixed

ultrasonication time is shown in Fig. 5.5a. It was observed that an increase in lipid amount caused corresponding increase in particle size. For a given concentration of surfactant, as amount of lipid increases, lipid molecules tend to coalesce. This is due to increasing interfacial tension between lipid and aqueous phase with increasing lipid leading to coalesce and increase in particle size.

When lipid amount was fixed, effect of surfactant concentration on particle size showed non-linear relation (Fig. 5.5a). Increase in P407 concentration decreased particle size. Beyond 5 %w/v concentration, particle size increased sharply. Apparently, intial decrease in particle size is due to reduction of interfacial tension between lipid and aqeous phase and stabilization of newly formed particles by P407 (due to stearic stabilizing effect) [33]. However, at higher concentrations, hydrophobic interactions between P407 molecules might dominate, leading to aggregation and increase in particle size.

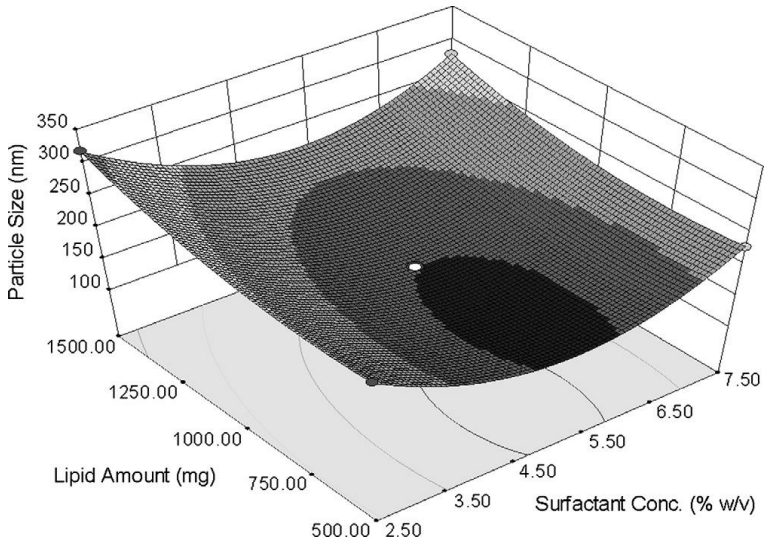

Fig. 5.5a: Response surface plot showing effect of surfactant concentration (X_1) and amount of lipid (X_2) on particle size of RLX-SLN (Y_1).

At fixed surfactant concetration, no significant curvature for ultrasonication time when compared with lipid amount is seen (Fig. 5.5b). This suggests that the factor is of minor importance in its effect on particle size.

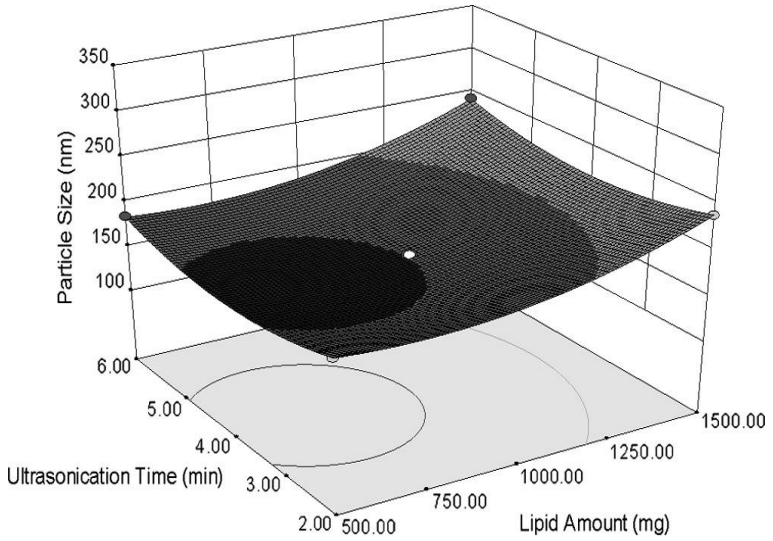

Fig. 5.5b: Response surface plot showing effect of amount of lipid (X_2) and ultrasonication time (X_3) on particle size of RLX-SLN (Y_1).

5.8.2.2 Effect of formulation variables on EE (Y_2)

The least-square second order polynomial equation at 95% confidence level is given below:

$$EE\ (Y_2) = +\ 91.00 + 4.88(X_1) + 11.63(X_2) - 3.00(X_3) - 3.50(X_1X_2) - 3.75(X_1X_3) - 1.25(X_2X_3) - 6.50(X_1^2) - 6.00(X_2^2) - 7.25(X_3^2)$$

Quadratic model was found to be significant with an *F*-value of 207.72 ($p < 0.0001$). Value of regression co-efficient ($r^2 = 0.9763$) indicated good correlation between response and selected factors. Regression co-efficients for X_1, X_2, X_3, X_1X_2, X_1X_3, X_1^2, X_2^2 and X_3^2 were significant (Table 5.4).

Table 5.4: Significance values for particle size and entrapment efficiency (EE)

Source	Particle size (Y_1)				EE (Y_2)			
	Sum of Squares	**DF**	**F-value**	***P*-value**	**Sum of Squares**	**DF**	**F-Value**	***P*-value**
Model	42071.07	9	2174.22	<0.0001*	2069.78	9	207.72	<0.0001*
X_1	1891.12	1	879.59	<0.0001*	190.12	1	171.73	<0.0001*
X_2	6328.13	1	2943.31	<0.0001*	1081.12	1	976.50	<0.0001*
X_3	8.00	1	3.72	0.0951	72.00	1	65.03	<0.0001*
X_1X_2	42.25	1	19.65	0.0030*	49.01	1	44.26	0.0003*
X_1X_3	25.00	1	11.63	0.0113*	56.25	1	50.81	0.0002*
X_2X_3	4.00	1	1.86	0.2148	6.25	1	5.65	0.0592
X_1^2	27302.21	1	12698.70	<0.0001*	177.89	1	160.68	<0.0001*
X_2^2	2330.21	1	1083.82	<0.0001*	151.58	1	136.91	<0.0001*
X_3^2	1996.42	1	928.57	<0.0001*	221.32	1	199.90	<0.0001*
Residual	15.05	7			7.75	7		
Lack-of -fit	8.25	3	1.62	0.3191[xx]	1.75	3	0.39	0.7681[xx]
Pure error	6.80	4			6.00	4		
Total	42086.12	16			2077.53	16		

* Significant at $\alpha < 0.05$. [xx]Not significant at $\alpha < 0.05$.

Fig. 5.5c shows the effect of lipid amount and surfactant concentration on EE at constant ultrasonication time. A steep curvature for EE when viewed from lipid axis indicates that, with increasing lipid amount, EE increases. This is expected because with increasing lipid amount, the lipophlic drug raloxifene hydrochloride gets better entrapped in the lipid matrix. Apparently, higher amount of lipid also provides additional number of particles into which raloxifene hydrochloride can get entrapped.

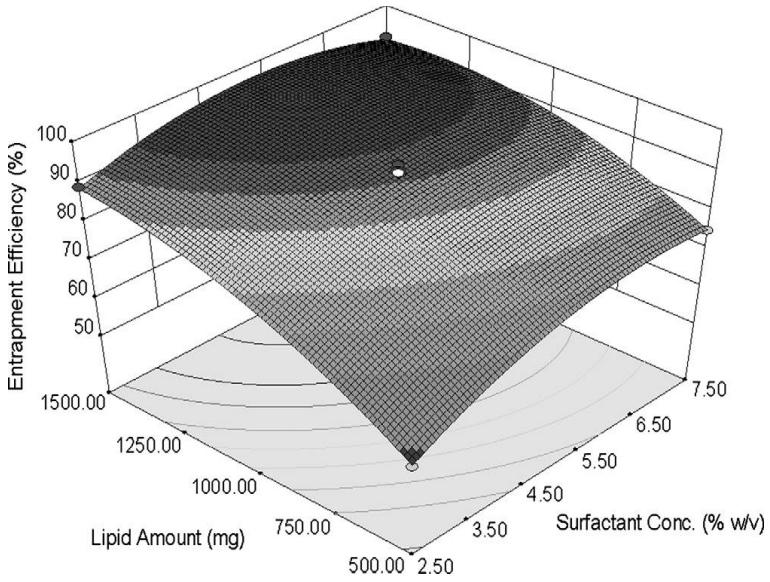

Fig. 5.5c: Response surface plot showing effect of surfactant concentration (X_1) and amount of lipid (X_2) on entrapment efficiency of RLX-SLN (Y_2).

From the polynomial equation for EE, it is evident that surfactant concentration had a positive effect on EE. From fig. 5.5c, at fixed ultrasonication time, EE significantly increased by increasing the surfactant and lipid amount. This effect may be explained by increased viscosity of medium due to increase of both lipid and surfactant that prevents rapid diffusion of raloxifene hydrochloride into the bulk of the medium, thus increasing EE [34]. With higher surfactant concentration, it is also possible that raloxifene hydrochloride gets entrapped in surfactnat layer covering SLN surface affording higher EE. Contrary to reported literature [35], we did not find significant reduction in EE at higher surfactnat concentration. This may be due to surfactant concentration range selected for our study. Curvature of ultrasonication time axis in fig. 5.5d suggests that this variable has low effect on EE.

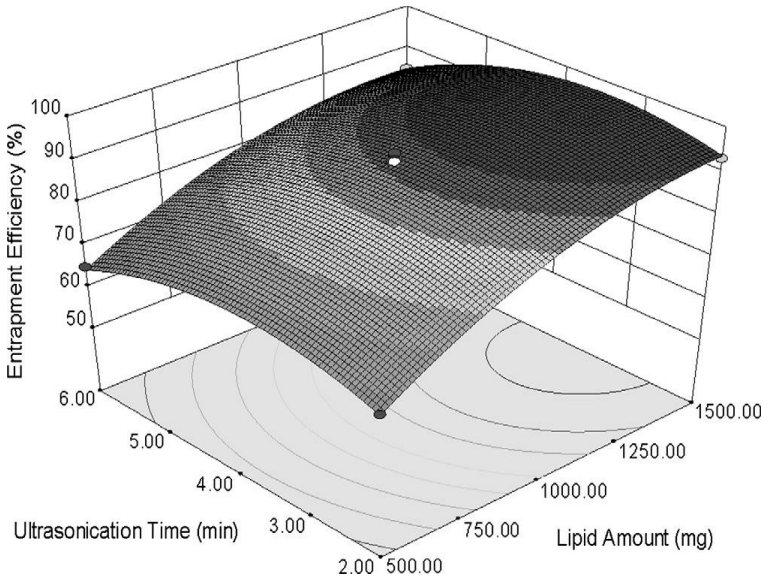

Fig. 5.5d: Response surface plot showing effect of amount of lipid (X_2) and ultrasonication time (X_3) on entrapment efficiency of RLX-SLN (Y_2).

5.8.3 Optimization and validation

Desireability function (0.984) was obtained form Design-Expert software v 8.0.7.1 to identify optimal conditions for RLX-SLN formulation. Optimal formulation was based on set criteria of minimum particle size and maximum EE. Conditions for optimal formulation as predicted by the software was as follows: surfactant concentration (P407) = 5.4 mg/ml, lipid (GB) amount = 1047.4 mg and ultrasonication time = 4.7 min. To prove validity of this statistical model, verification runs (n = 6) using these conditions were carried out. Wilcoxon signed rank test was used for estimation of statistically significant difference between experimental and theoretical values. At $\alpha = 0.05$, there was no statistically significant difference between actual and theoretical values for particle size ($P < 0.0625$) and EE ($P < 0.8438$), thus, affirming validity of proposed model. Optimized formulations had particle size (mean ± SD) of 167 ± 3 nm and EE of 93 ± 2%.

5.9 Characterization of lipid nanoparticles

From surface morphology studies by SEM (Fig. 5.6), it was observed that formulated lipid nanoparticles had near spherical shape with smooth surface morphology. Mean particle size for optimized formulation was 167 ± 3 nm with PDI of 0.2 ± 0.05 (n = 6). Low value of PDI indicated that using optimal conditions, we could manufacture stable SLN suspensions with a relatively narrow size distribution. Zeta potential value of optimal formulation was 23 ± 2 mV. Positive zeta potential could be attributed to surface presence of raloxifene hydrochloride molecules on SLN.

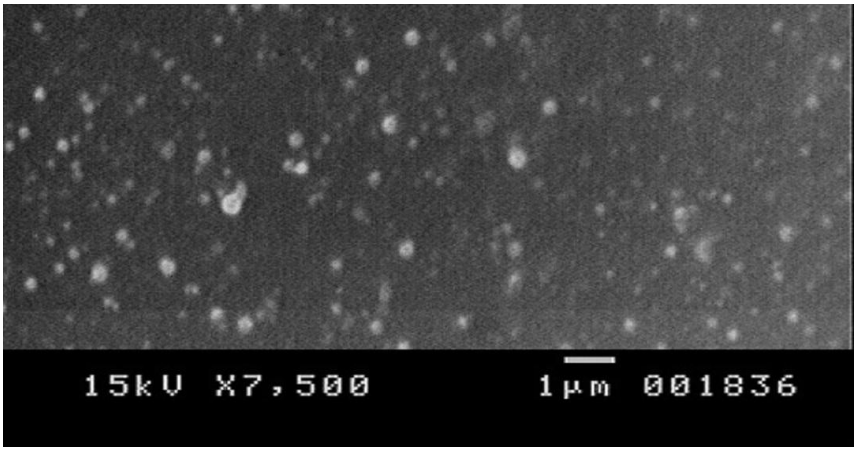

Fig. 5.6: Surface morphology by scanning electron microscopy of raloxifene loaded solid lipid nanoparticles (7500x).

Fig. 5.7 shows DSC thermograms for pure raloxifene hydrochloride, bulk GB, physical mixture of raloxifene hydrochloride and GB in the ratio 1:1, placebo (blank SLN) and RLX-SLN. For pure raloxifene hydrochloride, sharp endothermic peak at 265.0 °C was observed. Bulk GB showed melting endotherm at 72.3 °C. No shift in peak position for raloxifene hydrochloride or GB was observed in physical mixture indicating absence of interaction between raloxifene hydrochloride and lipid. For placebo and RLX-SLN, two peaks at 53.3 °C and 165.3 °C were observed that correspond to P407 and mannitol (used as cryoprotectant) respectively. Apparently, absence of raloxifene hydrochloride endotherm in

thermograms of SLN formulation indicates that majority of raloxifene hydrochloride was present in amorphous form within the lipid matrix.

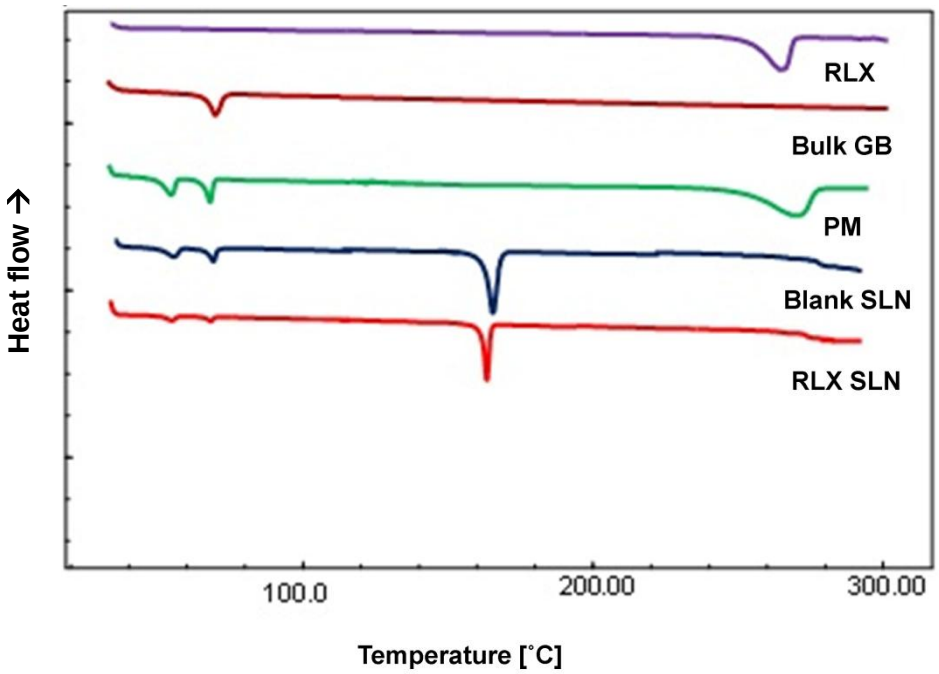

Fig. 5.7: Differential scanning calorimetric thermograms of (A) bulk raloxifene hydrochloride, (B) bulk glyceryl behenate (GB), (C) physical mixture of raloxifene hydrochloride and glyceryl behenate (PM), (D) blank solid lipid nanoparticles (without raloxifene hydrochloride) and (E) optimized solid lipid nanoparticle formulation with raloxifene hydrochloride (RLX-SLN).

Further, pXRD studies of pure raloxifene hydrochloride and RLX-SLN reinforced our hypothesis that crystallinity of raloxifene hydrochloride reduces in SLN formulation. pXRD data is presented in Fig. 5.8 for pure raloxifene hydrochloride (fig. 5.8a), physical mixture (fig. 5.8b) and SLN formulation (fig. 5.8c). For RLX-SLN samples, reduction in intensity and area was seen at following 2θ scattered angles: 14.567°, 15.869°, 19.241°, 21.108° and 22.781°.

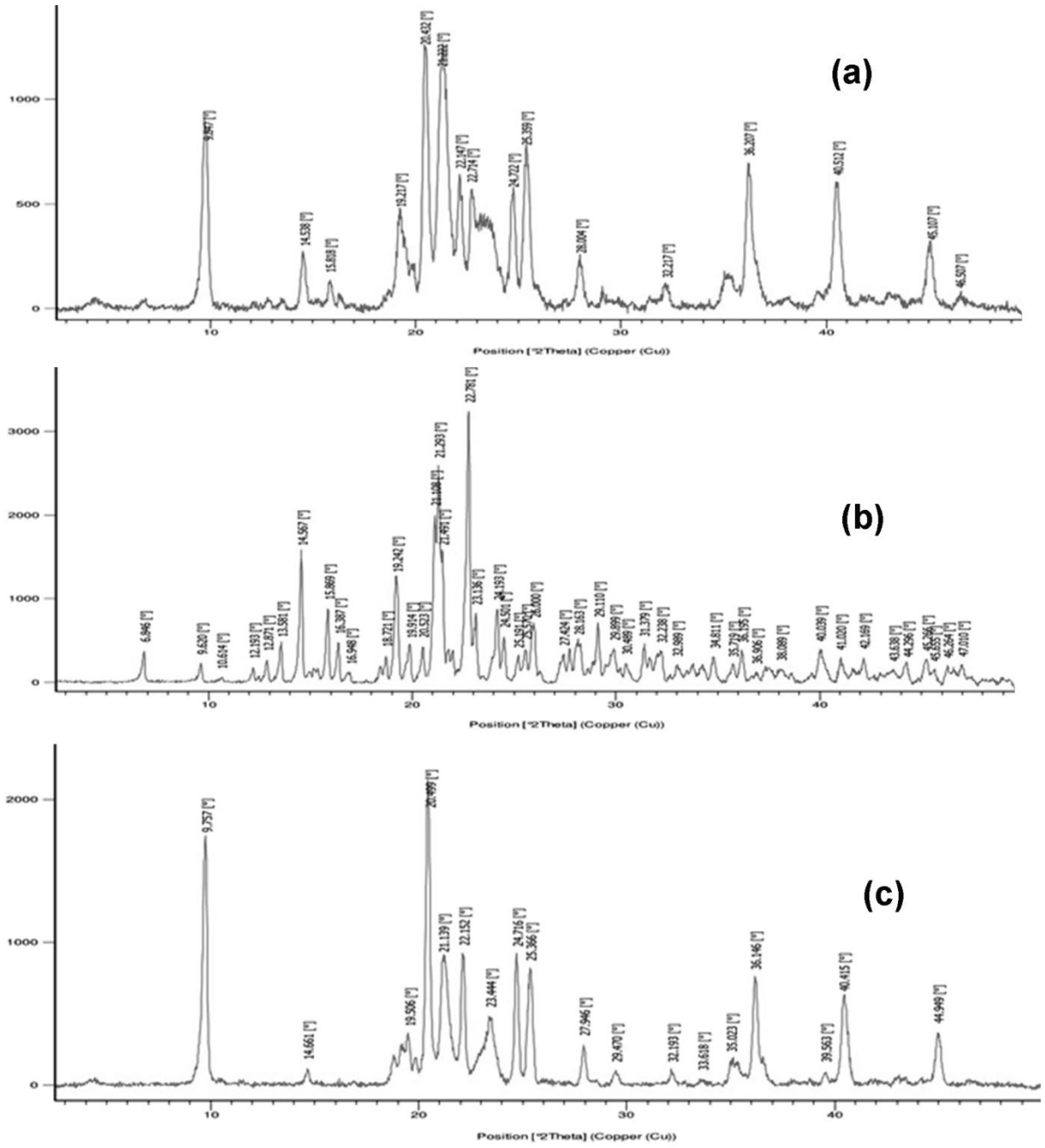

Fig. 5.8: X-ray diffractograms of (a) bulk raloxifene hydrochloride, (b) physical mixture of raloxifene hydrochloride and glyceryl behenate and (c) optimized solid lipid nanoparticle formulation with raloxifene hydrochloride.

5.10 In-vitro drug release studies

In-vitro drug release data is presented in Fig. 5.9. From the figure, apparently, free raloxifene hydrochloride completely released within 4 h. In contrast, release of raloxifene hydrochloride from optimized SLN formulation showed typical bi-phasic release pattern: initial rapid release phase that lasted 30 min, followed by slower release phase lasting up to 72 h. Initial phase of rapid release may be explained by surface presence of raloxifene hydrochloride molecules in SLN. The stearic stabilizer (P407) that covers surface of SLN can also entrap some raloxifene hydrochloride molecules. This will result in higher release rate initially. Second phase of drug release is much slower. This phase is controlled by diffusion of drug from lipid matrix.

We evaluated various models to understand drug release mechanism from SLN. From regression analysis, drug release from SLN was most appropriately described by reciprocal-powered time model (r^2 = 0.9803). In comparison, zero-order kinetics (r^2 = 0.5959), first-order kinetics (r^2 = 0.8556), and Higuchi kinetics (r^2 = 0.7807) showed relatively lower r^2 values. Time taken for 50% drug release ($t_{50\%}$) from SLN formulation was calculated as 29 min.

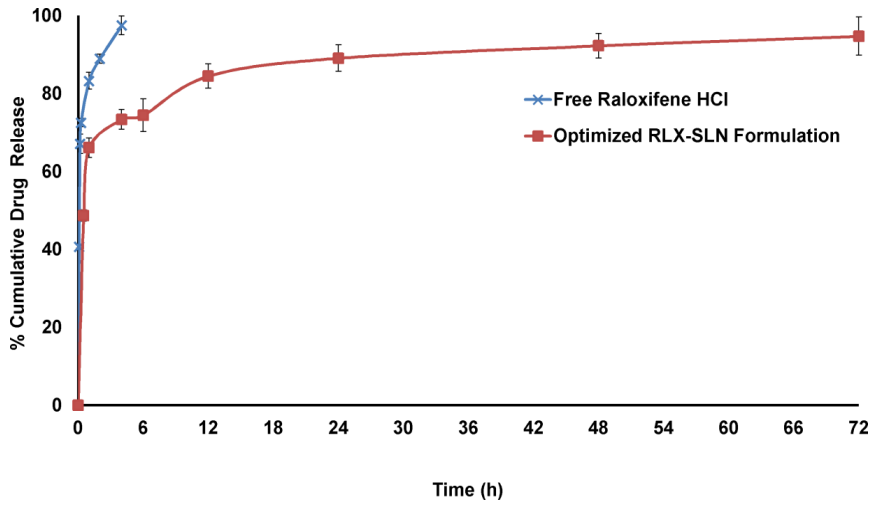

Fig. 5.9: In-vitro drug release profile in pH 7.4 buffer for RLX-SLN and free drug (used as a reference). Data are presented as mean ± SD (*n* = 3).

5.11 Stability studies

Stability estimation for optimized RLX-SLN formulation was done on basis of EE, particle size, zeta potential and PDI variations during three month study period. Results showed that, under refrigerated conditions (2-8 °C) for RLX-SLN, no significant ($P < 0.05$) changes in any of the assessed parameters occur. This is illustrated in fig. 5.10a.

However, it is reported that, upon ageing, drug expulsion from solid lipid matrix (due to crystallization of lipid) leads to reduction in EE [36, 37]. Therefore, to establish shelf-life of the optimized formulation, we considered time taken to reach 90% of initial EE (t_{90EE}) as an indicator. Formulations stored at room temperature (25 °C ± 2 °C and 60% ± 5% RH) were monitored for EE. As predicted, EE decreased with time; t_{90EE} was calculated as 6 months. Value of EE (at 95% C.I.) after 6 months of storage at room temperature ranged from 91.76% (lower C.I) to 94.23% (upper C.I) with a mean of 92%. The shelf-life data is represented in fig. 5.10b. From these studies, for reasons of better stability, we recommend storing RLX-SLN formulations under refrigeration (2-8 °C).

(a)

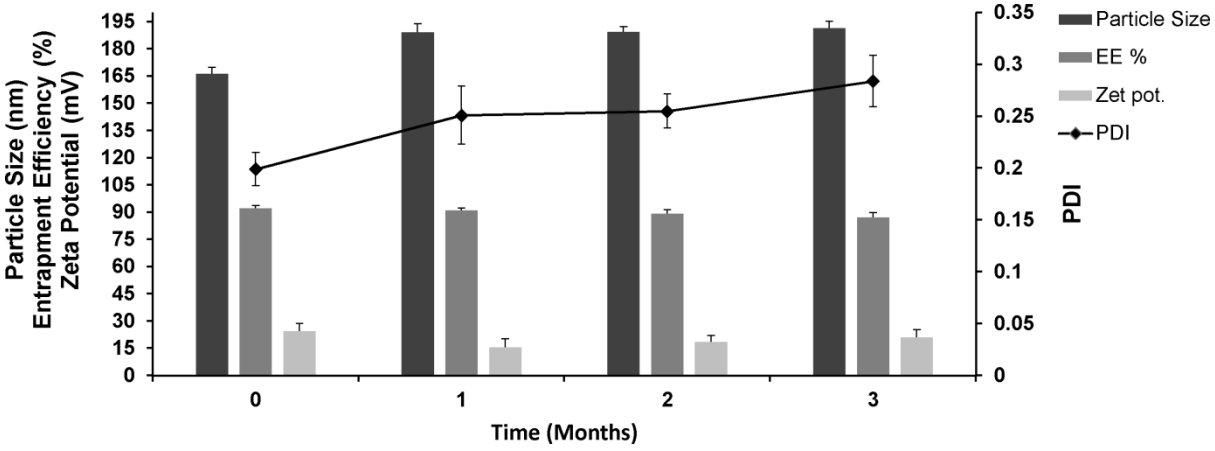

(b)

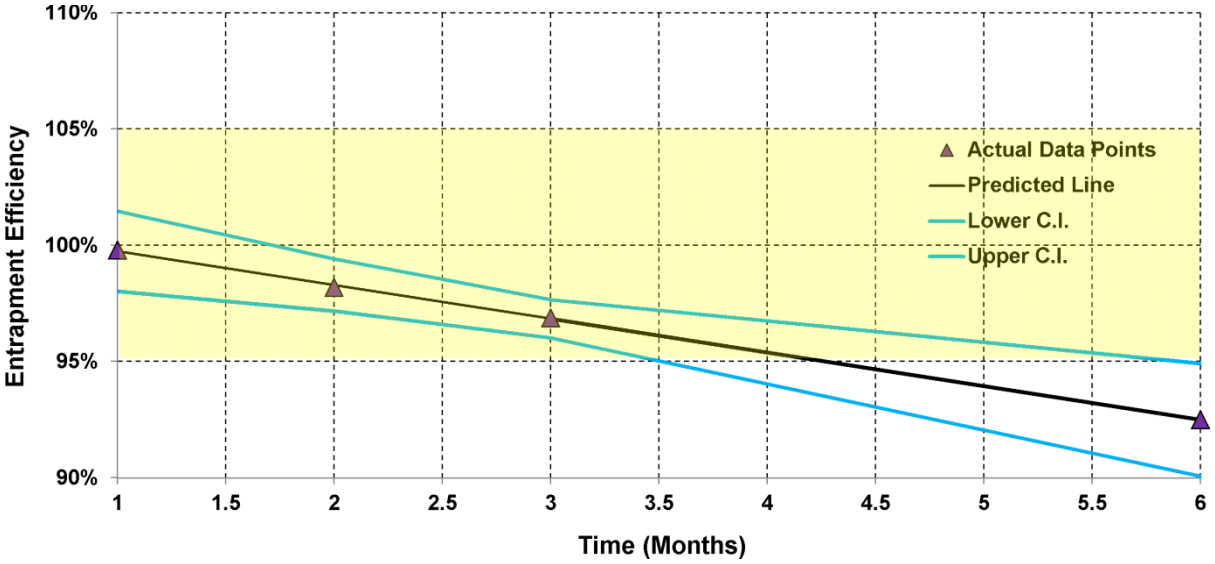

Fig. 5.10: Stability study data for RLX-SLN (a) assessment of particle size, EE, zeta potential and PDI at 2–8 ºC and (b) shelf life estimation of RLX-SLN at 25 ± 2 ºC and 60 ± 5% RH; C.I. indicates 95% confidence interval.

5.12 In-vivo pharmacokinetic studies in rats

For evaluating the effectiveness of optimized formulation in the in-vivo conditions, we performed pharmacokinetic studies for free raloxifene hydrochloride and optimized SLN, post oral and post intravenous (IV) administration in female Wistar rats. Pharmacokinetic parameters of raloxifene hydrochloride after oral administration are given in table 5.5.

Table 5.5: Pharmacokinetic parameters for raloxifene after oral administration of free raloxifene hydrochloride suspension and RLX-SLNs to rats (15 mg/kg, *n* = 6)

Parameter	Raloxifene hydrochloride suspension	RLX-SLN
C_{max} (ng/ml)	182.02 ± 17.18	376.71 ± 45.66***
T_{max} (h)	2.33 ± 0.52	1.33 ± 0.52**
$MRT_{(0-t)}$ (h)	9.21 ± 1.14	16.50 ± 0.91**
$AUC_{(0-t)}$ (µg·h/ml)	2.46 ± 0.46	7.99 ± 1.36 ***
F_{rel}	-	3.24

Each value represents the mean ± SD (*n* = 6). (**$P < 0.01$; ***$P < 0.001$)

The plasma drug concentration versus time profile is presented in Fig. 5.11. Compared to free raloxifene hydrochloride, significant increase ($P < 0.05$) in $AUC_{0\text{-}t}$ and C_{max} for RLX-SLN was seen. From the data, oral bioavailability of raloxifene hydrochloride increased by 3.2 folds in SLN formulation than free raloxifene hydrochloride. Apparently, loading raloxifene hydrochloride into lipid nanoparticles helped in bypassing extensive gut wall metabolism due to intimate association of drug with lipid; absorption through oral lymphatic region ensured an increase in bioavailability. Besides, mean residence time (MRT) for raloxifene hydrochloride from SLN formulations was significantly higher ($P < 0.05$) than free raloxifene hydrochloride.

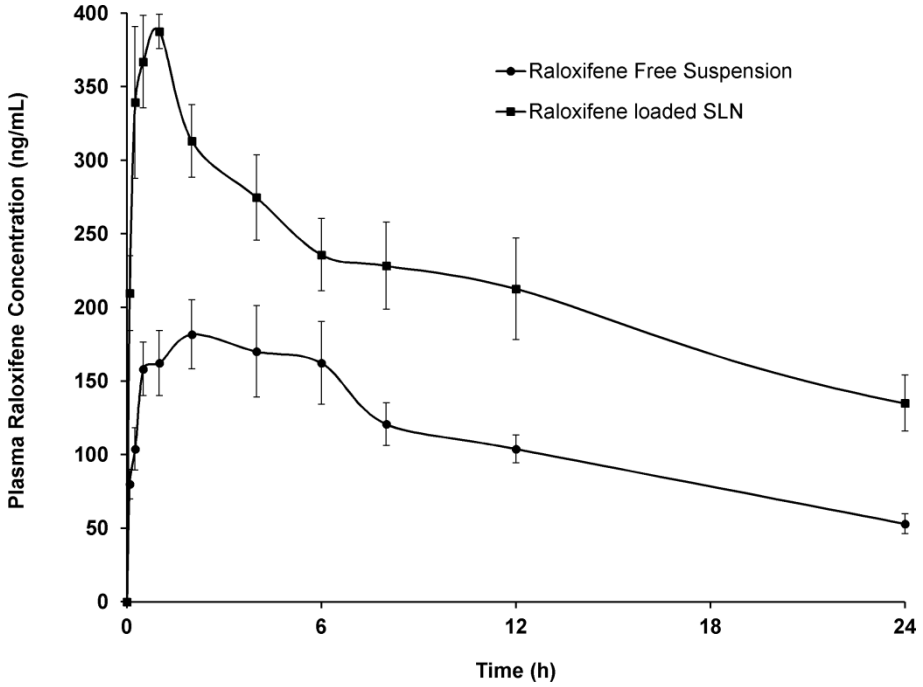

Fig. 5.11: Plasma concentration–time profile of raloxifene in female Wistar rats after oral administration of free raloxifene suspension and RLX-SLN (15 mg/kg). Data are given as mean ± SD ($n = 6$).

The IV pharmacokinetic study data presented in table 5.6 shows that both rate of elimination (K_e) and clearance were significantly ($P < 0.05$) lower for SLN than free raloxifene hydrochloride. Increase in MRT for raloxifene hydrochloride in SLN can be

correlated to reduced K_e and clearance. These in-vivo studies confirm our hypothesis that BA of raloxifene hydrochloride can be improved by using higher carbon chain lipid (GB) with an emulsifier-stabilizer (P407). Protective action of lipid coupled with lower clearance help in improving BA of raloxifene hydrochloride.

Table 5.6: Pharmacokinetic parameters after intravenous administration of raloxifene hydrochloride solution and RLX-SLNs to rats (2.4 mg/kg, $n = 3$)

Parameter	**Raloxifene hydrochloride solution**	**RLX-SLN**
K_e (1/h)	0.5343 ± 0.1218	0.1511 ± 0.0126*
V_d (L/kg)	0.0105 ± 0.0035	0.0052 ± 0.0010*
Clearance (L/kg.h)	0.0056 ± 0.0018	0.0007 ± 0.0002*
$t_{1/2}$ (h)	1.2971 ± 0.0590	4.5874 ± 0.3184**

Each value represents the mean ± SD ($n = 3$). (*$P < 0.05$; **$P < 0.01$)

5.13 Uptake of RLX-SLN into rat intestinal sacs

We investigated uptake of RLX-SLN at two different temperatures, 37 °C (Control) and 4 °C using rat everted gut sac model. It is reported that at lower temperatures (4 °C), energy dependent active processes like endocytosis could be blocked [30]. In our study, at 4 °C, there was significant ($P < 0.001$) reduction in relative apparent permeability (P_{app}) of RLX-SLN, with the uptake being reduced to 78% of that at equivalent concentrations. These results suggest that energy-dependent endocytic processes may be responsible for uptake of majority of SLN, while physical adhesion or free drug diffusion accounts for the remaining.

Many energy-dependent endocytic processes are reported for oral uptake of nanomedicine [24, 28]. Major processes include clathrin-mediated endocytosis, caveolae-mediated endocytosis, and clathrin-caveolae independent endocytosis (importantly, macropinocytosis). While clathrin and caveolae mediated endocytosis are receptor-mediated processes, macropinocytosis is actin-dependent non-specific transport mechanism that is not

mediated by receptors. In macropinocytosis, large (0.5 to 2 µm) vesicular structures at the cell surface called macropinosomes are formed; particles smaller than 2 µm can be internalized into enterocytes by this mechanism [25]. As macropinocytosis is non-specific pathway for endocytic uptake, we did not exclusively evaluate uptake of SLN by this pathway.

To elucidate cellular uptake pathways for SLN, we carried out investigations by treating with different chemical inhibitors of clathrin-mediated endocytosis and caveolae-mediated endocytosis. Chlorpromazine, a cationic, amphiphilic drug, is reported to inhibit clathrin-mediated endocytosis by causing clathrin to accumulate in late endosomes and reducing its availability on the enterocyte surface [37]. In our study, permeability of RLX-SLN reduced significantly by 46% ($P < 0.01$) (Fig. 5.12) compared to control. Based on the results, we conclude that clathrin mediated process contributes to uptake of RLX-SLN.

Caveolae are special type of lipid rafts rich in cholesterol and sphingolipids. They are flask-shaped invaginations on the plasma membrane that can engulf cargo molecules or carriers binding to their surface [24, 38]. The antifungal drug nystatin inhibits caveolae mediated uptake process by cholesterol sequestration [32]. From the results of our study, compared to control, treatment with nystatin caused 27% ($P < 0.05$) reduction in apparent permeability of SLN at equivalent concentrations (Fig. 5.12).

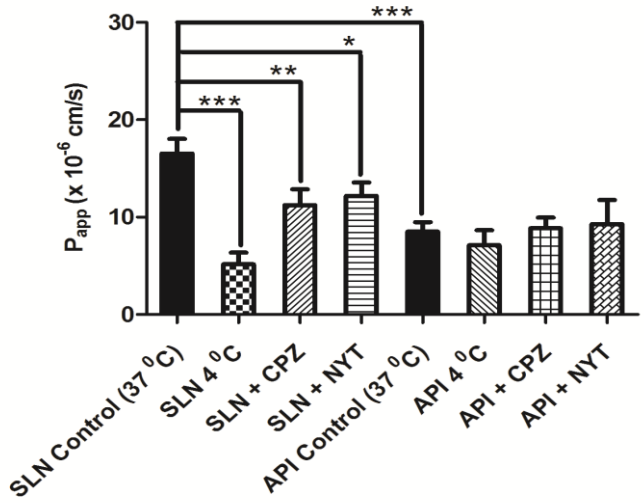

Fig. 5.12: Apparent permeability (P_{app}) of RLX-SLN in rat everted gut sac under different conditions; RLX-SLN incubated at 37 ºC was formulation control and raloxifene hydrochloride free suspension incubated at 37 ºC was API control. CPZ, Chlorpromazine and NYT, Nystatin. (*$P < 0.05$; **$P < 0.01$; ***$P < 0.001$ versus control) ($n = 3$).

Apparently, both clathrin and caveolae mediated endocytosis pathways are involved in uptake of RLX-SLN from rat intestine. Further, compared to free raloxifene hydrochloride, permeability of RLX-SLN was found to be 1.94 folds ($P < 0.001$) higher. For various treatment conditions, we did not observe significant difference in transport of free raloxifene hydrochloride. This suggests that free raloxifene hydrochloride does not undergo active endocytic uptake process. It is likely that free raloxifene hydrochloride is absorbed by simple passive diffusion process.

5.14 Lymphatic transport of RLX-SLN in rats

Upon oral administration, drugs loaded into lipid carriers can access lymphatic transport system by two mechanisms: (1) Through M-cells and gut-associated lymphoid tissue that consist of lymphoidal follicles forming Peyer's patches (2) Stimulating chylomicron production and transport via triglyceride rich lipoproteins [26]. In the latter case, these triglyceride rich lipoproteins preferentially access lymphatic capillaries where cells are arranged in overlapped manner with gaps. Thus, they gain entry into lymphatic system bypassing the portal hepatic circulation [27].

To understand the role of chylomicrons and lymphatic transport in RLX-SLN, we treated rats with lymphatic transport inhibitor, cycloheximide and studied the oral pharmacokinetic parameters. Cycloheximide is known to inhibit the lymphatic transport pathway without damaging other active and passive absorption pathways [29, 30]. Results from lymphatic transport study (Fig. 5.13) show that plasma concentration of CXI treated rats (treatment) was significantly ($p < 0.05$) lower than control group rats. In the treatment group,

peak plasma concentration (C_{max}) of raloxifene hydrochloride reduced by 34% and AUC_{0-t} reduced by 29%. This could be explained by inhibition of lymphatic transport of SLN by CXI. This study demonstrates the importance of lymphatic transport system in oral absorption of RLX-SLN.

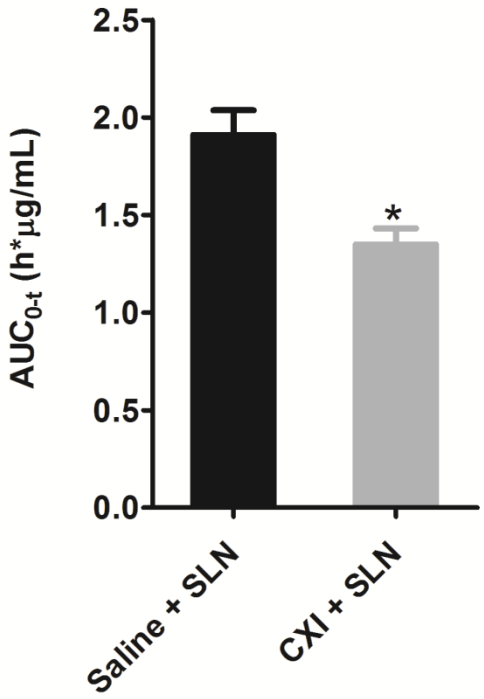

Fig. 5.13: The area under curve ($AUC_{0–t}$) values after oral administration of RLX-SLN to female Wistar rats treated with cycloheximide (CXI) or saline (control) (*$P < 0.05$) ($n = 6$).

5.15 Tissue-distribution studies

Tissue distribution studies were performed for raloxifene hydrochloride free suspension and RLX-SLN. Fig. 5.14 shows distribution pattern of free raloxifene hydrochloride and SLN in various organs at different time points. Peak concentration in all the organs was achieved between 2 h to 4 h. This can be correlated to short gastric emptying time and subsequent absorption of both raloxifene hydrochloride and RLX-SLN through intestinal region in rats.

Fig 5.14a shows comparative distribution of raloxifene hydrochloride in liver. From the figure, raloxifene hydrochloride from SLN accumulated to lesser extent in liver compared to free raloxifene hydrochloride. This can be explained by lymphatic uptake of RLX-SLN (previously discussed under section 5.14). Lipid nanoparticles reach lymphatic system either by direct endocytosis/transcytosis uptake by membranous epithelial cells (M-cells) covering Payer's patches in intestine or by partitioning into triglyceride-rich lipoprotein particles that are secreted into intestinal lymph [28].

Fig. 5.14b shows comparative distribution of raloxifene hydrochloride in spleen. Apparently, raloxifene hydrochloride from SLN was distributed to greater extent at all-time points (0.5 h to 12 h) compared to free raloxifene hydrochloride. Partial phagocytic uptake of SLN by macrophages and subsequent release into spleen may explain higher splenic distribution of SLN. Further, it was observed that free raloxifene hydrochloride distributed to greater extent than raloxifene hydrochloride from SLN in rat kidneys and lungs (Fig. 5.14c and 5.14d). Depending on surface charge, hydrophobicity and particle size, SLN preferentially accumulate in lymphoid organs [39].

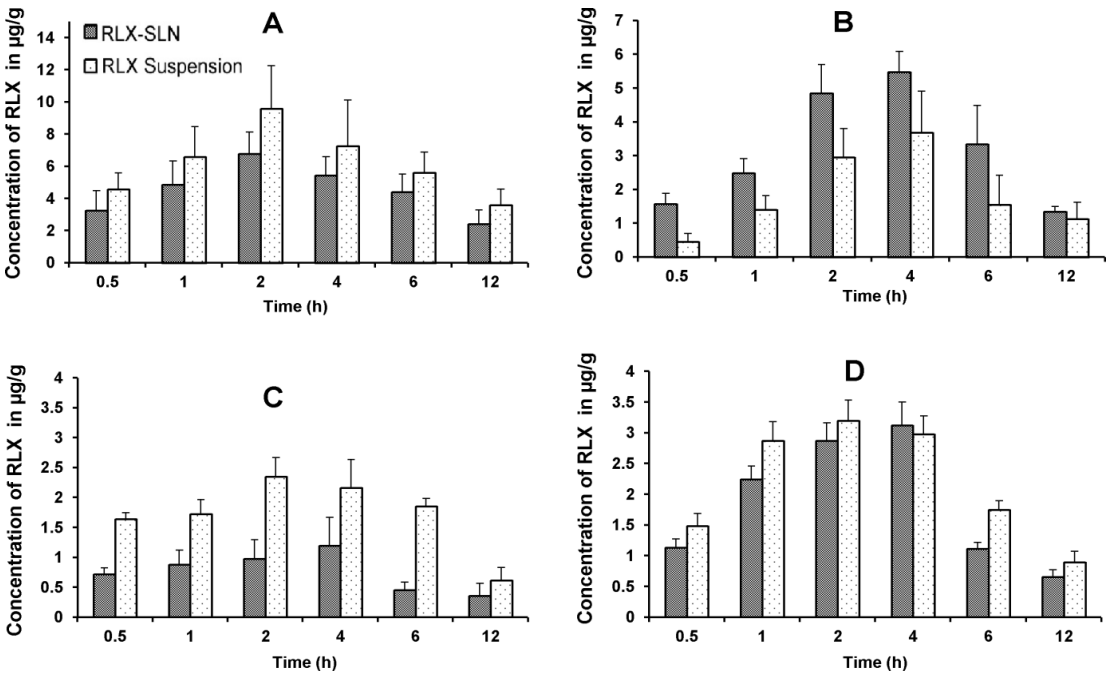

Fig. 5.14: Tissue distribution profile of raloxifene hydrochloride after oral administration of RLX-SLN, and free raloxifene hydrochloride (RLX) suspension to female Wistar rats (20 mg/kg) (*n* = 3 for each time point): (a) liver (b) spleen (c) kidneys (d) lungs.

5.16 Conclusions

The GB based solid lipid nanoparticles for raloxifene hydrochloride showed promise as effective carriers for enhancement of bioavailability in rats. Processing conditions for manufacture of these lipid nanoparticles were identified and optimized using DOE with good correlation between actual and predicted values. Oral bioavailability of raloxifene loaded into SLN formulation increased over 3.2 folds when compared to free suspension. It was also demonstrated that SLN formulations were taken up by endocytosis process. Higher plasma concentration of raloxifene hydrochloride from SLN was attributed to both portal absorption and intestinal lymphatic transport. Distribution of RLX-SLN to non-target tissues was lesser in comparison to free raloxifene hydrochloride. In conclusion, lipid nanoparticles for poorly soluble raloxifene was an effective approach in improving its oral bioavailability and in reducing dose of the drug which may prove beneficial in treatment of chronic disease like osteoporosis.

Polymeric nanocarriers

Poly(ε-caprolactone) Nanocapsules

5.17 Introduction

As discussed in the first chapter, polymeric nanoparticles can be produced by using either pre-formed polymers or by direct polymerization of monomers in the solution. Most of the methods reported in the literature employ the former method. Reasons for this could be the ease of production/scale-up and a reasonable control on particle size, distribution and the drug entrapment in the nanoparticles and predictability of in-vivo behaviour when using pre-formed polymers. Moreover, this method also precludes the use of many toxic chemicals like cross-linking agents that are commonly employed in the latter method.

Polymeric nanoparticles are classified either as nanospheres or nanocapsules depending on whether the drug is uniformly dispersed throughout the polymer matrix (nanospheres) or is concentrated in the core of a nanocapsule. Methods employed in manufacture of polymeric nanoparticles from pre-formed polymers include: solvent evaporation method, salting-out method, nanoprecipitation/solvent displacement method and dialysis method. Of late, methods employing supercritical fluid technology (RESS and RESOLV) are popular, especially when the formulation has to be scaled up or commercially viable.

5.17.1 Polymers used in formulation of nanoparticles

Polymers used in manufacture of nanoparticles can be broadly classified as (a) biodegradable polymers and (b) non-biodegradable polymers. Literature is replete with nanoparticles formulated with biodegradable polymers. Some of the frequently used biodegradable polymers are: poly-d,l-lactide-co-glycolide (PLGA); polylactic acid (PLA); poly-ε-caprolactone (PCL); chitosan; gelatin and poly-alkyl-cyano-acrylates (PAC). Despite their obvious advantages, only few of these polymers are commercially viable (for e.g.:

PLGA, PLA and PCL). Others like gelatin and chitosan are of natural or semi-synthetic origin and hence suffer from concerns like purity and batch-to-batch variability [40].

PCL was one of the earliest biodegradable polymers synthesized by the Carothers group in the early 1930s [41]. It can be degraded by microbial enzymes and is economical as compared to other biodegradable polymers like PLA and PLGA [42]. PCL is either prepared by ring-opening polymerization reaction of ε-caprolactone using a variety of anionic, cationic and co-ordination catalysts or by free radial ring-opening polymerization of 2-methylene-3-dioxepane [43]. It is a hydrophobic and a semi-crystalline polymer; its crystallinity decreases with increasing molecular weight [42]. Good solubility profile of PCL, low melting point (59–64 ºC) and an exceptional biocompatibility profile have resulted in extensive research with PCL in the area of drug delivery [44-46]. It degrades at a slower rate as compared to PLGA and PLA and is particularly suitable for sustained release dosage applications [47]. Literature is replete with the use of PCL in drug delivery [43, 48, 49]. PCL demonstrates high permeability to small molecules, high stability in the GI environment and a negligible tendency to generate acidic impurities during degradation (as compared to PLA or PGAs).

We selected PCL as a model biodegradable polymer for nano encapsulation of raloxifene hydrochloride because of the following reasons:

1. It is economical, biocompatible and shows a slow degradation profile as compared to PLA and PLGA.
2. It is highly stable in both in-vitro and in-vivo conditions
3. It does not generate acidic impurities upon degradation, unlike PLA and PLGA.

Nanoparticles and nanocapsules of PCL can be prepared by solvent evaporation, solvent diffusion or emulsion evaporation methods [50]. As discussed earlier, depending on

the manufacturing method used, the end product could either be a nanoparticle or a nanocapsule. For solvent evaporation/diffusion methods (where the end product is nanoparticle) it is essential that both the encapsulant and the encapsulating polymer must be the same phase [51]. However, in our case, raloxifene hydrochloride (encapsulant) was nearly insoluble in most of the common organic non-polar solvents like dichloromethane, acetonitrile, chloroform and acetone that are traditionally used in preparation of nanoparticles. Hence, employed a modified multiple emulsion (w/o/w) solvent evaporation technique to encapsulate raloxifene hydrochloride in PCL based nanocarrier system. Because we dissolved raloxifene hydrochloride and PCL in different phases and followed a multiple emulsion method for manufacture, the resulting formulation was a nanocapsule rather than a nanoparticle.

5.18 Experimental

5.18.1 Materials

Raloxifene hydrochloride was obtained as a gift sample from Apotex Research Pvt. Ltd. Bangalore, India. Poly-ε-caprolactone (PCL) was purchased from M/s Polysciences, Inc. (Warrington, PA, USA). Poloxamer 407 (P407) was procured form Signet Chemicals, Mumbai, India. Polyethylene glycol 400 (PEG 400), Dichloromethane (DCM) and Span 20 were purchased from Merck Ltd., Mumbai. All other chemicals used were of analytical grade and the solvents were of HPLC grade. Freshly collected Milli-Q water (Millipore, MA, USA) was used in preparation of aqueous mobile phase of HPLC analysis.

5.18.2 Methodology

Preparation of nanocapsules by double emulsion method is previously reported [52]. Several variables are involved in nanocapsule preparation by this method. Identifying and controlling critical variables helps in obtaining nanocapsules with reproducible and desired characteristics. Running design of experiments (DOE) is a logical way of understanding

critical variables involved in preparation. We used a hybrid design approach [53] to understand critical steps and optimize preparation conditions for nanocapsules.

To start with, we identified several factors that were likely to influence critical quality attributes of nanocapsules (entrapment efficiency and particle size). Selection of parameters and their levels was based on preliminary studies, prior experience, and on available literature [54]. Full factorial design is a good choice to understand influence of several factors on outcome of a process [55]. However, in full factorial design, as number of factors increase, number of trials increase exponentially.

When screening large number of factors, Plackett-Burman design (PBD) is more practical and frequently used alternative to full factorial design. It uses only a fraction of trials used in full factorial design and is suitable for initial screening of critical factors [56]. Limitation of PBD is that, with this design, we cannot identify interaction between factors. For this, higher resolution response surface methodology (RSM) designs are often used [56].

In this study, we used rotatable central composite design (RCCD), a sub-type of RSM design to identify multi-factor interactions and optimize processing conditions in preparation of drug loaded PCL nanocapsules. Influencing factors and their interactions (with each other) were studied in detail using Design Expert 8.0.7 software (Full version 8.0.7.1, Stat-Ease Inc., MN, USA). Further, we subjected optimized nanocapsules for in-vitro characterization and extensive pharmacokinetic evaluation using female Wistar rats. With tissue distribution studies in rats, we assessed differences in distribution pattern of drug loaded nanocapsules and free drug.

5.18.3 Experimental Design

We employed low resolution PBD for initial screening of significant variables affecting entrapment efficiency (EE) and particle size of nanocapsules. Total of eleven

different variables at two levels were studied. Variables studied were (A) Volume of PEG 400 in internal phase (0 and 2 ml); (B) internal to external phase volume ratio for first emulsion (1:20 and 1:2); (C) Effect of pre-sonication time (1 and 3 min); (D) ultrasonication time for second emulsion (5 and 10 min); (E) temperature used for evaporating solvent (25 °C and 45 °C); (F) vacuum pressure used for evaporating solvent (1 and 100 millibars); (G) ultrasonication time for first emulsion (1 and 3 min); (H) amount of PCL in organic phase (100 and 1000 mg); (J) concentration of surfactant in first emulsion (1 and 2.5% w/v); (K) internal to external volume ratio for second emulsion (1:10 and 1:2.5); and (L) amount of stabilizer per 100 ml in second emulsion (0.5 and 5 g).

Further, we selected three most significant factors from PBD (coded as X_1, X_2 and X_3) that influence EE (Y_1), particle size (Y_2) and studied their interaction effects using high resolution RCCD. The RCCD comprised of 20-run, 3-factor and 3-level design with 5 center point trials for reproducibility.

We used results from RCCD to construct second order polynomial models for process optimization in production of nanocapsules with minimum particle size and maximum EE. Design Expert software was extensively used for designing the sequence of trials and interpreting the results. Following polynomial model was used to model the responses:

$$Y = b_0 + b_1X_1 + b_2X_2 + b_3X_3 + b_{11}X_1^2 + b_{22}X_2^2 + b_{33}X_3^2 + b_{12}X_1X_2 + b_{13}X_1X_3 + b_{23}X_2X_3$$

Where, the b_i (for i =1, 2 and 3) are the linear effects, the bii's are the quadratic effects, the bij's (for i, j = 1, 2 and 3, i<j) are the interactions between the i^{th} and the j^{th} variables; the b_0 is the intercept. Selection of the optimized formulation was done on basis of constraints mentioned in Table 5.7.

Table 5.7: Variables and their levels in the Rotatable Central Composite Design

Factor	Levels used				
	-α	**-1**	**0**	**+1**	**+α**
Independent variables					
X_1= Amount of polymer (mg)	80	250	500	750	920
X_2= Ultra sonication time (min)	02	05	10	15	18
X_3= Amount of stabilizer in external phase (mg)	80	250	500	750	920
Dependent factors	**Constraints**				
Y_1= Particle size (nm)	Minimize				
Y_2= Entrapment efficiency (%)	Maximize				

5.18.4 Preparation of Nanocapsules:

We suitably modified previously reported double emulsion (w/o/w) method [52] for preparation of drug loaded nanocapsules. In brief, raloxifene hydrochloride (25 mg) was dissolved in 2 ml of PEG 400: Water (1:1) pre-mix to form internal phase of first emulsion. This was emulsified with 20 ml DCM containing PCL (amount varied as per experimental design) and 1% w/v Span 20 under ultrasonication (Vibra cell, Sonics, USA) for 1 min at fixed amplitude (100 W output). The first emulsion (w/o) was then added to 100 ml water containing P407 (amount varied as per experimental design) and subjected to ultrasonication for specified time period (varied as per experimental design) in an ice bath. After removing solvent under reduced pressure in a vacuum concentrator (Rotavapor R-210, Buchi, Switzerland), a dispersion of drug loaded nanocapsules in water was obtained. Free drug was removed by ultra-filtration (regenerated cellulose membrane, MWCO 3500 Da, Milipore, MA, USA) and final product was obtained. Placebo nanocapsules were prepared by following similar procedure without incorporating raloxifene hydrochloride. The scheme of preparation is illustrated in Fig. 5.15 below.

5.18.5 HPLC method for analysis of raloxifene hydrochloride

5.18.5.1 Method for analysis of EE, assay and in-vitro drug release study samples

Validated HPLC method described earlier was used for analysis of samples from EE, assay and in-vitro drug release studies. Before analysis, suitable dilution and processing was done for all samples.

5.18.5.2 Method for analysis of biological samples

For analysis of plasma samples, the method described earlier under bioanalytical method development validation section was used after suitable validation. Further, for tissue distribution study samples, we did a partial validation and also ensured the absence of interfering peaks by running blanks while analyzing samples from organ distribution studies.

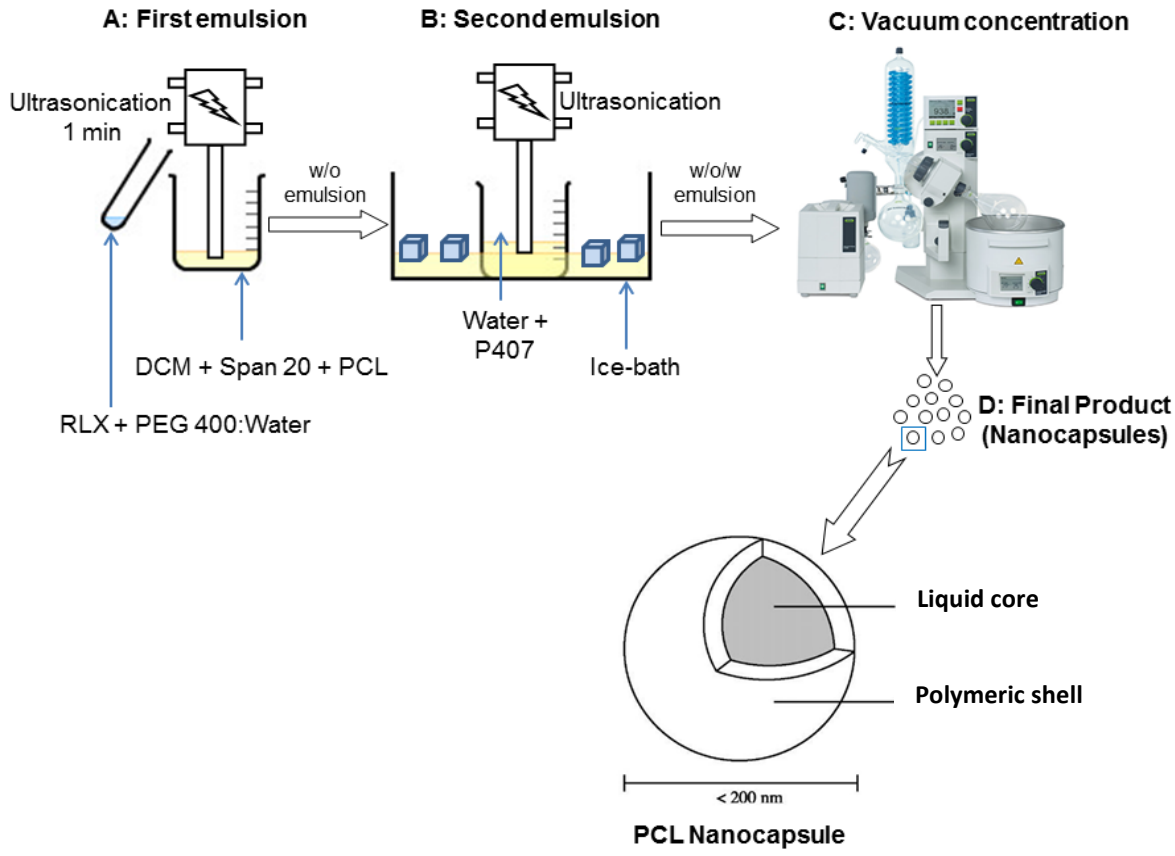

Fig. 5.15: Preparation method for raloxifene loaded polymeric nanocapsules

5.19 Characterization Studies

5.19.1 Particle Size and Zeta Potential

Zetasizer nano ZS (Malvern Instruments, Worcestershire, UK) was used to measure particle size, polydispersity index (PDI) and electrophoretic mobility (zeta potential) of nanocapsules. Intensity of scattered light was measured at an angle of 173º. In serial mode, 10 min set time was given to the instrument and 30 ms sample measurement time was maintained for all samples. Values of zeta potential and PDI provided by software attached to instrument were used in interpreting the results.

5.19.2 Entrapment Efficiency (EE)

After suitable dilution of samples, ultrafiltration method (regenerated cellulose membrane, molecular cut-off 3500 Da, Milipore, MA, USA) was used to estimate EE. Following equation was used to calculate EE:

$$EE\ (\%) = \ (W_{\text{total}} - W_{PCL})/W_{\text{total}} \ \times 100$$

Where, W_{PCL} is the amount of free raloxifene hydrochloride obtained in filtrate; W_{total} is total amount of raloxifene hydrochloride added to formulation.

5.19.3 Scanning electron microscopy (SEM) analysis

Scanning electron microscope (JSM-6360LV Scanning Microscope; Jeol, Tokyo, Japan) was used to examine surface morphology of drug loaded and placebo nanocapsules. To facilitate analysis, under vacuum, 100 µl of nanocapsule dispersion was placed on an aluminium stub and dried overnight. Sputter-coating of this with thin gold-palladium layer under argon atmosphere was carried using a gold sputter module in a high-vacuum

evaporator (JFC-1100 fine coat ion sputter; Jeol, Tokyo, Japan). Scanning of samples was done under an acceleration voltage of 15 kV and photomicrographs taken.

5.19.4 In-vitro drug dissolution and release studies

We used previously reported dialysis bag method for in-vitro drug release studies [57]. Drug release for both raloxifene hydrochloride free drug and drug loaded nanocapsules (n = 6) were studied. A sealed dialysis bag (Spectra/Por 3 dialysis membrane, MWCO 3500 Da) containing either nanocapsule formulation or free drug solution (prepared in water, pH 5.5, containing 1% w/v Tween 80), equivalent to 1.5 mg raloxifene hydrochloride was completely immersed in 500 ml dissolution media (phosphate buffer, pH 7.4 containing 0.1% w/v Tween 80). Uniform temperature of 37 °C was maintained and media was continuously stirred by a magnetic bead. 1 ml sample was withdrawn at pre-determined time intervals from dissolution media. A validated HPLC method was used to analyze these samples. For evaluation of drug release kinetics, the obtained release data was fitted into zero order, first order, Higuchi, reciprocal powered time model and Korsmeyer–Peppas models. Regression coefficient (r^2) and time for 50% dissolution ($t_{50\%}$) were calculated for the best-fit model. List of models and their mathematical relations used to fit drug release data is given below:

Zero order model: $F = k_0 t$, First order model: $\ln(1 - F) = -k_f\, t$,

Higuchi model: $F = k_H \sqrt{t}$, Reciprocal powered time model: $(1/F - 1) = m/t^b$

and Korsmeyer–Peppas model: $M_t/M_\infty = kt^n$

Where, F is fraction of drug released up to time t; k_0, k_f, k_H, m and b are model parameters. M_t is amount of drug released at time t, M_∞ is amount of drug released at infinite time, k is release kinetics constant, and n is exponent of release.

5.19.5 Stability studies

We subjected optimized nanocapsule formulation to stability testing as per International Conference on Harmonization (ICH) Q1A (R2) guidelines. For accelerated stability studies, optimized formulations (n = 3) were stored in sealed glass vials at 25 ± 2 °C/60 ± 5% RH in a stability chamber (Remi, Mumbai, India) for period of 3 months. Control samples at corresponding time intervals were kept at 2-8 °C. For long term stability studies, optimized formulations were stored in final pack (gray bromobutyl rubber stoppered glass vials with complete tear-off aluminum seal) at 5 °C ± 3 °C (refrigeration) for 6 months. At monthly intervals, samples were monitored for particle size, zeta potential, EE and PDI. GraphPad Prism version 5.03 for Windows software (GraphPad Software, San Diego, USA) was used for statistical evaluation.

5.19.6 In-vivo pharmacokinetic studies in rats

Pharmacokinetic studies were conducted in female Wistar rats weighing 180–220 g. Approval from institutional animal ethics committee was taken for all animal experiments. For rats used in oral pharmacokinetic study, overnight fasting of animals (12 h) was ensured before dosing. Animals were continued on fasting until 4 h after dosing. Thereafter, rat chow diet was provided *ad libitum*. In all the studies, freshly prepared raloxifene hydrochloride nanocapsule formulations were administered.

Pharmacokinetic studies were conducted post-oral (15 mg/kg) and post-intravenous (IV, 2.4 mg/kg) administration of free raloxifene hydrochloride suspension and raloxifene hydrochloride loaded NCs. For both oral and IV pharmacokinetic study, two groups with six animals in each group were made. While control group received free suspension (raloxifene hydrochloride suspended in 0.5 %w/v methyl cellulose, molecular weight 14000 Da, viscosity 15 cps), treatment group received optimized raloxifene hydrochloride nanocapsule

formulation. Similarly, in IV pharmacokinetic study, control group received free raloxifene hydrochloride solution (raloxifene hydrochloride dissolved in PEG 400: water pre-mix (1:1)) while the treatment group received raloxifene hydrochloride nanocapsule formulation.

Blood samples (0.15 ml) were collected from orbital sinus puncture of rats into microfuge tubes containing anti-coagulant (3.8% w/v sodium citrate). For oral pharmacokinetic studies, samples were collected at following time points: pre-dose, 0.17, 0.25, 0.5, 1, 2, 4, 6, 8, 10 and 12 h; sampling points for IV pharmacokinetic study were: pre-dose, 0.17, 0.25, 0.5, 1, 2, 4, 6 and 8 h. Plasma was separated from blood samples by centrifuging at 1000 × g at 4 °C for 10 min. Harvested plasma was stored at -70 °C temperature until further analysis. Validated HPLC method was used in analyzing these samples.

5.19.7 Assessment of raloxifene hydrochloride distribution to various organs

Female Wistar rats (180 – 220 g) (n = 12) were used to study organ distribution pattern. Rats were divided into two groups of six rats each. Each group was administered either free-raloxifene hydrochloride suspension or raloxifene hydrochloride loaded nanocapsules (20 mg/kg) by oral gavage. At 2 h and 4 h time points after dosing, three rats from each group were sacrificed. To remove residual blood, organs of interest (spleen, liver and kidney) were perfused with pH 7.4 PBS and separated from rat's body. Isolated organs were protected by freezing at -70 °C. Before analysis, organs were thawed back to room temperature. They were then minced and water equivalent to organ weight was added. To achieve fine paste-like consistency, homogenization was carried out in a tissue homogenizer (Remi, Mumbai, India). Acetonitrile, a protein precipitating agent (2 parts acetonitrile to 1 part of tissue homogenate) was then added to homogenized samples. Vortexing followed by

centrifugation (8000 × g for 20 min) gave clear supernatant. With a validated HPLC method, drug content was analyzed in this supernatant.

5.19.8 Statistical Analysis

To examine significance of difference between experimental results in RCCD, Analysis of Variance (ANOVA) was used. Overall regression relationship between response variable *Y* and entire set of *X* variables at 95% ($\alpha = 0.05$) significance level was determined by *F*-test. The co-efficient of multiple regression analysis (R^2) measured proportionate reduction of total variation in *Y* associated with set of *X* variables. Additionally, 'lack of fit' tests were used to assess regression model validity. In optimization step, to identify difference between predicted and actual values of responses, Wilcoxon sign rank test was used at 95% ($\alpha = 0.05$) significance level. To assess difference between means of accelerated stability study results, in-vitro drug release study results and organ distribution study results, unpaired Student t-test was used at 95% ($\alpha = 0.05$) significance level.

5.20. Results and Discussion

5.20.1 Preliminary Experiments using Plackett-Burman design

PBD was employed to screen factors that significantly influence EE and particle size. The design consisted of 12 trials at two levels for 11 different variables.

5.20.1.1 Influence of investigated factors on entrapment efficiency (Y_1)

For various factor combinations, EE for nanocapsules varied from 31% to 84% (data not shown). The fitted model describing influence of variables on EE is:

$$Entrapment\ Efficiency\ (Y_1)\ (\%) = 57.01 + 9.33*H - 7.18*L$$

As evident from above equation and Pareto chart (Fig. 5.16), factors that influenced EE of nanocapsules significantly ($P < 0.05$) were: H ─ amount of PCL in organic phase of first emulsion and L ─ amount of stabilizer in second emulsion.

Increased EE is expected with increase in polymer amount; as previously suggested [58], increase in polymer amount will result in higher viscosity of the medium limiting drug diffusion from inner phase to outer phase. Moreover, increased viscosity results in faster solidification of nanocapsules leading to higher EE [54].

EE was negatively influenced by amount of stabilizer in second emulsion; higher amount of stabilizer results in lower EE as it increases drug partitioning to external phase. Increased partitioning is a result of increased solubility of drug in external phase. Independent solubility study data confirms this hypothesis. Saturation solubility of raloxifene hydrochloride in 1% w/v and 5% w/v P407 aqueous solution was 218.9 ± 2.4 µg/ml and 357.5 ± 3.2 µg/ml respectively.

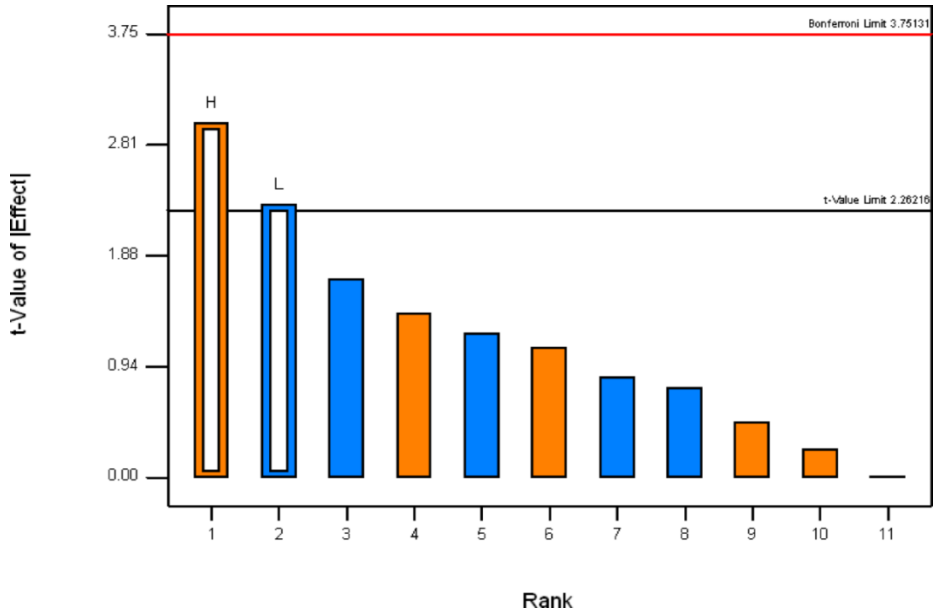

Fig. 5.16: Pareto chart showing significant factors in Plackett-Burman design that influence particle size of nanocapsules. H→ Amount of polymer and L→ Amount of stabilizer in external phase.

5.20.1.2 Influence of investigated factors on particle size (Y_2)

For various factor combinations, mean particle size for nanocapsules varied from 91 nm to 381 nm (data not shown). The fitted model describing influence of variables on the mean particle size is:

$$Particle\ Size\ (Y_2) = 247.36 + 27.28*D + 39.37*H + 24.12*K - 41.48*L$$

The above equation and Fig. 5.17 suggest that particle size is significantly ($P < 0.05$) influenced by (i) D ─ ultrasonication time for second emulsion, (ii) H ─ amount of PCL used, (iii) K ─ ratio of internal to external phase of second emulsion and (iv) L ─ amount of stabilizer in second emulsion.

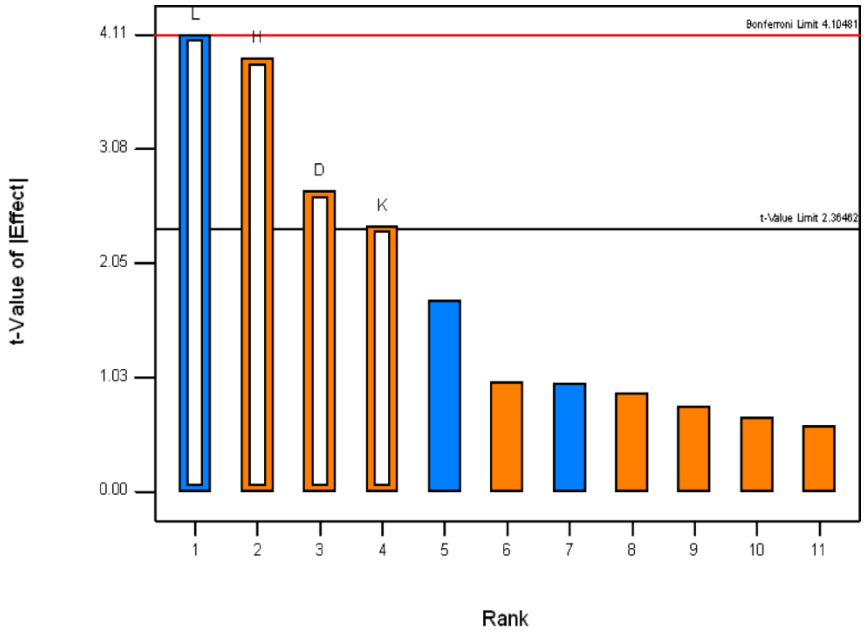

Fig. 5.17: Pareto chart showing significant factors in Plackett-Burman design that influence entrapment efficiency of nanocapsules. L→ Amount of stabilizer in external phase, H→ Amount of polymer, D→ Ultrasonication time for second emulsion and K→ Volume ratio for second emulsion.

Mean particle size increased with increase in polymer amount. This could be explained by increase in viscosity of organic phase with increasing polymer amount. As

viscosity increases, efficiency of ultra sonicator in breaking down emulsion to smaller droplets decreases due to decreased cavitation effect. Increase in particle size was seen when external phase volume of second emulsion was increased. Because overall bulk of the formulation is increased, it leads to decrease in ultrasonication efficiency and increase in particle size.

Particle size is expected to reduce with increase in ultrasonication time. This is because with increase in ultrasonication time, more energy goes into the system. However, contrary to this, with increasing ultrasonication time, an increase in particle size was seen. We observed that at higher ultrasonication time, local temperature of emulsion increases rapidly. This leads to rapid evaporation of solvent and decrease in overall volume of emulsion bringing particles closer to each other. Coalescence and particle aggregation is caused by proximity of these nascent semi-hardened nanocapsules shells.

Stabilizer amount had negative effect on particle size. With increase in amount of stabilizer, particle size of nanocapsules decreased. Decrease in size of nanocapsules is expected because higher amount of stabilizer helps in stabilization of smaller droplets by reducing interfacial tension and preventing them from coalescing into bigger droplets [54].

5.20.1.3 Experiments using Rotatable Central Composite Design (RCCD)

RCCD comprised of 20-run, 3-factor and 5-level design with 5 center point trials. Factors chosen to study interaction effects were: Polymer amount (X_1), ultrasonication time of second emulsion (X_2) and stabilizer amount in external phase (X_3). Influence of these factors on two responses, EE (Y_1) and particle size (Y_2) was studied (Table 5.8)

5.20.1.4 Effect of formulation variables on Entrapment Efficiency (Y_1)

The least-square second order polynomial equation for EE at 95% confidence level is given below:

$$EE\ (Y_1) = 52.85 + 4.29*X_1 - 0.39*X_2 - 13.37*X_3 - 1.44*X_1X_2 - 2.60*X_1X_3 - 0.71*X_2X_3 + 6.83*X_1^2 + 3.31*X_3^2$$

The quadratic model was significant with *F*-value of 43.17 ($P < 0.0001$). Value of regression co-efficient ($R^2 = 0.9753$) indicated good correlation between response and selected factors. The adjusted R^2 value for EE response was 0.9531. EE for various factor combinations varied from 41% (run 5) to 86% (run 20). Table 5.8 gives data for all trials taken. Regression co-efficient of X_1, X_3, X_1X_3, X_1^2 and X_3^2 were significant ($P < 0.05$) (Table 5.8).

Table 5.8: Actual experimental design and obtained response

Run	Amount of polymer (mg , X_1)	Ultrasonication time (min, X_2)	Amount of stabilizer in external phase (min, X_3)	Particle size (Y_1, nm)	Entrapment efficiency (Y_2, %)
1	750	15	250	199	84
2	500	10	80	189	80
3	500	18	500	234	55
4	500	10	500	185	54
5	500	10	920	195	41
6	750	15	750	216	47
7	500	2	500	185	53
8	500	10	500	199	54
9	500	10	500	181	52
10	500	10	500	191	51
11	500	10	500	184	52
12	750	5	750	199	54
13	250	5	750	152	48
14	500	10	500	189	52
15	250	15	250	178	73
16	80	10	500	131	61
17	250	15	750	176	49
18	250	5	250	178	72
19	920	10	500	188	79
20	750	5	250	192	86

Table 5.9: Significance values for entrapment efficiency and particle size

Source	Entrapment Efficiency (Y_1)				Particle Size (Y_2)			
	Sum of Squares	**DF**	**F-value**	***P*-value**	**Sum of Squares**	**DF**	**F-Value**	***P*-value**
Model	3555.49	8	43.17	<0.0001*	7792.08	9	17.29	<0.0001*
X_1	251.27	1	24.41	0.0004*	3475.47	1	69.39	<0.0001*
X_2	2.03	1	0.20	0.6658	1245.25	1	24.86	0.0005*
X_3	2442.34	1	237.25	<0.0001*	2.72	1	0.054	0.8206
X_1X_2	16.58	1	1.61	0.2306	0	1	0	1.0000
X_1X_3	54.01	1	5.25	0.0427*	338	1	6.75	0.0266*
X_2X_3	4.05	1	0.39	0.5435	144.5	1	2.88	0.1203
X_1^2	678.91	1	65.95	<0.0001*	1522.53	1	30.4	0.0003*
X_2^2	-	-	-	-	788.98	1	15.75	0.0026*
X_3^2	159.3	1	15.48	0.0023*	21.17	1	0.42	0.5303
Residual	113.24	11			500.87	10		
Lack-of -fit	94.28	6	4.15	0.0701^{++}	296.04	5	1.45	0.348^{++}
Pure error	18.95	5			204.83	5		
Total	3668.73	19			8292.95	19		

* Significant at $P < 0.05$. $^{++}$Not significant at $P < 0.05$ (non sgnificant lack-of-fit).
For modelling the response entrapment efficiency, non-significant factor X_2^2 was removed in the run to improve lack-of-fit value in the table.

From Fig. 5.18a, it is evident that EE increases with increasing polymer amount in organic phase. For reasons discussed earlier, polymer amount has positive effect on EE. From Fig. 5.18b, ostensibly, stabilizer amount has negative impact on EE. Reduction in EE is seen with increasing amount of stabilizer in external phase. The drug's solubility increases in external phase and it partitions out of internal phase leading to decrease in EE. The small value for co-efficient of term X_2 in the equation indicates that ultrasonication time alone has little impact on EE of raloxifene hydrochloride in nanocapsules. From co-efficient of X_1X_2 in the above equation, apparently, ultrasonication time appears to be involved in multi-factor interaction with factor X_1 in influencing EE of nanocapsules.

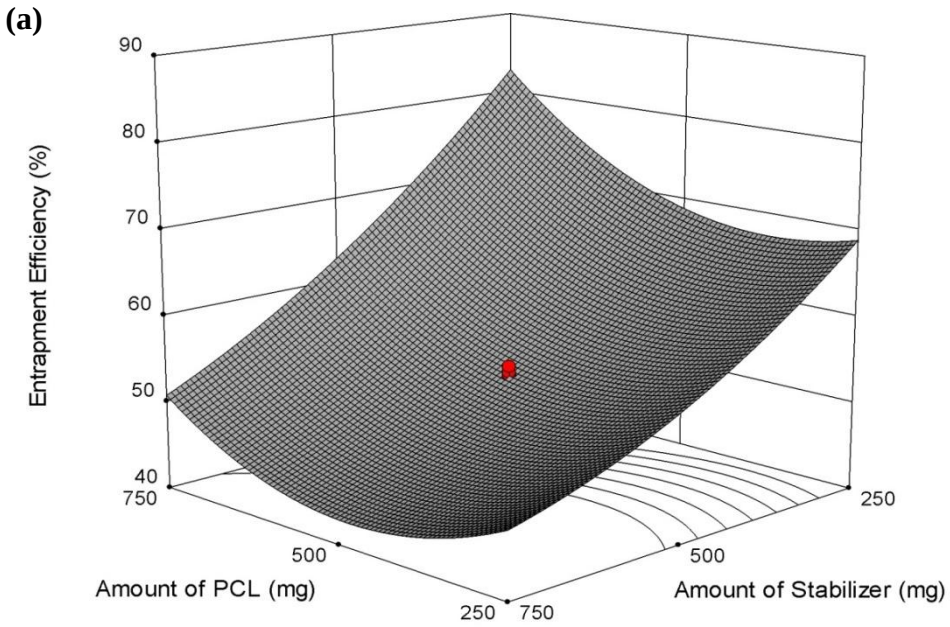

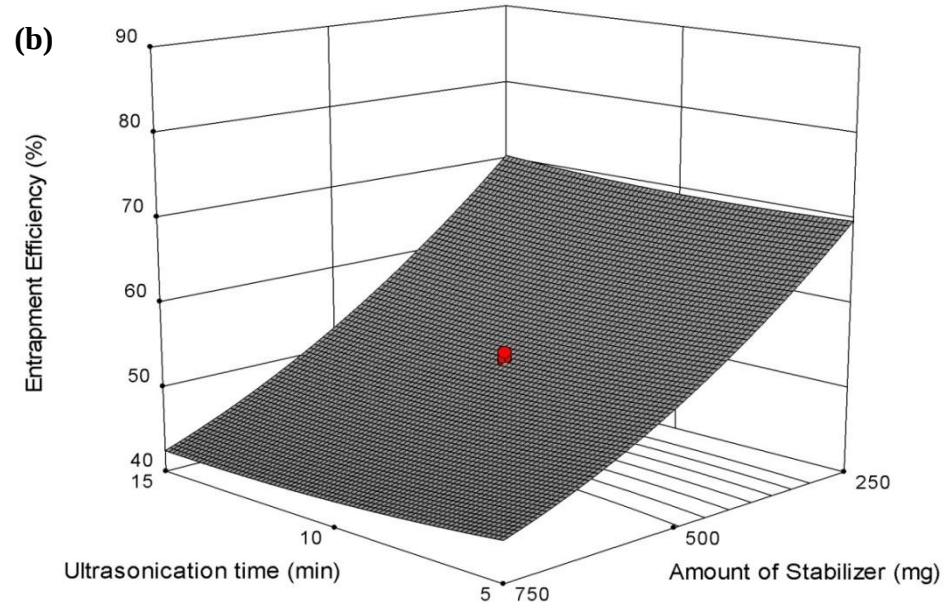

Fig. 5.18a: Effect of polymer amount (PCL) and stabilizer amount on entrapment efficiency and **Fig. 5.18b**: Effect of ultrasonication time and stabilizer amount on entrapment efficiency

5.20.1.5 Effect of formulation variables on particle size (Y_2)

The least-square second order polynomial equation for particle size at 95% confidence level is given below:

$$Particle\ Size\ (Y_2) = 188.19 + 15.95*X_1 + 9.55*X_2 + 0.45*X_3 + 0.000*X_1X_2 + 6.50*X_1X_3 + 4.25*X_2X_3 - 10.28*X_1^2 + 7.40*X_2^2 + 1.21*X_3^2$$

Of all tested models, quadratic model was found significant with *F*-value of 17.29 ($P < 0.0001$). Value of regression co-efficient ($R^2 = 0.9396$) for this equation indicated good correlation between response and selected factors. The residuals were distributed randomly around zero; there was no effect of experimental sequence on the trend of residuals. The adjusted R^2 value for particle size response was 0.8852. For different factor combinations, particle size varied from 131 nm (run 16) to 234 nm (run 3). Complete data is presented in Table 5.8. As shown in Table 5.9, at $\alpha = 0.05$, regression co-efficient were significant for X_1, X_2, X_1X_3, X_1^2 and X_2^2.

From Fig. 5.18c and 5.18d, it is apparent that amount of stabilizer in external phase (X_3) alone has little influence on particle size. This is contrary to the results of PBD where stabilizer amount had negative effect on particle size. This difference may be explained by difference in levels of stabilizer used in both these designs. In PBD, upper and lower levels of stabilizer were taken as 0.5 and 5 g respectively; stabilizer levels in RCCD design were 0.25, 0.5 and 0.75 g. The response Y_2 appears to be sensitive to stabilizer amount only at lower levels (below 0.25 g); at higher amount of stabilizer, this factor has little influence on particle size. However, as evident from large positive coefficient value in the equation, this factor displayed significant interaction effect with X_1. From Fig. 5.18d, it is apparent that particle size increased with increase in ultrasonication time. For reasons discussed earlier, ultrasonication time has positive effect on particle size of nanocapsules.

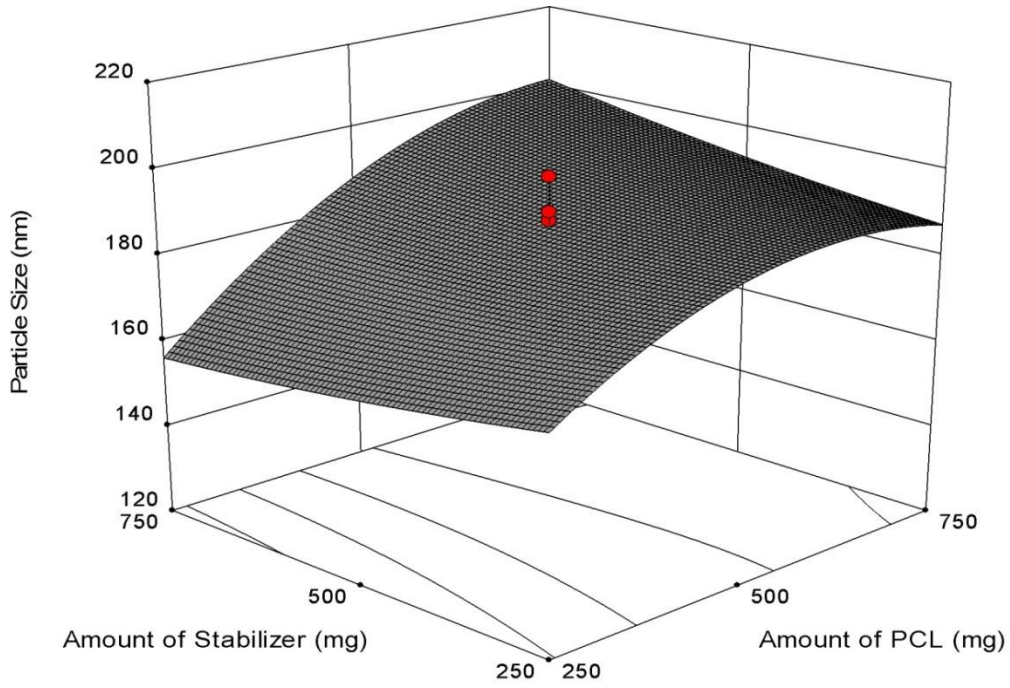

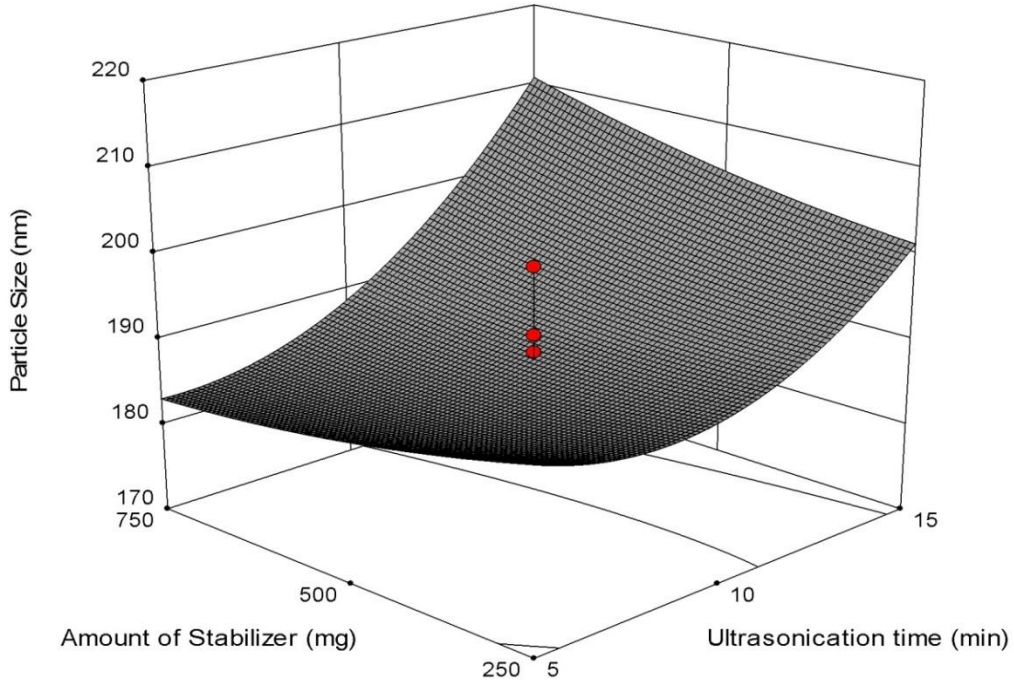

Fig. 5.18c: Effect of stabilizer amount and polymer amount (PCL) on particle size and **Fig. 5.18d:** Effect of stabilizer amount and ultrasonication time on particle size.

5.20.1.6 Optimization and validation

Desirability function of Design-Expert software v 8.0.7.1 was used to identify optimal conditions in manufacture of raloxifene hydrochloride nanocapsules. The value of desirability factor was 0.95. Set criteria of minimum particle size and maximum EE was used to predict optimal preparation conditions for nanocapsules. Optimal conditions for preparation of nanocapsules as predicted by software were: polymer amount in external phase = 750 mg; ultrasonication time = 7.53 min and stabilizer amount in external phase = 250 mg. Verification runs (n = 3) with suggested optimal conditions were carried out to prove the validity of this statistical model. Difference between actual and predicted values was checked using Wilcoxon signed rank test. At $\alpha = 0.05$, there was no statistically significant difference between actual and predicted values for particle size ($P < 1.0000$) and EE ($P < 0.7500$), thus affirming validity of the proposed model. Optimized formulations had particle size (mean ± SD) of 187.8 ± 4.75 nm and EE of 82.93 ± 3.31%.

5.20.1.7 Characterization of nanocapsules

The SEM image of nanocapsules (Fig. 5.19) showed almost spherical and uniform shape. Mean particle size value obtained from Zetasizer for optimized formulation was 187.8 ± 7.75 nm with poly dispersibility index (PDI) of 0.234 ± 0.004 (n = 3). Low value of PDI indicates that optimized conditions could be used to produce stable nanocapsules with a relatively narrow size distribution (Fig. 5.20). Zeta potential value of optimal formulation was -15.13 ± 0.35 mV. Free lactone groups in PCL polymer may be responsible for negative zeta potential values [59].

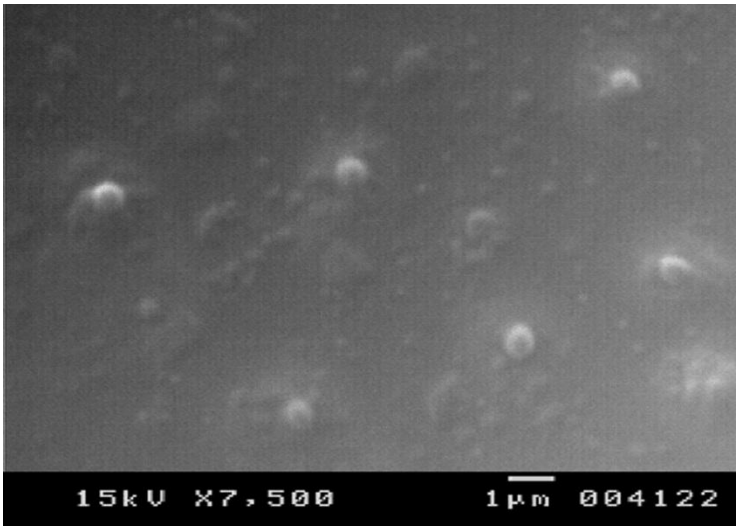

Fig. 5.19: Scanning electron micrograph of raloxifene loaded nanocapsules (×7500)

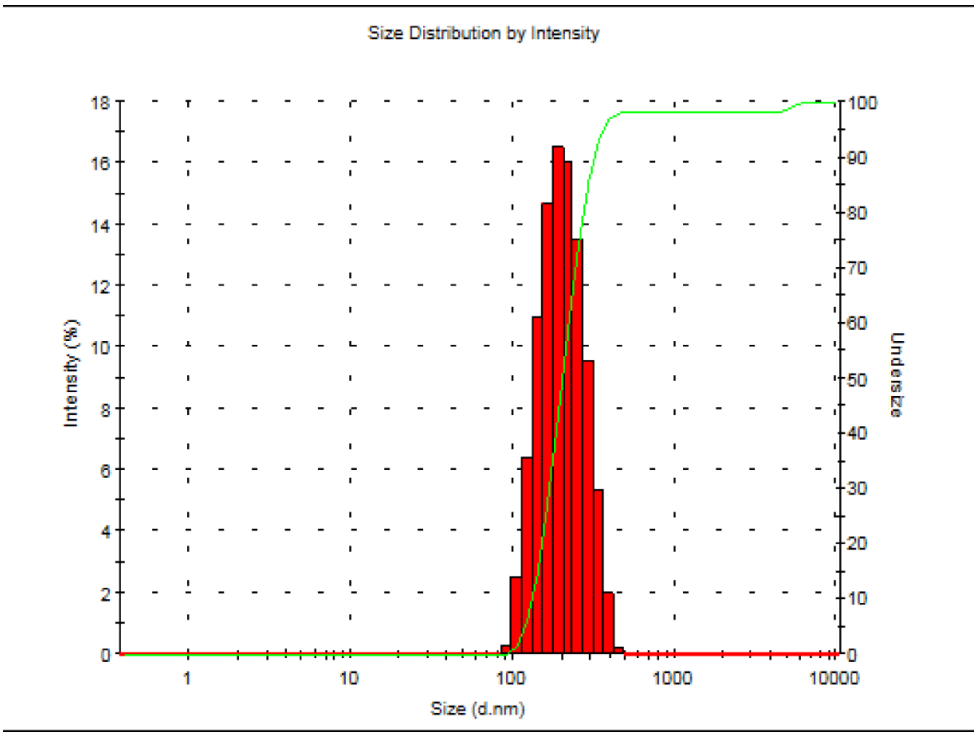

Fig. 5.20: Particle size distribution data for optimized nanocapsule formulation.

5.20.1.8 In-vitro drug release studies

Analysis of release profiles of drugs from polymeric nanocapsules can provide important information on the mechanisms involved. In reservoir-type system such as nanocapsules, drug release is preferentially governed by diffusion through the polymeric wall [60]. In-vitro studies were used to examine dissolution of raloxifene hydrochloride from free solution and release from drug loaded nanocapsules. In this study, only drug could traverse membrane pores, whereas, polymeric nanocapsules could not.

The results presented in Fig. 5.21 show that, within 4 h period, free raloxifene hydrochloride completely dissolves into the media. In case of raloxifene hydrochloride loaded nanocapsules, a slow and more sustained release pattern was observed.

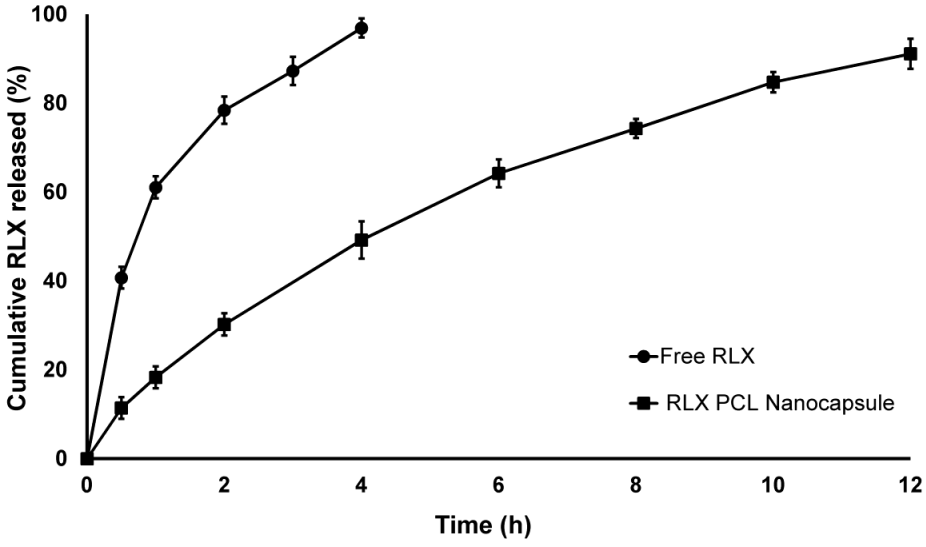

Fig. 5.21: In-vitro drug release profile of free raloxifene hydrochloride and optimized raloxifene hydrochloride loaded nanocapsule formulation in pH 7.4 buffer. Each point represents mean ± SD of three observations.

From the analysis, data showed best fit with Korsmeyer–Peppas model with good regression co-efficient value (r^2 = 0.9974). The Korsmeyer–Peppas model is a semi-empirical

model that uses single exponential equation to describe drug release process from a delivery system [60]. It has been used to evaluate release of drugs from polymeric devices and nanocapsules especially when mechanism of release is unclear or when more than one mechanism is involved in drug release [59, 61, 62].

The drug dissolution rate constant of free raloxifene hydrochloride (k = 58.085/min) was nearly three times higher than release rate constant from raloxifene hydrochloride loaded into nanocapsules (k = 20.337/min). Mechanisms involved in both these cases are different. In case of raloxifene hydrochloride loaded into PCL nanocapsules, initial desorption of surface bound drug occurs followed by the diffusion of raloxifene hydrochloride through polymeric wall of nanocapsules [63]. The value of exponent (n = 0.6653) indicated that drug release followed non-Fickian transport mechanism. Time taken for release of 50 % raloxifene hydrochloride from nanocapsules, calculated as $t_{50\%}$ was 4.30 h. For free raloxifene hydrochloride, $t_{50\%}$ was calculated as 0.674 h. Thus, polymeric nanocapsules of raloxifene hydrochloride were able to slow down drug release to a considerable extent compared to free raloxifene hydrochloride suspension.

5.20.1.9 Stability studies

Influence of storage conditions on stability of nanocapsules was assessed by analyzing data from EE, particle size, zeta potential and in-vitro drug release studies ($t_{50\%}$). For accelerated stability studies, optimal formulations (n = 3) were stored at 25 °C ± 2 °C/60% ± 5 % RH for 3 months. Long-term stability studies were performed by storing formulations in final pack (n = 3) at 5 °C ± 3 °C for period of 6 months. There was no significant change (P < 0.05) in any of the assessed parameters when raloxifene hydrochloride-nanocapsules were stored under refrigerated conditions at 2-8 °C. However, significant (P < 0.05) changes in EE and in-vitro drug release profile ($t_{50\%}$) were observed in

samples stored at room temperature (Fig. 5.22). The $t_{50\%}$ value shortened from 4.32 ± 0.24 h (fresh sample) to 1.46 ± 0.16 h (3 month old test sample); EE reduced from 82.9 ± 3.3% (fresh sample) to 61.6 ± 4.1% (3 month old test sample). No significant change in particle size or zeta potential was observed.

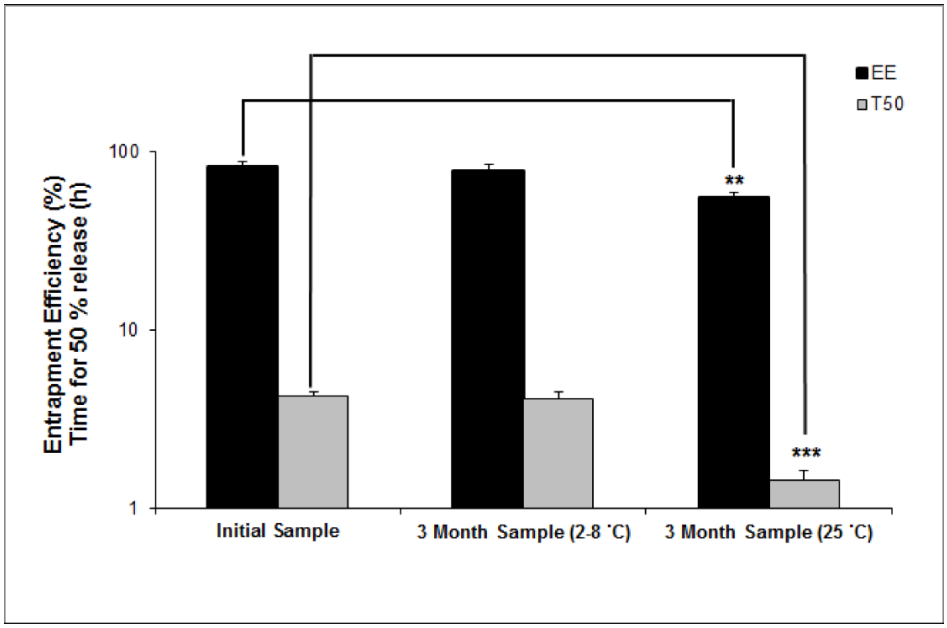

Fig. 5.22: Accelerated stability for optimized raloxifene hydrochloride loaded nanocapsules: Effect of storage temperature on EE (%) and $t_{50\%}$ (h). Each value represents mean ± SD (*n* = 3). *** $P < 0.001$, ** $P < 0.01$.

Reduction in $t_{50\%}$ value and EE could be again explained by partitioning behavior of drug into polymeric shell of nanocapsules during stability period which is primarily influenced by storage condition. With progress in time, polymer shell of nanocapsules becomes *richer* in drug content. In freshly prepared samples, initial release occurs due to desorption of surface bound drug followed by diffusion of drug through polymeric wall of nanocapsules [63]. Nonetheless, in aged samples, drug-enriched polymeric shell causes burst release effect. Thus, the in-vitro drug release profile for aged nanocapsule formulation shows a bi-phasic pattern – phase-I where over 50 % of entrapped drug is released within 2h and phase-II characterized by more sustained release due to diffusion of drug from core of

nanocapsules. Loss of entrapped drug from nanocapsules leads to a decrease in EE. This process is expedited when nanocapsule formulations are stored at accelerated temperature condition; this is expected because drug is present in molecular form in core of nanocapsules. At higher temperature, thermodynamic energy of drug molecules increases leading to a greater partitioning and diffusion of the drug out of the polymeric shell. This causes loss of entrapped drug and reduction in EE.

From long-term stability study data of 6 months in final pack, no appreciable change was observed in any assessed parameter for the nanocapsule formulation compared to initial time point data. Apparently, these formulations demonstrate acceptable stability when stored under prescribed storage conditions in final pack. We recommend storage of nanocapsule formulation under refrigerated conditions or freeze drying of the formulation to ensure better stability during storage.

5.20.1.10 In-vivo pharmacokinetic studies in rats

Table 5.10 presents pharmacokinetic parameters obtained after oral and IV administration of free raloxifene hydrochloride and raloxifene hydrochloride loaded nanocapsules in female Wistar rats.

Table 5.10: Pharmacokinetic parameters for raloxifene after administration of free raloxifene hydrochloride suspension (oral study), raloxifene hydrochloride solution (IV study) and drug loaded nanocapsules to rats

Pharmacokinetic parameters from oral study (15 mg/kg)		
Parameter	**Raloxifene hydrochloride suspension**	**Raloxifene hydrochloride nanocapsules**
C_{max} (ng/ml)	181.71 ± 28.19	400.21 ± 41.70***
T_{max} (h)	2.33 ± 0.52	2.10 ± 0.32
$MRT_{(0-\infty)}$ (h)	10.72 ± 2.04	13.25 ± 1.81*
$AUC_{(0-t)}$ (µg h/ml)	1.58 ± 0.28	3.25 ± 1.18 **

$T_{1/2}$ (h)	6.84 ± 1.12	9.08 ± 1.43*
F_{rel}	-	2.10

Pharmacokinetic parameters from IV study (2.4 mg/kg)

Parameter	Raloxifene hydrochloride solution	Raloxifene hydrochloride Nanocapsules
K_e (per h)	0.5343 ± 0.1218	0.1175 ± 0.0412**
V_d (L/kg)	0.0105 ± 0.0035	0.00172 ± 0.0014*
Clearance (L/kg/ h)	0.0056 ± 0.0018	0.0002 ± 0.0001**
$T_{1/2}$ (h)	1.2971 ± 0.0590	5.8984 ± 1.4240**

Each value represents the mean ± SD (n = 6). *** $P < 0.001$, ** $P < 0.01$, *$P < 0.05$

In Fig. 5.23, plasma drug concentration versus time profile of free raloxifene hydrochloride suspension and raloxifene hydrochloride loaded nanocapsules post-oral administration is presented. From oral pharmacokinetic data, in comparison to free raloxifene hydrochloride, significant increase ($P < 0.05$) in AUC_{0-t} and C_{max} for nanocapsules formulation was observed. Oral bioavailability increased by ~2.1 folds for nanocapsules formulation when compared with free drug suspension. Encapsulating raloxifene hydrochloride in polymeric nanocapsules helped the drug to bypass gut wall metabolism.

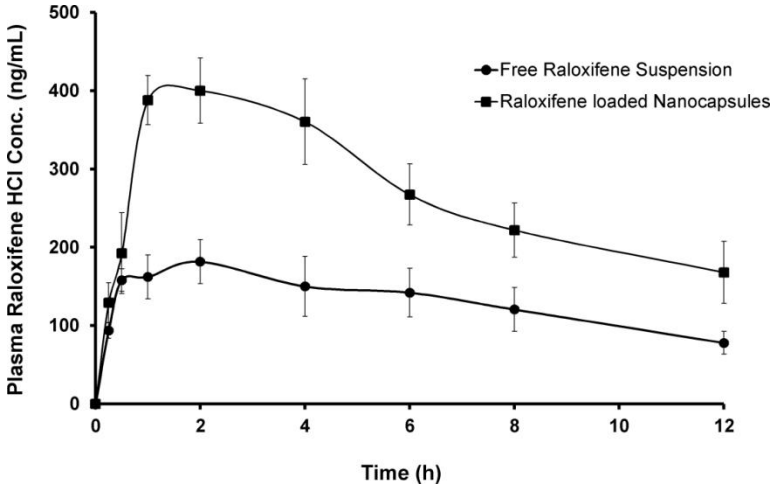

Fig. 5.23: Plasma concentration of raloxifene hydrochloride loaded nanocapsules compared with free raloxifene hydrochloride suspension (15 mg/kg) in rats after per-oral administration. Each value represents mean ± SD (n = 6).

Further, as suggested by several previously published reports [39, 64, 65], drug loaded nanocapsules were thought to be absorbed into lymphatic system by endocytosis process. From lymphatic system, these raloxifene hydrochloride loaded nanocapsules eventually reach systemic circulation [25, 66]. Mean residence time (MRT) for nanocapsules formulation (13.2 h) was significantly ($P < 0.05$) higher in comparison to MRT of free raloxifene hydrochloride (10.7 h). This could be due to reduced clearance of raloxifene hydrochloride loaded into nanocapsules formulation. IV pharmacokinetic data showed a significant reduction in both rate of elimination and clearance of drug loaded into nanocapsules compared to free raloxifene hydrochloride solution.

5.20.1.11 Organ distribution study

Post-oral dosing, highly perfused organs like liver, spleen and kidneys were isolated from rats to understand the difference in distribution pattern of free raloxifene hydrochloride and drug loaded nanocapsules. Time points for isolation of organs were selected based on T_{max} data obtained from oral pharmacokinetic studies. Fig. 5.24 presents the results of organ distribution study.

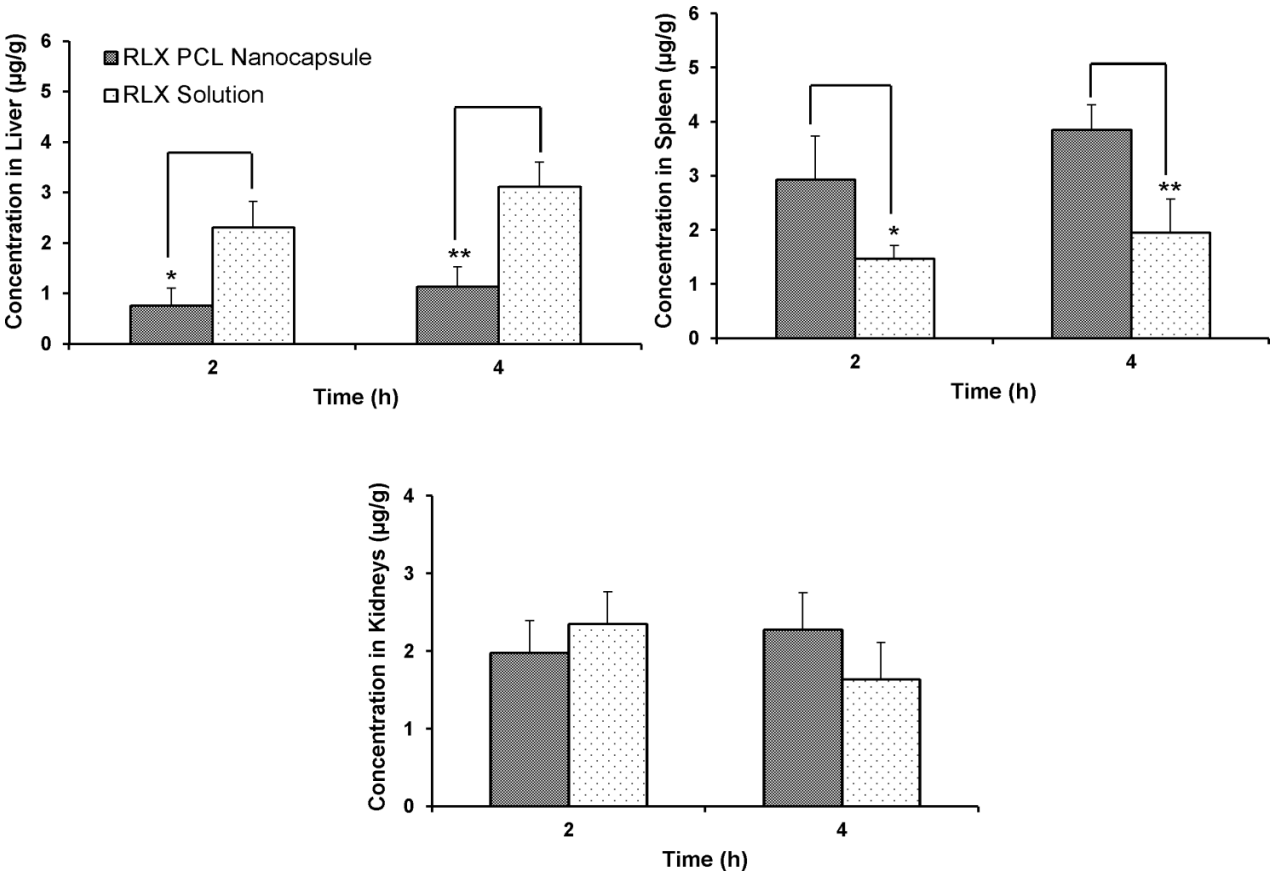

Fig. 5.24: Distribution profile of raloxifene hydrochloride in organs after per-oral administration of raloxifene hydrochloride loaded nanocapsules and free raloxifene hydrochloride suspension to rats at dose of 20 mg/kg (n =3 for each time point). ** $P < 0.01$ and *$P < 0.05$.

It is apparent that free raloxifene hydrochloride accumulates to a significant ($p < 0.05$) extent in liver compared to nanocapsules formulation. Alongwith glucuronidation in gut, raloxifene hydrochloride is also reported to undergo CYP-independent hepatic metabolism [67]. Though we did not identify any metabolites during our analysis, it is likely that accumulated drug undergoes extensive metabolism in the liver in a time dependent manner. Another possible explanation is that drug loaded nanocapsules undergo process of endocytic uptake by membranous epithelial cells (M-cells) covering Payer's patches in intestine [66]. They are further secreted into lymph and reach lymphatic system [68]. Higher accumulation of drug in spleen tissue from nanocapsules (Fig. 5.24) corroborates this hypothesis. In case of

kidneys, no significant difference in distribution pattern of raloxifene hydrochloride (from either free form or loaded nanocapsules) was seen. This is because majority of free raloxifene hydrochloride is excreted in feces and very small part of administered dose is excreted in urine [69].

5.21 Conclusions

PCL based nanocapsules for raloxifene hydrochloride were manufactured by double emulsion method (w/o/w). Important processing conditions for manufacture of these polymeric nanocapsules were identified and optimized using hybrid designs in DOE. Good correlation between actual and predicted values was obtained for the optimized formulation. Oral bioavailability of raloxifene delivered via PCL nanocapsules increased 2.1 folds when compared to free drug suspension. Distribution of nanocapsules to non-target tissues was lesser in comparison to raloxifene hydrochloride free suspension. In conclusion, formulating poorly soluble raloxifene in polymeric nanocapsules proved effective in improving its oral bioavailability and reducing clearance of the drug. This approach may prove beneficial in treatment of chronic disease like osteoporosis.

Chitosan-Soy lecithin hybrid nanoparticles

5.22 Introduction

Recently, nanoparticles produced from lipids and polysaccharides have received a great deal of attention. Both these materials are of natural/semi-synthetic origin and are considered safe and biocompatible.

Soybean lecithin is naturally-occurring phospholipid that is extracted during processing of soybean oil. Soy lecithin consists of three types of phospholipids– phosphatidylcholine, phosphatidylethanolamine and phosphatidylinositol [70-72] It is widely used in food and pharmaceutical industry for its emulsifier-stabilizer properties. Soy lecithin demonstrates strong anionic charge in aqueous media with zeta potential values lower than -40 mV [72]. In the past, it had been used to produce drug loaded liposomes [70, 71], micellar systems [73] and lipid based nanoparticles [72].

Chitosan is a biodegradable polycationic polymer obtained by deacetylation of chitin, a naturally occurring polysaccharide found in the crustacean shells [74, 75]. It contains numerous amino groups that impart strong cationic charge in acidic aqueous media. Chitosan exhibits mucoadhesive properties in GIT and increases the residence time of the nanocarrier formulations [76]. It is also possesses permeation enhancer effect in the GIT where it acts by opening tight junctions between enterocytes in the intestine [76]. Upon oral administration, chitosan is slowly degraded by chitinases that are secreted by the intestinal microorganisms and also by lysozymes [77, 78]

In the past, some research groups have reported the role of hybrid nanocarriers with soy lecithin and chitosan for drug delivery applications [73,76,79,80]. Nevertheless, the potency of these hybrid carrier systems in the oral delivery of low bioavailable drugs remains largely unexplored. We hypothesized that the anionic lipid soy lecithin can be an efficient carrier for the cationic, lipophilic raloxifene hydrochloride. Moreover, combination with

chitosan could further enhance the retention of these nanocarriers in GIT. Therefore, the primary aim of this study was to develop and characterize raloxifene hydrochloride loaded soy lecithin–chitosan hybrid nanocarriers.

According to recent reports [79, 81], soy lecithin alone (without chitosan) can make flat, hollow, sub-micron sized vesicles that could be utilized for drug delivery. Therefore, we also compared standalone soy lecithin vesicles (SLV) against soy lecithin–chitosan hybrid nanocarriers (LCNPs). To understand the usefulness of LCNPs under in-vivo conditions, we performed comparative oral and intravenous (IV) pharmacokinetic studies.

Several mechanisms have been proposed for oral uptake of nanomedicines [24]. Therefore, to unravel the mechanism(s) involved in the oral uptake of raloxifene hydrochloride loaded nanocarriers, we performed experiments using rat everted gut-sac model. Furthermore, we also studied tissue distribution profile and fecal excretion profile of free drug and drug loaded nanocarriers.

5.23 Materials

Raloxifene hydrochloride was obtained as a gift sample from Apotex Research Pvt. Ltd. Bangalore, India. Chitosan (100,000 – 300,000 Da) was purchased from M/s Polysciences, Inc. (Warrington, PA, USA). Soy lecithin was procured from Hi-media Laboratories, Mumbai, India. Ethanol was purchased from Merck Ltd., Mumbai. All other chemicals used were of analytical grade and the solvents were of HPLC grade. Freshly collected Milli-Q water (Millipore, MA, USA) was used in preparation of aqueous mobile phase of HPLC.

5.24 Preparation of Soy lecithin–chitosan nanoparticles:

Soy lecithin–chitosan nanoparticles (LCNP) were prepared by previously reported method with some modifications [79]. Soy lecithin (5% w/v) and raloxifene hydrochloride (25 mg) were dissolved in ethanol-water pre-mix (90:10). Aqueous solution of chitosan was prepared by stirring chitosan in 0.275N HCl solution overnight. To remove any undissolved chitosan, the solution was filtered through 0.45 µm membrane filter and filtrate collected. The final concentration of chitosan in aqueous solution was adjusted to 10mg/ml. Further, 4 ml of ethanolic soy lecithin-raloxifene hydrochloride solution was added to 46 ml aqueous chitosan solution at a constant rate of 2 ml/min using a polypropylene syringe (internal diameter 0.75 mm) under homogenization (Polytron PT 3100D, Kinematica, Lucerne, Switzerland) at 1200 rpm. In order to obtain soy lecithin–chitosan nanocarriers with different soy lecithin: chitosan ratios (5:1, 10:1, 20:1 30:1 and 40:1), an appropriate volume of 10 mg/ml chitosan solution was diluted with high purity water and then the aforementioned ethanolic injection procedure was followed. For preparation of standalone soy lecithin vesicles, a similar procedure was followed except for the use of chitosan in the aqueous phase. All the formulations were prepared in triplicate. The scheme of preparation is illustrated in Fig. 5.25 below.

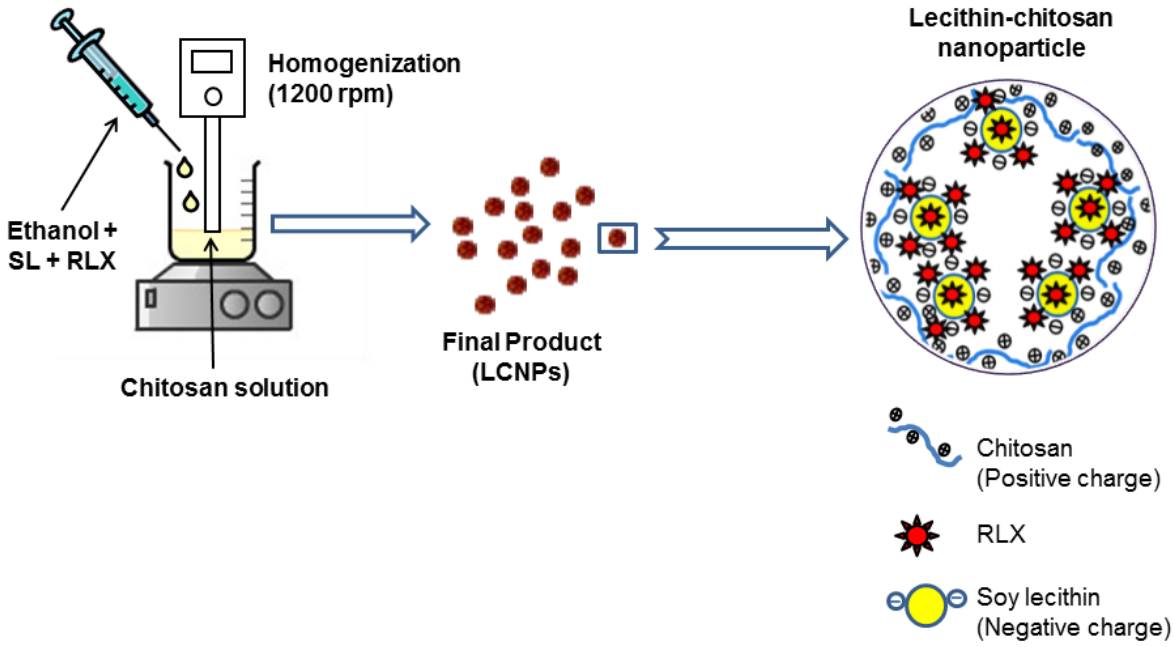

Fig 5.25: Preparation of raloxifene loaded soy lecithin chitosan hybrid nanoparticles

5.25 HPLC method for analysis of raloxifene hydrochloride

5.25.1 Method for analysis of EE, assay and in-vitro drug release study samples

The assay, entrapment efficiency (EE) and in-vitro drug release study samples were analysed after suitable dilution and processing using a validated HPLC method as described earlier.

5.25.2 Method for analysis of biological samples

Biological samples (plasma, tissue and mucoadhesion study samples) were analyzed by previously validated method developed in our lab [82]. The lower limit of quantification (LLOQ) in rat plasma was 50ng/ml. For all other biological matrices, partial validation was carried out prior to analysis. Further, we ensured the absence of interfering peaks by running blanks while analyzing samples from organ distribution and mucoadhesion studies.

5.26 Physicochemical characterization

5.26.1 Particle Size and Zeta Potential

Zetasizer Nano ZS (Malvern Instruments, Worcestershire, UK) was used to measure particle size, polydispersity index (PDI) and zeta potential (ζ-potential) of LCNPs. Intensity of scattered light was measured at an angle of 173º. Samples were measured in serial mode with 10 min set time and 30 ms sample measurement time. Values of ζ-potential and PDI provided by software attached to instrument were used in interpreting the results.

5.26.2 Entrapment Efficiency (EE)

After suitable dilution of samples, ultrafiltration method (regenerated cellulose membrane, molecular cutoff 3500 Da, Milipore, MA, USA) was used to estimate EE. Following equation was used to calculate EE:

$$EE\ (\%) = \ (W_{\text{total}} - W_{LCNP})/W_{\text{total}} \ \times 100$$

Where, W_{LCNP} is the amount of free raloxifene hydrochloride obtained in the filtrate; W_{total} is the total amount of raloxifene hydrochloride added to the formulation.

5.26.3 Thermal analysis using differential scanning calorimetry (DSC)

The change in enthalpy and melting temperature of raloxifene hydrochloride, soy lecithin, chitosan, blank LCNPs and drug loaded LCNPs were measured using DSC 60 (Shimadzu, Kyoto, Japan) instrument. Briefly, accurately weighted samples were taken in aluminium pans that were then crimp-sealed. In the DSC chamber, samples were allowed to equilibrate at 25 °C. Then, the samples were subjected to heating run over a temperature range of 25 to 300 °C at a heating rate of 5 °C/min. DSC thermograms were directly obtained from the software supplied with the instrument.

5.26.4 Fourier Transformed Infrared Spectroscopy (FT-IR)

To determine the possible interactions between raloxifene hydrochloride, chitosan and soy lecithin, FT-IR spectra were measured using bench top (Jasco, Japan) spectrometer. The LCNPs and corresponding blank LCNPs were lyophilized using a freeze dryer (Coolsafe 110-4, Scanvac, Denmark) to obtain a free-flowing powder. These freeze-dried LCNPs were then diluted with potassium bromide (KBr) and scanned. To obtain each spectrum, 256 scans at 4 cm^{-1} resolution were used.

5.26.5 In-vitro drug dissolution and release studies

The dialysis bag method was used for in-vitro drug release studies. Drug release for both free raloxifene hydrochloride and drug loaded LCNPs (n = 6) were studied. A sealed dialysis bag (Spectra/Por 3 dialysis membrane, MWCO 3500 Da) containing either LCNPs formulation or free drug solution (prepared in water with 1% w/v Tween 80, equivalent to 1.5 mg raloxifene hydrochloride) was immersed in 500 ml dissolution media (phosphate buffer, pH 6.8 containing 0.1% w/v Tween 80). The temperature was maintained at 37 °C by continuously stirring the media with a magnetic bead. Aliquots (1 ml) were withdrawn at pre-determined time intervals from dissolution media and were analyzed using HPLC. For evaluation of drug release kinetics, the drug release data were fitted into zero order, first order, Higuchi, reciprocal powered time model and Korsmeyer–Peppas models. From regression analysis, best-fit model was determined. The $t_{50\%}$, defined as the time taken for 50% drug dissolution was calculated. The models used to fit drug release data are given below:

Zero order model: $F = k_0 t$, First order model: $\ln(1 - F) = -k_f\, t$,

Higuchi model: $F = k_H \sqrt{t}$, Reciprocal powered time model: $(1/F - 1) = m/t^b$ and

Korsmeyer–Peppas model: $M_t/M_\infty = kt^n$

Where, F is fraction of drug released up to time t; k_0, k_f, k_H, m and b are model parameters. M_t is the amount of drug released at time t, M_∞ is the amount of drug released at infinite time, k is release kinetics constant, and n is exponent of release.

5.26.6 Absorption studies using everted gut sac model

5.26.6.1 Preparation of everted rat intestinal sac

Briefly, female Wistar rats (n = 3) were fasted overnight for 12 h but allowed water *ad libitum* before the experiment. After anesthetizing the rats with urethane, (1.25 g/kg, i.p.) entire small intestine was removed by cutting across the upper end of the duodenum and the lower end of the ileum. The mesentery was separated by manual stripping. The intestine was carefully flushed with normal saline (0.9% w/v NaCl) and different segments of the small intestine were identified. A length of 8 ± 0.5 cm (between upper ends of duodenum through the lower end of the ileum) was quickly cut and gently turned inside out over a glass rod. The everted intestine was then placed in a flat dish containing Krebs-Henseleit bicarbonate (KHB) buffer oxygenated with O_2/CO_2 (95%/5%) at 37 °C. One end of everted intestine was clamped and tied with a silk thread. From the open end, KHB buffer was filled into the intestinal sac using a 0.5 ml syringe. Then, the open end was sealed with another piece of silk thread. The sacs were then placed in individual incubation chambers containing oxygenated KHB buffer maintained at 37 °C.

5.26.6.2 Uptake studies in rat everted gut sac

To discern the uptake mechanism, everted gut sacs were incubated at 4 °C or in the presence of specific endocytic inhibitors like chlorpromazine (CPZ) (10 μg/ml) and nystatin (NYT) (25 μg/ml) at 37 °C. After a pre-set incubation time of 30 min, intestinal sacs were carefully removed, blotted onto filter paper and contents were collected. Sacs were rinsed

thrice with KHB buffer and rinsing were pooled with original content for analysis. Samples were analysed by a validated HPLC method.

5.26.6.3 In-vivo pharmacokinetic studies in rats

Female Wistar rats weighing 180–220 g were used for both oral and IV pharmacokinetic studies. Prior approval from the institutional animal ethics committee was taken for all the animal experiments. For the oral pharmacokinetics study, rats were kept on fasting for 12 h. After oral dosing of either raloxifene hydrochloride suspension or raloxifene hydrochloride loaded LCNPs, rats were continued on fasting for another 4 h. Thereafter, they were provided with rat-chow diet and water *ad libitum*. In all the studies, freshly prepared formulations were administered.

Drug–plasma profiles were drawn from data obtained after oral (15 mg/kg) and intravenous (IV, 2.4 mg/kg) administration of free raloxifene hydrochloride suspension and raloxifene hydrochloride loaded LCNPs. The animals (n = 12) were divided into two equal groups. One group, called the 'control group' received raloxifene hydrochloride suspension (free raloxifene hydrochloride suspended in 0.5% w/v methyl cellulose, molecular weight 14000 Da, viscosity 15 cps), while, the other group, called the 'treatment group' was administered LCNPs formulation. For the IV pharmacokinetic study, the control group was administered with raloxifene hydrochloride solution (raloxifene hydrochloride dissolved in PEG 400: water pre-mix (1:1)), while the treatment group received raloxifene hydrochloride LCNP formulation.

Blood samples (0.15 ml) were collected from orbital sinus puncture of rats into microfuge tubes containing anti-coagulant (3.8 %w/v sodium citrate). For the oral pharmacokinetic studies, samples were collected at following time points: pre-dose, 0.17, 0.25, 0.5, 1, 2, 4, 6, 8, 10 and 12 h; sampling points for the IV pharmacokinetics study were: pre-dose, 0.17, 0.25, 0.5, 1, 2, 4, 6 and 8 h. Plasma was separated from blood components by

centrifuging at 1000 × g at 4 °C for 10 min. Thus harvested plasma samples were stored at -70 °C until further analysis. As previously reported, a validated HPLC method was employed for analysing these samples.

5.26.6.4 Assessment of raloxifene hydrochloride distribution to various organs

Female Wistar rats (180–220 g) (*n* = 12) were deployed in this study. Two groups, with six animals in each group were made. The animals were administered either raloxifene hydrochloride suspension or LCNPs formulation (20 mg/kg) by oral gavage. Two hours post-dosing, three rats from each group were sacrificed. To remove residual blood, organs of interest (spleen, liver, lungs and kidney) were flushed with pH 7.4 PBS and later dissected from the rat's body. Isolated organs were protected by freezing at -70 °C. Before analysis, organs were thawed back to room temperature and were minced with water (equivalent to organ weight). To achieve a fine consistency, homogenization was carried out in a tissue homogenizer (Remi, Mumbai, India). Acetonitrile, a protein precipitating agent (2 parts acetonitrile to 1 part of tissue homogenate) was then added to these homogenized samples. Vortexing followed by centrifugation (8000 × g for 20 min, 4ºC) resulted in a clear supernatant. This supernatant was collected and drug content analysed by a validated HPLC method.

5.26.6.5 Rat faecal Analysis

Nine female Wistar rats were divided into 3 groups (*n* = 3, per group) and were orally administered one of the following: 4 ml water (control), 4 ml (raloxifene hydrochloride suspended in 0.5 %w/v MC, 15 mg/kg) or 4 ml (LCNPs, 15 mg/kg). All the rats were provided water and rat-chow diet *ad libitum*. Post dosing, the animals were housed in separate metabolic cages and their faecal matter were collected at two time periods: 0-24 h

and 24-48 h. The collected faecal matter was dried in a hot air oven (Remi, Mumbai, India) at 60 ºC to a constant weight.

For extraction of excreted drug, 0.5 g faecal matter was treated with 1 ml methanol: acetonitrile pre-mix (1:1), vortex-mixed for 5 minutes, centrifuged at 8,000 x g and straw-coloured supernatant collected. The supernatant was suitably diluted with methanol and analysed for drug content by validated HPLC method. Linearity (2–20 µg/ml) in faecal matter was established by externally spiking drug samples in the blank faecal matrix collected from control group rats. Limit of detection and limit of quantification for raloxifene hydrochloride in faecal matrix were 0.5 ± 0.04 and 1 ± 0.1 µg/ml respectively. The retention time of raloxifene hydrochloride was 6.2 ± 0.2 min. Cumulative amount of drug excreted in faecal matter was calculated using the formula:

$$\%\ \text{raloxifene hydrochloride Excreted} = \frac{Total\ amount\ of\ RLX\ recovered\ in\ fecal\ matter}{Amount\ of\ RLX\ administered}\ x\ 100$$

5.26.6.6 Mucoadhesion studies

Previously reported ex-vivo rat jejunum model was used to evaluate the mucoadhesion behaviour of LCNPs and free raloxifene hydrochloride suspension [83]. Briefly, female Wistar rats (300-350 g, n = 3) were sacrificed by cervical dislocation and a segment of their fresh intestine (jejunum) was separated from the body and cleaned thoroughly by rinsing with normal saline (0.9 %w/v NaCl solution in water) to remove all traces of food/faecal matter. The jejunum was cut into 2 cm segments and filled with 100 µl of LCNPs/free drug suspension in water (pH 6.5). (Before use, the LCNPs were subjected to ultrafiltration (regenerated cellulose membrane, molecular cut-off 3500 Da, Milipore, Billerica, MA) to remove free drug). The jejunum segments containing LCNPs were then

incubated in a petri plate containing phosphate buffered saline (PBS; pH 7.4) for 2h at 37 ºC. Thereafter, the tissue segments were thoroughly rinsed with PBS thrice to remove all loose/free LCNPs and any free raloxifene hydrochloride. The segments were then cut open with a midline incision to expose the internal surface of the intestinal tissue.

To determine the quantum of LCNPs attached to the mucus, the mucosal layer was separated from the exposed tissue by carefully scraping the mucus with a scalpel and collecting the debris. The mucosal debris was suspended in acidified methanol (acidified with glacial acetic acid) and subjected to ultrasonication to lyse the particles and release the drug. The samples were then left overnight at room temperature. On the following day, these samples were centrifuged at 8000×g for 20 min resulting in a clear supernatant which was collected and analysed for the drug content using a validated HPLC method. A similar procedure was followed with placebo LCNPs (without drug) to eliminate the interference from junk peaks. Externally spiked quality control samples of raloxifene hydrochloride in rat mucosal matrix, LQC = 150 ng/ml, MQC = 600 ng/ml and HQC = 1300 ng/ml were used as quality control standards for the HPLC analysis.

5.26.6.7 Statistical Analysis

To measure the difference between means of accelerated stability study results, in vitro drug release study results and organ distribution study results, unpaired Student t-test was used at 95% ($\alpha = 0.05$) significance level.

5.27 Results and discussion

5.27.1 Preparation and characterization of LCNPs

We prepared LCNPs using soy lecithin and chitosan in different ratios (5:1, 10:1, 20:1 30:1 and 40:1) and characterized them for size and surface charge (ζ-potential). The results are shown in Fig. 5.26a and 5.26b. The pH values of all these formulations were between 4.5

and 5.0; weight ratio of soy lecithin to raloxifene hydrochloride was kept constant (8:1, w/w) for all the formulations. Standalone raloxifene hydrochloride loaded soy lecithin vesicles were prepared without using chitosan.

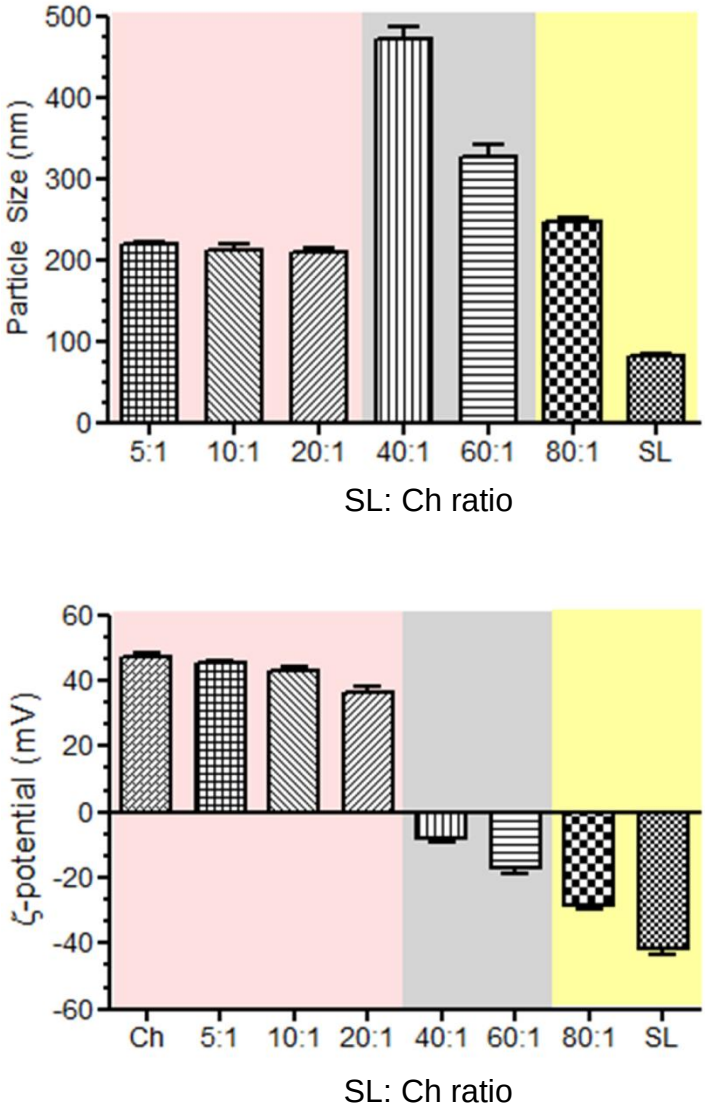

Fig. 5.26a: Effect of soy lecithin: chitosan ratio on particle size and **Fig. 5.26b:** Effect of soy lecithin: chitosan ratio on the ζ-potential of nanoparticles. Each observation represents mean ± SD (*n* = 3). SL–Soy lecithin; Ch–Chitosan and ζ-potential–zeta potential.

From Fig 5.26a, it is evident that the soy lecithin–chitosan ratio has a substantial bearing on particle size of the LCNPs. The obtained data could be placed into three distinct

zones. In the first zone, (from ratio 5:1 to 20:1) impact of soy lecithin–chitosan ratio on particle size is minimal. Particle size of LCNPs remains fairly constant in this zone (~ 210 nm). On the contrary, in the second zone (from ratio 40:1 to 60:1), particle size increases dramatically (~ 325 to 470 nm). Finally, in the third zone (80:1 ratio), the particle size again decreases (~ 250 nm). These results can be explained based on the changes in surface charge of LCNPs with changing soy lecithin–chitosan ratio (Fig. 5.26b).

Fig 5.26b shows the effect of soy lecithin–chitosan ratio on surface charge of LCNPs. The LCNPs are formed when protonated amine groups from chitosan form electrostatic linkages with negatively charged phosphate groups (PO_3^-) from soy lecithin [79, 84]. At acidic pH (4.5 to 5.0), amine groups (pKa ~6.2) on chitosan are protonated to $–NH_3^+$, while, phosphate groups (pKa ~1.5) on soy lecithin acquire a strong negative charge (PO_3^-) [79, 84, 85]. Further, from Fig. 5.26b, it is evident that the native chitosan demonstrates a strong positive surface charge (~ +45 mV), while the native soy lecithin shows a strong negative surface charge (~ -40 mV). However, the overall charge on LCNPs depends on the pH of the medium and proportion of each ingredient used [79, 84]. At a fixed pH (4.5-5.0), when ratio of soy lecithin–chitosan was varied, the ζ-potential, and hence, the particle size varied. In the first zone of Fig. 5.26b, when the soy lecithin–chitosan ratio was varied from 5:1 to 20:1, the ζ-potential values were ~40 to 45 mV. Correspondingly, particle size was low due to electrostatic repulsion and stabilization of the particles.

In the second zone (Fig 5.26b), when soy lecithin–chitosan ratio were 40:1 to 60:1, the magnitude of ζ-potential was near neutral (~ 0 to -20 mV). Therefore, the tendency for the particles to aggregate increased (due to low repulsive forces) and the particle size increased. Finally, with higher proportion of soy lecithin (third zone in Fig 5.26b), magnitude of ζ-potential increased in negative direction (~ -30 mV); therefore, once again the particles were stabilized by electrostatic repulsion and hence, the particle size reduced. Standalone soy

lecithin vesicles (without chitosan) demonstrated a very low particle size (~ 80 nm) and a high negative ζ-potential (~ -40 mV). Based on the results of particle size and ζ-potential, soy lecithin–chitosan ratio of 20:1 (with soy lecithin–raloxifene hydrochloride ratio of 8:1) was considered optimal. Further evaluations were done for the LCNPs bearing soy lecithin-chitosan ratio of 20:1. The optimal formulation of LCNPs had particle size of 208 ± 3 nm and ζ-potential of 36 ± 2 mV.

The EE for raloxifene hydrochloride was determined by ultrafiltration method and samples were analysed by a validated HPLC method. The results showed that the raloxifene hydrochloride was sufficiently entrapped in the optimal LCNPs formulation with an entrapment efficiency of 73 ± 3%.

The DSC thermograms of raloxifene hydrochloride, optimized LCNPs formulation, soy lecithin and chitosan are shown in Fig. 5.27. Raloxifene hydrochloride, being a crystalline material, displayed an endothermic peak at 265.5 ºC (Fig 5.27 (a)). However, in the thermogram of optimized LCNPs, this peak was not detected. Apparently, raloxifene hydrochloride was present in an amorphous state within the nanoparticle matrix. The strong endothermic peak at 165 ºC in the thermogram of LCNPs was attributed to mannitol that was used as a cryoprotectant during freeze-drying step (Fig 5.27 (b)). Soy lecithin demonstrated a broad peak between 90–100 ºC (Fig 5.27 (c)); the thermogram for chitosan demonstrated a prototype polysaccharide behaviour [86] with two distinct phases of degradation. The first phase (from 30–150 ºC) was attributed to the process of dehydration [86, 87]. The second phase (from 220–300 ºC), that resulted in the elevation of baseline, was attributed to the combustion of sample in the pan [86, 87]. Due to the amorphous nature of chitosan [86], no sharp endothermic peak was observed in this thermogram (Fig 5.27 (d)).

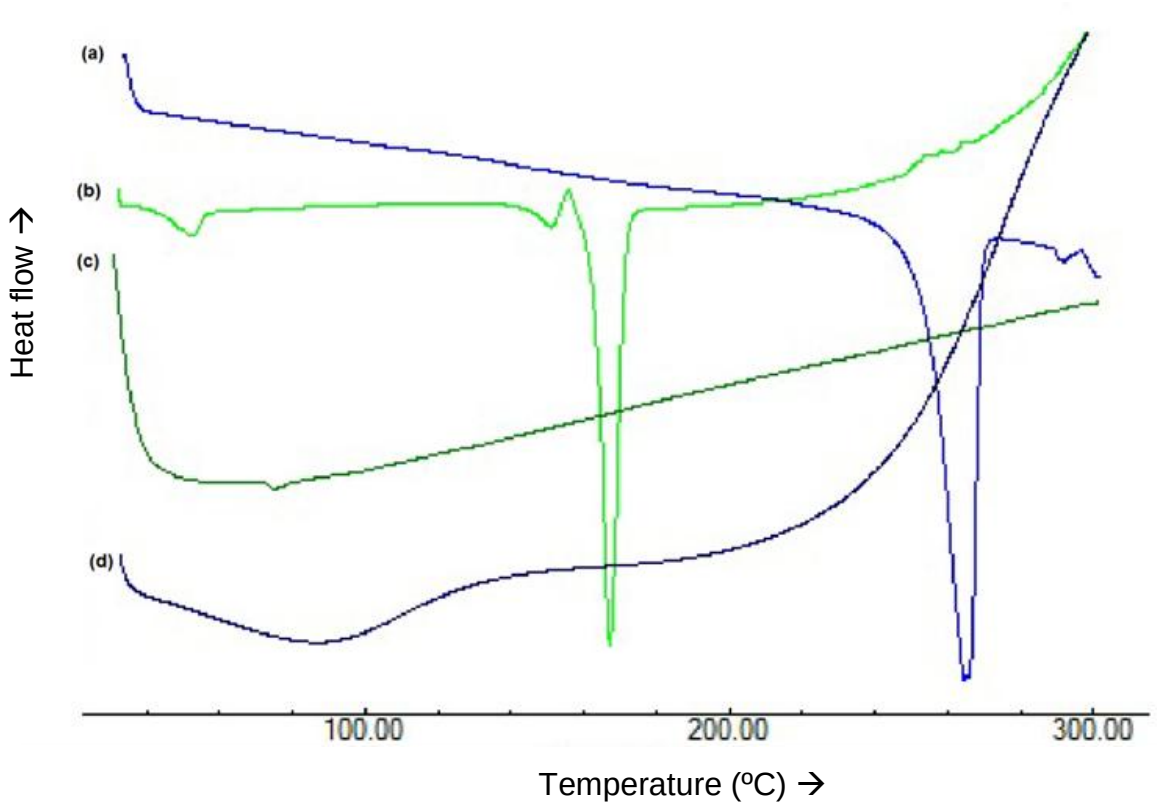

Fig. 5.27: DSC thermograms of (a) pure raloxifene hydrochloride; (b) optimized LCNPs formulation; (c) pure soy lecithin and (d) pure chitosan

The FT-IR studies were conducted for standalone chitosan, soy lecithin, raloxifene hydrochloride, their physical mixtures and the actual formulation. The data are presented in Fig. 5.28. For standalone chitosan, significant peaks at 3558 cm^{-1} (-NH stretching and -OH stretching), 1663 cm^{-1}(-NH bending) and 1422 cm^{-1} (-CH bending) were observed. For standalone soy lecithin, peaks appeared at 2925 cm^{-1} (-CH stretching), 1735 cm^{-1} (-C=O stretching), 1458 cm^{-1} (-CH bending) and 1236 and 1060 cm^{-1}(P=O stretching). In the physical mixture, slight shift of peak to 3379 cm^{-1} (-NH stretching) and 1094 cm^{-1} (P=O stretching) indicates that there was interaction between positively charged chitosan and negatively charged soy lecithin. From spectrum 4 (Fig. 5.28), it is evident that raloxifene hydrochloride was loaded into chitosan–soy lecithin nanoparticles. Characteristic peaks of raloxifene hydrochloride appear at: 2697 cm^{-1}, 2541 cm^{-1}, 1913 cm^{-1}, 1597 cm^{-1}, 1462 cm^{-1},

1356 cm^{-1}, 1258 cm^{-1}, 1120 cm^{-1}, 1042 cm^{-1}, 907 cm^{-1} and 835 cm^{-1} [88]. However, the most important peaks for raloxifene hydrochloride are found at 3151 cm^{-1} (due to -NH stretching) and 2954 cm^{-1} (due to Ph-OH bonds) [88]. During the formulation of nanoparticles, any kind of interaction with the polymer or lipid (e.g. hydrogen bonding) can lead to shift in frequency or splitting of absorption peaks.

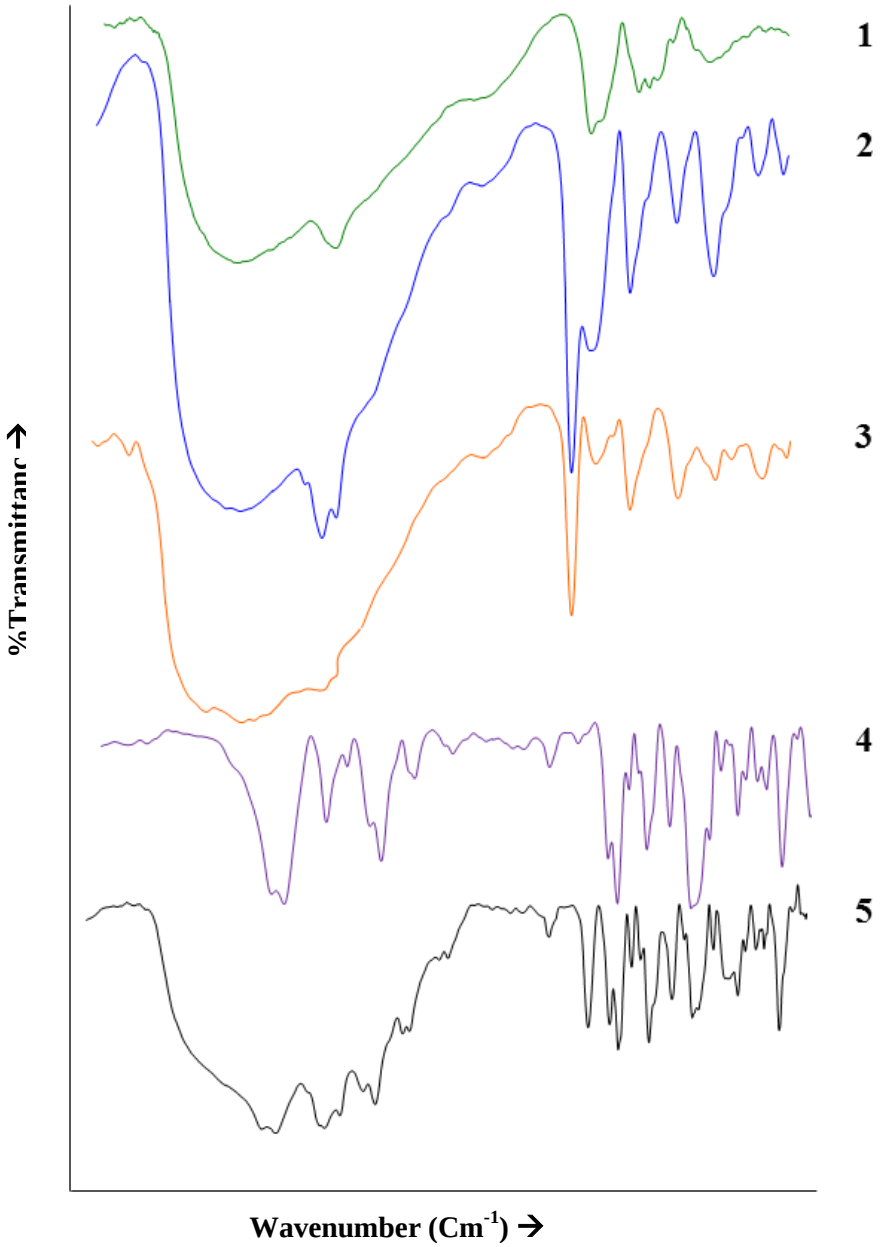

Fig. 5.28: Infrared spectra of: (1) pure chitosan; (2) pure soy lecithin; (3) physical mixture of chitosan and soy lecithin (without drug); (4) pure raloxifene HCl and (5) actual formulation.

5.27.2 In-vitro drug release study

The results presented in Fig. 5.29 demonstrate that free raloxifene hydrochloride completely dissolves into the media within 4h. However, in case of LCNPs, slow and more sustained drug release pattern was observed. From the analysis, data showed best fit with Korsmeyer–Peppas model with good regression co-efficient value (r^2 = 0.9823). The Korsmeyer–Peppas model is a semi-empirical model that uses single exponential equation to describe drug release process from a delivery system [60]. It has been used to evaluate the release of drugs from polymeric devices and nanoparticles, especially when the mechanism of release is unclear or when more than one mechanism is involved in the drug release [89, 90].

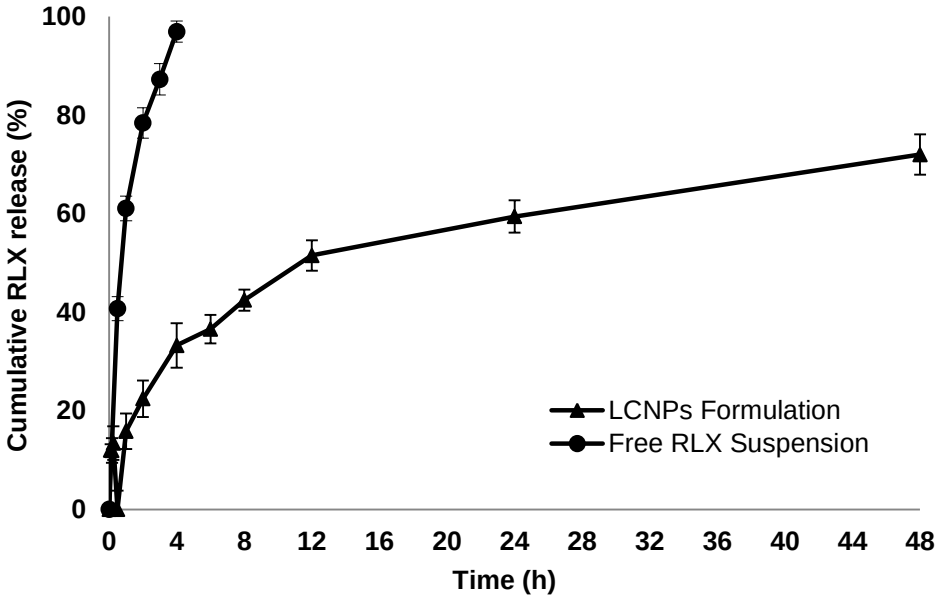

Fig. 5.29: In-vitro drug release data for raloxifene hydrochloride (RLX) and LCNPs

5.27.3 Absorption studies using everted gut sac model

The data from the everted gut sac study was expressed in terms of apparent permeability values of the drug. To distinguish between active and passive uptake mechanisms, we conducted this study at two different temperatures: 4 ºC and 37 ºC. It is

well-known that at 4 ºC, all the active uptake processes in the intestine are blocked [30]. Therefore, any significant differences in the uptake of raloxifene hydrochloride from LCNPs between 4 ºC and 37 ºC (normal body temperature, where the active uptake processes are functional) could indicate role of active processes in the intestinal uptake of LCNPs.

From our experiments, as depicted in Fig. 5.30, there was a significant increase ($P < 0.001$) in the apparent permeability of raloxifene hydrochloride from LCNPs at 37 ºC indicating that the LCNPs are internalized by active uptake processes. Further, at 4 ºC, even in the absence of all active uptake processes, raloxifene hydrochloride from LCNPs showed significantly ($P < 0.01$) higher permeability value than free raloxifene hydrochloride. Apparently, this increase in permeability could be attributed to mucus-binding capability of chitosan (which increases local retention time for LCNPs) and ability to open tight junctions between intestinal cells (by binding to phospholipase C and affecting the IP3/DAG pathway) [91, 92]. Tight junction opening by chitosan may lead to increased paracellular transport of raloxifene hydrochloride and hence, a higher permeability value [93].

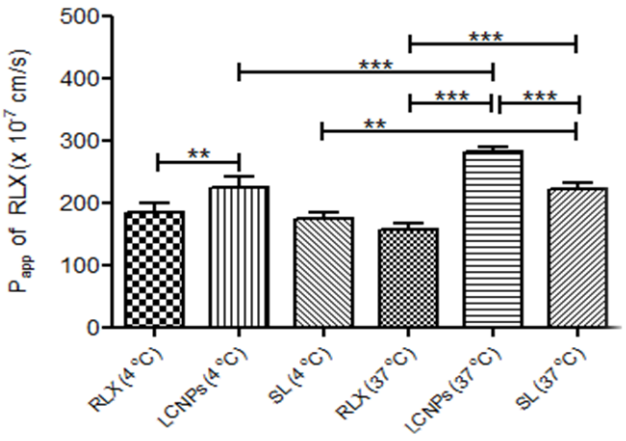

Fig 5.30: Apparent permeability (P_{app}) of raloxifene hydrochloride (RLX) in rat everted gut-sac model under various test conditions. (**$P < 0.01$;***$P < 0.001$ vs control) (Data represented as mean ± SD; $n = 3$).

Moreover, there was no significant difference in apparent permeability values for the control (free raloxifene hydrochloride) between 4 ºC and 37 ºC. This indicates that the free drug is absorbed into the intestine by a passive diffusion process. However, in standalone raloxifene hydrochloride loaded soy lecithin vesicles (SL) and LCNPs, the apparent permeability values at 37 ºC were significantly higher than that at 4 ºC. This indicates that both active and passive uptake mechanisms could play a part in the intestinal uptake of these drug loaded nanocarriers.

5.27.4 In-vivo pharmacokinetic studies

The effectiveness of the optimized raloxifene hydrochloride loaded LCNPs was assessed by performing oral and IV pharmacokinetic studies in female Wistar rats (n = 6). After loading into LCNPs, bioavailability of raloxifene hydrochloride increased significantly ($P < 0.05$) by over ~4.2 folds compared to free drug suspension at the same dose. This increase in bioavailability was attributed to protection of raloxifene hydrochloride from glucuronidation in the intestine by LCNPs, permeation enhancing effect of chitosan and also due to active uptake of LCNPs. The IV and oral pharmacokinetic parameters are presented in Table 5.11 and data plot is shown in Fig. 5.31.

Table 5.11: Pharmacokinetic parameters for raloxifene hydrochloride after administering free raloxifene hydrochloride suspension (oral study), raloxifene hydrochloride solution (IV study) and drug loaded LCNPs to female Wistar rats.

Parameter	Raloxifene hydrochloride free drug	Raloxifene hydrochloride loaded LCNPs
Pharmacokinetic parameters obtained from oral study (15 mg/kg)		
C_{max} (ng/ml)	186 ± 22.46	794.5 ± 61.3***
T_{max} (h)	2.1 ± 0.21	1.2 ± 0.14
$MRT_{(0-t)}$ (h)	12.83 ± 2.13	8.10 ± 2.91
$AUC_{(0-t)}$ (µg h/ml)	1.53 ± 0.39	6.46 ± 1.34**
$T_{1/2}$ (h)	8.70 ± 1.41	5.06 ± 1.65
F_{rel}	-------	4.2 folds
Pharmacokinetic parameters obtained from IV study (2.4 mg/kg)		
Ke (per h)	0.5343 ± 0.1218	0.14227 ± 0.0214**
Vd (L/kg)	0.0105 ± 0.0035	0.0046 ± 0.0021
Clearance (L/kg/h)	0.0056 ± 0.0018	0.0006 ± 0.0002**
$T_{1/2}$ (h)	1.2971 ± 0.0590	4.8712 ± 1.1831**

Each value represents the mean ± SD (n = 6); * P < 0.05; ** P < 0.01; *** P < 0.001

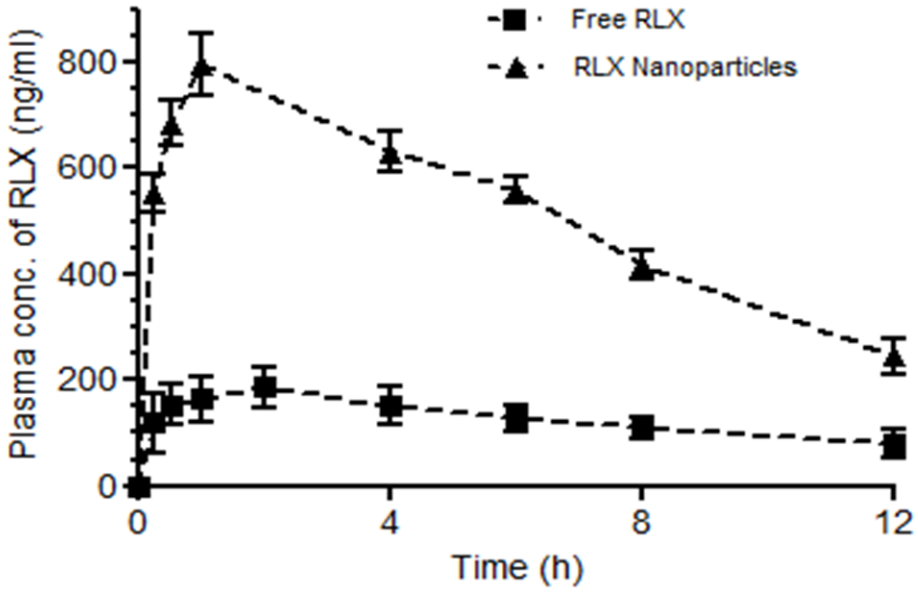

Figure 5.31: In-vivo oral pharmacokinetic profile of free raloxifene hydrochloride (RLX) suspension and raloxifene hydrochloride loaded soy lecithin chitosan nanoparticles in female Wistar rat model. All data points are represented as mean ± SD (n = 3).

5.27.5 Tissue distribution study

Rats (n = 3) were sacrificed two hours after oral administration of either raloxifene hydrochloride suspension or raloxifene hydrochloride nanoparticles (LCNPs). Highly perfused organs like spleen, liver, lungs and kidneys were then harvested from the rats. The time point for harvesting the organs was selected based on the T_{max} data obtained from oral pharmacokinetic study. The data from this study are presented in Fig. 5.32.

From the figure, ostensibly, compared to free raloxifene hydrochloride, the LCNPs accumulate to a significantly greater extent in liver ($P < 0.01$) and lungs ($P < 0.05$). Increased accumulation of raloxifene hydrochloride from LCNPs in liver can be co-related to an increase in apparent permeability value as compared to free drug (Fig. 5.30). An increase in permeability of raloxifene hydrochloride due to LCNPs leads to an increased entry of the drug via portal hepatic vein and accumulation in the liver [9, 94].

An increase in accumulation of LCNPs in lungs as compared to free drug can be explained by the surface charge of LCNPs. The formulation used for tissue distribution study demonstrated positive surface charge (38.2 ± 0.51 mV). It is now known that nanoparticles with strong positive charge tend to attract plasma proteins that deposit on them leading to reduction of the surface charge and aggregation of the particles in the blood [94]. These particle aggregates get trapped into tiny blood capillaries present in highly perfused organs like liver and lungs [94]. Therefore, it is logical that the LCNPs accumulate to a greater extent in the lungs and liver than other organs. In spleen and kidneys, 2h after oral dosing, we did not find statistically significant difference in the accumulation patterns of free drug and LCNPs (Fig. 5.32).

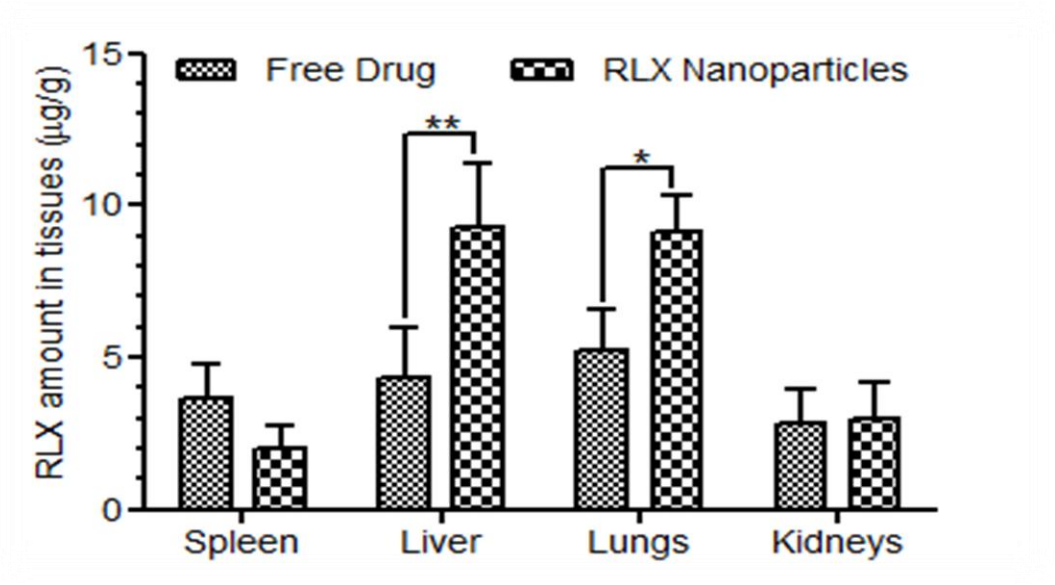

Fig. 5.32: Tissue pattern of raloxifene hydrochloride free drug and nanoparticles in female Wistar rats. Rats were sacrificed 2h post oral dosing (20 mg/kg) of either free drug or LCNPs. (**P < 0.01; *P < 0.05 *vs* control) (Data represented as mean ± SD; n = 3).

5.27.6 Faecal excretion study

This study was performed to understand the difference in excretion patterns of free drug and LCNPs. The data from this experiment are presented in Fig. 5.33 below.

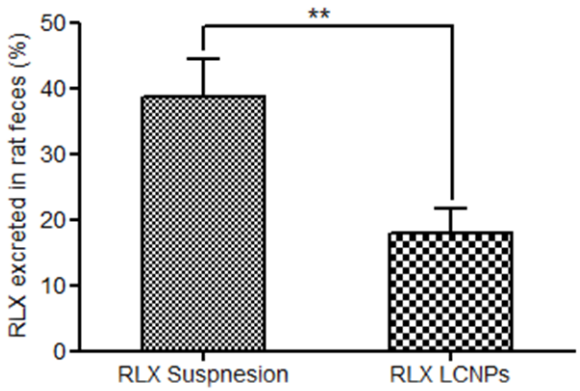

Fig.5.33: Faecal excretion study in female Wistar rats. Faces were collected at two time slots (0-24 h and 24-48 h) post oral administration of either free raloxifene hydrochloride (RLX) or LCNPs. **P < 0.01 *vs* control. Data represented as mean ± SD; n = 3.

From the figure, there was a statistically significant difference ($P < 0.01$) between the percentage of excretion of free drug suspension and LCNPs. In case of free drug suspension, ~40% of the orally administered dose (cumulative) of raloxifene hydrochloride was excreted in the faces in 48h period. However, at the same dose and same study period, LCNPs was excreted to an extent of only ~20% (cumulative excretion). This significant reduction in faecal excretion of LCNPs was possibly due to two reasons: (a) adhesion of LCNPs to the intestinal mucosa [83] and (b) increased permeability of raloxifene hydrochloride due to tight junction opening by chitosan.

5.27.7 Ex-vivo mucoadhesion studies

The mucoadhesion of nanoparticles immobilizes them in the intestine. Mucoadhesion mainly depends on the interaction of nanoparticle components with mucin glycoproteins [83]. Both non-specific (van der Waals) and specific (ionic) interactions with mucus membrane can contribute to mucoadhesion of nanoparticles [76, 83]. The data from this study is depicted in Fig. 5.34. From the figure, the LCNPs showed a significantly ($P < 0.01$) higher mucoadhesion character when compared with free drug suspension and standalone soy lecithin vesicles.

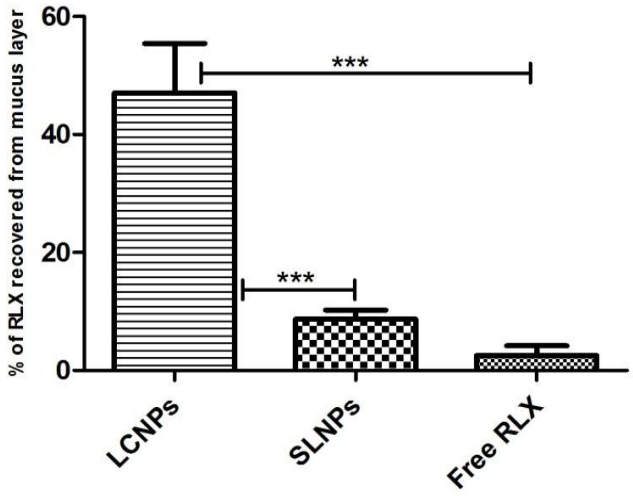

Fig. 5.34: Results from ex-vivo mucoadhesion study for free raloxifene hydrochloride and nanoparticles. Mucus samples were collected 2h after incubation with free drug/nanoparticles at 37 ºC. (***$P < 0.001$ *vs* control). (Data represented as mean ± SD; $n = 3$). LCNPs – soy lecithin chitosan nanoparticles; SLNPs – soy lecithin nanoparticles without chitosan and RLX – raloxifene hydrochloride.

After oral administration, the foremost barrier that nanoparticles encounter is the mucosal layer of the GIT [64, 95]. A vast majority of the administered particle population get enmeshed in the mucosal layer and are excreted via faeces during the mucus turnover cycle [64]. However, a small portion of the particles sneak through the mucus layer and come in contact with the intestinal epithelia where they are taken up by various active and non-active processes [64]**.** This depends on both particle size and surface charge present in that environment [64]**.**

For LCNPs, mucoadhesion may be beneficial because it increases the contact time of particles with GIT. However, as shown by S. Dünnhaupt et al [83], the mucoadhesion strength and particle penetration to the intestinal epithelia are inversely related. Thiolated

chitosan nanoparticles demonstrate "10-fold higher mucoadhesive property in comparison to penetration properties" [83]**.** Thus, for a better uptake from GIT, it is important that the nanoparticles should demonstrate just enough mucoadhesive strength to be retained in GIT and reach the intestinal epithelia from where they can be taken up. When we consider the results of oral pharmacokinetic study, faecal excretion study and ex-vivo mucoadhesion study in unison, we can hypothesize that the proposed LCNPs formulation has just enough mucoadhesion to be retained in GIT from where a fraction of the administered particles reach the intestinal epithelia and thereafter taken up by both active and non-active mechanisms. However, further studies need to be done in this direction to prove the proposed hypothesis.

5.28. Conclusions:

We developed soy lecithin-chitosan complex nanoparticles for oral delivery of raloxifene hydrochloride which has inherently poor oral bioavailability. The chitosan to soy lecithin ratio was optimized based on the surface charge and particle size. Oral bioavailability studies in female Wistar rats demonstrated a significant improvement (~4.2 folds) in the bioavailability of the drug. We also demonstrated that active uptake processes are involved in the intestinal uptake of these nanoparticles. Further, ex-vivo mucoadhesion studies proved that these nanoparticles are bound to the mucus layer of the intestine. In conclusion, the proposed nanocarrier system appears promising for effective oral delivery of poorly bioavailable drugs. Our investigations provide proof-of-concept for the use of soy lecithin-chitosan nanoparticles as oral delivery systems. However, further investigations to decipher exact uptake mechanism, distribution and comprehensive toxicity evaluation of these nanocarriers is necessary.

References:

1. Kalepu, S., M. Manthina, and V. Padavala, *Oral lipid-based drug delivery systems – an overview.* Acta Pharm Sin B, 2013. **3**(6): p. 361-372.

2. Wissing, S.A., O. Kayser, and R.H. Müller, *Solid lipid nanoparticles for parenteral drug delivery.* Adv Drug Deliver Rev, 2004. **56**(9): p. 1257-1272.

3. Müller, R.H., M. Radtke, and S.A. Wissing, *Solid lipid nanoparticles (SLN) and nanostructured lipid carriers (NLC) in cosmetic and dermatological preparations.* Adv Drug Deliver Rev, 2002. **54, Supplement**(0): p. S131-S155.

4. Muller, R.H., M. Radtke, and S.A. Wissing, *Nanostructured lipid matrices for improved microencapsulation of drugs.* Int J Pharm, 2002. **242**(1-2): p. 121-8.

5. Harde, H., M. Das, and S. Jain, *Solid lipid nanoparticles: an oral bioavailability enhancer vehicle.* Expert Opin Drug Deliv, 2011. **8**(11): p. 1407-24.

6. Radomska-Soukharev, A., *Stability of lipid excipients in solid lipid nanoparticles.* Adv Drug Deliv Rev, 2007. **59**(6): p. 411-8.

7. Mehnert, W. and K. Mäder, *Solid lipid nanoparticles: Production, characterization and applications.* Adv Drug Deliver Rev, 2001. **47**(2-3): p. 165-196.

8. Westesen, K. and H. Bunjes, *Do nanoparticles prepared from lipids solid at room temperature always possess a solid lipid matrix?* International Journal of Pharmaceutics, 1995. **115**(1): p. 129-131.

9. Manjunath, K. and V. Venkateswarlu, *Pharmacokinetics, tissue distribution and bioavailability of clozapine solid lipid nanoparticles after intravenous and intraduodenal administration.* Journal of Controlled Release, 2005. **107**(2): p. 215-228.

10. Manjunath, K. and V. Venkateswarlu, *Pharmacokinetics, tissue distribution and bioavailability of nitrendipine solid lipid nanoparticles after intravenous and intraduodenal administration.* J Drug Target, 2006. **14**(9): p. 632-45.

11. Schubert, M.A. and C.C. Müller-Goymann, *Characterisation of surface-modified solid lipid nanoparticles (SLN): Influence of lecithin and nonionic emulsifier.* European Journal of Pharmaceutics and Biopharmaceutics, 2005. **61**(1–2): p. 77-86.

12. Awad, T.S., et al., *Temperature scanning ultrasonic velocity study of complex thermal transformations in solid lipid nanoparticles.* Langmuir, 2008. **24**(22): p. 12779-84.

13. zur Mühlen, A., C. Schwarz, and W. Mehnert, *Solid lipid nanoparticles (SLN) for controlled drug delivery – Drug release and release mechanism.* European Journal of Pharmaceutics and Biopharmaceutics, 1998. **45**(2): p. 149-155.

14. Müller, R.H., D. Rühl, and S.A. Runge, *Biodegradation of solid lipid nanoparticles as a function of lipase incubation time.* International Journal of Pharmaceutics, 1996. **144**(1): p. 115-121.

15. Wavikar, P. and P. Vavia, *Nanolipidgel for enhanced skin deposition and improved antifungal activity.* AAPS PharmSciTech, 2013. **14**(1): p. 222-33.

16. Nabi-Meibodi, M., et al., *The effective encapsulation of a hydrophobic lipid-insoluble drug in solid lipid nanoparticles using a modified double emulsion solvent evaporation method.* Colloids Surf B Biointerfaces, 2013. **112**: p. 408-14.

17. Castelli, F., et al., *Characterization of indomethacin-loaded lipid nanoparticles by differential scanning calorimetry.* International Journal of Pharmaceutics, 2005. **304**(1-2): p. 231-238.

18. Singh, B., R. Kumar, and N. Ahuja, *Optimizing drug delivery systems using systematic "design of experiments." Part I: fundamental aspects.* Crit Rev Ther Drug Carrier Syst, 2005. **22**(1): p. 27-105.

19. Liu, F.I., et al., *Biodegradable polymeric microspheres for nalbuphine prodrug controlled delivery: in vitro characterization and in vivo pharmacokinetic studies.* Int J Pharm, 2003. **257**(1-2): p. 23-31.

20. Hickey, T., et al., *Dexamethasone/PLGA microspheres for continuous delivery of an anti-inflammatory drug for implantable medical devices.* Biomaterials, 2002. **23**(7): p. 1649-56.

21. Barzegar-Jalali, M., et al., *Kinetic analysis of drug release from nanoparticles.* J Pharm Pharm Sci, 2008. **11**(1): p. 167-77.

22. Barthe, L., et al., *The improved everted gut sac: a simple method to study intestinal P-glycoprotein.* International Journal of Pharmaceutics, 1998. **173**(1–2): p. 255-258.

23. Barthe, L., J. Woodley, and G. Houin, *Gastrointestinal absorption of drugs: methods and studies.* Fundam Clin Pharmacol, 1999. **13**(2): p. 154-68.

24. Sahay, G., D.Y. Alakhova, and A.V. Kabanov, *Endocytosis of nanomedicines.* J Control Release, 2010. **145**(3): p. 182-95.

25. Roger, E., et al., *Biopharmaceutical parameters to consider in order to alter the fate of nanocarriers after oral delivery.* Nanomedicine (Lond), 2010. **5**(2): p. 287-306.

26. Roger, E., et al., *Lipid nanocarriers improve paclitaxel transport throughout human intestinal epithelial cells by using vesicle-mediated transcytosis.* Journal of Controlled Release, 2009. **140**(2): p. 174-181.

27. Ali Khan, A., et al., *Advanced drug delivery to the lymphatic system: lipid-based nanoformulations.* Int J Nanomedicine, 2013. **8**: p. 2733-44.

28. Porter, C.J.H., N.L. Trevaskis, and W.N. Charman, *Lipids and lipid-based formulations: optimizing the oral delivery of lipophilic drugs.* Nat Rev Drug Discov, 2007. **6**(3): p. 231-248.

29. Dahan, A. and A. Hoffman, *Evaluation of a chylomicron flow blocking approach to investigate the intestinal lymphatic transport of lipophilic drugs.* Eur J Pharm Sci, 2005. **24**(4): p. 381-8.

30. Lind, M.L., et al., *Intestinal lymphatic transport of halofantrine in rats assessed using a chylomicron flow blocking approach: The influence of polysorbate 60 and 80.* European Journal of Pharmaceutical Sciences, 2008. **35**(3): p. 211-218.

31. Gao, F., et al., *Nanoemulsion improves the oral absorption of candesartan cilexetil in rats: Performance and mechanism.* Journal of Controlled Release, 2011. **149**(2): p. 168-174.

32. Zhang, Z., et al., *Solid lipid nanoparticles loading candesartan cilexetil enhance oral bioavailability: in vitro characteristics and absorption mechanism in rats.* Nanomedicine, 2012. **8**(5): p. 740-7.

33. Hao, J., et al., *Development and optimization of solid lipid nanoparticle formulation for ophthalmic delivery of chloramphenicol using a Box-Behnken design.* Int J Nanomedicine, 2011. **6**: p. 683-92.

34. Yang, Y.-Y., et al., *Effect of preparation conditions on morphology and release profiles of biodegradable polymeric microspheres containing protein fabricated by double-emulsion method.* Chemical Engineering Science, 2000. **55**(12): p. 2223-2236.

35. Shah, M., et al., *Oral solid compritol 888 ATO nanosuspension of simvastatin: optimization and biodistribution studies.* Drug Dev Ind Pharm, 2011. **37**(5): p. 526-37.

36. Souto, E.B., et al., *Development of a controlled release formulation based on SLN and NLC for topical clotrimazole delivery.* Int J Pharm, 2004. **278**(1): p. 71-7.

37. Muller, R.H., R. Shegokar, and C.M. Keck, *20 years of lipid nanoparticles (SLN and NLC): present state of development and industrial applications.* Curr Drug Discov Technol, 2011. **8**(3): p. 207-27.

38. Duncan, R. and S.C. Richardson, *Endocytosis and intracellular trafficking as gateways for nanomedicine delivery: opportunities and challenges.* Mol Pharm, 2012. **9**(9): p. 2380-402.

39. Moghimi, S.M., A.C. Hunter, and T.L. Andresen, *Factors controlling nanoparticle pharmacokinetics: an integrated analysis and perspective.* Annu Rev Pharmacol Toxicol, 2012. **52**: p. 481-503.

40. Kumari, A., S.K. Yadav, and S.C. Yadav, *Biodegradable polymeric nanoparticles based drug delivery systems.* Colloids Surf B Biointerfaces, 2010. **75**(1): p. 1-18.

41. Natta, F.J.v., J.W. Hill, and W.H. Carothers, *Studies of Polymerization and Ring Formation. XXIII.1 ε-Caprolactone and its Polymers.* J Amer Chem Soc, 1934. **56**(2): p. 455-457.

42. Sinha, V.R., et al., *Poly-epsilon-caprolactone microspheres and nanospheres: an overview.* Int J Pharm, 2004. **278**(1): p. 1-23.

43. Woodruff, M.A. and D.W. Hutmacher, *The return of a forgotten polymer—Polycaprolactone in the 21st century.* Prog Polym Sci, 2010. **35**(10): p. 1217-1256.

44. Chandra, R. and R. Rustgi, *Biodegradable polymers.* Prog Polym Sci, 1998. **23**(7): p. 1273-1335.

45. Okada, M., *Chemical syntheses of biodegradable polymers.* Prog Polym Sci, 2002. **27**(1): p. 87-133.

46. Nair, L.S. and C.T. Laurencin, *Biodegradable polymers as biomaterials.* Prog Polym Sci, 2007. **32**(8–9): p. 762-798.

47. Cai, Q., et al., *Biodegradation behaviour of poly(lactide-co-glycolide) induced by microorganisms.* Polym Degrad Stabil, 2001. **71**(2): p. 243-251.

48. Pohlmann, A.R., et al., *Poly(-caprolactone) microcapsules and nanocapsules in drug delivery.* Expert Opin Drug Deliv, 2013. **10**(5): p. 623-38.

49. Kaleemuddin, M. and P. Srinivas, *Lyophilized oral sustained release polymeric nanoparticles of nateglinide.* AAPS PharmSciTech, 2013. **14**(1): p. 78-85.

50. Mora-Huertas, C.E., H. Fessi, and A. Elaissari, *Polymer-based nanocapsules for drug delivery.* Int J Pharm, 2010. **385**(1-2): p. 113-142.

51. Rao, J.P. and K.E. Geckeler, *Polymer nanoparticles: Preparation techniques and size-control parameters.* Prog Polym Sci, 2011. **36**(7): p. 887-913.

52. Ubrich, N., et al., *Preparation and characterization of propranolol hydrochloride nanoparticles: a comparative study.* J Control Release, 2004. **97**(2): p. 291-300.

53. Negi, L.M., M. Jaggi, and S. Talegaonkar, *A logical approach to optimize the nanostructured lipid carrier system of irinotecan: efficient hybrid design methodology.* Nanotechnology, 2013. **24**(1): p. 015104.

54. Rahman, Z., et al., *Understanding the quality of protein loaded PLGA nanoparticles variability by Plackett-Burman design.* Int J Pharm, 2010. **389**(1-2): p. 186-94.

55. Daspaul, S., et al., *Optimization of polymeric nano drug delivery system using 3(2) full factorial design.* Curr Drug Deliv, 2013. **10**(4): p. 394-403.

56. Lewis, G., D. Mathieu, and P.-T.-L. R., *Screening: Designs for identifying active factors*, in *Pharmaceutical experimental design*. 1999, Marcel Dekker, Inc.: New York. p. 39-40.

57. Singh, S. and M.S. Muthu, *Preparation and characterization of nanoparticles containing an atypical antipsychotic agent.* Nanomedicine (Lond), 2007. **2**(2): p. 233-40.

58. Yang, Y.Y., T.S. Chung, and N.P. Ng, *Morphology, drug distribution, and in vitro release profiles of biodegradable polymeric microspheres containing protein fabricated by double-emulsion solvent extraction/evaporation method.* Biomaterials, 2001. **22**(3): p. 231-41.

59. De Melo, N.F., et al., *Benzocaine-loaded polymeric nanocapsules: study of the anesthetic activities.* J Pharm Sci, 2012. **101**(3): p. 1157-65.

60. Peppas, N.A., *Analysis of Fickian and non-Fickian drug release from polymers.* Pharm Acta Helv, 1985. **60**(4): p. 110-1.

61. Peppas, N.A. and J.J. Sahlin, *A simple equation for the description of solute release. III. Coupling of diffusion and relaxation.* Int J Pharm, 1989. **57**(2): p. 169-172.

62. Korsmeyer, R.W., et al., *Mechanisms of solute release from porous hydrophilic polymers.* Int J Pharm, 1983. **15**(1): p. 25-35.

63. de Melo, N.F., et al., *Poly(lactide-co-glycolide) nanocapsules containing benzocaine: influence of the composition of the oily nucleus on physico-chemical properties and anesthetic activity.* Pharm Res, 2011. **28**(8): p. 1984-94.

64. Ensign, L.M., R. Cone, and J. Hanes, *Oral drug delivery with polymeric nanoparticles: the gastrointestinal mucus barriers.* Adv Drug Deliv Rev, 2012. **64**(6): p. 557-70.

65. Galindo-Rodriguez, S.A., et al., *Polymeric nanoparticles for oral delivery of drugs and vaccines: a critical evaluation of in vivo studies.* Crit Rev Ther Drug Carrier Syst, 2005. **22**(5): p. 419-64.

66. Plapied, L., et al., *Fate of polymeric nanocarriers for oral drug delivery*. Curr Opin Colloid Interface Sci, 2011. **16**(3): p. 228-237.

67. Mizuma, T., *Intestinal glucuronidation metabolism may have a greater impact on oral bioavailability than hepatic glucuronidation metabolism in humans: a study with raloxifene, substrate for UGT1A1, 1A8, 1A9, and 1A10.* Int J Pharm, 2009. **378**(1-2): p. 140-1.

68. Nishioka, Y. and H. Yoshino, *Lymphatic targeting with nanoparticulate system.* Adv Drug Deliv Rev, 2001. **47**(1): p. 55-64.

69. Hochner-Celnikier, D., *Pharmacokinetics of raloxifene and its clinical application.* Eur J Obstet Gynecol Reprod Biol, 1999. **85**(1): p. 23-9.

70. Kelmann, R.G., et al., *Carbamazepine parenteral nanoemulsions prepared by spontaneous emulsification process.* Int J Pharm, 2007. **342**(1-2): p. 231-9.

71. Pavelic, Z., et al., *Development and in vitro evaluation of a liposomal vaginal delivery system for acyclovir.* J Control Release, 2005. **106**(1-2): p. 34-43.

72. Schubert, M.A., M. Harms, and C.C. Muller-Goymann, *Structural investigations on lipid nanoparticles containing high amounts of lecithin.* Eur J Pharm Sci, 2006. **27**(2-3): p. 226-36.

73. Hafner, A., et al., *Melatonin-loaded lecithin/chitosan nanoparticles: physicochemical characterisation and permeability through Caco-2 cell monolayers.* Int J Pharm, 2009. **381**(2): p. 205-13.

74. van der Lubben, I.M., et al., *Chitosan microparticles for mucosal vaccination against diphtheria: oral and nasal efficacy studies in mice.* Vaccine, 2003. **21**(13-14): p. 1400-1408.

75. Agnihotri, S.A., N.N. Mallikarjuna, and T.M. Aminabhavi, *Recent advances on chitosan-based micro- and nanoparticles in drug delivery.* J Control Release, 2004. **100**(1): p. 5-28.

76. Derakhshandeh, K. and S. Fathi, *Role of chitosan nanoparticles in the oral absorption of Gemcitabine.* Int J Pharm, 2012. **437**(1-2): p. 172-7.

77. Aiba, S., *Studies on chitosan: 4. Lysozymic hydrolysis of partially N-acetylated chitosans.* Int J Biol Macromol, 1992. **14**(4): p. 225-8.

78. Nagpal, K., S.K. Singh, and D.N. Mishra, *Chitosan nanoparticles: a promising system in novel drug delivery.* Chem Pharm Bull (Tokyo), 2010. **58**(11): p. 1423-30.

79. Sonvico, F., et al., *Formation of self-organized nanoparticles by lecithin/chitosan ionic interaction.* Int J Pharm, 2006. **324**(1): p. 67-73.

80. Chadha, R., S. Gupta, and N. Pathak, *Artesunate-loaded chitosan/lecithin nanoparticles: preparation, characterization, and in vivo studies.* Drug Dev Ind Pharm, 2012. **38**(12): p. 1538-46.

81. Senyigit, T., et al., *Lecithin/chitosan nanoparticles of clobetasol-17-propionate capable of accumulation in pig skin.* J Control Release, 2010. **142**(3): p. 368-73.

82. Ravi, P., N. Aditya, and R. Vats, *Development, validation, and pharmacokinetic application of liquid chromatographic method for estimation of raloxifene hydrochloride in rabbit plasma.* Acta Chromatogr, 2012. **24**(4): p. 559-573.

83. Dünnhaupt, S., et al., *Distribution of thiolated mucoadhesive nanoparticles on intestinal mucosa.* International Journal of Pharmaceutics, 2011. **408**(1-2): p. 191-199.

84. Gerelli, Y., et al., *Structure of Self-Organized Multilayer Nanoparticles for Drug Delivery.* Langmuir, 2008. **24**(20): p. 11378-11384.

85. Senyigit, T., et al., *Lecithin/chitosan nanoparticles of clobetasol-17-propionate capable of accumulation in pig skin.* Journal of Controlled Release, 2010. **142**(3): p. 368-373.

86. Dhawade, P. and R. Jagtap, *Characterization of the glass transition temperature of chitosan and its oligomers by temperature modulated differential scanning calorimetry.* Adv App Sci Res, 2012. **3**(3): p. 1372-1382.

87. Ruiz-Caro, R. and M.D. Veiga-Ochoa, *Characterization and Dissolution Study of Chitosan Freeze-Dried Systems for Drug Controlled Release.* Molecules, 2009. **14**(11): p. 4370-4386.

88. Jagadish, B., et al., *Enhanced Dissolution and Bioavailability of raloxifene Hydrochloride by Co-grinding with Different Superdisintegrants.* Chem Pharm Bull (Tokyo), 2010. **58**(3): p. 293-300.

89. Korsmeyer, R.W., et al., *Mechanisms of solute release from porous hydrophilic polymers.* International Journal of Pharmaceutics, 1983. **15**(1): p. 25-35.

90. Peppas, N.A. and J.J. Sahlin, *A simple equation for the description of solute release. III. Coupling of diffusion and relaxation.* International Journal of Pharmaceutics, 1989. **57**(2): p. 169-172.

91. Dodane, V., M. Amin Khan, and J.R. Merwin, *Effect of chitosan on epithelial permeability and structure.* International Journal of Pharmaceutics, 1999. **182**(1): p. 21-32.

92. Bravo-Osuna, I., et al., *In vitro evaluation of calcium binding capacity of chitosan and thiolated chitosan poly(isobutyl cyanoacrylate) core–shell nanoparticles.* International Journal of Pharmaceutics, 2007. **338**(1–2): p. 284-290.

93. Maestrelli, F., et al., *Influence of chitosan and its glutamate and hydrochloride salts on naproxen dissolution rate and permeation across Caco-2 cells.* Int J Pharm, 2004. **271**(1-2): p. 257-67.

94. Li, S.D. and L. Huang, *Pharmacokinetics and biodistribution of nanoparticles.* Mol Pharm, 2008. **5**(4): p. 496-504.

95. Cone, R.A., *Barrier properties of mucus.* Adv Drug Deliv Rev, 2009. **61**(2): p. 75-85.

Chapter 6

Pharmacodynamic Studies

6.1 Introduction

Osteoporosis is a major cause of functional impairment in elderly patients. It is a multi-factorial skeletal disease that is characterized by reduction in bone mass, disruption of bone microarchitecture and an increased risk to bone fracture. Osteoporosis may be localized or it may involve the whole skeletal system. The generalized osteoporosis can be either primary (postmenopausal or senile osteoporosis) or secondary [1].

Bone is a complex organ. It continuously undergoes the process of resorption and deposition to maintain the structural integrity of the skeletal system [1]. The balance between bone resorption and deposition are determined by two types of cells – osteoclasts and osteoblasts [1, 2]. The osteoclasts are responsible for bone resorption. They are specially modified cells that have highly active ion channels in their cell membrane that can pump protons to the extracellular space leading to decrease in local pH. The low pH dissolves the bone minerals leading to bone resorption [3]. On the other hand, the osteoblasts lay down minerals for new bone formation by hereto unclear mechanisms, thus re-building the lost bone [4]. The activities of osteoclasts and osteoblasts are intimately intertwined. In a typical bone remodelling cycle, osteoclasts get activated first leading to bone resorption [4]. This is followed by a brief “reversal” phase when the resorption “pit” is occupied by osteoblast precursors and the bone formation begins as progressive “waves” and fresh matrix of bone is laid down [4]. In general, bone formation takes longer than the bone resorption process. Both the osteoclasts and osteoblasts communicate with each other by molecular signalling pathways [5]. Endogenous factors like hormones (estrogen) and exogenous factors like diet and exercise can influence these signalling pathways leading to pathological conditions of the bone [5].

6.2 Factors influencing bone resorption and bone formation:

In normal adults, this fine balance between bone resorption and deposition if well preserved. However, this balance is disturbed in pathological conditions and bone resorption exceeds bone formation leading to loss of structural integrity of the bone which is generally termed as osteoporosis [5].

Hormones are one of the most important modulators of bone resorption and bone formation. It is known that estrogen [6], parathyroid hormone [7] and to some extent testosterone [8] can influence both bone development and maintenance. Amongst these hormones, estrogen directly modulates the process of bone formation by interacting with specific proteins and receptors present on the surface of osteoblasts and osteoclasts [9]. The interaction of estrogen with these receptors sets off a series of events within the cells that increase the osteoblast activity and interfere with the osteoblast-osteoclast communication [10]. The paradox in bone remodelling cycle is the osteoblasts release factors which stimulate osteoclasts and drive the bone resorption process [10].

The effects of estrogen on bone formation are modulated by interaction of estrogen with special type of receptors called estrogen receptor alpha [ERα], which binds and transports the estrogen into the nucleus of the bone cells where the ERα-estrogen complex act as a "switch" to turn-on specific genes. The ER alongwith other receptors like estrogen receptor-related receptor alpha (ERRα) are abundantly found on the cell surface of osteoblasts [10]. Estrogen is secreted into the blood stream and it also has significant effects on other tissues like breast and uterus [10]. Other than estrogen, Prostaglandins, particularly progtaglandin E2 (PGE2) are known to modulate bone resorption and formation [11]. How the hormones impact bone remodelling depends on how they modulate osteoclast or osteoblast activity.

6.3 Animal models for osteoporosis

Osteoporosis is a complex disease affected by many physiological, dietary, genetic and environmental factors. Therefore, choosing a right animal model for simulating a particular type of human osteoporosis is important. Carefully chosen animal models provide for a greater control on the experimental material and allows for testing of potential therapies [12]. Since 1994, the USFDA has mandated generation of data both from rats and well-validated larger animal models for preclinical evaluation of new experimental drug therapies at the clinical dose and five times the clinical dose [13]. Several animal models have been reported in literature that simulate human osteoporosis [14]. Some of the frequently used animal models are: non-human primates like monkeys (rhesus and cynomolgus), beagle dogs, cats, New Zealand white rabbits, ferrets, guinea pigs, sheep, rats and mice [14]. Of these, rodents – rats and mice are most commonly employed as animal models for simulation of human osteoporosis [14].

6.3.1 Rat as an animal model for postmenopausal osteoporosis

Ovariectomized rat model exhibits most of the characteristics of human postmenopausal osteoporosis [15]. There are several advantages of using rats as animal model for postmenopausal osteoporosis – they are inexpensive, easy to house and have quicker bone remodelling cycle. Moreover, there is extensive literature available about ovariectomized rat model including histomorphometric changes, biochemical markers, methodology for bone densitometry and evaluation of bone mechanical properties [16, 17]. Unlike primates, the rodents do not experience a natural menopause [17]. Therefore, ovariectomy has become a time-tested method to produce artificial menopause [17]. After ovariectomy, bone resorption exceeds bone formation initially, causing bone loss in rats [18]. In rats that have undergone bilateral ovariectomy, statistically significant bone loss is seen in the proximal tibial metaphysis after 14 days [18, 19], in the lumbar vertebral body after 60

days [18, 19] and in the femoral neck after 30 days [20]. In contrast, ovariectomy does not induce bone mass loss in epiphyses of long bones, distal tibial metaphysis, or caudal vertebrae [14]. Various experimental interventions to induce osteopenia and osteoporosis in rats are presented in Fig. 6.1.

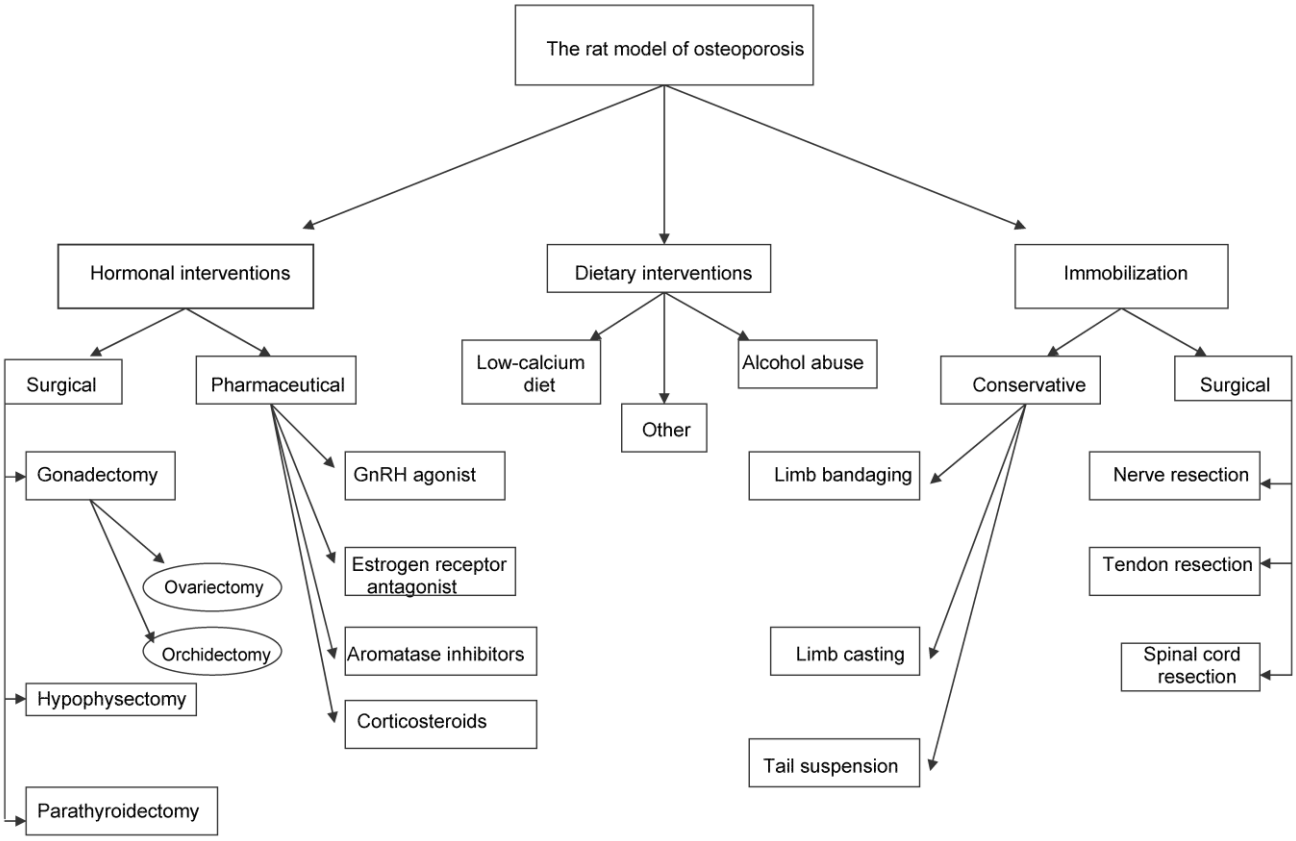

Fig 6.1: Experimental interventions to induce osteopenia and osteoporosis in rats. Figure source: Lelovas, P.P., et al., *The laboratory rat as an animal model for osteoporosis research.* Comp Med, 2008. **58**(5): p. 424-30.

Using rat model to express postmenopausal osteoporosis has some limitations. One potential drawback is the lack of Haversian remodelling in the rat skeletal system [12]. In humans, increased Haversian remodelling leads to cortical porosity; rats lack well-developed Haversian modelling system. Larger animals like rabbits, dogs and primates are considered more appropriate for study of Haversian remodelling [21]. However, despite this limitation,

osteopenia in rats due to age, ovariectomy (female rats) and immobilization bears a strong resemblance to human osteoporosis in both anatomical features and transitional states of the bones. In humans, low-impact fractures are common which are not easily reproduced in any animal model [21]. Nevertheless, according to World Health Organization definition, osteoporosis is considered to be present when the bone mineral density (BMD) values are more than 2.5 standard deviations lower than adult reference mean, with or without presence of fractures [22]. Therefore, even in absence of fractures, the rat model is still considered valid for screening of new therapies for treatment of osteoporosis.

6.4 Experimental design

This study was conducted in accordance with current legislation on animal experiments (Institutional Animal Ethical Committee (IAEC)) at BITS-Pilani, Hyderabad Campus. For this study, 34 female Wistar rats (250 ± 50 g), 10 weeks of age were housed in a pathogen-free animal house with 12-hour light and dark cycle. The rats were allowed free access to water and commercially available rat-chow diet. After 2 weeks of acclimatization, 4 rats (now twelve weeks old) were euthanized and their femora were carefully removed from the body (Naïve group – for obtaining baseline values). The adhering tissue was removed by treatment with 4 %w/v sodium hypochlorite solution for 2h and the cleaned bones were stored at -80 ºC by wrapping them in wet gauze soaked in phosphate buffered saline till further use.

6.5 Ovariectomy of rats and induction of post-menopausal osteoporosis

The remaining 30 rats were divided into two groups: ovariectomy group (n = 15) and sham operated group (n = 15). The castration procedure for the rats was performed after anesthetizing the rats with ketamine (90 mg/kg) and xylazine (10 mg/kg) administered through i.p. route. The ovariectomy was performed on both sides (bilateral ovariectomy)

using the double dorso-lateral approach [23]. For the sham operated group, similar surgical procedure was followed; sans ovariectomy .The experimental plan is summarized in Fig. 6.2.

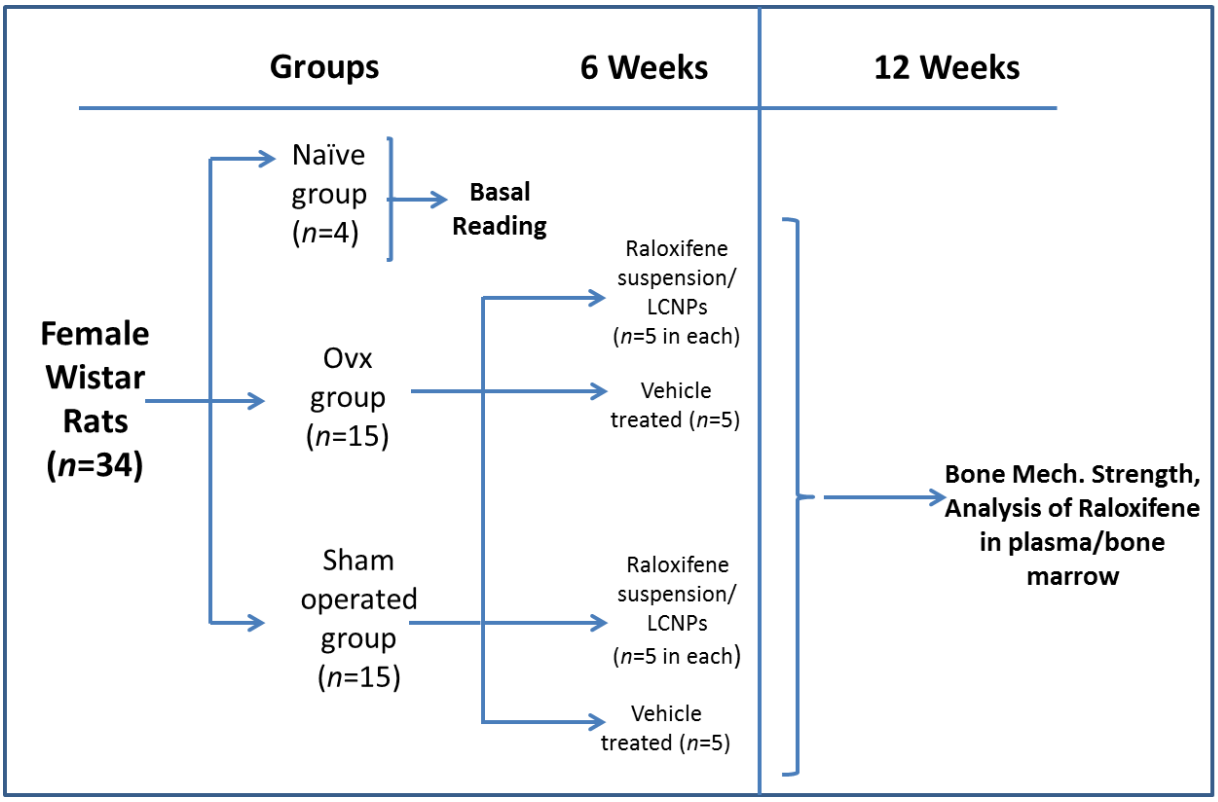

Fig. 6.2: Experimental plan for induction of post-menopausal osteoporosis and treatment. Naïve group indicates untreated and non-operated rats; ovx group indicates group of rats on which bilateral ovariectomy was performed; sham group indicates group of rats on which sham operation was performed without actual ovariectomy; LCNPs treated indicates group of rats treated with drug loaded soy lecithin-chitosan nanoparticles and vehicle treated group indicates group of rats treated with 0.5 %w/v aqueous dispersion of sodium carboxymethyl cellulose in water (pH 6.5).

6.5.1 Procedure for ovariectomy in rats:

For the surgery, the anaesthetized rat was laid in a prone position on the operating table and its legs were immobilized with surgical tapes. The bulged area on the back of the rat (between the last rib and the hip joint) was shaved clean of hairs on either side. Incisions were made in the shaved area with the help of a scalpel; thumb was placed at the uppermost

proximal area of the thigh for support [23]. The sharp incision of about 1.5 cm was made in the medial portion of the base of the distal phalanx [23]. This exposed the dorsolateral abdominal muscles (more specifically, the external oblique muscle). The muscle was then dissected to gain entrance into the peritoneal cavity where the ovary with the surrounding adipose tissue (fat) was visible. The adipose tissue was carefully pulled away from the incision site; ovary along with the attached uterine tube was identified. After the parts were identified, the distal uterine horn was ligated and ovary was carefully separated from the rat's body. The remaining uterine horn and other attachments were put back into the rat's abdominal cavity and the muscle was sutured with sterile biodegradable catgut sutures. Finally, the skin was sutured with 4.0 nylon thread and polyvinylpyrrolidone-iodine tincture (PVPI-tincture) was applied over the wound for asepsis [24]. Same procedure was repeated on the opposite side of the rat's body to complete bilateral ovariectomy. The sham operated group was treated in a similar way, except that, no real ovariectomy was performed in these rats.

After surgery, the rats were individually housed in a controlled pathogen-free environment at 21 ºC with 12-h light/dark cycle. They were fed with commercial rat-chow diet and water *ad libitum*. The polyvinylpyrrolidone-iodine tincture was applied daily to the wounds for a period of one week to prevent infection. The rats were left for 6 weeks to attain osteopenia [25, 26]. After 6 weeks, rats were treated with either raloxifene hydrochloride suspension (suspended in 0.5 %w/v sodium carboxymethyl cellulose aqueous dispersion) or LCNPs by oral gavage for next 12 weeks. A dose of 10 mg/kg/day was administered to the rats and volume of administration was fixed to 1 ml. The dose was selected based on previously published reports [27]. Equal number of rats in both sham operated and ovariectomized group served as vehicle control. The vehicle control group rats received only

vehicle – 0.5 %w/v aqueous dispersion of sodium carboxymethyl cellulose in water (pH 6.5) daily for 12 weeks by oral gavage.

At the end of twelve weeks, the rats were euthanized with high dose of ketamine and xylazine. Blood (1 ml) was immediately collected from the rat's body by cardiac puncture. Thereafter, both femoral bones were dissected out and were separated from adjacent tissue debris by treatment with 4 %w/v sodium hypochlorite solution for 2h. The bone samples were stored at -80 ºC by wrapping them in wet gauze soaked in phosphate buffered saline. These bones were later used to assess ex-vivo bone mechanical strength and microscopy studies. The bone marrow was separately collected from the tibiae by aspiration via syringe and pooled for analysis.

6.6 Measurement of bone mechanical strength

Three-point bending strength of femur mid-diaphysis was used to assess the baseline mechanical strength of the bones. The bone strength tester (model TK-252C) reported earlier was used to evaluate the bone strength [28-30] of the samples. Load-displacement curves generated by the instrument were used to calculate the ultimate load (N), stiffness (N/mm) and energy of failure (mJ) in the bone samples [30]. Readings from the naïve rats were considered as baseline readings. The sham operated rats served as control and ovariectomized rats served as the test group.

6.7 Analysis of drug content in bone marrow and plasma

The drug content in the pooled bone marrow was estimated by a previously validated HPLC method. Briefly, to 0.5 ml of pooled bone marrow, 1 ml acetonitrile: methanol (50:50, %v/v) pre-mix was added and vortex-mixed for 2 min. The sample was centrifuged (3000 x g) for 10 min, supernatant collected and concentrated to dryness under vacuum and reconstituted in 50 µl methanol. These samples were analysed using a validated HPLC

method. The limit of quantification of raloxifene hydrochloride in bone marrow was 150 ng/ml. Bone marrow samples were also collected from untreated rats and processed in a similar manner to ensure absence of interference of junk peaks with the drug peak. For analysis of drug content in plasma, bioanalytical method previously reported from our lab was used [31].

6.8 Results and Discussion

6.8.1 Measurement of bone mechanical strength

Three-point bending test was used to assess the bone strength at the femoral midshaft (Fig. 6.2). From the data, we have evidence that in the ovariectomized + vehicle treated group, compared to the vehicle treated sham operated group, there was a significant decrease in ultimate load, energy of failure and stiffness. Further, when compared with ovariectomized + vehicle treated group, rats from both raloxifene hydrochloride suspension treated group and LCNPs treated group showed a significant improvement in these bone mechanical parameters hinting towards the effectiveness of the treatment.

6.8.2 Analysis of drug content in bone marrow and plasma

The raloxifene hydrochloride content was estimated in plasma and bone marrow samples at the endpoint of the study. The data are presented in Fig. 6.3. There was evidence that in case of LCNPs treated group, the raloxifene hydrochloride content was significantly greater in both plasma and bone marrow matrices compared to raloxifene hydrochloride suspension treated rats at the endpoint. We suggest that in case of LCNPs, the higher bioavailability, sustained drug release pattern and slower clearance result in accumulation of the drug in bone marrow and blood plasma. This could prove clinically beneficial in treatment of chronic disease like post-menopausal osteoporosis.

(a)

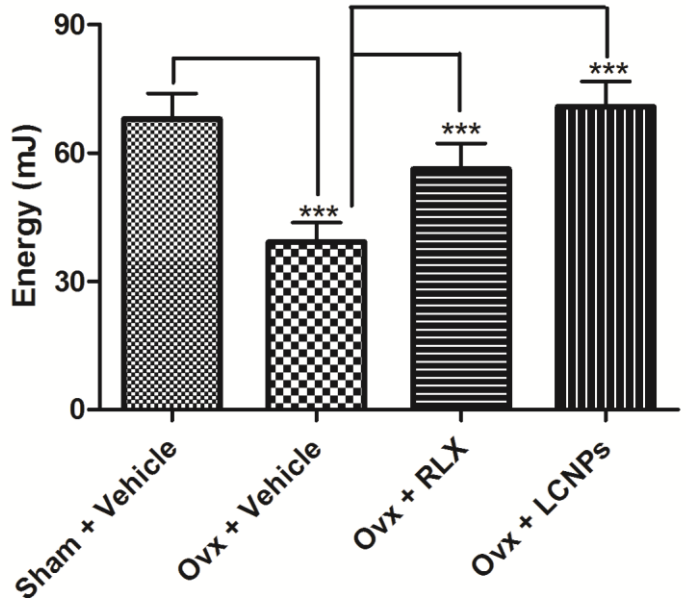

(b)

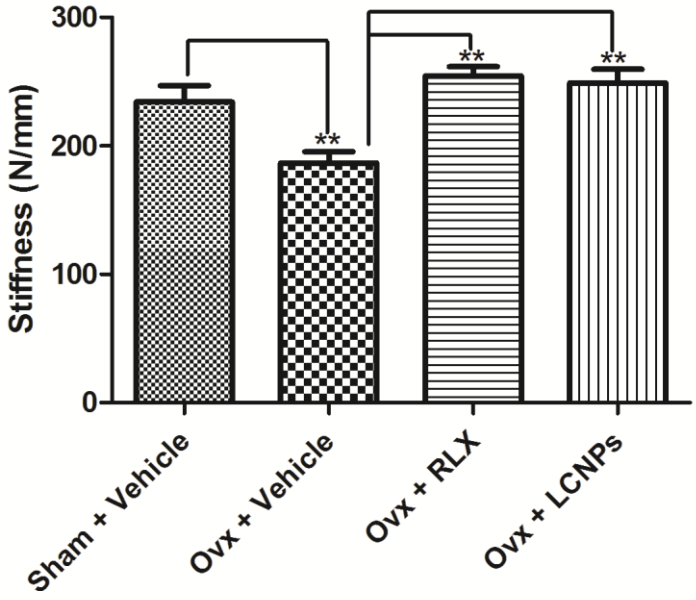

Fig. 6.3: Three-point bending test of rat femoral midshaft. The values of energy to failure (mJ) (a) and stiffness (N/mm) (b) were calculated from load-displacement curves. Values represent mean ± SD; n = 5 rats/group. (***P < 0.001, ** P < 0.01compared to sham/Ovx control group). RLX – raloxifene hydrochloride; LCNPs – soy lecithin chitosan nanoparticles; Ovx–ovariectomy group.

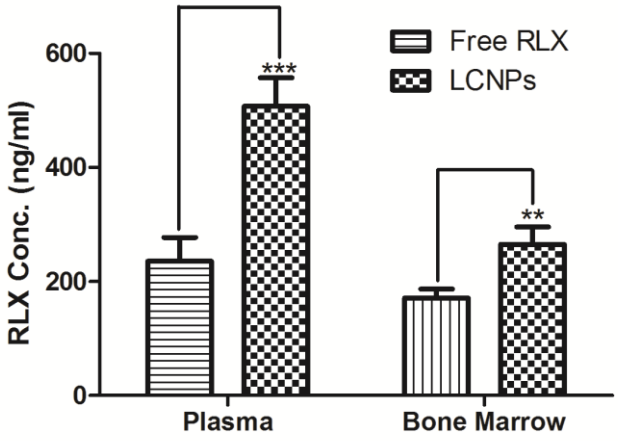

Fig. 6.4: Raloxifene hydrochloride (RLX) content estimated in plasma and bone marrow samples at endpoint of the study. The blood was collected by cardiac puncture and bone marrow was extracted and pooled from tibiae of the rats after euthanization. Values represent mean ± SD; n = 5 rats/group. (***P < 0.001, ** P < 0.01compared to sham/Ovx control group). RLX – raloxifene hydrochloride; LCNPs – soy lecithin chitosan nanoparticles.

6.9 Conclusions

We have shown that formulating selective estrogen receptor modulator (SERMs) like raloxifene into nanocarrier system (LCNPs) results in better oral bioavailability and greater accumulation in bone marrow than the traditionally available free drug. There was evidence that increased availability of the drug near the site of action could be beneficial in improving mechanical properties of the bone afflicted by post-menopausal osteoporosis. However, we hurry to caution that these investigations are only preliminarily in nature and data from other studies like mineralization of bone marrow cells, bone mineral density, histomorphometry and microcomputed tomography must be considered before drawing final conclusions. Nevertheless, our preliminary investigations show that use of appropriate nanocarriers for delivery of estrogens/SERMs could be a new strategy in treating post-menopausal osteoporosis.

References

1. Ammann, P. and R. Rizzoli, *Bone strength and its determinants.* Osteoporos Int, 2003. **14 Suppl 3**: p. S13-8.

2. Seeman, E., *From density to structure: growing up and growing old on the surfaces of bone.* J Bone Miner Res, 1997. **12**(4): p. 509-21.

3. Blair, H.C., et al., *Osteoclastic bone resorption by a polarized vacuolar proton pump.* Science, 1989. **245**(4920): p. 855-7.

4. Orwoll, E.S., *Toward an expanded understanding of the role of the periosteum in skeletal health.* J Bone Miner Res, 2003. **18**(6): p. 949-54.

5. Raisz, L.G., *Pathogenesis of osteoporosis: concepts, conflicts, and prospects.* J Clin Invest, 2005. **115**(12): p. 3318-25.

6. Prestwood, K.M. and L.G. Raisz, *Prevention and treatment of osteoporosis.* Clinical Cornerstone, 2000. **2**(6): p. 34-41.

7. Lips, P., *Vitamin D physiology.* Prog Biophys Mol Biol, 2006. **92**(1): p. 4-8.

8. Seeman, E., *The structural basis of bone fragility in men.* Bone, 1999. **25**(1): p. 143-7.

9. Zallone, A., *Direct and indirect estrogen actions on osteoblasts and osteoclasts.* Ann N Y Acad Sci, 2006. **1068**: p. 173-9.

10. Bonnelye, E. and J.E. Aubin, *Estrogen receptor-related receptor alpha: a mediator of estrogen response in bone.* J Clin Endocrinol Metab, 2005. **90**(5): p. 3115-21.

11. Forwood, M.R., *Inducible cyclo-oxygenase (COX-2) mediates the induction of bone formation by mechanical loading in vivo.* J Bone Miner Res, 1996. **11**(11): p. 1688-93.

12. Lelovas, P.P., et al., *The laboratory rat as an animal model for osteoporosis research.* Comp Med, 2008. **58**(5): p. 424-30.

13. Hartke, J.R., *Preclinical development of agents for the treatment of osteoporosis.* Toxicol Pathol, 1999. **27**(1): p. 143-7.

14. Turner, A.S., *Animal models of osteoporosis--necessity and limitations.* Eur Cell Mater, 2001. **1**: p. 66-81.

15. Aerssens, J., et al., *Interspecies differences in bone composition, density, and quality: potential implications for in vivo bone research.* Endocrinology, 1998. **139**(2): p. 663-70.

16. Jee, W.S. and W. Yao, *Overview: animal models of osteopenia and osteoporosis.* J Musculoskelet Neuronal Interact, 2001. **1**(3): p. 193-207.

17. Kalu, D.N., *The ovariectomized rat model of postmenopausal bone loss.* Bone Miner, 1991. **15**(3): p. 175-91.

18. Wronski, T.J., M. Cintron, and L.M. Dann, *Temporal relationship between bone loss and increased bone turnover in ovariectomized rats.* Calcif Tissue Int, 1988. **43**(3): p. 179-83.

19. Wronski, T.J., et al., *Long-term effects of ovariectomy and aging on the rat skeleton.* Calcif Tissue Int, 1989. **45**(6): p. 360-6.

20. Li, M., Y. Shen, and T.J. Wronski, *Time course of femoral neck osteopenia in ovariectomized rats.* Bone, 1997. **20**(1): p. 55-61.

21. Turner, R.T., et al., *Animal models for osteoporosis.* Rev Endocr Metab Disord, 2001. **2**(1): p. 117-27.

22. Kanis, J.A., *Assessment of fracture risk and its application to screening for postmenopausal osteoporosis: synopsis of a WHO report. WHO Study Group.* Osteoporos Int, 1994. **4**(6): p. 368-81.

23. Park, S.B., Y.J. Lee, and C.K. Chung, *Bone mineral density changes after ovariectomy in rats as an osteopenic model : stepwise description of double dorso-lateral approach.* J Korean Neurosurg Soc, 2010. **48**(4): p. 309-12.

24. Palacio, E.P., et al., *O Zoledronato no tratamento da osteoporose umeral em ratas: estudo prospectivo e randomizado.* Acta Ortopédica Brasileira, 2010. **18**: p. 90-95.

25. Sniekers, Y.H., et al., *Animal models for osteoarthritis: the effect of ovariectomy and estrogen treatment – a systematic approach.* Osteoarthritis and Cartilage, 2008. **16**(5): p. 533-541.

26. Hoegh-Andersen, P., et al., *Ovariectomized rats as a model of postmenopausal osteoarthritis: validation and application.* Arthritis Res Ther, 2004. **6**(2): p. R169-80.

27. Turner, C.H., M. Sato, and H.U. Bryant, *Raloxifene preserves bone strength and bone mass in ovariectomized rats.* Endocrinology, 1994. **135**(5): p. 2001-5.

28. Kumar, A., et al., *In vivo efficacy studies of layer-by-layer nano-matrix bearing kaempferol for the conditions of osteoporosis: a study in ovariectomized rat model.* Eur J Pharm Biopharm, 2012. **82**(3): p. 508-17.

29. Trivedi, R., et al., *Kaempferol has osteogenic effect in ovariectomized adult Sprague-Dawley rats.* Mol Cell Endocrinol, 2008. **289**(1-2): p. 85-93.

30. Srivastava, K., et al., *Greater Skeletal Gains in Ovary Intact Rats at Maturity Are Achieved by Supplementing a Standardized Extract of Butea monosperma Stem Bark that Confers Better Bone Conserving Effect following Ovariectomy and Concurrent Treatment Withdrawal.* Evid Based Complement Alternat Med, 2013. **2013**: p. 519387.

31. Ravi, P., N. Aditya, and R. Vats, *Development, validation, and pharmacokinetic application of liquid chromatographic method for estimation of raloxifene hydrochloride in rabbit plasma.* Acta Chromatogr, 2012. **24**(4): p. 559-573.

Chapter 7

Conclusions

7.1 Conclusions

Currently, nanotechnology holds an important position in drug delivery research. Nanotechnology based products have expanded the therapeutic horizon for many existing drugs with potential problems. With the help of nanocarriers, it is now possible to reach and maintain therapeutically useful drug levels in hereto inaccessible body sites. In the current research endeavour, we attempted to design different nanocarriers for the drug raloxifene hydrochloride which is a selective estrogen receptor modulator, useful in treatment of postmenopausal osteoporosis.

Development of robust analytical methods precedes formulation development. Therefore, analytical methods (UV and HPLC) were developed and extensively validated for various studies. Both the UV and HPLC methods were found to be selective towards raloxifene hydrochloride and were successfully employed in analysis of bulk drug and samples originating from preformulation/formulation studies. Methods to quantify the drug in the body fluids are essential pre-requisite for in-vivo studies. Therefore, bioanalytical method for analysis of drug in plasma was developed and validated using HPLC. The bioanalytical method was successfully employed for quantifying the drug in biological samples originating from pharmacokinetic and bio-distribution studies conducted in laboratory animals. The method was found to be adequately sensitive and selective towards the drug.

Preformulation studies are essential to gain knowledge about the physicochemical properties of the drug. They also aid in selection of appropriate excipients and conditions for the design of formulation. From the preformulation studies it was found that, raloxifene hydrochloride was crystalline material with a melting point of 267 ºC and that it demonstrates a pH dependent solubility. Highest solubility for raloxifene hydrochloride was found in the region of pH 4.5 to 6.0. The partition co-efficient of raloxifene hydrochloride was found to be

2.69 indicating the lipophilic nature of the drug. Drug-excipient compatibility data showed that raloxifene hydrochloride was compatible with most of the excipients used in the nanocarrier formulations. In liquid state, raloxifene hydrochloride was found to be stable below pH 7.3 and was sensitive towards extreme alkaline pH conditions.

For preparation of lipid based nanoparticles, warm o/w emulsion-solidification method was found suitable. Experimental results showed that SLNs were near spherical in shape with particle size less than 200 nm and with high encapsulation efficiency (>92%). From the in-vivo pharmacokinetics study in female Wistar rats, it was evident that oral bioavailability of raloxifene after incorporation into SLN improved by 3.24 folds compared to free drug. From the ex-vivo uptake studies using everted gut sac model, it was found that SLN were taken up by both clathrin and caveolae mediated endocytic pathways. Pre-treatment of rats with lymphatic uptake inhibitor, cycloheximide resulted in a significant reduction of area under plasma concentration curve (AUC) highlighting the importance of lymphatic route in transport of SLN. In conclusion, SLN seemed to be promising drug delivery systems that could significantly ($P < 0.05$) enhance the oral bioavailability of raloxifene.

Polymeric nanocapsules for raloxifene hydrochloride were prepared using the biodegradable polymer poly(ε-caprolactone). This polymer was selected based on its stability in the GIT and other economic benefits. Polymeric nanocapsules were chosen over nanoparticles for loading raloxifene because of the insolubility of the drug in traditional organic solvents used in the manufacture of nanoparticles. For preparation of nanocapsules, a modified multiple emulsion method (w/o/w) was followed which yielded a core-rich nanocarrier system. To optimize the manufacturing conditions, a hybrid-design approach was used. The hybrid-design approach comprised of a low-resolution screening design (Plackett–

Burman design) and a higher resolution rotatable central composite design which is a part of response surface methodology. This unique hybrid-design approach helped in selection and optimization of few important factors from many possible factors that could affect the properties of the nanocapsules. The optimized formulations were subjected to in-vitro and in-vivo evaluation. From the characterization results it was found that raloxifene loaded nanocapsules were spherical in shape with particle size less than 200 nm and high encapsulation efficiency (more than 80%). In-vivo pharmacokinetic studies in female Wistar rats showed that nanocapsules could improve oral bioavailability of raloxifene by 2.1 folds when compared to free drug. Further, IV pharmacokinetic studies in rats indicated that raloxifene loaded nanocapsule had significantly ($P < 0.05$) lower clearance and higher mean retention time in the body when compared to free drug. Therefore, it was concluded that the designed nanocapsules were promising dosage forms to improve oral bioavailability of raloxifene.

The third type of nanocarrier system developed to improve oral bioavailability of raloxifene was soy lecithin-chitosan hybrid nanoparticles. Of late, colloidal preparations with lipids and polysaccharides have proven useful as delivery systems for nasal, buccal or oral administration. The purpose of this part of the work was to prepare and characterize soy lecithin-chitosan nanoparticles (LCNPs) and to evaluate their capability in enhancing oral bioavailability of raloxifene. Another objective of this study was to assess the bio-distribution of LCNP after oral administration in female Wistar rats. From the results, it was found that the soy lecithin: chitosan ratio played a significant role in determining surface charge, particle size and stability of LCNPs. A ratio of 20:1 (soy lecithin: chitosan) was found optimal which yielded formulations with low particle size (159.3 ± 4.1 nm), positive zeta potential (38.2 ± 0.51 mV) and a moderate EE (65.2 ± 4.6 %). In-vitro drug release study showed a sustained

release pattern (less than 50 % release in 24 h) for LCNPs. Oral bioavailability study showed a significant ($P < 0.01$) improvement in systemic exposure of raloxifene in rats. The $AUC_{0\text{-}t}$ from LCNPs was 4.2 folds higher than free drug suspension. Bio-distribution studies indicated significantly ($P < 0.05$) lesser distribution of LCNPs to liver and spleen compared to free drug. Ex-vivo mucoadhesion studies showed that the LCNPs attached to the intestinal mucosa and are retained in the GIT for significantly longer duration. The final improvement in raloxifene's bioavailability could be due to a combination of permeation enhancing ability of chitosan, increased retention in the GIT and active uptake processes in the intestine.

To assess the usefulness of LCNPs in-vivo, pharmacodynamic experiments were designed using female Wistar rats. Raloxifene hydrochloride is used as a first line drug in treatment of postmenopausal osteoporosis. Rat is a well-established animal model for assessing therapeutic benefits of drugs used in treatment of postmenopausal osteoporosis. However, like other rodents, rats do not undergo a natural menopause. Therefore, to induce menopause artificially, bilateral ovariectomy was performed using the dorso-lateral approach.

Post-ovariectomy, 6 weeks induction period was allowed during which the rats became osteopenic. Thereafter, the rats were treated either with free drug or LCNPs formulation by oral gavage for next 12 weeks. At the end of 12 weeks, the rats were euthanized and blood, bone marrow & femoral bones were collected. Drug content in blood and bone marrow was analysed using validated HPLC method. Femoral bones were subjected to three-point bending test using bone strength tester. Load-displacement curves generated by the instrument were used to calculate stiffness and energy of failure in the bones.

From the results, there was evidence that in the ovariectomized + vehicle treated group, there was a significant decrease in ultimate load, energy of failure and stiffness when compared to the vehicle treated sham operated group, Further, when compared with

ovariectomized + vehicle treated group, rats from both free drug treated group and LCNPs treated group showed a significant improvement in the bone mechanical parameters hinting towards the effectiveness of the treatment.

From the plasma and bone marrow analysis, there was evidence that in case of LCNPs treated group, the raloxifene content was significantly ($P < 0.05$) greater in both plasma and bone marrow matrices when compared to free drug treated rats at the endpoint. It was suggested that higher bioavailability, sustained drug release pattern and slower clearance from LCNPs result in accumulation of the drug in bone marrow and blood plasma. This could prove clinically beneficial in treatment of chronic disease like post-menopausal osteoporosis. However, the results of these investigations are only preliminarily in nature and data from other studies like mineralization of bone marrow cells, bone mineral density, histomorphometry and microcomputed tomography must be considered before drawing final conclusions. Nevertheless, our preliminary investigations show that use of appropriate nanocarriers for delivery of estrogens/SERMs could prove to be a new and useful strategy in treating postmenopausal osteoporosis.

7.2 Future Scope and directions

In the present work, various types of nanocarriers for raloxifene hydrochloride were designed and evaluated for their efficacy under in-vitro and in-vivo conditions. In the pharmacodynamic studies, the effectiveness of selected formulation in treating rats induced with postmenopausal osteoporosis was compared with that of free drug. However, these results are only preliminarily in nature and data from other studies like mineralization of bone marrow cells, bone mineral density, histomorphometry and microcomputed tomography (µ-CT) must be considered before passing the final verdict about the usefulness of the formulations. Further, the effect of multiple-dosing and drug accumulation in other non-target organs needs for the selected nanocarrier formulation needs to be evaluated.

Appendix

LIST OF PUBLICATIONS (From Thesis Work)

1. Ravi PR, Aditya N, Kathuria H, Malekar S and Vats R. Lipid nanoparticles for oral delivery of raloxifene: Optimization, stability, *in vivo* evaluation and uptake mechanism. *European Journal of Pharmaceutics and Biopharmaceutics*; http://dx.doi.org/10.1016/j.ejpb.2013.12.015.

2. Aditya N, Ravi PR, Avula USR and Vats R. Poly (ε-caprolactone) nanocapsules for oral delivery of raloxifene: process optimization by hybrid design approach, *in vitro* and *in vivo* evaluation. *Journal of Microencapsulation*; http://dx.doi.org/10.3109/02652048.2014.885603.

3. Aditya N, Vats R and Ravi PR. Development, validation and pharmacokinetic application of liquid chromatographic method for estimation of raloxifene hydrochloride in rabbit plasma. *Acta Chromatographica*; 2012; 24(4):559–573.

LIST OF PUBLICATIONS (Outside Thesis Work)

1. Ravi PR, Aditya N, Patil S and Cherian L. Nasal *in situ* gels for rasagiline mesylate: improvement in bioavailability and brain localization. *Drug Delivery*; http://dx.doi.org/10.3109/10717544.2013.860501.

2. Ravi PR, Aditya N, Cherian L and Patil S. LC method for determination of rasagiline mesylate in different plasma matrices and its application to oral pharmacokinetic study in rabbits. *Journal of Chromatographic Science*; 2013; 51(1):1–7.

3. Abbas Z, Aditya N and Swamy NGN. Fabrication and *in vitro* evaluation of mucoadhesive, thermo reversible, in-situ gelling liquid suppository of chloroquine phosphate. *Indian Journal of Novel Drug Delivery*. 2013; 5(2):60–70.

4. Vats R, Aditya N and PR Ravi. Simple, rapid and validated LC determination of lopinavir in rat plasma and its application in pharmacokinetic studies. *Scientia Pharmaceutica*; 2011; 79(4):849–863.

5. Ravi PR, Vats R, Balija J, Adapa SP and Aditya N. Modified Pullulan Nanoparticles for Oral Delivery of anti-HIV Drug Lopinavir: Formulation and Pharmacokinetic Evaluation. *Carbohydrate Polymers*; http://dx.doi.org/10.1016/j.carbpol.2014.03.099.

6. Vats R, Ravi PR, Dalal V and Aditya N. Polymeric nanoparticles for oral delivery of lopinavir: optimization, physical characterization, *in vitro*, *ex vivo* and *in vivo* studies. *Drug Development and Industrial Pharmacy*; (Early Online 1-8) http://dx.doi.org/10.3109/03639045.2013.850710.

7. Ravi PR, Vats R, Dalal V and Aditya N. A hybrid design to optimize preparation of lopinavir loaded solid lipid nanoparticles and comparative pharmacokinetic evaluation with marketed lopinavir/ritonavir co-formulation. *Journal of Pharmacy and Pharmacology*; http://dx.doi.org/10.1111/jphp.12217.

8. Vats R, Varanasi KVS, Arla R, Veeraraghavan S, Rajak S and Murthy AN. Effect of multi-dose cilostazol on pharmacokinetic and lipid profile of atorvastatin in male Wistar rats. *Journal of Pharmacy and Pharmacology*; 2012; 64(11):1638–45.

9. Ravi PR, Vats R, Thakur R, Srivani S and Aditya N. Effect of grapefruit juice and ritonavir on pharmacokinetics of lopinavir in Wistar rats. *Phytotherapy Research*; 2012; 26(10):1490–5.

LIST OF CONFERENCE PRESENTATIONS (From Thesis Work)

1. Aditya N, R Vats, U Avula and PR Ravi. Design of polymeric nanocapsules for raloxifene hydrochloride by multiple emulsion method (w/o/w) using rotatable central composite design model in *10th International Nano Medicine and Drug Delivery (NanoDDS'12) Symposium, Atlantic City, NJ, USA*; 10/2012.

2. Aditya N, R Vats, H Kathuria and PR Ravi. Solid lipid nanoparticles for oral delivery of raloxifene: optimization, pharmacokinetic evaluation, bio-distribution and uptake studies. *13th International Symposium of Controlled Release Society, Indian Chapter, Mumbai, India*; 01/2013.

3. Aditya N, R Vats and PR Ravi. Self-organizing soy lecithin-chitosan nanoparticles for oral delivery of raloxifene. *3rd Nano Today Conference, Biopolis, Singapore*; 12/2013.

4. Aditya N, H Kathuria and PR Ravi. Raloxifene loaded SLN and NLC: comparison of in-vitro properties and in-vivo behavior after oral administration in rats. *3rd Nano Today Conference, Biopolis, Singapore*; 12/2013.

LIST OF CONFERENCE PRESENTATIONS (Outside Thesis Work)

1. Aditya N, Bhavya MV and Praveen KM. Formulation and characterization of controlled release benzoyl peroxide microsponges. *39th Annual Meeting and Exposition of Controlled Release Society, Quebec City, Canada*; 07/2012.

2. R Vats, PR Ravi and Aditya N. Polymeric nanoparticles of lopinavir to improve its oral bioavailability. *39th Annual Meeting & Exposition of the Controlled Release Society, Quebec City, Canada*; 07/2012.

3. R Vats, Aditya N and PR Ravi. Enhanced oral bioavailability of lopinavir from pullulan acetate nanoparticles: in vitro and in vivo evaluation. *3rd Nano Today Conference, Biopolis, Singapore*; 12/2013.

4. R Vats, Aditya N and PR Ravi. ADME of lopinavir loaded solid lipid nanoparticles in normal and hepatic impaired Wistar rats. *6th International Symposium on DMPK, NIPER, Mohali, India*; 2/2014.

Biography of Dr Punna Rao Ravi

Dr Punna Rao Ravi is working as Assistant Professor in Department of Pharmacy, BITS-Pilani, Hyderabad Campus. He obtained his B.Pharm, M.Pharm and PhD degrees in Pharmaceutical Sciences from BITS-Pilani University, Rajasthan. He has been working as a faculty member in BITS-Pilani since year 2000. He has many publications in reputed international and national peer-reviewed journals and has presented papers in scientific conference both in India and abroad. He has successfully completed government sponsored research projects and is expecting more grants from scientific funding agencies.

Biography of N. Aditya

Mr N. Aditya has completed his B.Pharm from KLES' College of Pharmacy, Hubli and M.Pharm from Government College of Pharmacy, Bangalore, both under the aegis of Rajiv Gandhi University of Health Sciences, Karnataka. Post M.Pharm, he has worked in formulation development departments of Strides Arcolab and Apotex Research Pvt Ltd., Bangalore where he was exposed to nuances of formulation development in semisolid and solid oral dosage forms. He joined BITS-Pilani, Hyderabad campus as a PhD scholar-cum-lecturer in July 2010. He has authored/co-authored research papers in renowned international and national peer-reviewed journals. He has also presented scientific posters/papers in reputed international and national conferences.